Redox reactions and antioxidant activities of organoselenium compounds and their nanocomposites

By

PAVITRA V. KUMAR

CHEM01201304031

BHABHA ATOMIC RESEARCH CENTRE, MUMBAI

A thesis submitted to the

Board of Studies in Chemical Sciences

In partial fulfillment of requirements for the Degree of

DOCTOR OF PHILOSOPHY

of

HOMI BHABHA NATIONAL INSTITUTE

January, 2017

Homi Bhabha National Institute

Recommendations of the Viva Voce Committee

As members of the Viva Voce Committee, we certify that we have read the dissertation prepared by **Pavitra V. Kumar** entitled **"Redox Reactions and Antioxidant Activities of Organoselenium Compounds and their Nanocomposites"** and recommend that it may be accepted as fulfilling the thesis requirement for the award of degree of Doctor of Philosophy.

Chairman - Dr. D. K. Palit	Palit	**Date:** 29/06/2017
Guide/Convener - Dr. K. I. Priyadarsini	K. Indira Priyadarsini	**Date:** 29.6.2017
Technical Advisor – Dr. B. G. Singh	BGSingh	**Date:** 29.6.2017
Member 1 - Dr. D. B. Naik		**Date:** 29-6-2017
Member 2 – Dr. P. A. Hassan		**Date:** 29-06-2017
External Member – Dr. G. Mugesh		**Date:** 29.06.2017

Final approval and acceptance of this thesis is contingent upon the candidate's submission of the final copies of the thesis to HBNI.

I/We hereby certify that I/we have read this thesis prepared under my/our direction and recommend that it may be accepted as fulfilling the thesis requirement.

Date: 29-06-2017

Place: BARC, Mumbai

(Guide)

STATEMENT BY AUTHOR

This dissertation has been submitted in partial fulfillment of requirements for an advanced degree at Homi Bhabha National Institute (HBNI) and is deposited in the Library to be made available to borrowers under rules of the HBNI.

Brief quotations from this dissertation are allowable without special permission, provided that accurate acknowledgement of source is made. Requests for permission for extended quotation from or reproduction of this manuscript in whole or in part may be granted by the Competent Authority of HBNI when in his or her judgment the proposed use of the material is in the interests of scholarship. In all other instances, however, permission must be obtained from the author.

Pavitra V. Kumar

DECLARATION

I, hereby declare that the investigation presented in the thesis has been carried out by me. The work is original and has not been submitted earlier as a whole or in part for a degree / diploma at this or any other Institution / University.

Pavitra V. Kumar

List of Publications arising from the thesis

Journal

1. Binding of a cyclic organoselenium compound with gold nanoparticles (GNP) and its effect on electron transfer properties

P. V. Kumar, B. G. Singh, N. Maiti, M. Iwaoka and K. I. Priyadarsini

J. Coll. Interf. Sci., **2014**, *436*, 179-185.

2. Degradation of peroxynitrite by simple, recyclable selenolanes

P. V. Kumar, B. G. Singh, A. Kunwar, M. Iwaoka and K. I. Priyadarsini

Bull. Chem. Soc. Jpn., **2016**, *89*, 490-497.

3. Effect of molecular interactions on electron-transfer and antioxidant activity of bis(alkanol)selenides: A radiation chemical study

P. V. Kumar, B. G. Singh, P. P. Phadnis, V. K. Jain and K. I. Priyadarsini

Chem. Eur. J., **2016**, *22*, 12189-12198.

4. Gold nanoparticles (GNP) induced redox modulation in organoselenium compounds: Distinction between cyclic vs. linear structures

P. V. Kumar, B. G. Singh, A. Ballal, V. K. Jain, M. Iwaoka and K. I. Priyadarsini

RSC Adv., **2016**, *6*, 69501–69508.

Conferences/Symposia

1. Enhanced glutathione peroxidase activity of selenocystine on binding with gold nanoparticles

P. V. Kumar, B. G. Singh and K. I. Priyadarsini

Ist National Conference on Advanced Oxidation Process, Thapar University, India, November, 2013.

2. Interaction of a cyclic organoselenium compound with gold nanoparticles

P. V. Kumar, B. G. Singh, M. Iwaoka and K. I. Priyadarsini

Trombay Symposium in Radiation & Photochemistry, Mumbai, India, January, 2014.

3. Degradation of peroxynitrite, a powerful and stealthy molecular oxidant by simple and recyclable selenium compounds

P. V. Kumar, B. G. Singh, M. Iwaoka and K. I. Priyadarsini

International Conference on Advanced Oxidation Processes, Munnar, India, September, 2014.

4. Pulse Radiolysis Studies of Selenobisethanol

P. V. Kumar, B. G. Singh, P. P. Phadnis, V. K. Jain and K. I. Priyadarsini

National Symposium on Radiation and Photochemistry, IIT Kanpur, India, March, 2015.

5. Comparison of hydroxyl radical reaction with linear and cyclic selenium compounds

P. V. Kumar, B. G. Singh, V. K. Jain, M. Iwaoka and K. I. Priyadarsini

Trombay Symposium on Radiation and Photochemistry, Mumbai, India, January, 2016.

6. Selenium- gold nano-conjugtates: preparation, characterization and redox reactions

P. V. Kumar, B. G. Singh, V. K. Jain and K. I. Priyadarsini

IUPAC International conference on Physical Organic Chemistry, Sydney, Australia, July, 2016.

To my family

ACKNOWLEDGEMENTS

It gives me immense pleasure to express my deepest and sincere gratitude to my guide, Dr. K. Indira Priyadarsini, Head, Chemistry Division for her aspiring guidance, constant encouragement and motivation. Her wide knowledge and logical way of thinking on scientific problems greatly helped me during the work.

I am deeply indebted to my research technical advisor Dr Beena G Singh, RPC Division for her invaluable guidance, positive and supportive attitude and continuous encouragement without which it would have not been possible to complete this research work.

I am privileged to thank Dr. B. N. Jagtap, Ex-Director, Chemistry group; Dr D. K. Palit, Head, RPC Division for their encouragement and support during my research work.

It is my great pleasure to thank Dr. D. B. Naik, RPC Division, Dr. P. A. Hassan, Chemistry Division for critical evaluation of my research activities and valuable suggestion as members of HBNI doctoral committee.

I also owe my sincere thanks to Dr V K Jain, Ex-Head, Chemistry Division; Dr P. P. Phadnis, Chemistry Division and Dr. M. Iwaoka, Tokai University, Japan, for providing the compounds for this study.

I would also like to thank Dr. A. Barik, RPC Division and Dr. Amit Kunwar, RPC Division for their support and healthy discussions during the research work. My heartfelt thanks go to all my lab mates and friends for their constant and unconditional support. I also sincerely thank CSIR for providing the research fellowship.

Finally, I am highly obliged to my family members for their constant love and support.

January, 2017 *Pavitra V Kumar*

CONTENTS

Section-B

Synopsis

Selenium (Se), 34th element of periodic table, discovered by Swedish chemist Joens Berzelius in 1817, was first considered as poison to living beings.[1] Excess exposure to selenium was found to be associated with loss of hair, nails and swelling at the fingertips, a condition known as "selenosis".[2] In 1957, Schwarz and Foltz identified selenium as a micronutrient in bacteria, mammals, and birds and later it was observed that selenium deficiency can cause onset of many diseases like, Parkinson's disease, cardiomyopathy, loss of immunity, etc.[3,4] The global interest in selenium biochemistry evolved after identification of selenium in bacterial enzymes like formate dehydrogenase and glycine reductase and at least 25 selenoproteins have been identified till date.[5] In 1973, presence of selenium at the active site of glutathione peroxidase (GPx), an important redox regulatory enzyme, emphasized the importance of selenium in the cellular redox biochemistry.[6] GPx catalyses reduction of oxidizing hydrogen peroxide (H_2O_2) and other hydroperoxides to less reactive water or alcohols using cellular thiols as substrates, where the reactions occur mostly through electron transfer. H_2O_2 and other hydroperoxides in presence of transition metals can lead to production of powerful oxidizing radicals like hydroxyl ($^{\bullet}OH$) radical and superoxide radicals. In the presence of intracellular nitric oxide, these radicals are further converted to other powerful oxidants like peroxynitrite ($ONOO^-$), carbonate ($CO_3^{\bullet-}$) and nitrogen dioxide ($NO_2^{\bullet}$) radicals.[7] All these free radicals and molecular oxidants are collectively termed as reactive oxygen species (ROS). Intracellular antioxidant system comprising of several enzymes, vitamins and thiols maintains the cellular redox status under normal

conditions. However under some conditions like radiation exposure, pollution, etc. can cause excess generation of ROS and lead to a condition known as “oxidative stress” which has been implicated in the onset of several diseases like diabetes, cancer, ageing etc. Under such conditions, supplementation with external antioxidants becomes necessary.

The presence of selenium at the active site of GPx prompted researchers to develop redox active organoselenium compounds as new GPx like antioxidants, where they can catalyze reduction of H_2O_2 in presence of thiols. The first organoselenium compound evaluated for GPx activity was an aromatic selenoamide, ebselen.[8] Following this, several organoselenium compounds based on ebselen moiety were synthesized and tested for GPx like activity.[9,10] These studies focused mainly on the presence of non-bonding interactions between selenium and hetero atom (O, N) to tune the GPx like activity of these compounds. In 2004, Back et al published that hydroxyl functionalized aliphatic monoselenides exhibited better GPx activity as compared to ebselen, due to formation of cyclic intermediates (spirodioxaselenanonanes).[11] Further, it was found that functionalization of aliphatic organoselenium compounds with electron donating groups like carboxylate ($-COO^-$), increased the GPx like activity whereas that with electron withdrawing groups like amino ($-NH_3^+$) and hydroxyl (-OH), decreased the GPx like activity.[12] Also, for a given functional group, the alkyl chain length has been found to play important role in GPx like activity of aliphatic monoselenides.[11,13]

Although most of the research on selenium based antioxidants was focused on synthesis and design of new GPx mimics, only a few studies were reported on their free

radical neutralizing activity. Selenium compounds like their sulfur analogues can react with free radicals like $^{\bullet}OH$ radical. The first report in this direction was published by Badiello et al who have reported $^{\bullet}OH$ radical reaction with selenourea (SeU), selenocystine (CysSeSeCys) and selenomethionine (SeM) using pulse radiolysis technique.[14] The free radical scavenging activity of these compounds was observed to be 10-100 times higher compared to their sulfur analogues.[15] Also, the selenium centered radical cations formed during the reaction were found to be more stable than the analogues sulfur based radicals. The selenium centered radical cations can exist either as monomer ($>Se^{\bullet+}$) or dimer radical cation ($>Se\therefore Se<)^{+}$ and the stability of these radicals is attributed to formation of two-centered three electron bond (2c-3e) also termed as hemi-bond, which is formed by overlapping of p-orbital of the oxidized selenium atom with the lone pair of the parent molecule. The nature and stability of these transients is governed by the non-bonding as well as bonding interaction of the selenium centre with the neighboring group/hetero atom (N, O etc.).[16] Due to higher covalent radii of selenium atom, these non-bonding interactions are more prevalent in organoselenium compounds than their sulfur analogues.

So far, in the literature, there is no attempt to provide correlation between free radical scavenging and GPx like activity in organoselenium compounds. Understanding the crucial electron transfer reactions and the nature and reactivity of the intermediates formed therein, is very important for the designing of new organoselenium compounds. Thus the aim of the present thesis work is to study redox reactions between free radical or molecular oxidants and simple organoselenium compounds, which are structurally

related. For this, three low molecular weight, water soluble organoselenium compounds e.g. trans-3,4-dihydroxyselenolane, (DHS), 3-monoamineselenolane (MAS) and bis(alkanol)selenides (SeROH) (Scheme 1) were chosen. DHS has been reported to show GPx like antioxidant activity and has also been shown to exhibit significant healing ability against indomethacin-induced stomach ulceration in mice.[17,18] MAS is a monoamino substituted analogue of DHS and has shown higher GPx activity than DHS.[17] Similarly, linear selenoethers, SeROH also exhibited GPx activity, where the length of the alkyl chain was found to play important role.[11,17] All these compounds are structurally related and have been investigated to understand how chemical structure correlates with their electron transfer reactions and antioxidant activity.

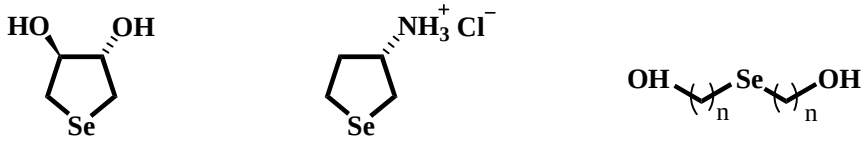

DHS **MAS** **SeROH; n=2, 3 and 4**

Scheme 1: *Chemical structures of trans-3,4-dihydroxyselenolane (DHS), 3-monoamineselenolane (MAS) and bis(alkanol)selenides (SeROH).*

The thesis has been divided into six chapters. Chapter one and two give general introduction and experimental details, respectively. The results of the different studies carried out are discussed in chapters three, four and five. In chapter three, one-electron transfer reactions of structurally related aliphatic selenoethers (SeROH) with $^{\bullet}OH$ radicals and other oxidizing radicals have been studied using nanosecond pulse radiolysis facility and the transients were detected by absorption spectroscopy. A

quantum chemical approach has been employed to correlate the nature and stability of the transients with structural properties of these compounds. Chapter four deals with the effect structure or functional groups present in cyclic and linear organoselenium compounds on their ability to scavenge peroxynitrite, a molecular oxidant. Chapter five explains the binding of linear and cyclic structural isomers of two organoselenium compounds with gold nanoparticles (GNP) and the role of selenium-GNP interactions in modulation of electron transfer reactions of these compounds. Chapter six gives summary and future scope of the study. A brief account of each chapter has been given below.

Chapter 1: General introduction

This chapter gives the general information about selenium and its chemistry and biology with emphasis on their physico-chemical properties, selenoproteins, the enzyme GPx and the important steps in the catalytic activity of synthetic GPx mimics. The generation of ROS, oxidative stress and the role of antioxidants in reducing ROS level has been discussed. Also, the basic principles of radiation chemistry and the use of pulse radiolysis in generation of ROS in studying electron transfer reactions in cellular system have been explained. A brief mention of various types of common antioxidants, with their advantages and limitations, has been given. The current status of research on selenium based antioxidants and pulse radiolysis studies on organoselenium compounds have been discussed in detail.

Chapter 2: Experimental techniques

A brief overview of the synthesis of the organoselenium compounds, along with all the other chemicals used in different studies has been included in the materials part. Details of different experimental techniques used in the current thesis have been illustrated. The working principle of nanosecond pulse radiolysis facility along with details of kinetics spectroscopy has been explained. Basic principles of instruments used for carrying out various studies such as stopped flow spectrometer, high performance liquid chromatography (HPLC) and details of the quantum chemical calculations have been given. Techniques employed for the characterization of nanoparticles such as dynamic light scattering (DLS), zeta (ζ) potential, surface enhanced Raman spectroscopy (SERS) etc. have also been described briefly.

Chapter 3: Pulse Radiolysis studies on reactions of free radical oxidants with organoselenium compounds

For the development of antioxidants, it is important to understand the various factors that can affect their interaction with ROS. Identifying various molecular descriptors and understand their role in stabilizing the intermediates formed during these reactions with ROS will help in the design of efficient antioxidants. Thus in this chapter reaction of three linear aliphatic selenoethers, bis(2-ethanol)selenide (SeEOH), bis(3-propanol)selenide (SePOH) and bis(2-butanol)selenide (SeBOH), with $^{\bullet}$OH radical were studied in detail using pulse radiolysis technique. The transients were characterized under different conditions like varying concentration of SeROH or proton, reaction with specific one-electron oxidant (like azide ($N_3^{\bullet}$) radical), etc. In all the three compounds, $(>Se\therefore Se<)^{+}$ radical was the major species formed having characteristics absorption

band at ~460-500 nm. The formation of $(>Se\therefore Se<)^{+}$ radical was attributed to association of parent SeROH molecule with one-electron oxidized SeROH ($>Se^{\bullet+}$). The nature, reactivity and yield of the transients formed was determined by employing their reaction with different redox couples like thionine ($Th^{2+}/Th^{\bullet+}$), 2,2'-azino-bis-ethylsulfonate ($ABTS^{2-}/ABTS^{\bullet-}$), etc. These results along with the equilibrium constant values for $(>Se\therefore Se<)^{+}$ radical formation indicated that the stability of $(>Se\therefore Se<)^{+}$ radical increased with increase in alkyl chain length. The yield of selenoxides ($SeROH_{ox}$) formed by disproportionation reaction of $(>Se\therefore Se<)^{+}$ radical and estimated by HPLC were found to increase with increase in alkyl chain length. Under similar conditions, analogues organosulfur compounds (SROH) did not produce sulfoxides ($SROH_{ox}$) and rather underwent radiolytic degradation to form formaldehyde (HCHO) and carbon (C)-centered radicals. To explain this differential behavior between organoselenium and organosulfur compounds, quantum chemical calculations were performed. The electron density analysis showed that the energy difference between highest occupied molecular orbital (HOMO) of parent molecule and singly occupied molecular orbital (SOMO) of ($>Se^{\bullet+}$) radical is an important factor in defining the stability of $(>Se\therefore Se<)^{+}$ radical. The larger energy difference between HOMO of SROH and SOMO of oxidized SROH ($>S^{\bullet+}$) led to poor overlapping of orbitals and consequently resulted in formation of a weak bond. It was also observed that the non-bonding interactions between the radical cation centre and α-C-H bond are prevalent in ($>S^{\bullet+}$) radical leading to formation of C-centered radicals. However, these interactions were non-significant in organoselenium compounds, therefore most of the ($>Se^{\bullet+}$) radicals were converted to $(>Se\therefore Se<)^{+}$ radicals. The formation of $(>Se\therefore Se<)^{+}$ radicals

was exothermic with a large negative energy change ($\Delta E\sim$ -14 kcal/mol), whereas similar reaction for organosulfur compounds was endothermic (ΔE= +122 kcal/mol). The formation of $(>S\therefore S<)^{+}$ radical was thermodynamically unfavorable as the process was associated with positive energy change. These results indicate that the non-bonding interactions existing in transients play important role in their stability and are greatly affected by change in structure or substitution of selenium by sulfur. Also, the stability of $(>Se\therefore Se<)^{+}$ radicals can be a useful parameter to understand the structure-activity correlation of organoselenium compounds.

To further understand the effect of structure on one-electron transfer reactions of organoselenium compounds, a comparison has been made between SeEOH and its cyclic analogue DHS. Although, both compounds formed $(>Se\therefore Se<)^{+}$ radical as major transient during $^{\bullet}$OH radical reaction, the stability and yield of this transient differed considerably. Also the yield of selenoxide was found to be ~2 times higher for DHS as compared to SeEOH and was attributed to the formation of stable $(>Se\therefore Se<)^{+}$ radical for DHS. Unlike SeEOH, DHS did not show formation of HCHO and C-centered radicals. These results were further supported by quantum chemical calculations, wherein it was observed that the non-bonding interactions between selenium and α-C-H bond of ($>Se^{\bullet+}$) radical are inhibited due to cyclic structure DHS. The stable transients ($(>Se\therefore Se<)^{+}$ radical) formed with DHS did not allow its radiolytic degradation, thereby resulting in higher yield of DHS_{ox} as compared to $SeEOH_{ox}$. These results directly correlate with their GPx activity, where DHS showed higher GPx activity than SeEOH. From these studies, it has been concluded that selenoxide formation decides the

antioxidant activity of selenoethers and the cyclic compounds are better antioxidants than their linear analogues.

Chapter 4: Reaction of peroxynitrite with organoselenium compounds: Role of chemical structure on antioxidant activity

To understand the effect of structure on redox reactions of organoselenium compounds with molecular oxidants, the reactions of DHS, MAS and SeEOH with peroxynitrite were studied. Peroxynitrite is a very powerful molecular oxidant which is formed by the diffusion controlled reaction of nitric oxide radical ($NO^{\bullet}$) with superoxide radical and is known to react with target bio-molecules via one-electron, two-electron and atom transfer reactions. The kinetics of the reaction of peroxynitrite with these compounds was studied by stopped flow technique and competition kinetics using dihydro rhodamine (DHR123) as reference solute and the bimolecular rate constant were estimated to be in order of ~10^3 $M^{-1}s^{-1}$. As, peroxynitrite reacts with carbon dioxide present in cells to form other powerful oxidants like nitrogen dioxide ($NO_2^{\bullet}$) and carbonate ($CO_3^{\bullet-}$) radicals, reactions of these compounds with $NO_2^{\bullet}$ and $CO_3^{\bullet-}$ radicals were also studied using pulse radiolysis technique. These compounds reacted with $CO_3^{\bullet-}$ radicals to form corresponding $(>Se\therefore Se<)^+$ radicals which were further converted to selenoxides as final products. However, they did not react with $NO_2^{\bullet}$ radical. The selenoxides (DHS_{ox}, MAS_{ox} and $SeEOH_{ox}$) were identified by ^{77}Se NMR and mass spectrometry (MS) and their yields were estimated by HPLC which followed the order DHS_{ox} > MAS_{ox} > $SeEOH_{ox}$. The selenoxides converted oxidizing NO_2^- to less reactive NO_3^-, followed by the regeneration of parent selenium

compounds, which is an important factor in their peroxynitrite reductase ability. Further, to evaluate their relative antioxidant activity these organoselenium compounds were tested for protection ability against peroxynitrite induced cellular toxicity and DNA damage. At a concentration of 1 mM, DHS showed significantly higher protection (70 ± 4%) against peroxynitrite induced DNA damage than that of MAS (37 ± 3%) and SeEOH (28 ± 3%). The antioxidant activity of these compounds was found to be in direct correlation with amount of selenoxide formed during reaction with peroxynitrite. These results indicated that the yield and stability of selenoxide formed during the reaction of organoselenium compounds with peroxynitrite is a very important factor for their peroxynitrite reductase like antioxidant activity.

Chapter 5: Studies on binding of organoselenium compounds with gold nanoparticles (GNP) and effect on their redox properties

The redox properties of organoselenium compounds can be modulated through formation of selenium-gold (Se-GNP) nanoconjugates. In this chapter, the binding of two organoselenium compounds, DHS (cyclic) and SeEOH (linear) with GNP of four different sizes (5 nm – 58 nm) was studied in detail. The formation of Se-GNP nanoconjugates was characterized by absorption spectroscopy, DLS, transmission electron microscopy (TEM) and ζ-potential measurements. The binding constant (K) was calculated from the absorption spectroscopic data, where it was observed that for a given size of GNP, SeEOH exhibited higher K value (~ 2 - 4 times) than that for DHS. Under identical conditions, the size of SeEOH-GNP nanoconjugates was found to be smaller than that of DHS-GNP nanoconjugates for all sizes of GNP. To understand the

mode of interactions between GNP and SeEOH/DHS, SERS measurements were carried out. The various SERS peaks were assigned by comparing with the Raman spectra of neat SeEOH/DHS and complemented by Raman bands obtained by using quantum chemical calculations. The results showed that the binding of SeEOH on GNP surface takes place via both selenium atom and side alkyl chain; whereas in DHS, the interactions mainly occur through selenium atom. The effect of this binding on electron transfer properties of SeEOH and DHS was studied by carrying out its reaction with $ABTS^{\bullet-}$ and $^{\bullet}OH$ radicals. Conjugation with GNP enhanced the rate of reaction of both SeEOH and DHS with $ABTS^{\bullet-}$ radical. Similarly the reactions of SeEOH and DHS with $^{\bullet}OH$ radical in absence and in presence of GNP1 (5 nm GNP) were studied. It was observed that not only the stability the of $(>Se\therefore Se<)^{+}$ radical formed during reaction of SeEOH with $^{\bullet}OH$ radical but also the yield of $SeEOH_{ox}$ increased in presence of GNP. However, no such effects were observed for DHS-GNP nanoconjugates. These results suggested that the binding of organoselenium compounds with GNP leads to modulation of electron density on selenium atom and thereby can modulate their electron transfer properties.

Chapter 6: Summary and future scope

This chapter summarizes the results of different studies carried out under this thesis work. A brief description on the contribution of the present work in development of selenium based antioxidants has been given. The future scope of the work has also been discussed briefly.

References

1. J. J. Berzelius, *Afhandl. Fys. Kemi Mineralogi*, 1818, **6**, 42.

2. O. H. Muth and W. Binns, *Annals of the New York Academy of Sciences*, 1964, **111**, 583–590.

3. K. Schwarz and C. M. Foltz, *J. Am. Chem. Soc.*, 1957, **79**, 3292-3293.

4. L. A. Papp, J. Lu, A. Holmgren and K. K. Khanna, *Antioxid. Redox Signal*, 2007, **9**, 775-806.

5. J. B. Jones and T. C. Stadtman, *J. Bio. Chem.*, 1981, **256**, 656-663; J. E. Cone, R. M. DelRio, J. N. Davis and T. C. Stadtman. *Proc Natl Acad Sci*, 1976, **73,** 2659-2663.

6. J. T. Rotruck, A. L Pope, H. E. Ganther, A. B. Swanson, D. G. Hafeman and W. G. Hoekstra, *Science*, 1973, **179**, 588-590.

7. W. H. Koppenol, J. J. Moreno, W. A. Pryor, H. Ischiropoulos and J. S. Beckman, *Chem. Res. Toxicol.*, 1992, ***5***, 834-842; G. E. Arteel, K. Briviba and H. Sies, *FEBS Lett.*, 1999, ***445***, 226-230.

8. H. Sies, *Free Rad. Bio. Med.*, 1993, **14**, 313-323.

9. B. K. Sharma and G. Mugesh, *J. Am. Chem. Soc.*, 2005, **127**, 11477–11485.

10. K. P. Bhabak and G. Mugesh, *Chemistry*, 2007, **13**, 4594-601.

11. T. G. Back, *Angew. Chem. Int. Ed.*, 2004, **43**, 1268-1270.

12. P. Prabhu, P. P. Bag, B. G. Singh, A. Hodage, V. K. Jain, M. Iwaoka and K. I. Priyadarsini, *Free Rad. Res.*, 2011, **45**, 461–468.

13. B. G. Singh, S. A. Nadkarni, V. K. Jain and K. I. Priyadarsini, *RSC Adv.*, 2015, **5**, 66621-66627.

14. R. Badiello and E.M. Fielden, *Int. J. Rad. Bio.*, 1970, **17**, 1-14; M. Tamba and R. Badiello, *Int. J. Rad. Bio.*, 1973, **23**, 435-445; M. Tamba, S. Bonora and R. Badiello, *Zeitschrift fur Naturforschung - Section B J. Chem. Sci.*, 1974, **29**, 571-572.

15. B. Mishra, P. A. Hassan, K. I. Priyadarsini, H. Mohan, *J. Phys. Chem. B*, 2005, **109**, 12718–12723.

16. B. G. Singh, E. Thomas, S. N. Sawant, K. Takahashi, K. Dedachi, M. Iwaoka and K. I. Priyadarsini, *J. Phys. Chem. A*, 2013, **117**, 9259−9265.

17. K. Arai, F. Kumakura, M. Takahira, N. Sekiyama, N. Kuroda, T. Suzuki and M. Iwaoka, *J Org. Chem.*, 2015, **80**, 5633−5642; B. G. Singh, E. Thomas, F. Kumakura, K. Dedachi, M. Iwaoka, and K. I. Priyadarsini, *J. Phys. Chem. A*, 2010, **114**, 8271–8277;

18. S. Chakraborty, S. Yadav, M. Subramanian, K. I. Priyadarsini and M. Iwaoka, *Free Radic. Res.*, 2012, **46**, 1378-1386; S. Chakraborty, S. Yadav, M. Subramanian, M. Iwaoka and S. Chattopadhyay, *Biochim. Biophys. Acta*, 2014, **1840**, 3385-3392.

List of abbreviations

ABTS:	2,2'-azino-bis(3-ethylbenzothiazoline-6-sulfonic acid)
B3LYP:	Becke non local model and Lee−Yang−Parr nonlocal correlation functionals
Cys:	Cysteine
CysSeSeCys:	Selenocystine
DFT:	Density functional theory
DTPA:	Diethylene triaminepentaacetic acid
DHS:	Trans-3,4-dihydroxy-1-selenolane
DHR123:	Dihydrorhodamine
DTT:	Dithiothretol
DLS:	Dynamic light scattering
DMEM:	Dulbecco's modified Eagle's medium
GSH:	Glutathione
GNP:	Gold nanoparticles
GPx:	Glutathione peroxidase
GSSG:	Oxidized glutathione
HOMO:	Highest occupied molecular orbital
HPLC:	High performance liquid chromatography
ID:	Iodothyronine deiodinase
LINAC:	Linear electron accelerator
LDL:	Low density lipoprotein

MTT:	Dimethyl thiazolyldiphenyl tetrazolium salt
MS:	Mass spectrometery
MAS:	3-amino-1-selenolane
PCM:	Polarizable continuum model
NBO:	Natural bond order
NADPH:	Nicotinamide adenine dinucleotide phosphate
NMR:	Nuclear magnetic resonance
OS:	Oxidative stress
ROS:	Reactive oxygen species
SeROH:	Bis(alkanol)selenides
SeCys:	Selenocysteine
SMD:	Solvent density model
SOD:	Superoxide dismutase
SERS:	Surface enhanced Raman spectroscopy
SelP:	Selenoprotein P
TrxR:	Thioredoxin reductase
TEM:	Transmission electron microscopy
TFA:	Trifluro acetic acid

LIST OF FIGURES

conditions (Absorbed dose=167 Gy). Inset (A) and (B) show the linear variation in the amount of formaldehyde formed as a function of absorbed dose.

LIST OF TABLES

Chapter 1

General introduction

In this introduction chapter, details on the physico-chemical properties of selenium, its importance as a micronutrient and its role in biology are given. The general information about reactive oxygen species (ROS), methods of generation of ROS, oxidative stress, enzymatic and non-enzymatic antioxidants and principles of radiation chemistry have been also included. The chapter also covers a brief literature review on sulfur and selenium based antioxidants and their current status. The motivation behind the present Ph.D work and a brief outline of thesis is included at the end.

1.1 Discovery of selenium

Selenium, a member of chalcogen family with atomic number 34, was accidently discovered by Jons Jacob Berzelius in 1817 while analyzing a red colored deposit on the wall of lead chambers used in the production of sulphuric acid.[1] Due to its resemblance with tellurium which was named after a Latin word 'tellus' (means earth), it was named as 'selenium' after the Greek word 'selene' (means moon). In the same year, he also discovered an ore 'eucairite' having unusually high selenium content and reported the discovery of selenium as a new element in 1818.

1.2 Atomic structure and periodic properties of selenium

Selenium belongs to the 16th group of periodic table and shares with other elements like, oxygen, sulfur, tellurium and polonium. Collectively, members of this group are called as chalcogens. Of these, oxygen and sulfur are non-metals, selenium and tellurium are metalloids and polonium is a radioactive metal.

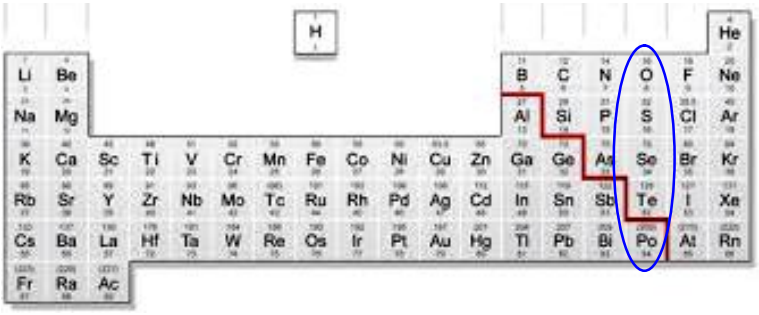

Fig.1.1: *Position of selenium in periodic table.*

The electronic configuration of selenium is [Ar]4s^{2}4p^4 with six electrons in its valance shell. To achieve noble gas configuration, selenium can either gain two electrons

or loose six electrons. Accordingly, selenium in its chemical form has been observed to exhibit variable oxidation states ranging from -2 to +6 as listed in table 1.1. Elements down the group, show decrease in both ionization energy and electron affinity while atomic radius increases. This makes selenium more electropositive in comparison to its lower analogues. Table 1.1 lists the periodic properties of sulfur and selenium.

Table 1.1: *Comparison of periodic properties of sulfur and selenium.*

Properties	Sulfur	Selenium
Electronic configuration	$[Ne]3s^2\ 3p^4$	$[Ar]4s^2\ 4p^4$
Ionization potential (eV)	10.4	9.75
Electronegativity (Pauling scale)	2.5	2.4
Oxidation states	-2, -1, 0, +2, +4 and +6	-2, -1, 0, +2, +4 and +6

1.3 Physico-chemical properties

1.3.1 Physical properties

Selenium is found in nature as an impurity in pyrites ores of copper and iron and sulfide ores of copper, lead, nickel, etc. The total crustal abundance of selenium is 0.13 ppm. There are six naturally occurring isotopes of selenium of which ^{80}Se (49.8%) and ^{78}Se (23.7%) are the most abundant ones. Selenium has been found to exist in three allotropic forms- black, red and gray. Black selenium has irregular and complex structure consisting of polymeric rings and exhibits a black luster. The red form of selenium has a monoclinic crystal structure and exists in three forms i.e. α, β, and γ forms. Gray form of selenium has a hexagonal crystal lattice consisting of helical polymeric chains and is the

most stable form. The red and black forms of selenium are insulators while gray form of selenium has semiconductor properties and used in electronics and solar cell applications.

1.3.2 Chemical properties

Selenium forms a variety of compounds in both inorganic and organic form, due to its ability to exhibit variable oxidation states. The most common oxidation states observed in inorganic forms are +4 and +6. The compounds with +4 oxidation state show both oxidizing and reducing properties whereas those with +6 oxidation state exhibit only oxidizing properties. Some of the important inorganic selenium compounds are selenium dioxide (SeO_2), sodium selenite (Na_2SeO_3) and sodium selenate (Na_2SeO_4). The organic selenium (or organoselenium) compounds in general have selenium in -2 and +2 oxidation states. However +4 and +6 oxidation states are also observed in some of organoselenium compounds like seleninic acid and selenones. The general structures of different forms of organoselenium compounds are given in scheme 1.1.

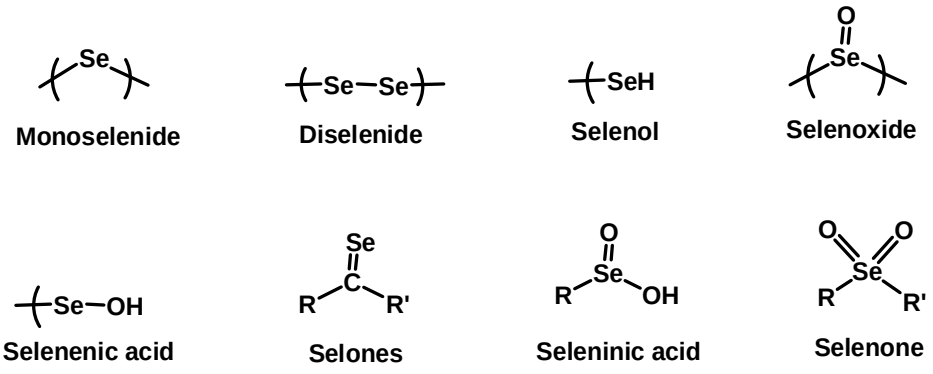

Scheme 1.1: *General motif of different types of organoselenium compounds.*

The monoselenides or selenoethers are the selenium equivalents of ethers and thioethers. These are the most prevalent organoselenium compounds and can be prepared

in laboratory either by alkylation of alkali metal selenide salts (e.g. sodium selenide) or by alkylation of selenolates. These compounds are generally nucleophilic in nature. Diselenides are comparatively more stable than monoselenides and are used for synthesis of selenols (RSeH) which are the selenium equivalents of alcohols and thiols. These compounds are relatively unstable and oxidize readily to their corresponding diselenide.

Table 1.2: *Reduction potential of sulfur and selenium compounds.*

Reduction potential (E° vs NHE, V)	Sulfur	Selenium	Reference
Dithiothretol (DTT)/diselenothretol (DST)	-0.327[a]	---[b]	[2]
Cysteine (Cys)/selenocysteine (SeCys)	-0.238 [a]	-0.383 [a]	[2]
Cystamine (CysA)/selenocystamine (SeCysA)	-0.236 [a]	-0.352 [a]	[2]
Glutathione (GSH)/Selenoglutathione (GSeH)	-0.256 [a]	-0.457 [a]	[3]
Methionine (Met)/Selenomethionine (SeMet)	----	1.21	[4]
methylphenylsulfide/ methylphenylselenide	-1.45[c]	-1.09 [c]	[5]

a- values are corresponding to two-electron reduction process; b-could not be estimated even in excess of DTT and assumed that it has lower reduction potential than DTT;c- values are corresponding to one-electron reduction process.

The reduction potential values of organoselenium compounds are more negative than their analogous sulfur compounds as listed in table 1.2. Therefore, organoselenium compounds are expected to participate in redox reactions more easily than their sulfur counterparts. Another important property that differentiates the chemical properties of

organoselenium compounds from their sulfur analogues is their acid dissociation constant (pKa) values. The pKa value of –SeH group in SeCys is ~5.2 whereas Cys exhibits pKa value of ~8.6.[6] Due to the lower pKa value, selenols exist in deprotonated form (selenolate ($-SeO^-$)) whereas thiols exist in protonated form at physiological pH. In addition, the C-Se bond distance in organoselenium compounds (C–Se 198 pm) is higher than that in organosulfur compounds (C–S 181 pm). As a result the C-Se bond (~58 kcal/mol) is weaker and can be easily cleaved in comparison to C-S bond (65 kcal/mol).

1.4 Selenium in biology

1.4.1 Selenium toxicity

Selenium was initially recognized for its toxicity in animals and humans. The toxicity of selenium was observed for the first time in 13th century by Marco Polo in North West China where he described a condition of lack of vitality, hair loss shedding of hooves in horses after grazing some plant species in that area. Later in 1560 in Columbia and in 1860 in South Dakota similar disorders were observed in grazing animals. At that time, the real cause of these disorders was unknown and the condition was named as 'alkali disease' due to its association with alkaline seeps which were being used as watering source in that area. In early 1930, H. G. Knights discovered similar incidence of alkali disease in livestock grazed in area of high selenium soil.[7] Further 'alkali disease' was also reported in horses and sheep fed on plants that can accumulate high levels of selenium in its tissues.[8,9] These symptoms were later named as 'blind staggers' by Rosefeld and co-workers and was attributed to high selenium consumption.[10] In 1943, Nelson et. al. showed that ingestion of seleniferous diet can lead to development of hepatic cell adenoma and low grade

carcinoma in rat and introduced the carcinogenic nature of selenium.[11] Selenium was continued to be considered as absolute poison, until 1957 when Schwartz and Foltz identified its role in preventing the liver necrosis caused due to vitamin E deficiency in animals.[12] Later in 1973, presence of selenium in bacterial enzymes like formate dehydrogenase and glycine reductase was identified.[13] During the same time, it was also discovered that selenium occupies the active site of redox regulatory enzymes like, glutathione peroxidase (GPx) and thioredoxin reductase (TrxR).[14] Subsequently, several others confirmed that selenium deficiency is associated with the onset of many diseases like Keshan disease, Kashin-Beck disease, loss of immunity, adverse mood states, cardiovascular diseases and other neurodegenerative diseases.[15] With increasing evidences on the health benefits of selenium, it is now recognised that selenium is an important micronutrient for humans.

1.4.2 Selenium as micronutrient/supplement

An adequate amount of selenium is required for optimal health. As per World Health Organization (WHO), the minimum daily requirement of selenium is 21 µg/per day for men and 16 µg/per day for women.[16] Accordingly, selenium intake higher than the daily recommended nutritional dose is considered as selenium supplementation. The upper safe limit as per the European Food Safety Authority (EFSA) guidelines is 300 µg/day for adults, 250 µg/day for children aged 15 to 17 years and 60 µg/day for children aged 1 to 3 years.[17] The dietary sources of selenium are broccoli, mushrooms, cabbage, radishes, onions, garlic, fish (Tuna), whole grains, meat, wheat and Brazil nuts. Other than dietary intake, selenium supplementation has also received considerable attention in recent years.

The compounds available for selenium supplementation include the inorganic forms (sodium selenite, sodium selenate), organic forms (SeMet, methylselenocysteine (MeSeCys)) and high selenium enriched yeast, which contains selenium mostly in the form of SeMet with methylselenol (MeSeH), SeCys, selenohomocysteine, selenoadenosine, etc. as minor components.[18]

1.4.3 Selenoproteins

Animals including humans obtain selenium primarily in the form of SeMet by consuming plant products. SeMet obtained from these sources acts as a precursor for the synthesis of SeCys. SeCys is considered as the 21st amino acid and has specific genetic codon for its incorporation in to proteins. The groups of proteins that contain SeCys as an integral part of their polypeptide chains are defined as selenoproteins and these proteins are responsible for most of the physiological functions mediated by selenium. Till date, around 100 selenoproteins have been discovered with a largest set of 59 selenoproteins in a unicellular brown alga (a harmful bloom for fisheries) and 25 selenoproteins in humans.[19] In mammals, GPx, TrxR and iodothyronine deiodinase (DIO) are important selenoenzymes which are involved in redox regulation, protein folding and thyroid hormone metabolism.[20,21] A brief description of some of these selenoproteins is given below.

TrxR: It is a member of the pyridine nucleotide-disulfide oxidoreductase family which catalyzes the reduction of thioredoxin (Trx) by using nicotinamide adenosine dinucleotide phosphate (NADPH). In mammals, TrxR exists in three isoforms: cytosolic (TrxR1), mitochondrial (TrxR2), and thioredoxin glutathione reductase (TGR/TrxR3).[22] The mammalian TrxRs have selenium in the active site and are of high molecular mass (55kDa)

with broad substrate specificity. Mammalian TrxR directly reduces not only Trx from different species but also many non-disulfide substrates such as selenite, lipid hydroperoxides and hydrogen peroxide (H_2O_2). The activity of mammalian TrxR is due to presence of SeCys which acts as the active site of the enzyme.

Selenoprotein P (SelP)

SelP, an extracellular glycoprotein, was discovered in humans in 1993. It is the most abundant selenoprotein found in plasma and constitutes more than 50% of plasma selenium reserves.[23] SelP is mainly produced in the liver and then secreted into the plasma. It is also expressed in other tissues such as brain and heart. It plays important role in maintaining homeostasis and the transport of selenium in tissues.[24] It eliminates peroxynitrite ($ONOO^-$), a molecular oxidant produced from the reaction of superoxide ions with nitric oxide and reduces inflammation.[25]

DIO: These enzymes constitute a family of three integral membrane proteins having similar structures. DIO1 and DIO3 are plasma membrane proteins, whereas DIO2 is localized in the ER membrane. All DIO's are oxido-reductases with SeCys residue in the active site, that participates in thyroid hormone metabolism by catalyzing the activation (DIO1, DIO2) or inactivation (DIO3) of tetraiodothyroxine (T4), triiodothyro-nine (T3), and reverse-triiodothyronine (rT3).[26] These thyroid hormones regulate various metabolic processes, such as lipid metabolism, thermogenesis, growth and hearing. These enzymes are also needed for the normal development of the fetal brain.[27]

GPx: GPxs are a family of enzymes with antioxidant functions. The GPx family comprises of eight isoforms, but only five members have a SeCys residue and can catalyze the reduction of H_2O_2 and organic hydroperoxides using GSH as a reducing cofactor.[28] Among its family members, GPx1 is highly sensitive to changes in oxidative stress conditions.[29] It is a ubiquitous homotetrameric protein localized in the cytosol and mitochondria. GPx2 is a homotetrameric enzyme expressed mainly in the gastrointestinal system mucosa. The function of GPx2 is to protect intestinal epithelium from oxidative stress against the ingested pro-oxidants and to guarantee mucosal homeostasis. GPx3 is the only extracellular enzyme of the GPx family. It is a glycosylated homotetrameric protein produced into the cells of the proximal tubular epithelium and in the parietal cells of Bowman's capsule of the kidney. Unlike GPx1, GPx3 shows more restricted hydroperoxides substrate specificity. Although it can reduce H_2O_2 and organic hydroperoxides, its activity is 10 fold lower than that of GPx1. GPx4 is a monomeric intracellular enzyme and can directly use phospholipid hydroperoxide as substrate.[30] GPx6 is a close homolog of plasma GPx3 and its specific functions are not known.

The catalytic activity of GPx has been attributed to SeCys residue present at its active site. In the reduced form, the SeCys moiety is present in GPx in selenols form (E-SeH). Following reaction with hydroperoxides, selenol form is oxidized to selenenic acid (E-SeOH) which in presence of cellular glutathione (GSH) form is regenerated back to active selenol form selenenyl sulfide (E-Se-SG). The attack of a second GSH molecule at the E-Se-SG intermediate regenerates E-SeH. During this cycle, GSH is converted to its disulfide form (GSSG) which is reduced back to GSH using NADPH and thus redox balance is maintained by conversion of GSSG to GSH (scheme 1.2).

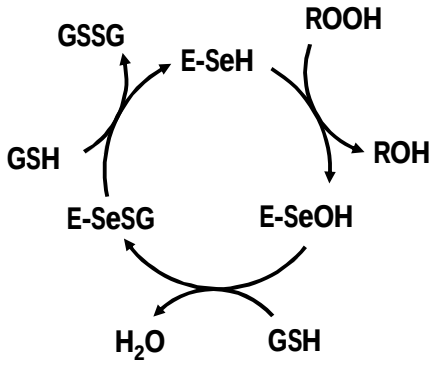

***Scheme 1.2**: Reaction mechanism for the catalytic reduction of peroxides by GPx.*

1.5 Reactive oxygen species (ROS), oxidative stress and antioxidants

ROS is a collective term for various oxygen and nitrogen containing molecular and free radical species which are in general oxidizing in nature. ROS are endogenously produced in every cell during cellular respiration as by products and serve as cell signaling agents. The controlled generation of ROS is essential for normal functioning of cellular system. The generation of ROS is controlled by various compounds present in cells, known as antioxidants. Under normal conditions, there is a balance between levels of these ROS and antioxidants and this balance is known as redox homeostasis. However, in response to external perturbations like, altered environmental conditions, exposure to ionizing radiations or during pathological processes like inflammation, the level of ROS is increased significantly. This disturbs the redox homeostasis and leads to a condition known as “oxidative stress”. The classical definition of oxidative stress is an imbalance between oxidants and antioxidants in favor of the oxidants, potentially leading to damage of cellular organelles like, DNA, proteins, lipid membrane etc.

1.5.1 ROS: Biological role

Some of the biologically important ROS are discussed below.

Superoxide radical ($O_2^{\bullet-}$): Formation of the $O_2^{\bullet-}$ radical can be considered to be the initial step for the formation of other ROS. In cells, it is generated by the single electron reduction of molecular oxygen (O_2) using NADPH or nicotinamide adenosine dinucleotide (NADH) as the electron donor as shown in equation 1.1.

$$2O_2 + NAD(P)H \rightarrow 2O_2^{\bullet-} + NAD(P) + H^+ \quad (1.1)$$

Under diseased conditions, over expression of xanthine oxidase (XO) enzyme leads to formation of $O_2^{\bullet-}$ radical and H_2O_2.[31] $O_2^{\bullet-}$ radical is also generated non-enzymatically in the mitochondrial respiratory chain. $O_2^{\bullet-}$ radical compared with other free radicals, is a less reactive species which can exist in solution for a considerable time and thus diffuse before reacting with other free radicals or with other target molecules. Being a charged species, $O_2^{\bullet-}$ radical can cross biological membranes via anion channels.

H_2O_2: H_2O_2 is a mild oxidizing agent and does not react with most of the biomolecules readily. It is produced in cells in mitochondria, peroxisomes and lysosomes and act as a signaling molecule for numerous biological processes like cell proliferation, apoptosis, etc. The cellular concentration of H_2O_2 varies from 1 nM-100 nM depending on cell component. The toxic effects of H_2O_2 mainly arise from its conversion to hydroxyl ($^{\bullet}OH$) radical which is a highly oxidizing species. The conversion takes place in the presence of transition metals ions like Fe^{2+} (reaction known as Fenton reaction) as shown in equation 1.2.[32]

$$Fe^{2+} + H_2O_2 \rightarrow Fe^{3+} + OH^- + {}^{\bullet}OH \qquad (k = 10^3\text{-}10^4\ M^{-1}s^{-1}) \qquad (1.2)$$

Peroxyl radicals ($ROO^{\bullet}$): Peroxyl radicals are important species contributing significantly to free radical mediated oxidative stress. Organic hydroperoxides produced from the hydrogen abstraction reaction of peroxyl radicals with organic molecules in presence of oxygen are also powerful oxidants. Peroxyl radicals have the ability to induce chain reactions and their reactions with membrane lipids induce peroxidation which causes structural changes leading to the loss of membrane integrity.

$^{\bullet}$OH radical: In cells $^{\bullet}$OH radical is produced as a product of Fenton reaction (equation 1.2) and Haber-Weiss reaction as shown in equation 1.3.

$$H_2O_2 + O_2^{\bullet-} \xrightarrow{Fe^{3+}} O_2 + OH^- + {}^{\bullet}OH \qquad (k = 10^4\text{-}10^6\ M^{-1}s^{-1})^{33} \qquad (1.3)$$

$^{\bullet}$OH radical is a strong oxidizing species and can cause damage virtually to all types of biomolecules like lipid, DNA and proteins. $^{\bullet}$OH radical is non-specific in its reactions with target molecules and cannot be eliminated by enzymatic reactions. The important antioxidants for detoxification of $^{\bullet}$OH radical include GSH, vitamin E, manintol, melatonin, etc.

Nitric oxide ($NO^{\bullet}$): $NO^{\bullet}$ is a signal transducing radical formed by nitric oxide synthase in endothelial and neuronal cells by enzymatic conversion of L-Arginin to L-citrulline.[34] It plays important role in vascular muscle relaxation, platelet aggregation and blood pressure regulation. It can undergo both one-electron oxidation and reduction reactions to form nitrosonium (NO^+) and nitroxyl ions (NO^-), respectively. Under aerobic conditions, it

reacts with molecular oxygen (k=2.4 x10^6 $M^{-1}s^{-1}$) to form nitrogen dioxide ($NO_2^{\bullet}$) radical while in presence of superoxide radical it forms peroxynitrite as shown in equation 1.4.[35] The metabolites of $NO^{\bullet}$ are more reactive than $NO^{\bullet}$ itself (E^o_{NO}= +0.39, E^o_{NO2}= +0.99 and E^o_{ONOO-}=+1.20 V). $NO^{\bullet}$ interacts with proteins by binding to Fe^{2+} ions present in heme group or iron sulfur complexes in different enzymes leading to deactivation of the enzymes. Through this mechanism, $NO^{\bullet}$ has also been shown to inhibit the activity of a number of enzymes like XO, GPx and NADPH oxidase.

$$NO^{\bullet} + O_2^{\bullet -} \rightarrow ONOO^{-} \qquad (k= 6.7 \times 10^9\ M^{-1}s^{-1}) \qquad (1.4)$$

Peroxynitrite ($ONOO^-$): Peroxynitrite is a biological oxidant generated in several cell types including neutrophils, macrophages etc.[36] It is also one of the key contributors of oxidative stress in cells and is known to react with sulfhydryls groups, lipids, proteins, DNA etc. It has a pKa of 6.8 and exists in equilibrium with its protonated form, peroxynitrous acid (ONOOH). While, peroxynitrite reacts with substrates by either one- or two-electron oxidation or oxygen atom transfer reactions; peroxynitrous acid shows $^{\bullet}$OH radical like properties.[37] Peroxynitrite is a relatively stable species and can be stored for several days at low temperature. Peroxynitrous acid decays very fast through isomerization to give nitrate with a half-life of less than a second at physiological pH and 37°C.

Peroxynitrite also reacts with carbon dioxide (CO_2) present at ~5 mM concentration in cells, with a second order rate constant of 5.7 x 10^4 $M^{-1}s^{-1}$ at 37 ºC to form carbonate ($CO_3^{\bullet -}$) radical and $NO_2^{\bullet}$ radical.[38] $CO_3^{\bullet -}$ radical is a one-electron oxidant (E^o= +1.50 V), while $NO_2^{\bullet}$ radical is both an oxidizing (E^o= 1.04 V) and nitrating agent.[39] Excess

generation of peroxynitrite in biological systems can result in peroxidation of lipids, oxidation of thiol residues in proteins, depletion of antioxidants, displacement of metals from metalloproteins, DNA oxidation and nitration of protein tyrosine residues.[40] All these reactions have been implicated in many pathological conditions including reperfusion injury, atherosclerosis and neurodegenerative diseases.

1.5.2 Cellular defense system

To maintain redox homeostasis, cells utilize various antioxidants. Based on the mode of action these antioxidants can be classified into two broad classes-i) enzymatic antioxidants and ii) non-enzymatic antioxidants. Details of these antioxidants are given below.

1.5.2.1 Enzymatic antioxidants

These are the main components of cellular defense system and react with free radicals in catalytic manner. These include GPx, TrxR, superoxide dismutase (SOD), catalase etc. The functions of GPx and TrxR have been discussed earlier in section 1.4.3.

SOD: SOD is found in three isoforms. In prokaryotes, SOD is reported to contain redox active manganese (MnSOD) or iron (FeSOD) metal centers. In eukaryotes and some bacterial species SOD exists as copper metalloenzyme in which copper and zinc occupy the active site. It is an endogenously produced intracellular enzyme and is predominantly located in liver, blood cells and brain tissue. SOD plays major role in the protection of cells against oxidative damage. It catalyzes the dismutation of $O_2^{\bullet-}$ radical into O_2 and H_2O_2 as shown in equation 1.5.

$$2O_2^{\bullet -} + 2H^+ \xrightarrow{SOD} O_2 + H_2O_2 \qquad (k= 2.4 \times 10^9\ M^{-1}s^{-1}) \qquad (1.5)$$

Catalase: Mammalian catalase is a complex of four identical subunits. Each subunit has a molecular weight of approximately 60 kDa and contains a single hematin (Fe(III)-porphyrin IX) group. The heme group is responsible for catalase's enzymatic activity. It catalyzes the decomposition of H_2O_2 to O_2 and H_2O as shown in equation 1.6.

$$2H_2O_2 \xrightarrow{catalase} 2H_2O + O_2 \qquad (1.6)$$

1.5.2.2 Non-enzymatic antioxidants

These are the low molecular weight compounds, supplied either endogenously or exogenously to cells. The examples include vitamin C, D and E, carotenoids, polyphenols, thiols etc. Vitamin C is a water soluble compound and is an efficient free radical scavenger.[41] Vitamin D, in particular vitamin D2 and D3 have been found to inhibit iron dependent lipid peroxidation.[42] Vitamin D has also been found to prevent cancer cell growth and stimulate cell death via apoptosis resulting in prevention of breast, prostate and ovarian cancers.[43] Vitamin E is fat soluble and found mainly in lipid membrane. It is the major chain breaking species for lipid peroxidation where it reacts with lipid peroxyl radical.[44] Both vitamin C and E work in synergistic way and vitamin C can regenerate the oxidized form of vitamin E. Along with these, folic acid (from vitamin B group) has also shown potential towards scavenging of free radicals and repair of biomolecules. Carotenoids are naturally found in plants and fruits as colorful pigments. They consist of tetraterpenoid structure with polyene backbone chain.

Several natural phenolic compounds show efficient antioxidant activity and these include polyphenols and phenolic acids. Flavonoids constitute a large group of naturally occurring plant phenolic compounds. The antioxidant activity of phenols is substantially increased by one or two methoxy substitutions, like in case of curcumin and its derivatives.[45] Polyphenols are dietary compounds present in fruits, vegetables, tea, wine, etc. Phenolic acids such as p-hydroxy benzoic acid, vanillinic, p-coumaric, caffeic, ferulic, rosamarinic, etc., are widely distributed in plant kingdom. They are weak acids and usually exist as esters or glycosides. Epidemiological studies have shown that regular dietary intake of polyphenols can reduce the incidence of cancer.[46] Considering all these health benefits, several of phenolic compounds are now being therapeutically used as antioxidants.

Sulfur compounds are present in almost all cell types in the form of proteins, amino acids, non protein thiols, etc., and GSH is one of the most important cellular thiols. It acts as a substrate for ROS detoxifying enzymes like GSH transferase and GPx. During detoxification of ROS, GSH is oxidized to GSSG. The GSH/GSSG ratio is an indicator of cellular redox state. GSH has been found to scavenge several ROS like $^{\bullet}OH$ radical, H_2O_2, peroxynitrite and thus plays an important role in regulation of cellular redox homeostasis.[47] Amino acids like Cys and homocysteine have been reported to scavenge H_2O_2, $^{\bullet}OH$ radical, peroxynitrite and hypochlorus acid and reduce transition metals mediated oxidation of low density lipoprotein.[48] The level of Cys modification is being used as a clinical marker of oxidative stress.

Other than endogenously present sulfur compounds, various naturally occurring and synthetic organosulfur compounds have also been evaluated for diverse biological effects including antioxidant activity, anti-inflammatory properties, inhibition of platelet aggregation, reduction of systolic blood pressure, and cholesterol levels.[49,50] For example, S-allylcysteine and S-allylmercaptocysteine extracted from aged garlic have shown potent antioxidant activity in terms of reduction of hydroperoxides and inhibition of $NO^{\bullet}$ production.[51] Similarly, sulforaphane, an important organosulfur compound present in young sprouts of broccoli and cauliflower, has been found to exhibit anti-inflammatory properties in vascular endothelial cells. [52] It was also found to prevent hyperglycemia induced biochemical dysfunction of endothelial cells and protect the heart against ischemia–reperfusion injury in rats.[53] Compounds like, S-allyl-L-cysteinesulfoxides, trans-1-propenyl-L-cysteinesulfoxide, S-allylmercaptocysteine, have the ability to prevent ROS production, vascular inflammation, reduce low density lipid content and inhibit platelet aggregation.[54]

1.6 Organoselenium compounds as antioxidants

Due to the similarity in chemical properties of sulfur and selenium, it was anticipated that organoselenium compounds, having selenium in less toxic chemical form can be explored as antioxidants. Further, involvement of redox active SeCys in GPx catalytic cycle inspired researchers to explore synthetic selenium compounds as potential GPx mimics. Herein, the organoselenium compounds studied as antioxidants are briefly discussed under two categories-i) synthetic GPx mimics and ii) ROS scavengers.

1.6.1 Synthetic GPx mimic

The first organoselenium compound tested for GPx like activity was ebselen (compound 1 in scheme 1.3), an aromatic selenoamide, by H. Sies in 1984.[55] Different groups have proposed different mechanisms for GPx like activity of ebselen with the latest one given by Mugesh and co-workers.[56] The current understanding is that, in presence of thiols ebselen initially forms a selenenyl sulfide intermediate which then undergoes disproportionation to form diselenide. The diselenide reacts with hydroperoxide to form selenenic acid which regenerates the active selenenyl sulfide intermediate using thiol as substrate.

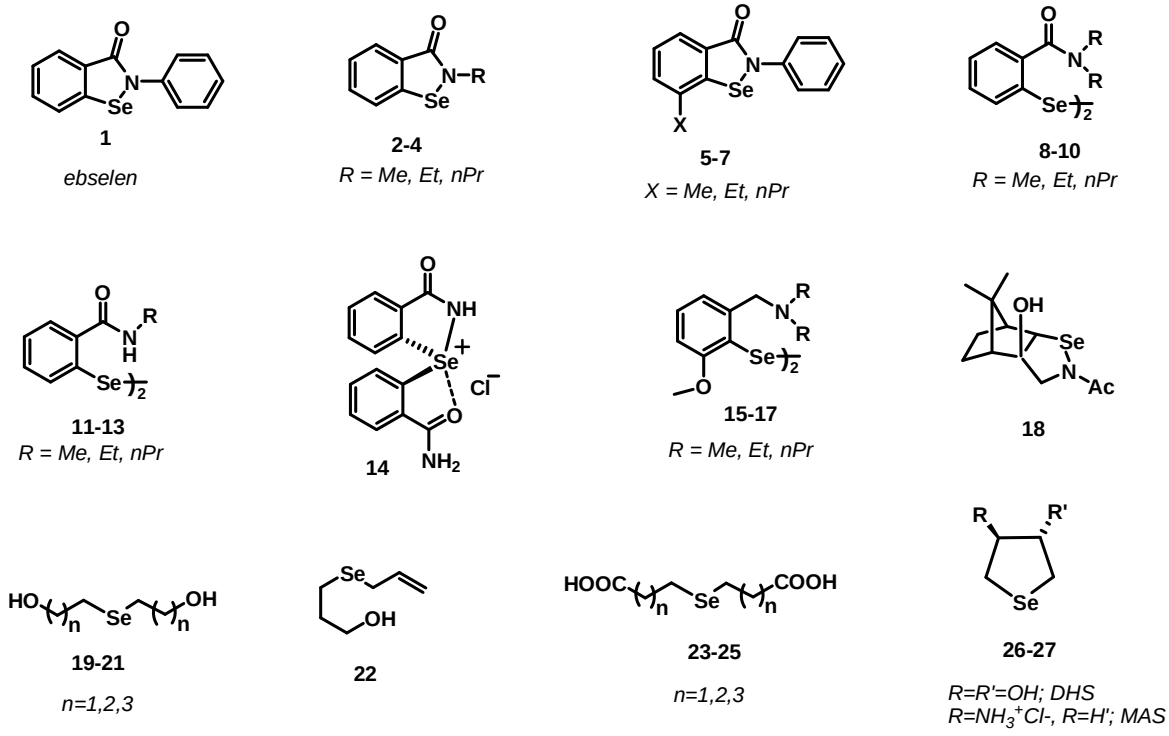

Scheme 1.3: *Chemical structures of organoselenium compounds having GPx like activity.*

As, the formation of diselenide from selenenyl sulfide intermediate is the rate determining step, several modifications have been done by inserting suitable substituents at phenyl ring and at ortho position to selenium (compounds 2-7; scheme 1.3).[57,58] The studies showed that the stability of selenenyl sulfide intermediate plays an important role in GPx like activity of these compounds. The strong non-covalent Se--N or Se--O interactions in the selenenyl sulfide intermediates of ebselen and its derivatives facilitate a nucleophilic attack of thiol (or thiolate) at selenium instead of the desired attack at sulfur. This process known as 'thiol exchange' reaction hampers the formation of selenol, the active form in the catalytic cycle. The chemical structures of some of the important organoselenium compounds are given in scheme 1.3.[59]

The studies carried out by Iwaoka et. al. on tertiary amine substituted aromatic diselenides and monoselenides (compounds 8-10; scheme 1.3) indicated that the proximate nitrogen base activates the selenol intermediate (-SeH) into the kinetically more reactive selenolate anion (-Se^{-}) while direct Se-N interaction in the selenenic acid intermediate (-SeOH) effectively prevents its further oxidation into other oxidized selenium species.[60] Back et.al. reported a camphor derived selenoamide (compound 18; scheme 1.3) which acts as a procatalyst reacting rapidly with the thiol to produce selenenyl sulfide intermediate.[61] This intermediate then participates in the reduction of the peroxide thus exhibiting a GPx like activity. The studies carried out on aromatic selenides showed that presence of methoxyl (-OMe) group at ortho position to selenium reduced strength of Se--N interactions in the selenenyl sulfide intermediates and the thiol exchange reactions at selenium.[62] Similar results were reported by Wirth et.al. where the bis-ortho substitution in

aromatic diselenides and close proximity of oxygen to selenium atom have been found to enhance GPx like activity.[63] Further, to understand the effect of functionalization, Back and co-workers studied the GPx like activity of functionalized aromatic cyclic seleninate esters and spirodioxyselenuranes.[64] Also, it was observed that the presence of electron-donating substituents stabilize the transition state during GPx cycle of seleninate esters while electron-withdrawing groups lead to destabilization of transition state and thus reduce the GPx like activity.[65] Recently, our group reported a compound 2,2′-diselenobis(3-amidopyridine) (NictSeSeNict) having higher activity than ebselen which is attributed to formation of a stable selone intermediate rather than selenenyl sulfide intermediate in ebselen and its derivatives.[66]

Although, extensive studies have been carried out to establish structure-activity relationship in case of aromatic selenides and diselenides, such detailed investigations on aliphatic form of organoselenium compounds are limited. In 2002, Back and co-workers reported a series of aliphatic diselenides (compounds 19-21; scheme 1.3) and allyl selenides (compound 22; scheme 1.3) that exhibited GPx like activity.[67] They showed that allyl selenides on reaction with hydroperoxides form selenoxides which being unstable underwent sigmatropic rearrangements leading to formation of selenenic esters. This pathway provided a rapid catalytic reduction of hydroperoxides and therefore allyl selenides showed higher GPx like activity than diselenides. Some of the important aliphatic organoselenium compounds studied for GPx like activity, are shown in scheme 1.3 (compounds 16-25; scheme 1.3).[68]

GPx like activity has also been found to be influenced significantly by the chemical substitution and interactions between selenium and the neighboring hetero atom. For example, the hydroxyl (OH) substituted linear selenoether, bis(3-propanol)selenide (SePOH) showed higher GPx like activity as compared to ebselen due to formation of a stable five membered cyclic intermediate, spirodioxaselenanonane.[69] Similarly, trans-3,4-dihydroxy-selenolane (DHS), a cyclic organoselenium compound (compound 26) was found to exhibit higher GPx like activity than its linear analogue bis(2-ethanol)selenide (SeEOH).[70] In functionalized monoselenides, carboxylate (COO^-) substituted monoselenides (25) showed higher GPx like activity than those substituted with -OH and amino ($-NH_3^+$) groups.[71] Also, it has been observed that compounds with functionalization at γ -position (or connected through propyl chain) to selenium centre showed much better GPx activity as compared to their homologues. In a recent report, it was shown that the oxidized form of selenoglutathione, a selenium analogue of glutathione exhibits higher GPx like activity than diphenyldiselenide, a standard compound for the GPx assay.[72]

1.6.2 ROS scavenging selenium antioxidants

Organoselenium compounds along with GPx like catalytic activity can also exhibit ROS neutralizing activity. In this direction a few organoselenium compounds have been tested for their scavenging activity against biological relavant ROS like, peroxynitrite, singlet molecular oxygen and free radicals like $^{\bullet}OH$, $NO^{\bullet}$, etc. Compounds like, diphenyl diselenide, ebselen, selenocystine (CysSeSeCys), SeMet, etc. have been reported to scavenge peroxynitrite efficiently and prevent peroxynitrite induced oxidation and nitration reactions.[73] The real-time chemiluminescence studies carried out on selenourea derivatives

and tertiaryselenoamides showed that these compounds exhibited $O_2^{\bullet-}$ radical scavenging activity.[74] Similarly, ebselen and its derivatives showed scavenging of singlet molecular oxygen where it was observed that these compounds had higher reactivity as compared to their sulfur analogs and involve a charge transfer complex as intermediate.[75] In another study it was found that monoselenide analogue of ebselen scavenges singlet oxygen however the corresponding diselenides did not show any activity.[76] Brumaghim and co-workers showed that metal chelated organoselenium compounds particularly N,N′-Dimethylimidazoleselone prevented iron and copper mediated DNA damage more efficiently than analogous sulfur compounds.[77] Recently, Kumar et.al reported multifunctional ebselenols which were found to exhibit higher scavenging activity for lipid peroxyl radicals as compared to α-tocopherols.[78]

In the study of organoselenium compounds as free radical scavengers, pulse radiolysis technique has been used as a convenient tool. The details of the pulse radiolysis studies carried out on organoselenium compounds are discussed in chapter 3 and only the main highlights are mentioned here. The GPx active compound ebselen and its derivatives were reported to scavenge peroxyl ($ROO^{\bullet}$) radicals with a rate constant in the order of 10^8 $M^{-1}s^{-1}$ which is comparable to vitamin E and ascorbic acid. [79] Similarly, the studies carried out on reaction of $^{\bullet}OH$ radical with SeMet showed that it exhibited higher free radical scavenging activity as compared to its sulfur analogue, Met.[80] The studies carried out on reaction of $^{\bullet}OH$ radical with a series of aliphatic organoselenium compounds, 1, ω-bis(methylse1eno)alkanes ($MeSe(CH_2)_nSeMe$; (n=1-5)), revealed that selenium compounds on one-electron oxidation form selenium centered radical cations with higher stability than their sulfur counterparts.[81] The rate constant values for the reaction of

different ROS with some of the important organoselenium compounds are listed in table 1.3.

***Table.1.3**: Rate constants for the reactions of ROS with organoselenium compounds.*

Compounds	Trimethylperoxyl radical ($CCl_3O_2^{\bullet}$), $M^{-1}s^{-1}$	$^{\bullet}OH$ radical, $M^{-1}s^{-1}$	Peroxynitrite, $M^{-1}s^{-1}$
Ebselen[82]	$2.9x10^8$	---	$2.0x10^6$
2-(methylseleno)-benzoic acid-N-phenylamide[81,83]	$3.9x10^8$	---	$2.7x10^3$
MeSeCys[84]	$1.1x10^9$	---	$2.0x10^3$
SeMet[85,86]	$3.4x10^8$	$1.4x10^{10}$	$2.4x10^3$
CysSeSeCys[87]	---	$8.1x10^9$	---
SeCysA[88]	$8.3x10^6$	$1.3x10^{10}$	$7.2x10^5$
Diselenopropanoic acid (DSePA)[68a,84,87]	$2.7x10^8$	$1.8x10^{10}$	$1.4x10^3$
GPx[89]	---	---	$8.0x10^6$
DHS[90]	$8.8x10^8$	$9.0x10^9$	---

1.7 Generation of free radicals by radiation chemical methods and pulse radiolysis

The in-vitro antioxidant activity of any compound is evaluated in terms of its ability to scavenge ROS. For this, controlled generation of sufficient concentration of ROS and its monitoring in real time scale is required. This can be achieved by radiation-chemical methods and sometimes by chemical reactions. Here, the principles and details of radiation chemistry are discussed below.

Radiation-chemical methods: These methods are widely used to generate free radicals and study their reactions. High-energy radiations such as X-ray, γ- ray, charged particles (α-

particles, protons), etc. on interaction with matter initially cause excitation and ionization of the medium. This is followed by several cascades of reactions in small reactive zones, known as spurs, leading to formation of different free radicals and ions. This process of generating radicals and ions by using high-energy radiations is called radiolysis. The basic terms related to radiation chemistry are discussed below.

Absorbed dose: When a system is exposed to radiation, the energy absorbed in the material will depend on nature and energy of radiation and also on composition of material. Out of incident radiation only a fraction of energy is utilized by the system leading to chemical changes. The amount of energy absorbed in unit mass of the material is called absorbed dose. The SI unit of absorbed dose is Gray (Gy) which is equal to 1 Joule/kg. The absorbed dose can also be expressed by the unit of Rad (100 ergs/gm), where, 1 Gy = 100 rads.

Radiation chemical yield: The yield of products formed or reactants consumed on interaction of matter with radiation is expressed in terms of radiation-chemical yield (known as G value). It is defined as number of species produced or consumed per 100 eV of energy absorbed and generally written in the form of atoms or molecules/100 eV. The SI unit of G value is μmol/J where, 1 molecule/100 eV=0.1036 μmol/J.

Radiolysis of water is a powerful method to generate specific ROS and to measure their reactivity. The details on interaction of water molecules with ionizing radiations and nature of species formed thereof are discussed below.

Water radiolysis: The energy absorbed by water molecules can lead to various radiation-chemical reactions such as direct ionization and excitation of water molecules etc. The

excited water molecules can undergo hemolytic bond dissociation forming hydrogen (H) atom and $^{\bullet}OH$ radical. Also H_2O^+ formed by direct ionization can undergo ion-molecule reaction and form $^{\bullet}OH$ radical and hydronium $(H_3O)^+$ ion. The electrons produced by direct ionization lose their energy by causing further ionization and get thermalized followed by stabilization provided by solvation with water molecules from surrounding medium. These electrons are known as solvated or hydrated (for water) electrons (e_{aq}^-). The initial reactions occurring through water-radiation interactions are described in scheme 1.4.

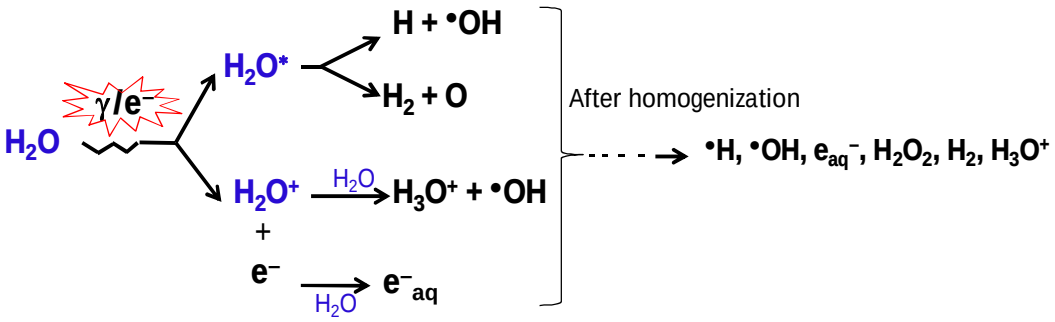

Scheme 1.4: *Interaction of water with radiation.*

Nature and reactions of important primary species formed due to water radiolysis are discussed below.

a) Hydrated electrons (e_{aq}^-): e_{aq}^- is a powerful reducing agent (E^0= -2.9 V). It shows strong absorption with wavelength maxima at 715 nm (ε_{715nm}=1.85 x $10^4 dm^3 mol^{-1} cm^{-1}$). This feature makes it easy to monitor the reaction of e_{aq}^- using absorption spectrophotometry. The reaction of any substrate (S^n, n is charge on substrate) with e_{aq}^- can be expressed as:

$$e^-_{aq} + S^n \rightarrow S^{n-1} \qquad (1.7)$$

b) H-atom: H atom acts as a weak base with pKa of 9.6. It is less reducing (E^0=-2.3 V) than e^-_{aq}. It is not an important reducing species at neutral and alkaline pH but is the main reducing species at acidic pH. H atom can react via H-abstraction and addition to double bond. Its reactions can be observed by following the absorption of reactants or products formed during the reaction.

c) $^\bullet$OH radicals: $^\bullet$OH radical is a strong oxidizing agent with standard reduction potential of +2.72 V at acidic pH and +1.89 V at neutral pH. It is non-specific in its reaction and can react with solute molecules via H-abstraction, addition to double bond, one-electron oxidation and displacement reactions. $^\bullet$OH radical has a very weak absorption in UV region with wavelength maxima at ~230 nm and therefore difficult to be detected directly. Therefore its reactions are generally observed by following the formation of transient species during the reaction.

The primary radicals generated by radiolysis of water are both oxidizing and reducing in nature and also non-specific in their reactions. Therefore, secondary radicals are utilized to perform exclusive redox reactions. Some of the important secondary radicals are discussed below.

a) Azide radicals ($N_3^\bullet$): $N_3^\bullet$ radical is produced by reaction of azide ions (N_3^-) with $^\bullet$OH radical. $N_3^\bullet$ radical is specific one electron oxidant with a reduction potential of 1.33 V ($N_3^\bullet/N_3^-$) vs NHE.

$$N_3^- + {}^\bullet OH \rightarrow N_3^\bullet + OH^- \qquad (k= 1.2 \times 10^{10}\ M^{-1}s^{-1})^{91} \qquad (1.8)$$

b) $CO_3^{\bullet-}$ radical: $CO_3^{\bullet-}$ radical is strong oxidizing agent and react with solute molecules through electron transfer reaction. Its reduction potential is +1.58 V ($CO_3^{\bullet-}/CO_3^{2-}$) vs NHE. $CO_3^{\bullet-}$ radical is formed by reaction of $^\bullet$OH radical with carbonate ions (CO_3^{2-}).[91]

$$CO_3^{2-} + {}^\bullet OH \rightarrow CO_3^{\bullet-} + OH^- \qquad (k= 4.0 \times 10^{8}\ M^{-1}s^{-1}) \qquad (1.9)$$

c) $NO_2^\bullet$ radical: $NO_2^\bullet$ radical is a weak oxidizing radical (E^0=0.99 V vs NHE) compared to $^\bullet$OH and $N_3^\bullet$ radical. It is formed on reaction of $^\bullet$OH radical with nitrite (NO_2^-) ions. $NO_2^\bullet$ radical react with solute molecules via one-electron transfer reactions.[91]

$$NO_2^- + {}^\bullet OH \rightarrow NO_2^\bullet + OH^- \qquad (k= 1.0 \times 10^{10}\ M^{-1}s^{-1}) \qquad (1.10)$$

d) $CCl_3O_2^\bullet$ radical: $CCl_3O_2^\bullet$ radical is an important radical which is employed as a model peroxyl radical in pulse radiolysis studies to study oxidation reaction of solute. These radicals are oxidizing in nature and can react with solute molecules via H-abstraction or electron transfer reactions. It is generated by reaction of primary radicals with carbon tetrachloride (CCl_4) in presence of isopropanol and molecular oxygen according to equation 1.11 to 1.14.

$$(CH_3)_2CHOH + {}^\bullet OH/{}^\bullet H \rightarrow (CH_3)_2{}^\bullet COH + H_2O/H_2 \quad (k= \sim 10^{12}\ M^{-1}s^{-1})^{92} \qquad (1.11)$$

$$(CH_3)_2{}^\bullet COH + CCl_4 \rightarrow (CH_3)_2CO + {}^\bullet CCl_3 \qquad (k= 7.0 \times 10^{8}\ M^{-1}s^{-1})^{93} \qquad (1.12)$$

$$CCl_4 + e_{aq}^- \rightarrow {}^\bullet CCl_3 + Cl^- \qquad (k= 1.9 \times 10^{10}\ M^{-1}s^{-1})^{93} \qquad (1.13)$$

$$^{\bullet}CCl_3 + O_2 \rightarrow CCl_3O_2^{\bullet} \qquad (k= 3.3 \times 10^9\ M^{-1}s^{-1})^{93} \quad (1.14)$$

To achieve totally oxidizing condition, e_{aq}^- is converted to $^{\bullet}$OH radical by saturating the solution with nitrous oxide (N_2O). e_{aq}^- reacts with N_2O with a rate constant of 8.7 x10^9 $M^{-1}s^{-1}$ to form $^{\bullet}$OH radical. This makes the $G_{\bullet OH}$ to increase up to 0.6 μmol/J. The solution still contains H atom which does not react with N_2O and contributes to ~10% of primary radicals formed.

$$e_{aq}^- + N_2O \rightarrow N_2 + O^- \rightarrow {}^{\bullet}OH + OH^- \qquad (k= 8.7 \times 10^9\ M^{-1}s^{-1})^{91} \quad (1.15)$$

For maintaining totally reducing conditions, $^{\bullet}$OH radical can be scavenged leaving e_{aq}^- and H atom in the solution. However, e_{aq}^- and H atom differ in their mode of reactions therefore it is desirable to convert all primary radicals in to a single reducing species. This can be achieved by using N_2O saturated solution of some organic solute like 2-propanol or t-butanol. In general, t-butanol is preferred over 2-propanol, as radical from t-buatnol is quite unreactive and does not interfere in absorption spectra of other species.

Other methods to generate free radicals: Free radicals can be generated by using chemical, electrolytic, photochemical and sonolysis methods. For example, $NO^{\bullet}$ radical can be generated in controlled manner by copper ions catalysed decomposition of S-nitroglutathione in presence of ethylenediaminetetraacetic acid (EDTA). Another important radical 2,2'-azino-bis (3-ethylbenz-thiazoline-6-sulfonic acid) ($ABTS^{\bullet-}$) can be prepared by oxidizing $ABTS^{2-}$ to $ABTS^{\bullet-}$ using potassium persulfate ($K_2S_2O_8$) as shown in equation 1.16.

$$2ABTS^{2-} + S_2O_8^{2-} \rightarrow 2ABTS^{\bullet-} + 2SO_4^{2-} \quad (1.16)$$

$NO^{\bullet}$ radical can also be prepared by photolysis of sodium nitroprusside. Similarly, $CO_3^{\bullet-}$ radicals can be generated by flash photolysis of sodium carbonate solution.

1.8 Motivation for present work

For a selenium compound to act as an efficient antioxidant, it must exhibit GPx activity, free radical scavenging capability, water solubility and less toxicity. In the last one decade, there is a significant progress in the design and synthesis of GPx active organoselenium compounds. In present thesis, an attempt has been made to correlate between free radical scavenging and GPx like activity in organoselenium compounds. Electron transfer reactions play important role in defining antioxidant activity of these compounds, therefore it is necessary to study these reactions and understand the nature of the transients formed therein, for the designing of new organoselenium compounds. Therefore the primary focus of the thesis is to study electron transfer reactions between a group of organoselenium compounds and ROS. In this context, we also made a comparison between electron transfer reactions of selenium and sulfur compounds. Further, studies on metal nanoparticles bound selenium compounds present a new area of interest and has great potential to modulate antioxidant ability of selenium compounds. With this motivation, important objectives of the present thesis work are listed as:

1. To study electron transfer reactions of structurally related organoselenium compounds with free radicals and to identify various molecular descriptors which can play role in stabilization of transients. The studies include reaction of oxidizing

free radicals like $^{\bullet}OH$, $CCl_3O_2^{\bullet}$, $N_3^{\bullet}$ etc. with organoselenium compounds using nanosecond pulse radiolysis technique and characterization of the intermediates by absorption spectroscopy in real time scales. This is followed by correlation of various molecular parameters and nature of transients with antioxidant activity of these compounds using experimental results and quantum chemical calculations.

2. To understand the structure-activity relation in organoselenium compounds for their reaction with molecular oxidants like peroxynitrite. This study includes understanding of reaction kinetics, characterization of reaction products and estimation of in-vitro antioxidant activity of structurally related organoselenium compounds.
3. To understand the structure dependent interaction of organoselenium compounds with gold nanoparticles (GNP) and its effect on their redox properties. The studies include characterisation of binding of two structurally related organoselenium compounds with GNP and to understand the effect of this binding on electron transfer properties of these compounds.

For these investigations three different types of compounds i.e. DHS, MAS(3-amineselenolane) and SeROH(bis(alknaol)selenides) as shown in scheme 1.5 have been employed. DHS is a low molecular weight organoselenium compound with GPx like activity. MAS is a monoamine substituted analogue of DHS with enhanced GPx like activity while SeROH are linear selenoethers having structural similarity with DHS.[73,94]

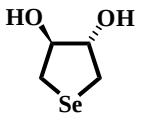

trans-3,4-dihydroxyselenolane
DHS

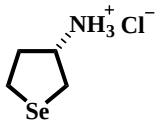

3-monoamineselenolane
MAS

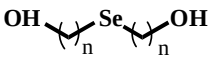

bis(alkanol)selenide (SeROH)

n=2; SeEOH,
3; SePOH and
4; SeBOH

Scheme 1.5: *Chemical structures of the organoselenium compounds studied in present thesis.*

1.9 Outline of the thesis

The thesis has been divided into six chapters. **Chapter one** gives the general information about physico-chemical properties of selenium, its role in biology, ROS, sulfur and selenium antioxidants, etc. **Chapter two** gives the details of the chemical and instrumental techniques used in the present work. **Chapter three** discusses the one-electron transfer reactions of structurally related aliphatic selenoethers (SeROH) with $^{\bullet}OH$ radicals and other oxidizing radicals using nanosecond pulse radiolysis facility. It includes characterization and quantification of various transients and products formed during these reactions. A quantum chemical approach has been employed to correlate the nature and stability of the transients with structural properties of these compounds. **Chapter four** deals with the effect structure or functional groups present in cyclic and linear organoselenium compounds on their ability to scavenge peroxynitrite. In **chapter five**, the binding of SeEOH and DHS with GNP have been explored and the effect of this binding on electron transfer reactions of these GNP conjugates has been studied. **Chapter six** gives summary and future scope of the work carried out in this thesis.

Chapter 2

Experimental

In this chapter, the materials, techniques and experimental conditions used for carrying out different studies are discussed. The chapter also summarizes the concepts and principles of techniques used to analyze the experimentally observed results.

2.1 Introduction

The research work presented in the thesis includes identification of various primary and secondary reactions of organoselenium compounds with ROS (free radicals and molecular oxidants). To understand this, it is necessary to characterize the transient intermediates formed during their short lifetime. For this, pulse radiolysis technique coupled with absorption detection was used to generate free radicals and to characterize the resulting transient species in real time scales. The reaction kinetics for the degradation of peroxynitrite using organoselenium compounds has been studied using stopped flow spectrometer. The products formed in these reactions were characterized by high performance liquid chromatography (HPLC), nuclear magnetic resonance (NMR) and mass spectroscopy (MS). Further, to study the interaction of organoselenium compounds with GNP, GNP samples of different sizes were prepared and characterized using techniques like, dynamic light scattering (DLS), absorption spectroscopy, transmission electron microscopy (TEM) and zeta (ζ)-potential. The structural orientation was characterized by using surface enhanced Raman spectroscopy (SERS).

2.2 Synthesis details

2.2.1 Synthesis of organoselenium compounds

In the present thesis, low molecular weight and water soluble organoselenium compounds have been studied for their reaction with ROS and their chemical structure are given in scheme 1.5. These compounds were reported by Prof M. Iwaoka's group, Tokai University, Japan and Dr V. K. Jain's group, BARC therefore the synthesis details have

not been included in this thesis.[95,96] However, for the clarification, only the chemical reactions are presented below.

a) DHS: 1,3-butadiene diepoxide was treated with a freshly prepared aqueous solution of sodium hydrogen selenite (NaHSe) under anaerobic conditions and the resultant compound (DHS) was extracted with ether. Further treatment of DHS with meta-chloroperoxybenzoic acid (m-CPBA) in dichoromethane (CH_2Cl_2) yielded its selenoxide (DHS_{ox}) as given in scheme 2.1.

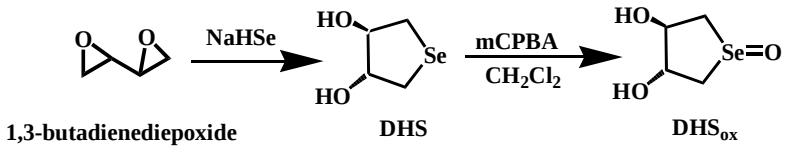

Scheme 2.1: *Synthesis scheme for DHS and DHS_{ox}.*

b) MAS: Sodium borohydride ($NaBH_4$) was heated with selenium powder in anhydrous ethanol under nitrogen (N_2) environment and was followed by addition of anhydrous solution of mesylated asparagininol. The reaction mixture was further treated with hydrochloric acid (HCl) and the resultant product (MAS) was extracted from aqueous layer using diethyl ether. Selenoxide of MAS (MAS_{ox}) was obtained quantitatively by treating MAS with hydrogen peroxide (H_2O_2) as shown in scheme 2.2.

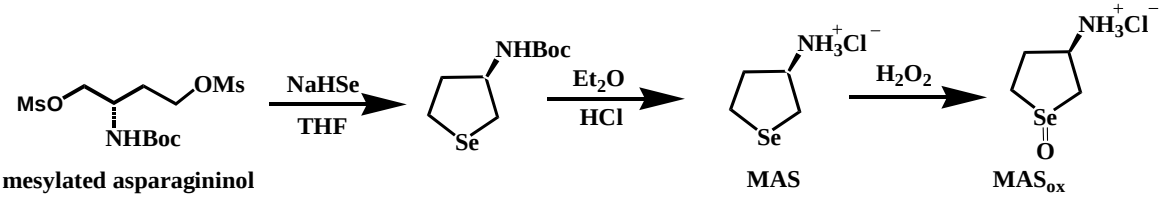

Scheme 2.2: *Synthesis scheme for MAS and MAS_{ox}.*

c) SeROH: Elemental selenium was reduced with $NaBH_4$ in ice cold water in anaerobic conditions, followed by addition of 2-bromoethanol to give a pale yellow solution of SeEOH as shown in scheme 2.3. Similarly, SePOH and SeBOH were prepared using 3-bromopropanol and 4-bromobutanol. Corresponding selenoxides ($SeROH_{ox}$) were prepared by incubating aqueous solution of SeROH compounds with hydrogen peroxide (H_2O_2) in 1:1 equivalents as represented in scheme 2.4.

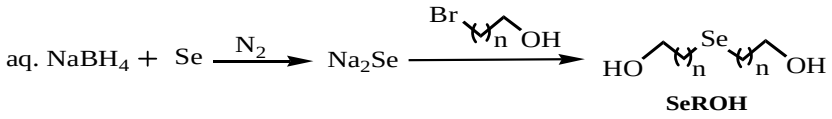

Scheme 2.3: *Synthesis scheme for SeROH (n=1; SeEOH, 2; SePOH and 3; SeBOH) compounds.*

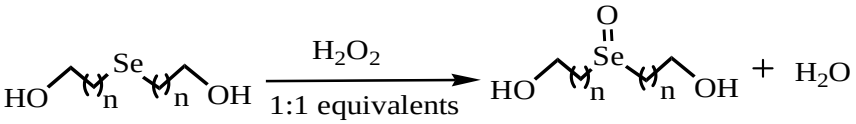

Scheme 2.4: *Synthesis scheme for $SeROH_{ox}$.*

The characterization of organoselenium compounds was done using ^{1}H, ^{13}C and ^{77}Se NMR and the characterization data are as follows:

DHS: ^{1}H NMR (500 MHz in$CDCl_3$) δ*:* 2.10 (d, *J*=5.0 Hz, 2H), 2.87 (dd, *J*=4.0 and11.0 Hz, 2H), 3.16 (dd, *J*=4.0 and 11.0 Hz, 2H), 4.27 (m,2H); ^{13}C NMR (125.65 MHz) δ: 26.8, 78.9; ^{77}Se NMR(95.35 MHz) δ: 65.6.

MAS: ^{1}H NMR (D_2O): δ=2.15–2.29 (m, 2H), 2.81–2.87 (m, 2H), 2.95–3.00 (m, 1H), 3.09–3.14 (m, 1H), 3.92–3.97 ppm (m, 1H); ^{13}C NMR (D_2O) δ=21.5, 27.9, 38.0, 58.5 ppm; ^{77}Se NMR (D_2O): δ=136.0 ppm.

SeEOH: ^{1}H NMR: (in D_2O) δ: 2.69 (t, *J* = 6.6 Hz, 2H), 3.71 (t, 2 H, *J* = 6.6 Hz). ^{13}C NMR (in D_2O) δ: 25.5, 61. ^{77}Se NMR (in D_2O) δ: 85.

SePOH: ^{1}H NMR: (in D_2O) δ: 1.65-1.75 (q, 2H, *J* = 6.9 Hz), 2.46 (t, 2H, *J* = 7.5 Hz), 3.47 (t, 2H, *J* = 6.3 Hz). ^{13}C{^{1}H} NMR (in D_2O) δ: 19.3, 31.9, 61.0. ^{77}Se NMR (in D_2O) δ: 139.

SeBOH: ^{1}H NMR (in D_2O) δ: 1.54 (m, 4H), 2.52 (t, 2H, J = 6.9 Hz), 3.48 (t, 2H,). ^{13}C NMR (in D_2O) δ: 19.1, 30.9, 46.2. ^{77}Se NMR: (in D_2O) δ: 141.

2.2.2 Synthesis of peroxynitrite

Peroxynitrite was synthesized by azide ozonization method.[97] Ozone was generated by passing dry oxygen (500 ml/min) through an ozone generator (Universal ozone system, Mumbai) undergoing dual dielectric discharge. Ozone gas was passed through alkaline (0.1 M NaOH) solution sodium azide solution (0.1 M) with a flow rate of 0.3 mL/min at 4 ºC. The reaction taking place in the reaction solution can be expressed as equation (2.1).

$$O_3 + N_3^- \rightarrow ONOO^- + N_2 \qquad (2.1)$$

The reaction solution turned to pale yellow colour which indicated the formation of peroxynitrite. The yield of peroxynitrite was estimated by monitoring the absorbance of peroxynitrite at 302 nm ($\varepsilon_{302\ nm}$=1705 M^{-1} cm^{-1}). After 3 hours of passing ozone, no

significant change was observed in the yield of peroxynitrite, so further ozonisation was stopped. The peroxynitrite stock solution was stored at -20 °C for future experiments.

2.2.3 Synthesis of GNP

GNP was prepared by following the well known Turkewich method with slight modification.[98] For this, aqueous solution of potassium tetrachloroaurate ($KAuCl_4$) was treated with trisodium citrate (Na_3-citrate) as shown in fig. 2.1(A). The size of GNP was varied by varying the reaction conditions and concentration of the reactants (i.e. $K[AuCl_4]$ and Na_3-citrate).

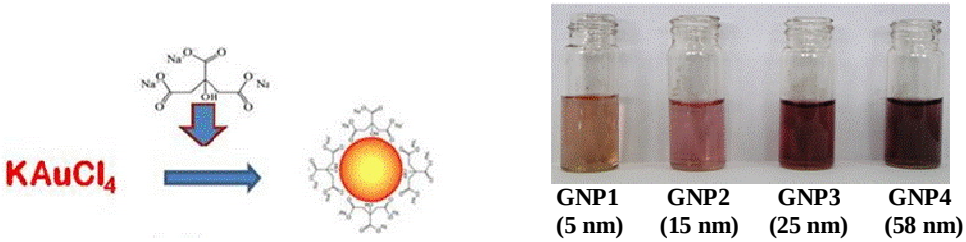

Fig. 2.1: *(A) Synthesis scheme of GNP by Turkewich method. Fig. (B) shows the images of GNP samples of different size (5-58 nm).*

For synthesis of small particles (5 nm sized GNP-GNP1), ice cold solution of 0.1 mM K[AuCl4] was mixed with Na_3-citrate (0.1 mM) and $NaBH_4$ (1 mM), the brown colored solution was stirred for 5 minutes in ice-bath.[99] Pinkish wine-red colored particles (15 nm sized GNP-GNP2) were prepared by mixing aqueous solution of 0.1 mM K[AuCl4] with 4 mM Na_3-citrate and the solution was kept at room temperature for 2 days. Wine red colored GNP (25 nm sized GNP-GNP3) was prepared by mixing aqueous solution of 0.25 mM K[AuCl4] with 10 mM Na_3-citrate and stirred for 2 days at room

temperature. Purple colored GNP solution (58 nm sized GNP-GNP 4) was prepared by addition of solid Na_3-citrate (294 mg, 10mM) to aqueous solution of 0.25 mM K[AuCl4]. The representative images of the GNP samples are shown in fig. 2.1(B).

To remove unconsumed Au^{3+} salt and Na_3-citrate, the GNP2, GNP3 and GNP4 solution were centrifuged at 7000 rpm, 6000 rpm and 5500 rpm respectively at 4 °C for 10 minutes. The pellet formed was redispersed in water and centrifuged again. This process was repeated 3 times to ensure complete removal of unreacted salts. Concentration of gold atoms in the GNP samples was estimated using a Continuum Source Flame Atomic Absorption Spectrometer (AAS, Contra AA 300, Analytik Jena, Germany) equipped with a 300 W xenon (Xe) arc lamp, at wavelengths 242 79 nm. The pellet formed at the end of the third cycle was dissolved in 1% hydrochloric acid (extra pure). The samples were aspirated in the AAS and concentration of gold atoms was estimated from the calibration curve of Au^{3+} standards. The yield of GNP samples in terms of conversion of gold ion (Au^{3+}) to gold atom was estimated to be 95 ± 5, 43 ± 5, 32 ± 3 and 30 ± 3 % for GNP1, GNP2, GNP3 and GNP4, respectively.

2.3 Pulse Radiolysis

2.3.1 Principle: In pulse radiolysis, the system under investigation is irradiated with an intense short pulse of high energy electrons to generate a significant concentration of transient species and the resulting transient species/free radicals are monitored during their short lifetime by a suitable physical techniques such as optical absorption, conductivity, electron spin resonance and fluorescence.

For pulse radiolysis experiments, the solution under study was kept at a distance of ~12 cm from the titanium electron beam window (beam diameter ~ 1 cm) and irradiated with an electron beam of 7 MeV energy and 100 ns pulse width using Linear Electron Accelerator (LINAC) facility.[100] Light beam from a Xe arc lamp was passed through the irradiated sample and the transmitted light was focused onto photomultiplier tube through monochromator. The signal produced in photo multiplier tube (PMT) is transferred to oscilloscope and then to computer for real time processing as shown in fig.2.2. Details of the LINAC instrument are given in the following sections.

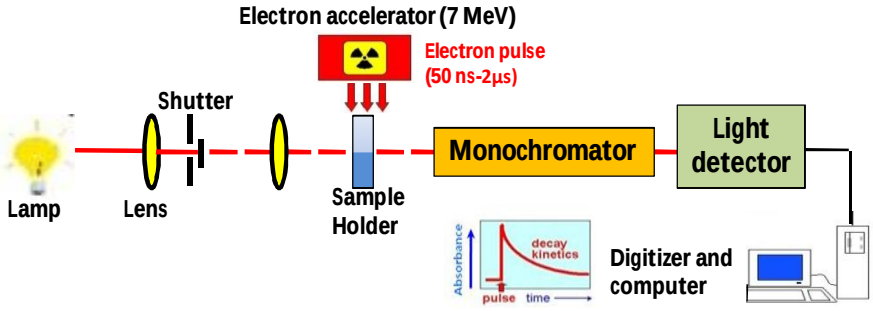

Fig. 2.2: *Flow chart representation of LINAC pulse radiolysis facility.*

2.3.2 LINAC Facility

The main components of LINAC instrument are described as below:

a) Electron gun: It generates electrons using the principle of thermionic emission of electrons from metal surface. It consists of three major components cathode, tungsten filament and anode. The electrons are ejected from the tungsten pellet (cathode) and further attracted towards the anode which is made up of a stainless steel tube. The electrons are then focused by a gap lenses into a deflection chamber which consists of two parallel upper

and lower copper plates having potential of +10 KV and +2 KV respectively. A negative potential of 8 KV is applied to upper plate for the required nanosecond pulse duration which makes both plates at a potential of +2 KV and allow the electron beam pass for that duration. The electron beam of specified pulse width then passed through and enters into the waveguide for further acceleration.

b) Waveguide: A waveguide is a rectangular tube pumped to a pressure of 10^{-7}torr. The electrons enter in waveguide with energy of 43 KeV and accelerated to 7 MeV in waveguide. This is done by means of axial electric field associated with electromagnetic wave (RF frequency) traveling down the circular waveguide. The inductive irises fitted in the waveguide helps to match the phase velocity of electromagnetic waves with that of electron.

c) Working: A pulse generator which is preset at 50 pulses per second (pps), triggers the R.F. pulses. The beam divider ratio is kept normally at 3 so that for every third R.F. pulse, one electron pulse is available for acceleration. Further, a train of pulses from the pulse generator triggers a sequential delay pulse generator (SDPG). Out of three pulses, first pulse activates an electromechanical shutter, second pulse activates Xenon arc lamp pulse power supply (to boost the analyzing light intensity for monitoring the fast events) and third pulse triggers the oscilloscope. As the oscilloscope is triggered by a pulse from the SDPG, the pre-trigger information ranging for duration of 600 ns to 1 μs prior to the arrival of the electron pulse is used to mark the monitoring level as well as the incident light intensity (I_0). Fine adjustments in SDPG with respect to time allows the electron pulse and

its effect to be recorded on the flat portion of the boosted lamp profile, during which time the output of the analyzing light remains steady.

2.3.3 Kinetic spectrophotometer

***a) Light source and optical set-up*:** The light source is composed of a Xe arc lamp of 450 W (Kratos model LH 151). Initially arc is struck by using 20 KV power supply, between two electrodes and then onwards the lamp which operates on a power of 18 V and current of 25 A. For monitoring the weak absorption signal of transients and improve signal to noise ratio, the lamp is boosted in milli second time scale using a power supply. To minimize the photodecomposition of sample, a shutter is placed between the lamp and sample holder. It also protects the photomultiplier tube from fatigue due to continuous illumination and is opened just before the boosting of the analyzing light.

The sample cell is made up of quartz with path length of 1 cm. The cell is placed in an aluminum cell holder and its alignment remains same every time when it is placed. The optics is aligned in such a way that the electron beam and the light beam cross each other inside the cell at right angles. The analyzing light after passing through the sample falls on the monochromator (Kratos, model GM 252) which covers wavelength range of 180 to 850 nm. Slit width of the monochromator is variable from 0.01-6.0 mm, to give band width of 0.1-19.8 nm.

b) Detection and data processing: The transmitted light is detected by a photomultiplier tube (PMT, Hamamtsu model R-955), which has a uniform spectral response in the wavelength range 180-850 nm region. A back-off device is used to compensate constant (-

ve DC) output of the PMT (I_0) before the arrival of the electron pulse. The signals detected by PMT are measured by a fast pulse amplifier, an oscilloscope, and signal recorder. Oscilloscope (100MHz) and signal recorder (computer) are used for recording and storage of transient signal.

2.3.4 Transient absorbance measurements

The intensity of the transmitted (I_t) light passing through a sample containing transient produced due to exposure to electron beam is given by:

$$I_t = I_0 10^{-\varepsilon c l} \tag{2.2}$$

Here, I_0 represents the light intensity in the absence of any absorbing species in the sample cell (i.e. light intensity transmitted immediately before electron pulse), c is the molar concentration of the absorbing species, ε is its molar absorptivity and l is optical path length of the sample cell. The light intensity is converted into voltage signal by PMT and resistors, therefore the output voltage is directly proportional to the intensity. If V_0 and V_t are output voltage obtained corresponding to I_0 and I_t, then V_t is given by:

$$V_t = V_0 10^{-\varepsilon c l} \tag{2.3}$$

Due to various chemical processes, the concentration of the absorbing species produced by the electron pulse changes with time resulting in change in I_t and V_t. From equation 2.3, at any time t, the absorbance (A_t) will be given by:

$$A_t = \log(I_o / I_t) = \log(V_0 / V_t) \tag{2.4}$$

The plot of A_t as a function of wavelength and time will give the transient absorption spectrum and kinetic trace respectively. These are useful in characterization of the transient species and to measure the rate of chemical process, respectively.

2.3.5 Absorbed Dose measurement

The absorbed dose was measured by using thiocyanate (SCN^-) dosimeter.[101] It contained aerated aqueous solution of 10 mM potassium thiocyanate. The major primary species produced by water radiolysis are $^\bullet OH$ radical, e_{aq}^- and H atom. Among these e_{aq}^- and H atoms are scavenged by dissolved oxygen (250 μmol/dm^3) whereas $^\bullet OH$ radical react with SCN^- according to following equations:

$$^\bullet OH + SCN^- \xrightarrow{3X10^9\, M^{-1}s^{-1}} SCN^\bullet + OH^- \qquad (2.5)$$

$$SCN^\bullet + SCN^- \rightarrow SCN^\bullet + (SCN)_2^{\bullet-} \qquad (2.6)$$

According to Beer-Lambert law, for a path length of 1 cm, the absorbance (ΔA) due to $(SCN)_2^{\bullet-}$ radical will be given by,

$$\Delta A = conc.of\ (SCN)_2^{\bullet-}\ x\ \varepsilon \qquad (2.7)$$

Where ε is the extinction coefficient of $(SCN)_2^{\bullet-}$ radical ($\varepsilon_{475\ nm}$=7600 M^{-1} cm^{-1}) at 475 nm. If G (number of radical/100eV) is the radiation chemical yield of $(SCN)_2^{\bullet-}$ radical then, for a given absorbed dose, the concentration of $(SCN)_2^{\bullet-}$ radical will be given by equation 2.8,

$$Conc.of\ (SCN)_2^{\bullet-} = \frac{G}{100\ eV/L\ x\ N}\ x\ Absorbed\ dose \qquad (2.8)$$

Where, N is Avogadro number. Substituting equation 2.8 in equation 2.7, we get,

$$\Delta A = \frac{G}{100\ eV/L\ x\ N}\ x\ Absorbed\ dose\ x\ \varepsilon \qquad (2.9)$$

Above equation can be rearranged to get absorbed dose from the experimentally measured value of ΔA.

$$Absorbed\ dose = \frac{\Delta A\ x\ N\ x 100\ eV/L}{G\varepsilon} \qquad (2.10)$$

Substituting the values for G and ε for $(SCN)_2^{\bullet -}$ radical at 475nm, the above expression can be written in the simplified form as

$$Absorbed\ dose = \Delta A\ x\ 2.7\ x\ 10^{21}\ eV/L \qquad (2.11)$$

The absorbed dose can be converted into Gy by using the following equation

$$Absorbed\ dose = \Delta A\ x\ 2.7\ x\ 10^{21}\ eV/L\ x\ 1.602\ x\ 10^{-19}\ J/eV \qquad (2.12)$$

$$Absorbed\ dose = \Delta A\ x\ 432.1\ x\ J/Kg\ or\ Gy \qquad (2.13)$$

2.4 Steady state irradiation

The radiolysis products of organoselenium compounds were examined by irradiating solutions using Cobalt-60 (^{60}Co) source. ^{60}Co undergoes beta (β) particle emission to form metastable ^{60}Ni which comes to ground state by emitting two γ-rays of energy 1.17 and 1.33 MeV per disintegration with a half life of 5.27 years as shown in scheme 2.5.

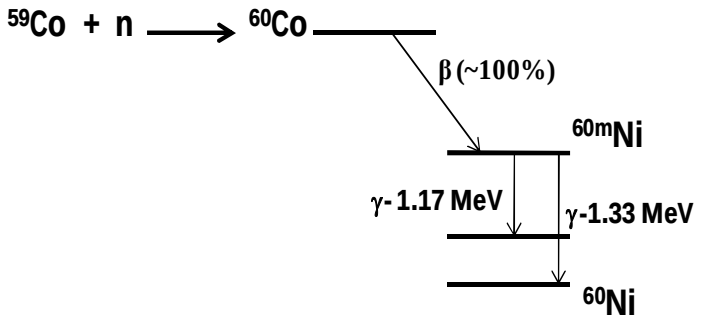

Scheme 2.5: *Schematic representation of decay of ^{60}Co.*

The ^{60}Co source used was obtained from Board of Radiation and Isotope Technology (BRIT) and installed in Modular Lab, BARC. The samples under study were kept in a cylindrical shaft which can be moved mechanically. For radiation exposure, the shaft is moved downwards where it is surrounded by ^{60}Co rods arranged in such a fashion that samples experience uniform radiation field. The source is equipped with digitally controlled movement of shaft to achieve accurate dose delivery. The absorbed dose rate delivered by the source was ~13 Gy/minute as measured by Fricke dosimeter and the dosimeter details are discussed below.

Fricke dosimeter solution contains aerated aqueous solution of 1 mM ferrous ammonium sulfate and 1 mM NaCl in 0.4 M H_2SO_4 (pH 0.46). The primary radicals generated by γ-radiolysis of water in the dosimeter solution oxidize ferrous (Fe^{2+}) ion to ferric (Fe^{3+}) ion. The reactions involved are:

$$Fe^{2+} + {}^{\bullet}OH \rightarrow Fe^{3+} + OH^{-} \qquad (2.14)$$

$$e^{-}_{aq} + H^{+} \rightarrow H \qquad (2.15)$$

$$H + O_2 \rightarrow HO_2 \tag{2.16}$$

$$Fe^{2+} + HO_2 \rightarrow Fe^{3+} + HO_2^- \tag{2.17}$$

$$HO_2^- + H^+ \rightarrow H_2O_2 \tag{2.18}$$

$$2Fe^{2+} + H_2O_2 \rightarrow 2Fe^{3+} + 2OH^- \tag{2.19}$$

The G-value of Fe^{3+} ions ($G(Fe^{3+})$) is calculated using following equation

$$G(Fe^{3+})_{O_2} = 3g(e_{aq}^-) + 3g(H) + g(OH) + 2g(H_2O_2) \tag{2.20}$$

Where, 'g' denotes the radiolytic yield of primary species formed by radiolysis of water and 'G' denotes the yield of secondary species generated by reaction of primary species with solute molecules. Using the radiolytic yield of the primary radicals produced from water radiolysis, G (Fe^{3+}) comes out to be 15.5. The amount of Fe^{3+} formed is estimated by its absorbance at 304 nm ($\varepsilon_{304\ nm}$ =2205 M^{-1} cm^{-1}). The absorbed dose is measured by the following relation:

$$\textbf{Absorbed dose} = \frac{\mathbf{9.684x10^6xA}}{\varepsilon l \rho\ \mathbf{G}} \text{Gy} \tag{2.21}$$

Where, A is the change in absorbance of dosimeter solution before and after irradiation. ρ (1.024) is the density (g cm^{-3}) of dosimeter solution and l is the path length in cm.

2.5 Stopped flow technique

The kinetics of the reaction between peroxynitrite and organoselenium compounds was studied by employing a BioLogic SFM-300 stopped flow absorption spectrometer (from BioLogic Scientific Instruments, France) equipped with single mixing mode. It is a rapid mixing technique which is used to study the chemical kinetics of fast reactions, with half lives in the range from milliseconds to minutes in solution. In this method, the reactants are injected simultaneously into a mixing chamber and the progress of the reaction is followed by monitoring a change in absorbance of either reactant or product in the spectrophotometer cell.

The main components of the stopped-flow instrument are given in fig.2.3 and discussed below.

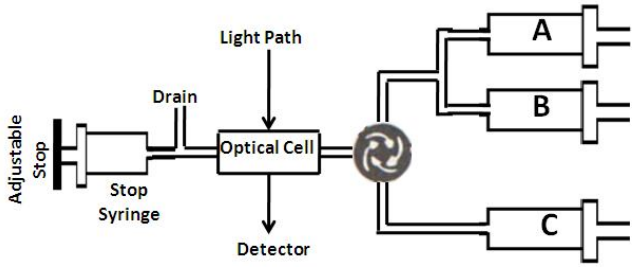

Fig. 2.3: *Basic components of stopped-flow instrument.*

1) Sample Unit: It comprises of drive syringes (A, B and C in fig. 2.3) of 10.0 ml volume and flow lines. They are provided with the drive rams to push the syringes up during the experiment. The sample-handling unit operates on pneumatic pressure of 8 bar provided by compressed N_2 gas.

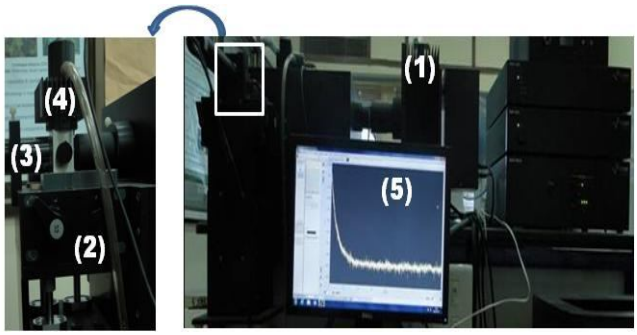

2) Auto-stop mechanism: The sample flow is stopped by an opposing piston that is linked to a sensing switch that triggers the measuring device. The movement of the valve and the return cylinder are both controlled by the applied pressure.

3) Optical cell & detector: The optical cell made up of quartz was used. It has orthogonal viewing ports so that it gives a choice of 2 mm and 10 mm path length. The cell volume of optical cell is 25 µl. The transmitted light is detected by PMT.

4) Light source: It consists of Xe arc light source (150W Xe and Xe/Hg lamp) which is powered by power control lamp supply. It also includes grating monochromator operating in the wavelength range 180-800 nm with 1 nm wavelength step.

5) Output unit: The incoming signal from detector is processed using analogue to digital converter (ADC) and displayed on monitor of computer. A signal-offset facility is provided which allows small changes in the signal to be amplified.

2.6 Kinetic treatment of experimental data

Treatment of kinetic data forms an integral part of the experimental procedure. For pulse radiolysis and stopped flow experiments experimental traces were fitted to first and second order kinetics. The basis of fitting is explained below.

2.6.1 First order processes

For a given reaction, $R \longrightarrow P$ the rate of reaction can be measured either in terms of disappearance of reactant (R) or formation of product (P).

$$-\frac{d[R]}{dt} = k[R] \qquad (2.22) \qquad \text{or} \qquad \frac{\boldsymbol{d[P]}}{\boldsymbol{dt}} = \boldsymbol{k[R]} \qquad (2.23)$$

Where, [R] represents the concentration of R and k is the rate constant or the specific rate of reaction. The dimension of k is $(\text{time})^{-1}$. Integration of equation (2.22) from start time (t=0) to time of observation (t), gives

$$\ln [R]_t - \ln [R]_0 = -kt \qquad (2.24)$$

If A_0 and A_t are the absorbancies of R at start time and at any time t, respectively, then equation (2.24) can be rewritten as:

$$\log [A]_t - \log [A]_0 = -0.4343kt \qquad (2.25)$$

The slope of the linear fit of log (A_t) as a function of time (Fig.2.4 (A)) gives the rate constant (k) for the reaction.

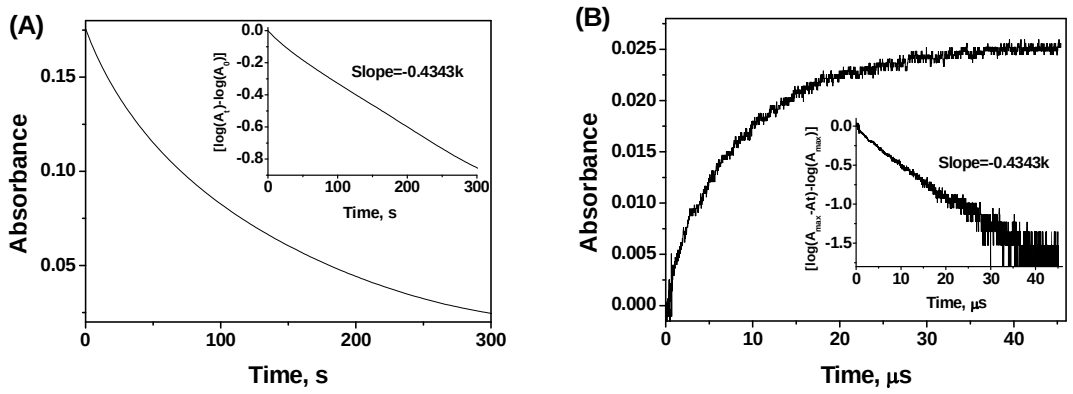

Fig. 2.4: *Absorption-time plot of (A) reactants and (B) products. Insets in figs. (A) and (B) show the fitting of absorbance of reactants and products in accordance with equation 2.25 and 2.26, respectively.*

If R does not absorb in an observable wavelength range, but the product P absorbs, then, equation (2.26) can be expressed in terms of absorbance of product as:

$$\log[A_{max}-A_t] - \log[A_{max}] = -0.4343kt \qquad (2.26)$$

Where, A_{max} represents the limiting absorbance represented by the plateau in the absorption vs. time curve and A_t is the absorbance of P at time t (Fig.2.4 (B)). The half life ($t_{1/2}$) of the reaction will be given by,

$$t_{1/2} = \frac{0.693}{k} \qquad (2.27)$$

2.6.2 Second order processes

For a bimolecular reaction, $R + R \longrightarrow Products$ the rate equation is represented by the following equation:

$$-\frac{d[R]}{dt} = k[R]^2 \tag{2.28}$$

Integration of equation 2.28 under the limits t=0 to t, gives

$$\frac{1}{[R]_t} - \frac{1}{[R]_0} = 2kt \tag{2.29}$$

Substituting the concentration terms by absorbance, we get

$$\frac{1}{A_t} - \frac{1}{A_0} = \frac{2kt}{\varepsilon l} \tag{2.30}$$

where, A_t represents the absorbance due to R at time t at wavelength λ, where product P does not have significant absorption. Above equation represents a linear relation between $1/A_t$ and time. The slope of the linear fit of $1/A_t$ as a function of time will give the rate constant ($2k/\varepsilon l$) for the reaction (Fig.2.5 (A)).

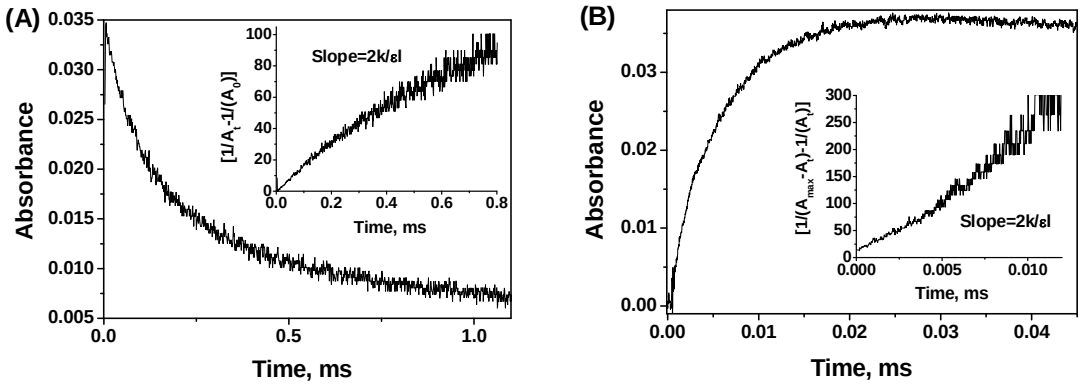

Fig. 2.5: *Absorption-time plot of (A) reactants and (B) products. Insets in figs. (A) and (B) show the fitting of absorbance of reactants and products in accordance with equation 2.30 and 2.31, respectively.*

This equation can also be written in terms of absorbance of product (P), if reactants do not absorb at the monitoring wavelength,

$$\frac{1}{\boldsymbol{A}_{\mathbf{max}} - \boldsymbol{A}_t} - \frac{1}{\boldsymbol{A}_t} = \frac{2\boldsymbol{kt}}{\varepsilon \boldsymbol{l}} \tag{2.31}$$

where A_t represents the absorbance due to P. The absolute rate constant 2k is obtained from the linear plot of $1/A_t$ against t (Fig.2.5 (B)). For a second order process, it is necessary to know the value of the molar extinction coefficient, ε, or in other words the concentrations of the transient species at specified time, in order to calculate the absolute rate constant from the observed absorption signal.

2.6.3. Pseudo first order reactions

The bimolecular reaction can also show a first order kinetics. This is done by taking one of the reactants in large excess, so that its concentration does not change significantly compared to other reactant and can be considered constant during the course of the reaction. These reactions are called as pseudo first order reaction.

If R and S react with each other and $[S_0] >> [R_0]$, then

$$R + S \longrightarrow Products \tag{2.32}$$

the rate equation for the above reaction can be written as:

$$-\frac{d[R]}{dt} = k[S][R] = k_{obs}[R] \tag{2.33}$$

The quantity k_{obs} (=k[S]) is the pseudo first order rate constant with unit s^{-1}. The unit of the second order specific rate constant k is $M^{-1}s^{-1}$. On integration under the limits t=0 to t, equation 2.33 becomes,

$$\ln [R]_t - \ln [R]_0 = -k_{obs}\, t \tag{2.34}$$

The term $[R]_t$ and $[R]_0$ refer to the concentrations at time t and at the beginning of the reaction i.e., (t=0). If A is the absorbance of species R at a particular wavelength λ where the absorption due to solvent, solute and other species are negligible, the term [R] can be substituted with absorbance, i.e A,

$$ln\left(\boldsymbol{A_t}\right) - ln\left(\boldsymbol{A}_0\right) = -\boldsymbol{k_{obs}t} \tag{2.35}$$

This equation can be written as:

$$log\left(\boldsymbol{A_t}\right) - log\left(\boldsymbol{A}_0\right) = -0.4343\boldsymbol{k_{obs}t} \tag{2.36}$$

For a reaction in which the species R does not absorb at wavelength λ but the product absorbs, the equation can be written as:

$$log\left(\boldsymbol{A_{max}} - \boldsymbol{A_t}\right) - log\left(\boldsymbol{A_{max}}\right) = 0.4343\boldsymbol{k_{\varphi}t} \tag{2.37}$$

The term A_{max} represents the maximum absorbance at the plateau in the absorbance vs. time trace. The bimolecular rate constant (k) is estimated from the linear plot of k_{obs} as a function of concentration of reactants.

2.6.4 Competition kinetics

In general, the rate constant for a given reaction is estimated by following the absorbance of either of reactant or product. However, sometimes due to overlapping absorbance of reaction components or absence of significant absorbance in the observable region, direct monitoring of the reaction becomes difficult. To resolve this, competition kinetics can be employed. This includes use of a standard compound which can react with given reactant in competition with the reaction being studied. When two reactants R_1 and R_2, both of which react with Q individually to form products P_1 and P_2, respectively, are taken together; there is a competition between R_1 and R_2 for Q to give products P_1 and P_2 respectively, as shown in scheme 2.6.

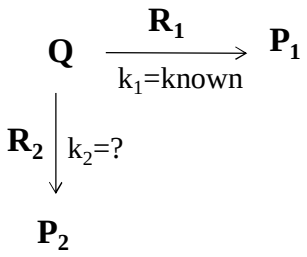

Scheme 2.6: *Representative scheme for the competitive reaction mechanism.*

Here, the reactant R_1 is taken as standard which reacts with Q with a known rate constant of k_1 to give product P_1. If k_2 is the rate constant for the reaction of R_2 with Q to give product P_2, then the fraction of P_1 formed in absence and in presence of R_2 will be given by equation 2.38.

$$\frac{[P_1]_s}{[P_1]_0} = \frac{k_1[R_1]}{(k_1[R_1]+k_2[R_2])} \qquad (2.38)$$

On rearrangement, equation 2.38 can be written as,

$$\frac{[P_1]_0}{[P_1]_s} = 1 + \frac{k_2[R_2]}{k_1[R_1]} \quad (2.39)$$

The concentration of P_1 in equation can be replaced by its absorbance (A) and equation 2.39 can be written as,

$$\frac{A_0}{A_s} = 1 + \frac{k_2[R_2]}{k_1[R_1]} \quad (2.40)$$

Where, A_0 and A_s are the absorbences of P_1 in absence and presence of R_2. The plot of A_o/A_s (absorbance ratio) vs $[R_2]/[R_1]$ yields a straight line with an intercept of unity. The slope represents k_2/k_1 and knowing the value of k_1, k_2 can be calculated. In the present study, competition kinetics was used for the estimation of the bimolecular rate constant for the reaction of organoselenium compounds with $^{\bullet}OH$ radical and peroxynitrite and discussed individually in chapters 3 and 4, respectively.

2.7 HPLC

Principle: HPLC is a technique used to separate mixtures into their individual components based on their relative affinity towards two phases. This is based on the preferential interaction of analyte with polar or non-polar phases. It includes binding of analyte with a stationary phase (a solid) and a mobile phase (liquid). The mobile phase flows through the stationary phase under high pressure (~400-600 atmospheres) and carries the components of the mixture with it. Eluted samples are then passed through absorbance based detector

where chromatogram is generated. The components of a basic HPLC system are shown in fig.2.6.

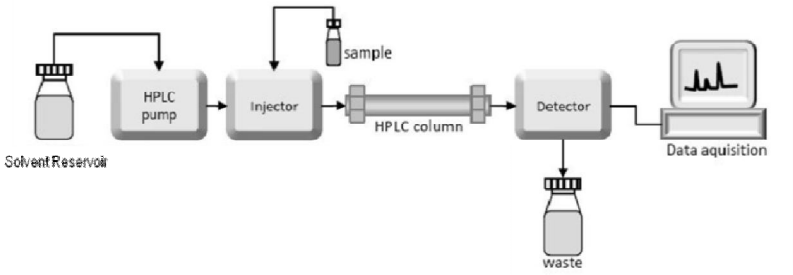

Fig. 2.6: *Basic components of HPLC instrument.*

In the present work, ELICO HP-464 instrument was used for HPLC measurements and the experimental details are given below.

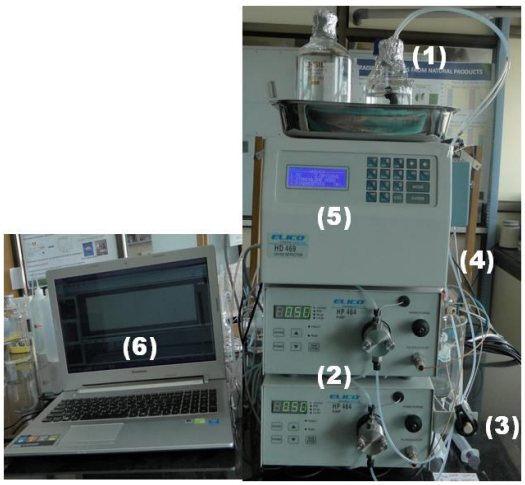

1) Solvent reservoir: Mobile phase or eluents are contained in solvent reservoirs (glass bottles). The mobile phase is a mixture of polar and non-polar liquid components whose concentrations are varied depending upon the polarity of the analyte.

2) Pump: The instrument is assisted by two independent pumps which can provide desired flow rate and eluent composition. For all HPLC studies in present work, isocratic method was used with a flow rate of 1.0 ml/minute.

3) Sample injector: An injector is used to introduce the sample into the continuously flowing mobile phase stream. It is composed of a fixed volume thin diameter loop (20 µl) which is connected to inlet of column.

4) Columns: The column used was a 250 mm long reverse phase C-18 column (Pronstil, particle size-5.0 µm) made up of polished stainless steel with an internal diameter of 4.6 mm.

5) Detector: The analytes eluted through the column are passed through a UV-Visible absorption detector (HD-469) having Deuterium/Tungsten (D_2/W) lamp as a light source.

6) Data collection devices: The detector is wired to the computer data station to generate the chromatogram on its display and to process, store and reprocess chromatographic data using Elichrom version 1.1.4 software.

HPLC measurements were carried out for qualitative and quantitative estimation of selenoxides and formaldehyde formed during reaction of organoselenium compounds with different oxidants. The selenoxides were estimated by monitoring the selenoxides (direct method) or by monitoring oxidized thiols (GSSG/DTT_{ox} in indirect method) peaks at 240 nm where the reaction mixture was eluted using 5:95 v/v acetonitrile-water solution containing 0.1% trifluroacetic acid (TFA). The yield of formaldehyde was estimated in terms of its dinitro phenylhydrazine (DNPH) derivative which was eluted using 60:40 v/v acetonitrile-water containing 0.1% TFA and monitored by absorption detection at 345 nm.[102]

2.8 Nanoparticles characterization

To study the interaction of organoselenium compounds with GNP, the samples were prepared and characterized using different techniques, some of which are discussed below.

2.8.1 DLS

DLS estimates the hydrodynamic diameter of colloidal particle by utilizing their intrinsic properties i.e., Brownian motion and ability to scatter the incident light.

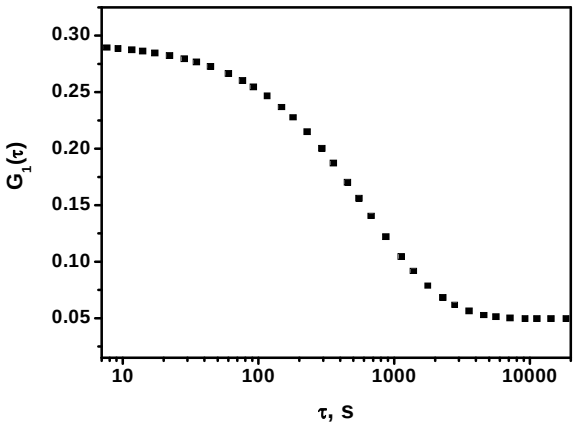

Fig. 2.7: *Representative DLS measurement output in the form of decay of ($G_1(\tau)$) as a function of time (τ).*

Due to the Brownian motion, the position of the particle changes with time and results in fluctuation in the intensity pattern of the scattered light. These intensity fluctuations in scattered light are directly proportional to the movement of the particles mathematically can be expressed by intensity auto-correlation function $G_2(\tau)$ given in equation 2.42. If I(t) is the intensity of light at any time t and $I(t+\tau)$ is the intensity after a

time delay of τ, then rate of change in scattering intensity is given by $G_2(\tau)$. From this, electric field correlation function ($G_1(\tau)$) is calculated that describes correlated particle movements and is given in equation 2.41.[103]

$$\boldsymbol{G_2(\tau) = \frac{1}{T}\int_0^T I(t)I(t+\tau)d\tau} \quad \text{and} \quad \boldsymbol{G_2(\tau) = B\left[1+\beta\,|G_1(\tau)|^2\right]} \tag{2.41}$$

Where, B is baseline and β is instrument response. Using the intensity measurements, G_1 (τ) is and plotted a function of time as shown in fig. 2.7, from which the decay constant (Γ) and diffusion coefficient (D) are calculated using equation 2.42.

$$\boldsymbol{G_1(\tau) = e^{-\Gamma\tau}} \quad \text{and} \quad \Gamma = -\boldsymbol{Dq^2} \tag{2.42}$$

Where q^2 reflects the distance the particle travels. The hydrodynamic diameters of the particles are calculated from the D values using Stokes-Einstein equation.[104]

$$\boldsymbol{D = \frac{kT}{6\pi\eta R}} \tag{2.43}$$

Where, k is Boltzmann constant, T is temperature, η is viscosity and R is radius of the particle. In the present work, DLS measurements were carried out on a Malvern 4800 Autosizer employing 7132 digital correlator. The light source used was a He-Ne laser being operated at 632 nm with a maximum output power of 2 W. Measurements were made at 90° scattering angle and at variable laser power depending on the scattering intensity. G_1 (τ) is analyzed by the method of cumulants using the mean and variance of the distribution as the fitted parameter.

2.8.2 ζ-potential measurements

Colloidal solutions are often characterized by a net charge at the particle surface which affects the distribution of ions in the surrounding interfacial region. This results in formation of an electrical double layer around each particle as shown in fig. 2.8. The inner layer in which the ions are strongly bound is known as stern layer, whereas the outer layer where the counter ions are more diffused is called the surface of hydrodynamic shear or slipping plane. The potential at slipping plane is known as ζ-potential.[105]

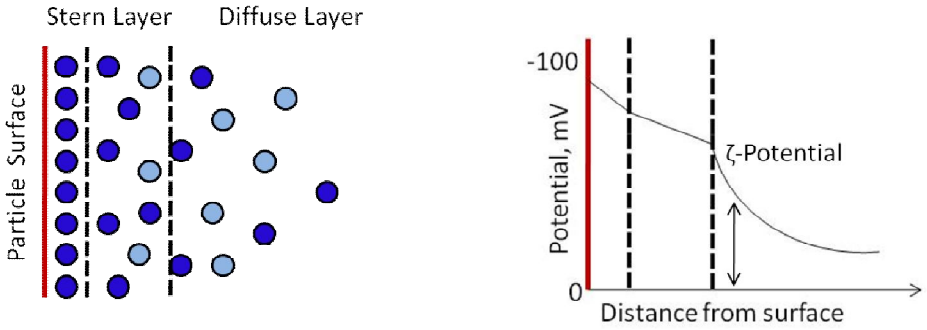

Fig. 2.8: *Distribution of counter ions on particle surface and ζ-potential.*

Under electric field, charged colloidal particles move towards oppositely charged electrode with electrophoretic mobility, U_E which depends on the magnitude of charge on the surface of the particles. U_E is related to ζ–potential by Henry equation (equation 2.44).

$$\boldsymbol{U_E} = \frac{2\varepsilon\zeta\, \boldsymbol{f(ka)}}{3\eta} \qquad (2.44)$$

Where, ε-dielectric constant, η-viscosity and f (ka) is Henry's function. For aqueous solutions and moderate electrolyte concentration, f (Ka) is 1.5, and is referred to the Smoluchowski approximation.

In the present work, ζ-potential measurements were performed on a Zetasizer Nano (Malvern Instruments, Ltd.). A sample cell with two gold electrodes was used and voltages up to 200 V were applied to the cell to induce electrophoresis. The light from He-Ne laser with wavelength 580 nm was incident on the sample and the scattered light was collected by charge coupled detector (CCD). The phase change between incident light and scattered light is detected by oscilloscope and further analyzed using PALS (Phase Analysis Light Scattering) technique to estimate U_E from which ζ–potential is calculated using equation 2.44.

2.9 SERS

SERS is a Raman spectroscopic technique that provides greatly enhanced Raman signal from Raman-active analyte molecules absorbed on metal surfaces.[106] If wavelength of light source matches with surface plasmon resonance (SPR) band of nanoparticles, it produces Raman signals with a very high multiplication factor and termed as surface enhanced resonance Raman spectroscopy (SERRS).

For the characterization of binding between GNP and organoselenium compounds, SERS technique was used. The measurements were carried out at room temperature using the 660 nm line from a DPSS laser (Ignis 660-500) M/s Laser Quantum Ltd. England. The laser power used to record the Raman spectrum was 50 mW and the spot size on the

sample was ~ 50µ. For this, the sample solution was taken in a standard 1cm x 1cm cuvette and the Raman scattered light was collected at 90° scattering geometry. The scattered light was detected using a CCD (Synapse, Horiba JobinYvon) based monochromator (Triax550, Horiba JobinYvon, France) together with an edge filter, covering a spectral range of 200-1700 cm^{-1}. Before sample measurements, the spectrometer calibration was carried out using benzene: CCl_4 mixture (1:1 v/v) and indene.

The assignment of spectral peaks was done using Raman spectra of pure organoselenium compounds taken on a micro-Raman spectrophotometer (SEKI Technotron) with excitation at 532 nm (power ~20 mW at sample position). Raman spectra of these compounds were also calculated theoretically by using quantum chemical calculations, the details of which are given in section 2.11.

2.10 Assay for determination of antioxidant activity

2.10.1 Cellular toxicity assay

To estimate the antioxidant activity of organoselenium compounds against peroxynitrite induced cellular damage, cell toxicity measurements were done using MTT assay.[107] For this Chinese hamster ovary (CHO) cells were grown in 96 well plate in DMEM culture medium supplemented with 10% fetal calf serum at a density of 2 X 10^3cells/well in 5% CO_2 humidified atmosphere at 37°C. After 16–18 h, the cells were treated with different concentrations of organoselenium compounds (0.1-1 mM) for 4 hours. To remove extracellular organoselenium compound, cells were washed with 1X phosphate buffer saline (PBS) three times. To this, 0.5 mM of peroxynitrite was added and

rapidly mixed with the buffer to distribute the peroxynitrite across the well. After 5 minutes, the PBS was removed and replaced with culture medium. The cells were incubated for 24 hours and viability was determined by a colorimetric MTT assay. For this, 5 µl of MTT (5 mg/ml) solution was added to each well and incubated for 4 hours. Addition of MTT leads to formation of formazan which can be seen as blue crystals under the microscope. This was followed by addition of 100 µl of sodium dodecyl sulphate (SDS) dissolved in 0.01 M HCl (0.1g/1ml) and further incubated to 12 hours. The amount of formazan formed is directly proportional to number of live cells and can be monitored by measuring its absorbance at 532 nm. The cell viability was calculated by using equation 2.45.

$$\%Viability = \frac{A_{test}}{A_{control}} X 100 \qquad (2.45)$$

Where, A_{test} is the absorbance of test sample and $A_{control}$ is the absorbance of cells in the absence of any treatment. Cell viability was expressed as percentage (%) viability compared to the control (100%). Results were expressed as mean ± S.E.M. from two independent experiments, each one assayed in triplicate.

2.10.2 Gel electrophoresis

To estimate the protection ability of organoselenium compounds towards ROS induced damage to bio molecules, DNA damage assay was performed.[108] ROS can cause damage to DNA molecules by various ways i.e. base modification, strand break, etc. Strand breaking of DNA leads to change in its structure which can be utilised to estimate

the extent of damage. Herein, plasmid pBR322 DNA has a super coiled (SC) structure which on exposure to ROS (radiation/peroxynitrite) changes to open circular (OC) due to single strand break. These two forms of pBR322 DNA move with different speeds under application of electric field and therefore can be separated by using gel electrophoresis method. For the assay, 1µl of pBR322 (250ng/µl) was mixed with (50 µM-1 mM) organoselenium compounds and final volume was made up to 19 µl. To this 1 µl of peroxynitrite (10 mM) was added and incubated for 5 minutes at 20°C. Reaction samples were mixed with 4 µl of bromophenol dye (6X). Equal volume (20 µl) of each sample was loaded on 1.5% agarose gel stained with ethidium bromide and subjected to electrophoresis. For radiation experiments, similar protocol was used and DNA damage was induced by γ-radiation (8Gy) instead of peroxynitrite. Gel images were taken using UV transilluminator and analysed by GeneTools software (Version 08-3d.3.SynGene). The percentage protection was calculated in terms of reduction in damage to SC DNA relative to damage obtained in radiation control as given in equation 2.46. For this, the fraction (I) of SC DNA was calculated for each sample and fraction of SC DNA ($I_{control}$) for control experiment was taken as unity. The results were represented as mean ±S.E.M. from two independent experiments, each one assayed in triplicate.

$$\%\,protection = \frac{\left(I_{test} - I_{ROS}\right)}{\left(I_{control} - I_{ROS}\right)} X 100 \qquad (2.46)$$

Where, I_{test} is the fraction of SC DNA treated with ROS in presence of organoselenium compounds, I_{ROS} is the fraction of super coiled DNA treated with ROS.

2.11 Computational studies

Computational calculations are based on solution of Schrodinger equation,

$$\hat{H}\psi = \hat{E}\psi \tag{2.47}$$

Where, H is the Hamiltonian operator and E is the corresponding Eigen value of wave function ψ and represents energy of the system. There are many methods for solving the many-body Schrodinger equation based on the expansion of the wave function in Slater determinants. These can be classified in two broad categories as described below.[109]

Ab-Initio methods: These methods involve solution of Schrodinger equation directly from theoretical principles and that do not include any experimental data based approximations. The simplest type of ab-initio electronic structure calculation is the Hartree–Fock (HF) method in which the correlated electron–electron repulsion is not specifically taken into account.

Semi-empirical methods: These methods are also based on the HF methods, but include many approximations and parameters obtained from empirical data. The use of empirical parameters allows inclusion of electron correlation effects and becomes important for treatment of large molecules where the HF method becomes expensive.

Density functional theory (DFT): It is among the most popular and versatile methods available in computational chemistry. For an N-body system, earlier methods involved use of 3N variables which makes the calculation both time and cost consuming. DFT allows the determination of the properties of a many-electron system using the spatially dependent

electron density functional. In many cases the results of DFT calculations for solid-state systems agree quite satisfactorily with experimental data.

Although density functional theory has its conceptual roots in the Thomas–Fermi model, DFT was put on a firm theoretical footing by the two Hohenberg–Kohn theorems (H–K). The first H–K theorem lays the groundwork for reducing the many-body problem of N electrons with 3N spatial coordinates to 3 spatial coordinates, through the use of functionals of the electron density. The second H–K theorem defines energy functional for the system and proves that the correct ground state electron density minimizes this energy functional. The major problem with DFT is that the exact functionals for exchange and correlation are not known except for the free electron gas. However, approximations exist which permit the calculation of certain physical quantities quite accurately. The most widely used approximations are:

1. Local-density approximation (LDA)
2. Local spin density approximation (LSDA)
3. Generalized gradient approximations (GGA)
4. Meta generalized gradient approximations (meta-GGA), etc.

DFT calculations involve use of different functionals which can be divided in three categories as given below.[109]

1. Exchange functionals: Slater exchange functional (S), Becke exchange fnctionals (B), X alpha exchange (X) etc.

2. Correlation functional: Lee, Yang, and Parr (LYP- includes both local and non-local terms), Becke 95 (B95- gradient-corrected correlation functional) etc.
3. Hybrid functionals: B3LYP (uses the non-local correlation provided by the LYP expression, and VWN functional III for local correlation), BMK (Boese and Martin's τ-dependent hybrid functional) etc.

B3LYP is a hybrid functional in which the exchange energy from Becke's exchange functional is combined with the exact energy from HF theory. Along with the component exchange and correlation functionals, three parameters define the hybrid functional, specifying how much of the exact exchange is mixed in. B3LYP with basis sets like 6-31 and 6-311 with (s,p) diffusion corrections has been widely used to characterize selenium compounds and different reaction intermediates.

As solvation plays an important role in defining the reaction mechanism and stability of reaction intermediates. Therefore it is essential to use a proper salvation model for the reaction system. Broadly, solvation models can be classified in two classes:

a) Implicit model
b) Explicit model

Implicit models are based on the assumption that solute can be considered as surrounded by a homogeneously polarizable medium. This model represents the solvent as a perturbation to the solute Hamiltonian. The most commonly implicit model is polarizable continuum model (PCM).[110] Further, PCM model can be associated with solvent density model (SMD) which separates the free energy of solvation into two components. The first

component is the bulk-electrostatic contribution arising from a self-consistent reaction field (SCRF) treatment. The second contribution arises from short-range interactions between the solute and solvent molecules in the first solvation shell, known as cavity–dispersion–solvent-structure (CDS) and is proportional to the solvent-accessible surface areas (SASAs) of the individual atoms of the solute.

In the present study, the quantum chemical calculations were performed by adopting the GAMESS suite of programs on a PC-based LINUX cluster platform.[111] The geometry of the compounds and intermediates were optimized in gaseous phase by extensive variation in initial confirmation at B3LYP/6-31+G(d,p). The most stable transient structures were further optimized in water using PCM-SMD model.[110] The optimized structures were verified as global minima structure by performing the frequency calculation. The energetics of the reactions was calculated by estimating the difference in the zero-point corrected B3LYP energy of the products and the reactants. To estimate the strength of non bonding interactions (E_{nb}) in intermediates formed during reaction of organoselenium compounds with free radicals, natural bond order (NBO) analysis was done at B3LYP/6-31+G (d,p) level using a Gaussian09 software.[112] Raman spectra of organoselenium compounds was calculated at B3LYP/6-31+G (d,p) level by using the optimized geometry of organoselenium compounds in water. To generate the Raman spectra, the change in the energy (E) of the system is calculated as a function of geometry (R) and external electric field (F) where the intensity of different Raman modes is proportional to the change in polarizability of the compound as shown in equations 2.48 and 2.49.[109]

$$\textbf{Raman intensity } \alpha \left(\frac{\partial \alpha}{\partial \boldsymbol{q}} \right) \tag{2.48}$$

OR $$\textbf{Raman Intensity } \alpha \left(\frac{\partial^3 \boldsymbol{E}}{\partial \boldsymbol{R} \partial \boldsymbol{F}^2} \right) \tag{2.49}$$

Where, α is the polarizability of given compound and q is the electronic charge. Identification and assignment of different Raman modes was done using MacMolPlt v7.6.1 by utilizing the direction of polarizability tensor. Visualization of the geometry and relevant molecular orbitals was done by following the Chemmissian software (version V4.38).

2.12 Other techniques

The characterization of organoselenium compounds and their selenoxides was done using NMR and MS techniques. The proton (^{1}H), carbon (^{13}C) and selenium (^{77}Se) NMR spectra of DHS, DHS_{ox}, MAS and MAS_{ox} were recorded on Bruker Avance-II 500 MHz spectrometer equipped with a magnetic field of 11.74 Tesla and operating at 500 MHz (for ^{1}H) and 95.43 MHz (for ^{77}Se). The NMR spectra of SeROH compounds were recorded on Bruker Avance-II 300 MHz spectrometer with magnetic field strength of 7.05 Tesla and operating at 300.13 Hz (for ^{1}H) and 57.25 MHz (for ^{77}Se). ^{1}H NMR chemical shifts were relative to internal DMSO peak (δ = 2.49 ppm) whereas ^{77}Se{^{1}H} NMR chemical shifts were taken relative to external diphenyl diselenide (Ph_2Se_2) in $CDCl_3$ (δ 463.0 ppm relative to Me_2Se (0 ppm)). The peak assignments were done using reported NMR data for these compounds. Mass spectra were recorded on a JEOL JMS-T100LP mass

spectrometer under atmospheric pressure chemical ionization (APCI+). The size of GNP was measured using Libra-120 plus TEM instrument (Carl Zeiss, Germany) operated at 120 kV as the accelerating voltage. For this, a small volume (~10 µl) of GNP solution was placed on carbon coated copper grid and dried at room temperature (~28-30 °C). Other analytical tools such as pH meter, fluorometer (Hitachi F-4500) and absorption spectrophotometer (JASCO V-630 spectrophotometer) were used wherever required.

Chapter-3

Pulse Radiolysis studies on reactions of free radical oxidants with organoselenium compounds

In this chapter, reactions of $^{\bullet}OH$ radical with aliphatic linear selenoethers with varying alkyl chain length (SeROH) were studied using pulse radiolysis technique. The selenium centered radicals produced during this reaction were characterized by monitoring their kinetic and spectral properties. The quantitative analysis of the products was done using steady state radiolysis followed by HPLC measurements. To correlate the nature and yield of transients with antioxidant activity of SeROH, studies were performed on GPx activity and DNA protection ability against radiation induced damage. The energetics of the different steps involved in these reactions was estimated by quantum chemical calculations.

3.1 Introduction

Free radicals are species that are capable of independent existence containing one or more unpaired electrons, which makes them very reactive. In cells, free radicals are produced during processes like metabolism and mitochondrial electron transfer.[113,114] High levels of free radicals can cause imbalance in cellular redox system leading to oxidative stress. Among different free radicals, $^{\bullet}$OH radical is a very strong oxidising radical and reacts with target molecules in non-selective manner. The $^{\bullet}$OH radicals reactions are in general, very fast and cannot be studied by simple kinetic spectrometric techniques like stopped flow etc. In this regard, pulse radiolysis technique offers a convenient tool to generate $^{\bullet}$OH radicals and study its reactions with various substrates in nano to milli second time scale. Due to the importance of thiols in several biological systems, extensive research has been carried out to understand the reaction of $^{\bullet}$OH radical with organosulfur compounds using pulse radiolysis.[115,116] The different types of transients formed during one-electron transfer processes of organosulfur compounds like thiols (RSH), sulfides (RSR), disulfides (RSSR) have been well characterized which include sulfur centered radical cations ($>S^{\bullet+}$), disulfide radical anions ($-(SS^{\bullet-})-$), dimer radical cation ($(>S\therefore S<)^{+}$) and neutral radicals ($RS^{\bullet}$). The major work on sulfur based radicals has been contributed by Asmus and co-workers.[117,118,119] He proposed that the initial reaction of $^{\bullet}$OH radical with organosulfur compounds takes place at sulfur centre to form hydroxy sulfauranyl radical ($>S\therefore OH$). The initially formed ($>S\therefore OH$) radical would react with another sulfur molecule to form $((>S)_2OH)^{\bullet}$ radical complex which then undergoes dehydroxylation to

give $(>S\therefore S<)^{+}$ radical. The proposed structures of these transients are given in scheme 3.1.

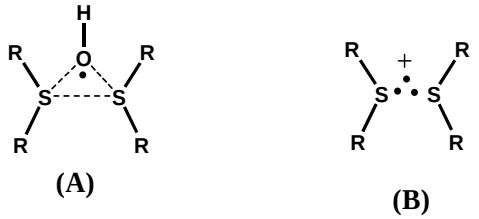

Scheme 3.1: *Structures of* $((>S)_2OH)^{\bullet}$ radical and $(>S\therefore S<)^{+}$ radical.

The formation of $(>S\therefore S<)^{+}$ radical was proposed to take place by association of $(>S^{\bullet+})$ radical with unoxidized sulfur molecule via formation of a two centre-three electron (2c-3e) bond.[120] This bond arises due to overlapping of unpaired electron in p-orbital of $(>S^{\bullet+})$ radical with lone pair of another sulfur atom of unoxidized molecule.[121] Out of the three electrons involved in bonding, two electrons resides in bonding (σ) orbital and one electron in anti-bonding (σ*) orbital as shown in fig. 3.1 and is written as 2σ/1σ* bond.

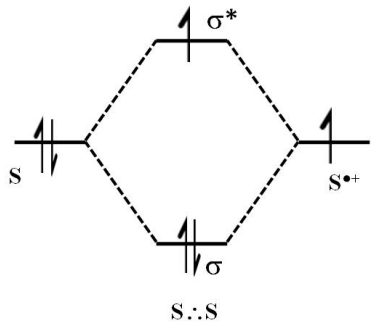

Fig. 3.1: *Molecular orbital representation of 2c-3e bond.*

The presence of one electron in σ* orbital weakens the bond and the overall bond order of 2c-3e bond is 0.5. Therefore, this bond is also known as hemi bond. These type of

transient species can be easily detected by absorption changes due to allowedness of σ to σ* electronic transitions. Supportive information on the existence of hemi bond has been provided by quantum chemical calculations and confirmed by electron para magnetism (EPR) and X-ray studies.[122] In unsubstituted aliphatic monosulfides e.g. dimethyl sulfide, the $(>S\therefore S<)^{+}$ radical formed during their reaction with $^{\bullet}OH$ radical, undergoes radical-radical reaction to form corresponding sulfoxide.[123] Similar results were not observed for functionalized sulfides.[124] The formation and nature of these transient species has been found to be greatly affected by neighbouring group participation. Presence of hetero atoms like N, O, etc., in proximity to sulfur atom, have been found to influence the spectral and redox properties of the transients. For example, the reaction of $^{\bullet}OH$ radical with Met at acidic pH, formed ($>S^{\bullet+}$) which was further converted to $(>S\therefore S<)^{+}$ radical.[125] At neutral pH, ($>S^{\bullet+}$) radical undergoes irreversible decarboxylation through formation of 5-membered cyclic intermediate involving (S∴N) bond.[126]

Selenium belonging to the same group as sulfur, participates in electron transfer reactions in a similar way as sulfur. Being more electropositive, selenium can be easily oxidized and can participate in redox reactions more easily as compared to analogous sulfur compounds. Although extensive studies on the free radical induced electron transfer reactions of organosulfur compounds have been performed, such reactions are not widely explored for organoselenium compounds. The first study on pulse radiolysis of organoselenium compounds was reported by Badiello et al in 1969, where he showed that the reaction of $^{\bullet}OH$ radical with selenourea results in formation of a charged complex having two molecules of selenourea.[127] Similar studies were carried out on CysSeSeCys

and SeMet, however, the structure of this charged complex remained unclear at that time.[128,129] In 2004, Mishra et al showed that the charged complex formed in selenourea is a selenium centered dimer radical cation ($(>Se\therefore Se<)^{+}$) which is formed by a intermolecular 2c-3e bond between two selenium atoms.[130] Unlike their sulfur analogues (thiourea), this transient was found to be reactive towards molecular oxygen and degrades to form elemental selenium.[131] Similar results were observed for reaction of $^{\bullet}OH$ radical with 1,1'-dimethyl-2-selenourea.[132] Asmus and co-workers also showed that $(>Se\therefore Se<)^{+}$ radical acts as the redox intermediate between SeMet and its oxide ($SeMet_{ox}$).[133] Further, the rate of reaction with $^{\bullet}OH$ radical and stability of transients formed therein have been found to be greatly affected by nature of functional groups present in organoselenium compounds. A comparative study on reaction of $^{\bullet}OH$ radical with SeCys, SeCysA and DSePA carried out by Mishra et. al. showed that the compounds having electron donating group like, carboxylate (COO^{-}) were easier to undergo oxidation than those having electron withdrawing groups and the reactivity of these compounds is guided by electron density on selenium atom.[87] Also the hydroxyselenouranyl adduct ($>Se\therefore OH$) of DSePA forms a stable selenium centered radical cation ($>Se^{\bullet+}$) while that of CysSeSeCys and SeCysA were destabilized and undergo fragmentation to form selenyl radical which further get converted to triselenide radical adduct. In another study by Koppenol group, the role of SeCys in electron transfer reactions was explored and it was shown that SeCys acts as an efficient catalyst in coupling one and two electron transfer processes, which otherwise are quite slow.[134]

Similar to organosulfur compounds, the presence of hetero atom in organoselenium compounds has been observed to affect the nature of transients through formation of 2c-3e bond between selenium and hetero atom. Due to higher covalent radius of selenium, these interactions are more favorable in selenium compounds than in their sulfur analogues resulting in higher thermodynamic and kinetic stability of selenium based radicals having (Se∴X; X=N, O, etc.).[121,133] A study from our group on SeMet and Met has shown that even though the initial reaction of •OH radical with both SeMet and Met is similar, extent of decarboxylation reaction is lower in SeMet and attributed to higher stability of its radical cation as compared to that of Met.[135] Similarly, experimental and theoretical studies reported by Asmus and co-workers showed that aliphatic selenides are more reactive towards free radicals and the resultant selenium based transients are more stable than those from analogous sulfides.[136] In another study involving the effect of chain length on the nature and stability of transients formed during one-electron transfer reactions of aliphatic selenocarboxylic acids, it was observed that bis(propyl carboxylic acid) undergoes significantly lower radiolytic degradation (via decarboxylation reaction) compared to its homologues due to formation of thermodynamically stable five membered ring in (>Se∴O) radical.[137]

From the studies carried out so far on electron transfer reactions of organoselenium compounds, it has been inferred that factors like electronic energy levels, stability of transients, neighboring group participation, etc., have important role in defining the electron transfer reactions of organoselenium compounds. Therefore, it is very important to understand the correlation between various molecular descriptors with the structure,

substitution and antioxidant activity of these compounds. Present work aims at identification of various molecular descriptors that affects the electron transfer reactions, nature of transients and their effect on overall antioxidant activity of organoselenium compounds. For this, the study has been divided in two sections. Section A discusses the effect of alkyl chain length on electron transfer reactions of three linear aliphatic selenoethers SeEOH, SePOH and SeBOH.[95] Section B, explores the importance of structure on the nature of transient formed. For this a comparison has been done between electron transfer properties of SeEOH and its cyclic analogue DHS.[70,90] The chemical structure of these compounds are given in scheme 3.2.

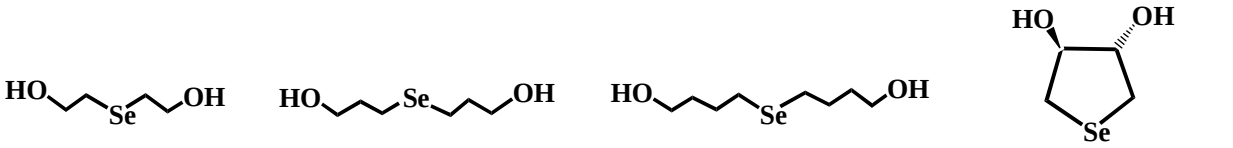

bis(2-ethanol)selenide (SeEOH) | bis(3-propanol)selenide (SePOH) | bis(4-butanol)selenide (SeBOH) | 3,4-dihydroxyselenolane (DHS)

Scheme 3.2: *Chemical structures of the SeROH compounds.*

3.2 Materials and Methods

Pulse radiolysis technique was used for the study of free radical reactions of SeROH and transient characterization. The instrumental details of this technique are discussed in chapter 2. The average absorbed dose used for most of the experiments was 9 ± 1 Gy; if different doses are used, they are mentioned accordingly. The reaction products were identified and quantified by HPLC. Quantum chemical calculations were performed by adopting the GAMESS suite of programs on a PC-based LINUX cluster platform.

3.3 Results and discussion

Section-A

Electron transfer reactions of linear organoselenium compounds: Effect of alkyl chain length

3.3.1 Pulse radiolysis studies

Pulse radiolysis studies were carried out to study the reaction of $^{\bullet}OH$ radical with SeROH compounds and the results from individual compound are presented below.

3.3.1.1 SeEOH

The reaction of $^{\bullet}OH$ radical with SeEOH was studied by radiolysing N_2O saturated aqueous solution at pH 7. Fig. 3.2(A) shows the time resolved transient absorption spectrum generated by the reaction of $^{\bullet}OH$ radical with 50 μM SeEOH. The absorption spectrum showed two absorption bands with maxima at 320 nm and 490 nm. The species absorbing at 320 nm was formed readily within 2 μs whereas the transient absorbing at 480 nm is formed slowly (~20 μs) compared to that absorbing at 320 nm. To differentiate the nature of transients, decay traces at 320 nm and 490 nm were recorded and analyzed (Fig. 3.2(B)). The transient absorbing at 320 nm decayed by following first order kinetics, with a rate constant of $(3.8 \pm 0.2) \times 10^3\ s^{-1}$, while that absorbing at 490 nm followed second order kinetics with $2k/\varepsilon l$ value of $(9.4 \pm 0.3) \times 10^5\ s^{-1}$, where ε is the extinction coefficient of transient at 490 nm.

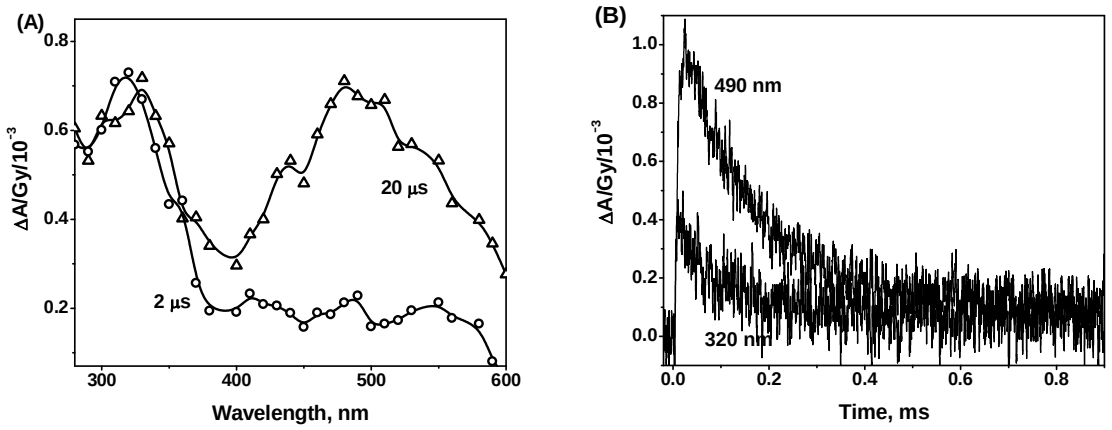

Fig. 3.2: *(A) Time resolved transient spectra (at 2 μs and 20 μs) generated on pulse radiolysis of N_2O saturated aqueous solution of 50 μM SeEOH at pH 7. Fig. (B) shows the absorbance-time plot of transients at 320 nm and 490 nm.*

To characterize the transients, their absorption spectra were recorded at different concentration of SeEOH (0.1 mM-2.5 mM) as shown in fig. 3.3(A). At 100 μM of SeEOH, the transient absorption spectrum showed a prominent absorption maximum at 320 nm and another broad absorption band with a maximum at 490 nm (Fig. 3.3(A)-a). Increasing the concentration to 1 mM and 2.5 mM, although generated similar spectral pattern, the absorbance at 490 nm increased significantly, while that at 320 nm was little influenced (Fig. 3.3(A)-b&c). As shown in fig. 3.3 (B), the absorbance at 490 nm increased gradually with increase in SeEOH concentration (0.05 mM-1 mM) while no significant changes were observed in the absorbance at 320 nm.

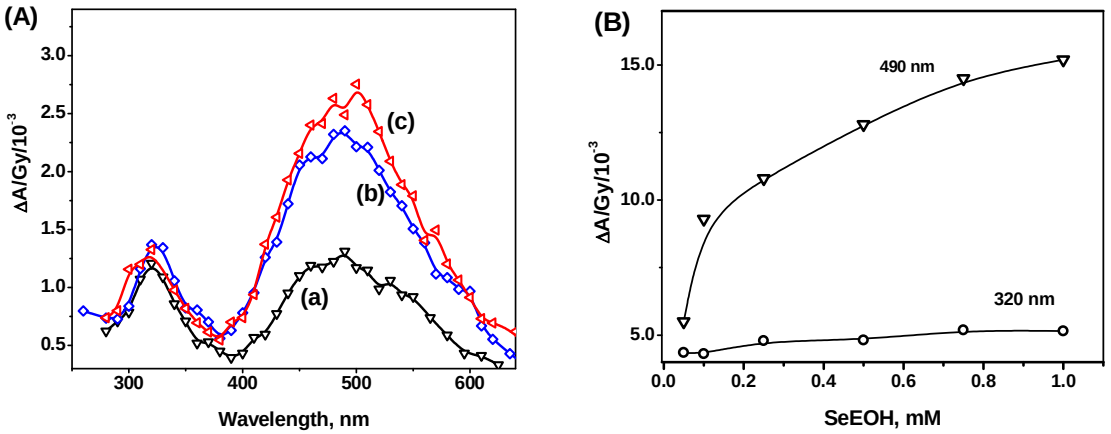

Fig. 3.3: *(A) Transient absorption spectra obtained at 10 µs after pulse radiolysing N_2O saturated aqueous solution of (a) 100 µM, (b) 1 mM and (c) 2.5 mM SeEOH at pH 7. Fig. (B) shows the variation of absorbance of transients absorbing at 320 nm and 490 nm as a function of SeEOH concentration.*

Earlier reports on the reaction of $^{\bullet}OH$ radical with selenium compounds have shown that $^{\bullet}OH$ radical initially adds to selenium center to form (>Se∴OH) radical as shown in equation 3.1. The (>Se∴OH) radical can form $(>Se\therefore Se<)^{+}$ radical by direct replacement of OH^{-} by parent SeEOH molecule (equation 3.2). Also it can undergo proton catalyzed elimination of OH^{-} to form ($>Se^{\bullet+}$) radical followed by addition of parent SeEOH molecule resulting in formation of $(>Se\therefore Se<)^{+}$ radical (equation 3.3 and 3.4). Both these processes would depend on the concentration of SeEOH. As shown in fig. 3.3(B), the absorbance at 490 nm increased with increase in SeEOH concentration, therefore, the transient absorbing at 490 nm was attributed to the formation of $(>Se\therefore Se<)^{+}$ radical.

$$> Se + {}^{\bullet}OH \rightarrow (> Se\therefore OH) \qquad (3.1)$$

$$> Se \therefore OH \xrightarrow{>Se} (> Se \therefore Se <)^{+} + OH^{-} \quad (3.2)$$

$$(> Se \therefore OH) \xrightarrow{H^{+}} > Se^{\bullet +} + H_2O \quad (3.3)$$

$$> Se^{\bullet +} \rightleftharpoons (> Se \therefore Se <)^{+} \quad (3.4)$$

The absorption band at 320 nm may be either due to the formation of (>Se∴OH) radical or (>$Se^{\bullet +}$) radical. This was resolved by monitoring the absorbance at 320 nm in the presence of different concentration of phosphate ($H_2PO_4^-$) ion (proton donor).[138] (>Se∴OH) radical in presence of $H_2PO_4^-$ ions would undergo proton catalyzed dehydration to form (>$Se^{\bullet +}$) radical leading to decrease in the absorbance due to (>Se∴OH) radical. Fig. 3.4(A) shows that the absorbance at 490 nm increased monotonically with increase in $H_2PO_4^-$ ion concentration while no significant change was observed for absorbance at 320 nm. This rules out the possibility of transient absorbing at 320 nm to be a (>Se∴OH) radical. Further, at pH 1, due to very high proton concentration, (>Se∴OH) radical will be quantitatively converted to (>$Se^{\bullet +}$) radical. Fig. 3.4(B) shows the overlay of transient spectra generated by reaction of $^{\bullet}$OH radical with 50 µM SeEOH at pH 7 (spectrum (a) in fig 3.4 B) and pH 1 (spectrum (b) in fig 3.4 B). Due to low concentration of SeEOH, extent of dimerization reaction would be suppressed and only (>$Se^{\bullet +}$) radical is expected to be observed. However, the transient spectrum at pH 1, showed absorption maximum only at 490 nm whereas the absorption band at 320 nm was not observed. Further, as shown in fig. 3.2, the absorbance at 320 nm did not change

significantly with increase in SeEOH concentration. This confirms that absorbance at 320 nm is neither due to (>Se∴OH) radical nor due to ($>Se^{\bullet+}$) radical.

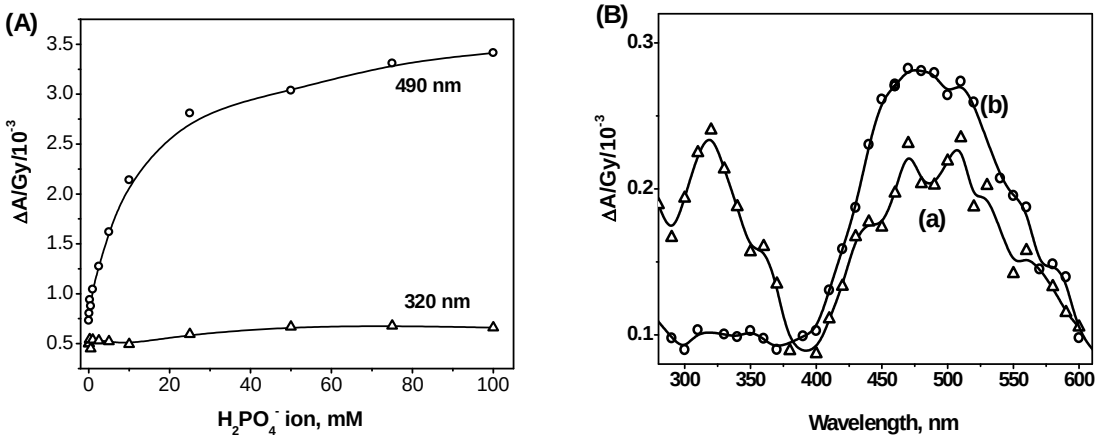

Fig. 3.4: *(A) Variation in transient absorbance at 320 nm and 490 nm as a function of $H_2PO_4^-$ ion concentration. Fig. B shows the transient absorption spectra obtained at 20 μs after pulse radiolysing N_2O saturated aqueous solution of 50 μM SeEOH at (a) pH 7 and (b) pH 1.*

On close observation of the decay and formation kinetics of the 320 nm absorbing species as a function of SeEOH and proton concentration, it can be noticed that this absorption band is formed very fast as compared to the $(>Se\therefore Se<)^+$ radical, and is not the precursor or successor of $(>Se\therefore Se<)^+$ radical. The first order decay of the transient absorbing at 320 nm, which is independent of SeEOH and proton concentration, can be envisaged to the formation of a carbon centered radical of the type α-(hydroxyl ethyl) seleno methyl radical ($HOCH_2CH_2SeCH_2^{\bullet}$). Such radicals can be formed by rearrangement of (>Se∴OH) radical at α-position to the selenium centre followed by elimination of water

and formaldehyde (HCHO) molecules via Barton reaction (path II in scheme 3.3).[124b] Similar mechanism has been proposed by Schoneich et al for the reaction of $^{\bullet}$OH radical with organosulfur compounds and has been supported by detection of HCHO formed as the side product.[124b] Based on these results, it was concluded that the reaction of $^{\bullet}$OH radical with SeEOH leads to formation of two main transients namely, ($HOCH_2CH_2SeCH_2^{\bullet}$) radical and $(>Se\therefore Se<)^{+}$ radical and shown in scheme 3.3.

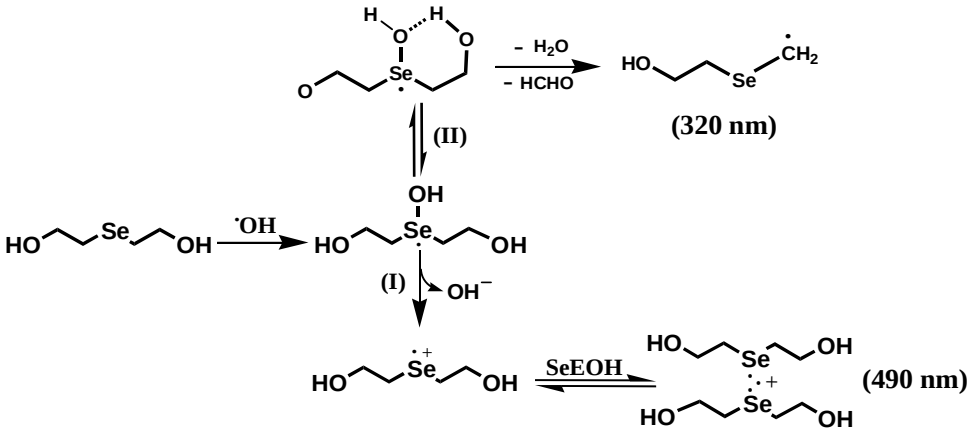

Scheme 3.3: *Reaction scheme showing formation of possible transients during reaction of* $^{\bullet}$*OH radical with SeEOH.*

3.3.1.2 SePOH

Similar to SeEOH, the reaction of $^{\bullet}$OH radical with SePOH was carried out at different concentration of SePOH (50 µM-5 mM) (Fig. 3.5 (A)). At 50 µM, the transient spectrum (spectrum (a) in fig. 3.5) was broad in the range from 200 nm to 600 nm with absorption maximum at around 370 nm. With increase in SePOH concentration from 50 µM to 250 µM (spectrum (b)), the absorbance in the wavelength range 350-380 decreased while that at 500 nm increased considerably with evolution of a shoulder band at 460 nm.

At higher concentration (1 mM, spectrum (c)) the transient absorption spectrum did not show any band at 370 nm but displayed two absorption maxima, one at 320 nm and another at 460 nm-500 nm.

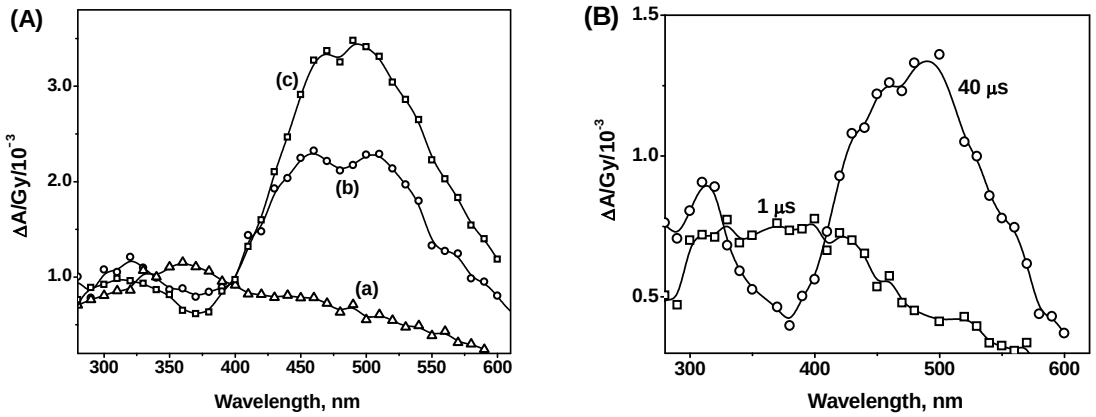

Fig. 3.5: *(A) Transient spectra recorded at 5 μs after pulse radiolysing N_2O saturated aqueous solution of (a) 50 μM, (b) 250 μM and (c) 1 mM SePOH at pH7. Fig. (B) shows the time resolved transient absorption spectra generated on pulse radiolysis of N_2O saturated aqueous solution of 0.1 mM SePOH at pH 7.*

Fig. 3.5(B) shows the time resolved transient spectra generated by reaction of $^{\bullet}OH$ radical with 0.1 mM SePOH at pH 7. The transient spectrum at ~1 μs showed broad absorption maximum at 350 – 370 nm, which decayed with the evolution of a new absorption band with maximum at 500 nm at ~40 μs after the pulse. To characterize the transients, absorption-time plots were recorded at 370 nm, 460 nm and 500 nm and fitted to first order decay kinetics (Fig. 3.6). The rate constant values were estimated to be (1.2 ± 0.2) x 10^3 s^{-1}, (2.7 ± 0.2) x 10^3 s^{-1} and (3.6 ± 0.3) x10^3 s^{-1} for the decay of absorption-time

plot at 370 nm, 460 nm and 500 nm, respectively, indicating that the three different transients are not of the same nature.

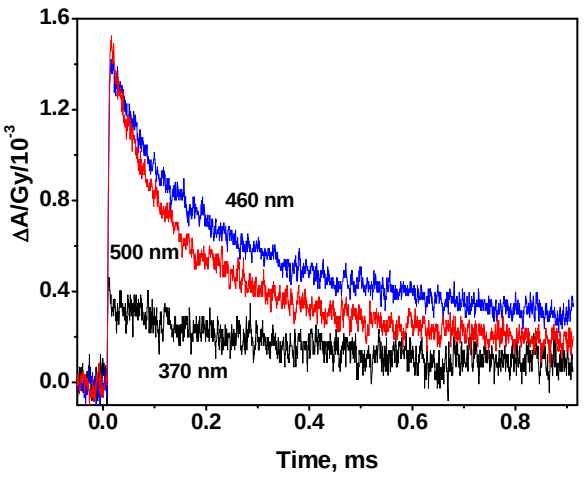

Fig. 3.6: *Absorption-time plot of transients absorbing at 370 nm, 460 nm and 500 nm formed during the pulse radiolysis of N_2O saturated solution of 100μM SePOH at pH 7.*

To assign these bands, the transient absorption spectrum of 100 μM SePOH was recorded in absence and in presence of 5 mM phosphate buffer (Fig. 3.7(A)). As seen in spectrum (a), in the absence of phosphate buffer, a broad absorption band with maxima at ~370 nm was observed with negligible absorbance at 460 nm. However, in presence of 5 mM phosphate buffer (spectrum (b)), the absorbance at 370 nm disappeared with evolution of 460 nm absorbance band. Further, the absorbencies at 370 nm, 460 nm and 500 nm were monitored as a function of $H_2PO_4^-$ concentration (0.05 mM-2.5 mM). As shown in fig. 3.7(B), with increase in $H_2PO_4^-$ concentration (0 to 2.5 mM) the absorbance at 370 nm decreased while that at 460 nm and 500 nm increased. This indicated that the transient absorbing at 370 nm is (>Se∴OH) radical.

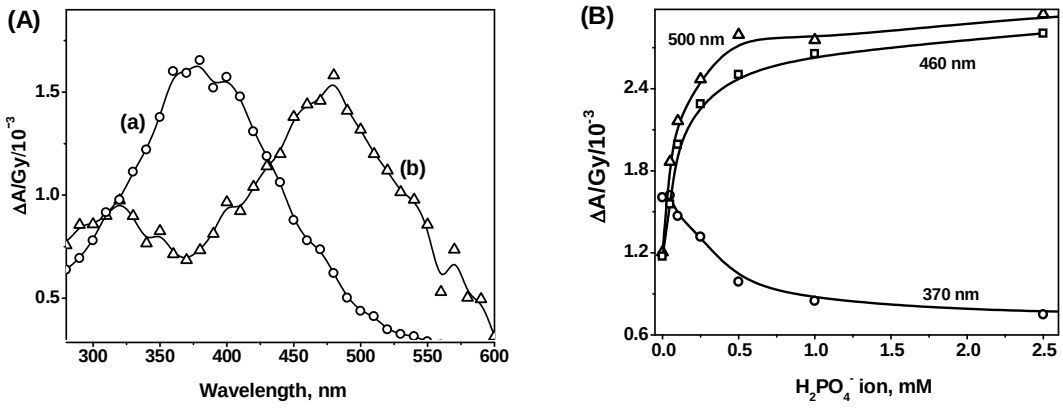

Fig. 3.7: *(A) Transient absorption spectra obtained at 20 µs after pulse radiolysis of N_2O saturated aqueous solution of 100 µM SePOH in absence (a) and in presence of (b) 5 mM phosphate buffer. Fig. (B) shows the variation in absorbance of transients (at 370 nm and 500 nm) at 20 µs after pulse radiolysing N_2O saturated aqueous solution of SePOH as a function of $H_2PO_4^-$ ions at pH 7.*

These studies indicate that (>Se∴OH) radical absorbing at 370 nm can decay by different competing pathways i.e. uncatalyzed spontaneous dissociation (k_d) (Path I in scheme 3.4), acid catalyzed elimination of hydroxide ion (k_h) (Path II in scheme 3.4) and reaction with another SePOH molecule (k_s) (Path III in scheme 3.4).[137]

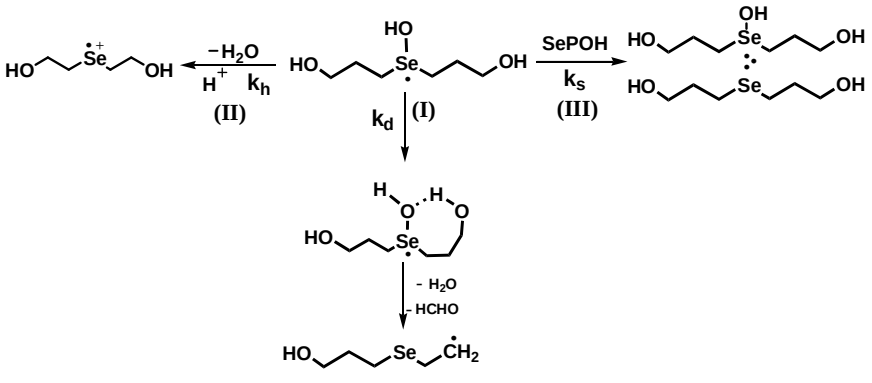

Scheme 3.4: *Different pathways for decay of (>Se∴OH) radical of SePOH.*

The experimentally observed rate constant (k_{obs}) for the decay of (>Se∴OH) radical can be expressed as given in equation 3.5.

$$k_{obs} = k_s[SePOH]^{+} k_h[H^+]^{+} k_d \quad (3.5)$$

The individual components were estimated by performing two different sets of experiments. In the first experiment, k_{obs} values were followed as a function of SePOH concentration, at pH 7 (Fig. 3.8). This resulted in a linear graph where the slope and intercept gives k_s and ($k_h[H^+]$ + k_d), respectively. In the second experiment, k_{obs} was followed as a function of H^+ ion concentration (inset of fig. 3.8), keeping SePOH concentration fixed and the slope and intercept of the linear plot were equal to k_h and (k_d + k_s[SePOH]).

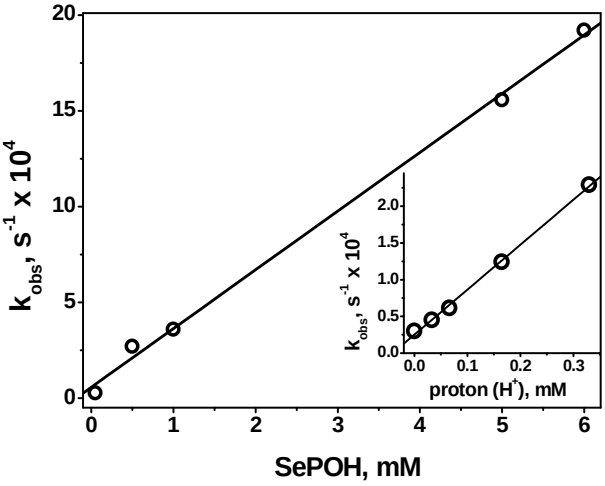

Fig. 3.8: *Linear increase in the rate constant for the decay of (>Se∴OH) radical as a function of SePOH concentration. Inset shows variation in the rate constant for the decay of (>Se∴OH) radical with change in proton concentration.*

Using these relations, k_s, k_h and k_d values were estimated to be (3.0 ± 0.1) x 10^8 $M^{-1}s^{-1}$, (6.8 ± 0.4) x 10^7 $M^{-1}s^{-1}$ and (2.5 ± 0.4) x 10^3 s^{-1}, respectively. The calculated value of k_d matched well with experimentally obtained value of k_{obs} of 100 µM SePOH (2.9 x 10^3 s^{-1}) in nanopure water where the contribution of $k_h[H^+]$ and k_s[SePOH] is negligible.

The absorbing species at 460 nm and 500 nm could be either (>$Se^{\bullet+}$) radical or (>Se∴Se<)$^+$ radical. To resolve this, absorbencies at 460 nm and 500 nm were followed as a function of SePOH concentration, where it was observed that the absorbance at both 460 nm and 500 nm increased with increase in SePOH concentration at a fixed concentration of phosphate buffer (Fig. 3.9). Like the 500 nm absorbing species, 460 nm transient also increased with increasing parent concentration, however the decay pattern (Fig. 3.6) at two wavelengths was different indicating that even though both the transients are formed through (>Se∴OH) radical, they appear to have different structures.

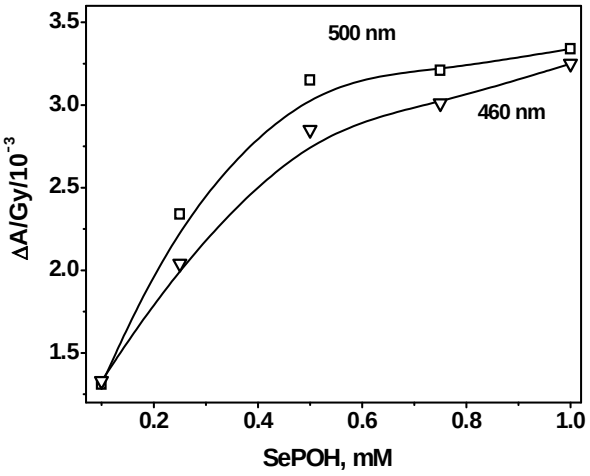

Fig. 3.9: *The variation in absorbance of transients absorbing at 460 nm and 500 nm as a function of SePOH concentration at pH 7.*

This was further confirmed by performing the reaction with $N_3^{\bullet}$ radical, a specific one electron oxidant.[139] The transient spectrum generated on reaction of 1 mM SePOH with $N_3^{\bullet}$ radical showed only one peak with maximum at 460 nm. As $N_3^{\bullet}$ radical is a specific one-electron oxidant, it will oxidize SePOH to SePOH radical cation (>$Se^{\bullet+}$) (equation 3.6), which can combine with parent molecule (SePOH) to form (>$Se\therefore Se<)^+$ radical (equation 3.4).

$$> Se + N_3^{\bullet} + \rightarrow > Se^{\bullet+} + N_3^- \qquad (3.6)$$

Fig. 3.10(A) shows the transient absorption spectrum generated by reaction of $N_3^{\bullet}$ radical with 1 mM SePOH. Unlike, $^{\bullet}$OH radical reaction, the transient spectrum generated by $N_3^{\bullet}$ radical produced only one absorption band with wavelength maximum at 460 nm and the decay profile of the transients both at 460 nm and 500 nm was similar (inset of fig. 3.10(B)). These results suggest that the species absorbing at 460 nm is (>$Se\therefore Se<)^+$ radical (equation 3.4) formed through the one-electron oxidation. As transient absorbing at 500 nm is not observed for $N_3^{\bullet}$ radical reaction with SePOH, it indicates that the later is not formed through (>$Se^{\bullet+}$) radical. Therefore, formation of 500 nm transient is proposed to take place by association of (>$Se\therefore OH$) adduct with the parent SePOH (equation 3.7). Similar kinds of transients have been proposed to be formed during reaction of $^{\bullet}$OH radical with dimethylsulfide by Schoneich et al.[124a]

$$> Se\therefore OH + > Se \rightarrow > (HO)Se\therefore Se < \qquad (3.7)$$

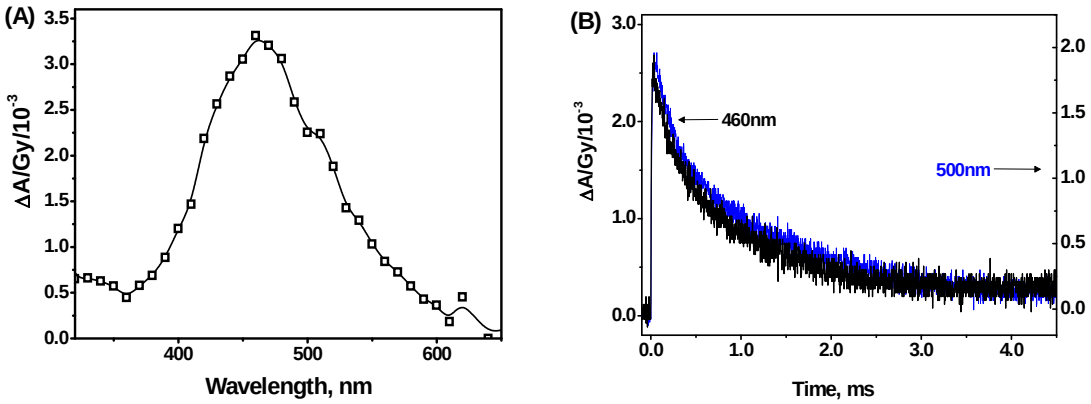

Fig. 3.10: *Transient absorption spectrum obtained at 40 μs after pulse radiolysing N_2O saturated aqueous solution of 0.1 M sodium azide containing 1 mM SePOH at pH 7. Inset shows overlay of absorption-time plot of transients absorbing at 460 nm and 500 nm.*

3.3.1.3 SeBOH

The transient spectra generated by radiolysing N_2O saturated aqueous solution of SeBOH showed similar features as that of SeEOH and SePOH. As seen in fig. 3.11, the spectra showed absorption band at 500 nm and another weak absorption band at ~320 nm. To characterize the transients, their spectra were monitored as a function of SeBOH concentration ((a)-50 μM, (b)- 100 μM and (c)- 500 μM). With increase in SeBOH concentration, the absorbance at 500 nm increased significantly with no other spectral changes. This indicated that the transient absorbing at 500 nm is the major species formed during the reaction of $^{\bullet}OH$ radical with SeBOH. In another experiment, the absorbance at 500 nm was monitored as a function of $H_2PO_4^-$ ion concentration, where the absorbance at 500 nm was found to increase with increase in $H_2PO_4^-$ ion concentration as shown in inset

of fig. 3.11. Based on these results and in analogy with that of SeEOH and SePOH, the transient absorbing at 500 nm was attributed to $(>Se\therefore Se<)^{+}$ radical.

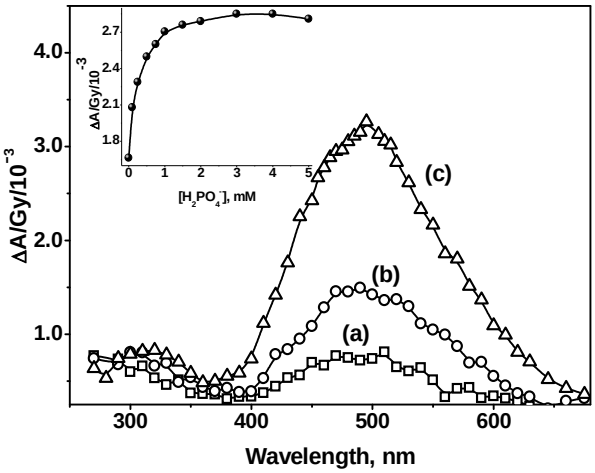

Fig. 3.11: *Transient absorption spectra obtained at 5 μs after pulse radiolysing N_2O saturated aqueous solution of (a) 50 μM, (b) 100 μM and (c) 500 μM SeBOH at pH 7. Inset shows the variation in absorbance of transient absorbing at 500 nm as a function of $H_2PO_4^-$ ion concentration.*

To confirm this, the reaction of SeBOH with $N_3^{\bullet}$ radical was carried out. As seen in fig. 3.12, the transient absorption spectrum generated by reaction of 1 mM SeBOH with $N_3^{\bullet}$ radical showed single absorption band with maximum at 500 nm with similar spectral features as obtained from the reaction with $^{\bullet}$OH radical. This confirmed that the transient absorbing at 500 nm is $(>Se\therefore Se<)^{+}$ radical.

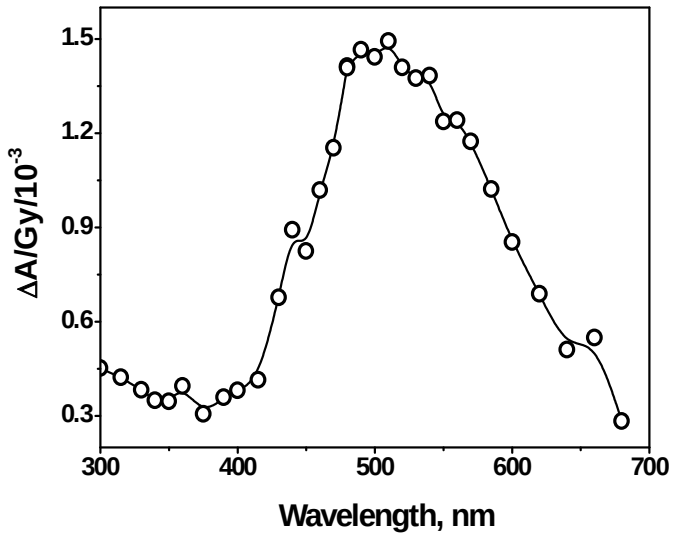

Fig. 3.12: *Transient absorption spectra generated at 5 μs after pulse radiolysing N_2O saturated aqueous solution of 0.1 M NaN_3 containing 1 mM SeBOH at pH 7.*

Since $^{\bullet}$OH radical is non-selective in its reactions, it can also react with SeROH via H-abstraction from alkyl chain, leading to formation of C-centered radicals. To assess the contribution of the transients formed by H-abstraction in the transient absorption spectra, the reaction of H atom with SeROH was carried out. Fig. 3.13 represents the transient absorption spectra generated by reaction of H atom with SeEOH, SePOH and SeBOH. It is clear from the spectra that none of these compounds on reaction with H atom produced any transient having absorption 280-600 nm wavelength regions. From this, it can be concluded that the transient spectra generated by pulse radiolysis of N_2O saturated solution of SeROH is obtained by direct electron transfer reaction only and have no contribution from H-abstraction reaction.

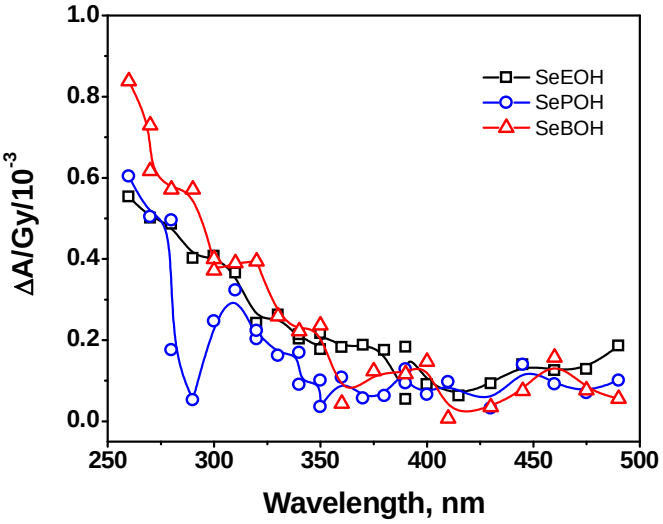

Fig. 3.13: *Transient absorption spectra generated at 40 µs after pulse radiolysing N_2 saturated aqueous solution containing 0.1 M perchloric acid ($HClO_4$), 1 mM t-butanol and 0.5 mM SeROH.*

As discussed earlier in chapter 2, the rate constant ($k_{SeROH+•OH}$) for the reaction of $^{•}$OH radical with SeROH compounds can be calculated by following the formation of $(>Se\therefore Se<)^{+}$ radical, however, since $(>Se\therefore Se<)^{+}$ radical exists in equilibrium with $(>Se^{•+})$, this can lead to error in $k_{SeROH+•OH}$ measurements. Therefore, $k_{SeROH+•OH}$ was determined by employing competition kinetics (details given in chapter 2) using isopropanol (ISP) as reference solute.[140] ISP reacts with $^{•}$OH radical with a bimolecular rate constant of $k_{ISP+•OH}=1.9 \times 10^{9}$ $M^{-1}s^{-1}$ as shown in equation 3.8. Also, as discussed earlier, the reaction of $^{•}$OH radical with SeROH compounds results in formation of $(>Se\therefore Se<)^{+}$ radical as shown in equation 3.9 where $k_{SeROH+•OH}$ represents the bimolecular rate constant for the reaction of $^{•}$OH radical with SeROH compounds. For a solution containing both SeROH and ISP, there will be competition for $^{•}$OH radical by both

SeROH and ISP, depending on their concentrations. Therefore the amount of $(>Se\therefore Se<)^+$ radical formed will decrease as a function of ISP concentration.

$$^{\bullet}OH + ISP \xrightarrow{k_{ISP+^{\bullet}OH}} products \quad (3.8)$$

$$^{\bullet}OH + > Se \xrightarrow{k_{SeROH+^{\bullet}OH}} (> Se \therefore Se <)^+ + products \quad (3.9)$$

If A_0 and A are the absorbances of $(>Se\therefore Se<)^+$ radical at 500 nm in absence and presence of ISP then $k_{SeROH+^{\bullet}OH}$ can be estimated from equation 3.10.

$$\frac{A_o}{A} = 1 + \frac{k_{ISP+^{\bullet}OH}}{k_{SeROH+^{\bullet}OH}} \frac{[ISP]}{[SeROH]} \quad (3.10)$$

'A' was monitored as a function of ISP concentration (0-1 mM) keeping SeROH concentration fixed at 4 mM. Plotting $(A_0/A-1)$ v/s [ISP]/[SeROH], the slope was obtained as $k_{ISP+^{\bullet}OH}/k_{SeROH+^{\bullet}OH}$ from which $k_{SeROH+^{\bullet}OH}$ values were calculated. The results obtained, as listed in table 3.1, showed that $^{\bullet}$OH radical reacts with SeROH with a near diffusion controlled rate constant which did not change with alkyl chain length of SeROH compounds.

3.3.1.4 Reaction with $CCl_3O_2^{\bullet}$ radical

$CCl_3O_2^{\bullet}$ radicals are model peroxyl radicals and can be conveniently generated by pulse radiolysis.[141] As seen in fig. 3.14(A), the reaction of $CCl_3O_2^{\bullet}$ radicals with SeEOH, SePOH and SeBOH generated transient spectra with absorption maxima at 460 nm, 480 nm and 500 nm, respectively, similar to those observed for $^{\bullet}$OH radical reactions. The

decay pattern of the transients obtained from the reaction of SeROH with $CCl_3O_2^{\bullet}$ radicals showed similarity with $(>Se\therefore Se<)^+$ radical. In analogy with reaction of SeROH with $^{\bullet}OH$ radical and $N_3^{\bullet}$ radical, these bands were assigned to $(>Se\therefore Se<)^+$ radical.

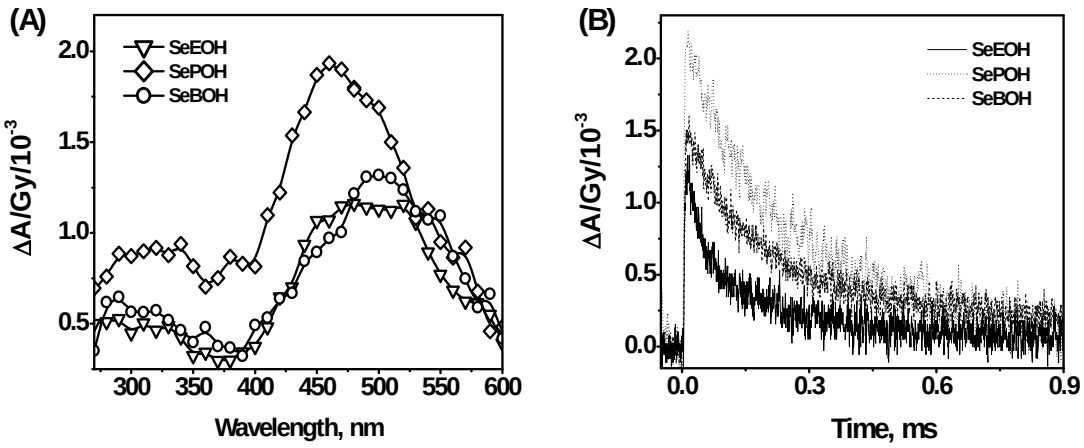

Fig. 3.14: *(A) Transient absorption spectra obtained at 5 μs after pulse radiolysing aqueous solution of 2 mM SeROH in an aqueous matrix containing 4% carbon tetrachloride (CCl_4), and 48% isopropanol at pH 7. Fig. (B) shows the absorbance time decay traces of 2 mM SeROH in above said matrix at 480 nm, 460 nm and 500 nm, respectively.*

Fig. 3.14(B) shows the absorption-time plot for the decay of $(>Se\therefore Se<)^+$ radical generated during reaction of $CCl_3O_2^{\bullet}$ radical with SeROH. These radicals followed second order decay kinetics with $2k/\varepsilon l$ value of $(9.2 \pm 0.5) \times 10^5$, $(7.6 \pm 0.6) \times 10^5$ and $(5.8 \pm 0.4) \times 10^5$ s^{-1} for SeEOH, SePOH and SeBOH, respectively. These results showed that the $(>Se\therefore Se<)^+$ radical of SeEOH is less stable than that generated from SePOH and SeBOH. The bimolecular rate constant for the reaction of $CCl_3O_2^{\bullet}$ radical with SeROH was

estimated by employing competition kinetics using $ABTS^{2-}$ as reference solute (Table 3.1).[142] $CCl_3O_2^{\bullet}$ radical reacts with $ABTS^{2-}$ to with a rate constant of $k_{ABTS^{2-}+CCl3O2\bullet}$ to form $ABTS^{\bullet-}$ radical as shown in equation 3.11, formation of which can be monitored by following is absorbance at 645 nm.

$$CCl_3O_2^{\bullet} + ABTS^{2-} \xrightarrow{k_{ABTS^{2-}+CCl_3O_2^{\bullet}}} CCl_3O_2^{-} + ABTS^{\bullet-} \quad (3.11)$$

$$CCl_3O_2^{\bullet} + > Se \xrightarrow{k_{SeROH+CCl_3O_2^{\bullet}}} CCl_3O_2^{-} + (> Se \therefore Se <)^{+} \quad (3.12)$$

On addition of SeROH, both $ABTS^{2-}$ and SeROH (equation 3.12) will react competitively with $CCl_3O_2^{\bullet}$ radical and the bimolecular rate constant ($k_{SeROH+CCl3O2\bullet}$) for the reaction of SeROH with $CCl_3O_2^{\bullet}$ radical will be given by equation 3.13.

$$\frac{A_o}{A} = 1 + \frac{k_{SeROH+CCl_3O_2^{\bullet}}}{k_{ABTS^{2-}+CCl_3O_2^{\bullet}}} \frac{[SeROH]}{[ABTS^{2-}]} \quad (3.13)$$

Where A_0 and A are the absorbancies of $ABTS^{\bullet-}$ radical at 645 nm, in absence and presence of 10-100 μM SeROH.

Table 3.1: *Rate constant values for the reaction of SeROH with $^{\bullet}OH$ and $CCl_3O_2^{\bullet}$ radicals.*

Compounds		SeEOH	SePOH	SeBOH
Rate constant (k) $x10^9$ $M^{-1}s^{-1}$	$k_{SeROH+\bullet OH}$	10.0 ± 0.1	7.3 ± 0.1	9.7 ± 0.1
	$k_{SeROH+CCl3O2\bullet}$	0.48 ± 0.04	0.88 ± 0.03	1.13 ± 0.06

The estimated values for $k_{SeROH+CCl3O2}$• are listed in table 3.1. The results showed that the reactivity of SeROH compounds towards $CCl_3O_2^{\bullet}$ radical increases with increase in alkyl chain length of SeROH.

3.3.1.5 Estimation of the equilibrium constant for the formation of (>Se∴Se<)$^+$ radical

As discussed earlier, the reaction of $^{\bullet}$OH radical leads to formation of $(>Se)^{\bullet+}$ radical and $(>Se\therefore Se<)^+$ radical as shown in equation 3.3 and 3.4. The formation of $(>Se)^{\bullet+}$ radical was very fast (~10^9 $M^{-1}s^{-1}$) while $(>Se\therefore Se<)^+$ radical was found to be formed at comparatively lower rate (~10^5 $M^{-1}s^{-1}$). Formation of $(>Se\therefore Se<)^+$ radical can be defined by the equilibrium between $(>Se)^{\bullet+}$ radical and $(>Se\therefore Se<)^+$ radical and is independent of primary reactions involved in formation of $(>Se)^{\bullet+}$ radical as shown in equation 3.4. The equilibrium constant (K_{eq}) for this reaction was calculated by following the absorbance of $(>Se\therefore Se<)^+$ radical at pH 7 and pH 1 as a function of SeROH concentration (0.1 mM- 1 mM) according to equation 3.14.[80]

$$\frac{1}{A} = \frac{1}{A_{\max}} + \frac{1}{K_{eq} A_{\max}} \frac{1}{[SeROH]} \qquad (3.14)$$

Where, A is the absorbance of $(>Se\therefore Se<)^+$ radical of SeROH at 500 nm. Fig. 3.15 (A & B) shows the linear plot for variation in absorbance of $(>Se\therefore Se<)^+$ radical as a function of SeROH concentration (0.1 mM-1 mM) at pH 7 and pH 1, respectively.

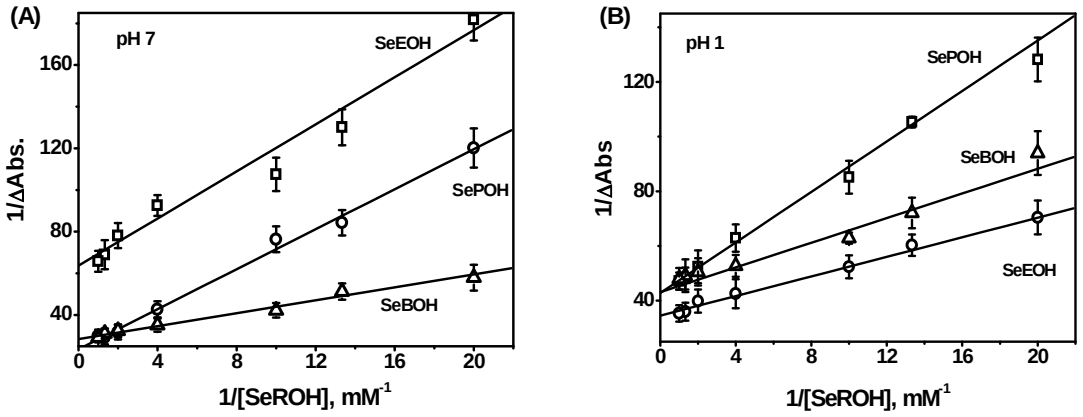

Fig. 3.15: *Double reciprocal plot for variation in absorbance of* $(>Se\therefore Se<)^{+}$ *radical at 500 nm as a function of SeROH concentration (0.1 mM-1 mM) at (A) pH 7 and (B) pH 1.*

The ratio of the intercept and slope of the linear plots gave the K_{eq} values at pH 7 and pH 1, which are listed in table 3.2. It is evident that the K_{eq} value for the $(>Se\therefore Se<)^{+}$ radical decreased in the order SeBOH > SeEOH > SePOH.

Table 3.2: *The decay rate constants and equilibrium constant for the formation of* $(>Se\therefore Se<)^{+}$ *radical.*

Compounds	Equilibrium constant (K, M^{-1}) x 10^4		$(>Se\therefore Se<)^{+}$ radical decay rate constant	
	pH 1	pH 7	First order (k, s^{-1}) x10^3 (at low SeROH conc.)	Second order (k, $M^{-1}s^{-1}$) x10^8 (at high SeROH conc.)
SeEOH	2.0 ± 0.2	1.1 ± 0.2	4.0 ± 0.3	15.2 ± 0.8
SePOH	0.8 ± 0.1	4.2 ± 0.3	3.5 ± 0.2	10.3 ± 0.3
SeBOH	3.5 ± 0.2	2.8 ± 0.3	3.2 ± 0.2	9.4 ± 0.2

The absorption-time plot of the $(>Se\therefore Se<)^+$ radical showed complex decay kinetics. At lower concentration (<1 mM), the $(>Se\therefore Se<)^+$ radical decayed by first order kinetics and shifted to second order at higher concentrations (>1 mM). As, there is an equilibrium between $(>Se)^{\bullet+}$ radical and $(>Se\therefore Se<)^+$ radical (equation 3.4), at lower concentration of SeROH, $(>Se)^{\bullet+}$ radical is the dominant species, which may undergo deprotonation or neutralization through first order kinetics as given in equation 3.15 and 3.16. Therefore, at lower concentrations of SeROH, $(>Se\therefore Se<)^+$ radical was observed to decay by first order kinetics.

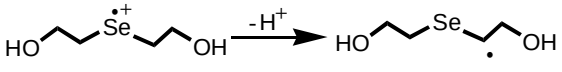

(3.15)

$$> Se^{\bullet+} + H_2O \rightarrow (> Se\therefore OH) + H^+ \qquad (3.16)$$

However, at higher concentrations (~2 mM), the equilibrium is mainly shifted towards right direction i.e. $(>Se\therefore Se<)^+$ radical formation, which can undergo radical-radical reaction and follow second order decay kinetics as shown in equation 3.17.

$$2(> Se\therefore Se<)^+ \rightarrow\!> Se^{2+} + 3Se< \qquad (3.17)$$

The absorption –time plots of $(>Se\therefore Se<)^+$ radical of SeROH compounds were fitted to second order to give decay rate constant values in the form of $2k/\varepsilon l$, where ε is the extinction coefficient of $(>Se\therefore Se<)^+$ radical. To get the actual value of k, the ε values of $(>Se\therefore Se<)^+$ radical were calculated using transient absorption spectra of SeROH at pH 1, where formation of $(>Se\therefore Se<)^+$ radical is quantitative and the $G_{\bullet OH}$ (0.27 μmol/J) can be

directly considered as $G_{(>Se\therefore Se<)+}$. Using $G_{(>Se\therefore Se<)+}$ as 0.27 μmol/J, the calculated ε values of $(>Se\therefore Se<)^+$ radical were (7.3 ± 0.2) x 10^3, (9.8 ± 0.5) x 10^3 and (7.9 ± 0.3) x 10^3 $M^{-1}cm^{-1}$ for $(>Se\therefore Se<)^+$ radical of SeEOH, SePOH and SeBOH, respectively. Substituting these values in 2k/εl, k values were calculated and are listed in table 3.2. The results indicated that the rate constant for the decay of $(>Se\therefore Se<)^+$ radical decreased with increase in alkyl chain length, which may be due to the steric interference from alkyl chain during radical-radical reactions and the same may be responsible for the increase in stability of $(>Se\therefore Se<)^+$ radical with increase in alkyl chain length.

3.3.2 Oxidizing vs. reducing transients formed during reaction of $^{\bullet}OH$ radical with SeROH

The different types of radicals produced during the reaction of SeROH with $^{\bullet}OH$ radical can be oxidizing or reducing in nature. The $(>Se\therefore Se<)^+$ radical which is the main observed transient will be oxidizing in nature while the C-centered radicals will be reducing in nature. The redox properties of these transients can be studied by monitoring their reaction with suitable redox couples.

3.3.2.1 Oxidizing radicals

In the present study, the oxidizing ability of the $(>Se\therefore Se<)^+$ radical was estimated by utilizing their reaction with $ABTS^{2-}$ ($ABTS^{\bullet-}/ABTS^{2-}$, E^0=+0.67 V vs NHE). The $(>Se\therefore Se<)^+$ radical of SeROH will oxidize $ABTS^{2-}$ to $ABTS^{\bullet-}$ and the resultant reaction

can be monitored by following the absorbance of $ABTS^{\bullet-}$ at 645 nm ($\varepsilon_{645nm} = 1.3 \times 10^4$ $M^{-1}cm^{-1}$) as shown in equation 3.18.

$$\boldsymbol{ABTS}^{2-} + (> \boldsymbol{Se} \therefore \boldsymbol{Se} <)^{+} \rightarrow \boldsymbol{ABTS}^{\bullet-} + 2 > \boldsymbol{Se} \qquad (3.18)$$

For this, N_2O-saturated aqueous solutions of 5 mM SeROH containing 10-100 µM $ABTS^{2-}$ were pulse irradiated. Due to high concentration of SeROH, contribution of $(>Se)^{\bullet+}$ radicals will be minimum and $(>Se\therefore Se<)^{+}$ radical will be the predominant species (90-95%). As, the reactivity of $(>Se\therefore Se<)^{+}$ radical would reflect its stability, bimolecular rate constant for the reaction of $(>Se\therefore Se<)^{+}$ radical with $ABTS^{2-}$ was estimated and the values are listed in table 3.3. The results indicated that the $(>Se\therefore Se<)^{+}$ radical of SeEOH is a stronger oxidant compared to SePOH and SeBOH. As the reaction between $(>Se\therefore Se<)^{+}$ radical and $ABTS^{2-}$ is stoichiometric and takes place with a nearly diffusion controlled rate constant, the G-value of $ABTS^{\bullet-}$ radical estimated under the present experimental condition can be directly equated to the amount of $(>Se\therefore Se<)^{+}$ radical.

Table 3.3: *The* G-value *and rate constant for the reaction of* $(>Se\therefore Se<)^{+}$ *radical with* $ABTS^{2-}$.

Compounds	Reaction with oxidising radical ($ABTS^{\bullet-}$/ $ABTS^{2-}$)	
	G-value, µmol/J	Rate constant ($k_{(>Se\therefore Se<)^{+}+ABTS^{\bullet-}}$), $M^{-1}s^{-1}$
SeEOH	0.22 ± 0.03	(6.0 ± 0.3) x 10^9
SePOH	0.34 ± 0.02	(3.6 ± 0.2) x10^9
SeBOH	0.31 ± 0.03	(4.1 ± 0.2) x10^9

The estimated G-value of the $(>Se\therefore Se<)^+$ radical of SeROH are listed in table 3.3. The results indicated that G-value of the $(>Se\therefore Se<)^+$ radical was the lowest for SeEOH followed by SeBOH and SePOH. From these results, it can be seen that the reactivity of $(>Se\therefore Se<)^+$ radical and the estimated G-value for $(>Se\therefore Se<)^+$ radical are not in the same order. Although the $(>Se\therefore Se<)^+$ radical of SeEOH showed highest reactivity towards $ABTS^{2-}$, the estimated G-value of $(>Se\therefore Se<)^+$ radical was the least.

3.3.2.2 Reducing radicals

The total reducing radicals which include α-reducing radicals (equation 3.15) and other C-centered radicals (path II in scheme 3.3) were estimated by monitoring the G-value of methyl viologen ($MV^{\bullet+}$) radical produced by the reduction of MV^{2+}. For this, N_2O saturated aqueous solutions containing 5 mM of SeROH and (10 µM - 100 µM) MV^{2+} were pulse radiolyzed and the formation of $MV^{\bullet+}$ at 605 nm was monitored. [143] The reaction system containing SeEOH did not show any signal at 605 nm, while that produced from SePOH and SeBOH reduced MV^{2+} with rate constant in the order of ~ 10^8 -10^9 $M^{-1}s^{-1}$. Similar reaction pattern was observed with other systems like duroquinone (DQ; $DQ/DQ^{\bullet-}$, E^0=-0.26 V).[144] The low reducing ability of the radical derived from SeEOH was also confirmed from its reaction with thionine (Th; $Th^{2+}/Th^{\bullet+}$, E^0=+0.06 V), where the rate constant was (7.4 ± 0.2) x 10^8 $M^{-1}s^{-1}$, while the radicals from SePOH and SeBOH reacted with the rate constants of ~10^9 $M^{-1}s^{-1}$.[145] The bimolecular rate constant values along with the respective G-value of reducing radicals are given in table 3.4.

Table 3.4: *The* G-value *and the rate constant values for the reaction of reducing radicals with different redox couples.*

Comp.	Reaction with reducing radicals					
	G-value, μmol/J			Rate constant (k), $M^{-1}s^{-1}$ x10^9		
	$Th^{2+}/Th^{\bullet+}$	$MV^{2+}/MV^{\bullet+}$	$DQ/DQ^{\bullet-}$	$Th^{2+}/Th^{\bullet+}$	$MV^{2+}/MV^{\bullet+}$	$DQ/DQ^{\bullet-}$
SeEOH	0.11 ± 0.02	No reaction	No reaction	0.74 ± 0.02	No reaction	No reaction
SePOH	0.13 ± 0.02	0.14 ± 0.02	0.13 ± 0.01	2.6 ± 0.3	0.94 ± 0.05	0.76 ± 0.03
SeBOH	0.13 ± 0.01	0.17 ± 0.02	0.15 ± 0.04	1.9 ± 0.1	1.4 ± 0.2	2.0 ± 0.2

As shown in table 3.4, the G-values of reducing radicals were comparable for SeEOH, SePOH and SeBOH. The combined G-value of transients (both oxidizing and reducing radicals) for SeEOH, SEPOH and SeBOH was found to be ~55%, ~78% and ~80% of the initial $^{\bullet}OH$ radical (0.6 μmol/J) generated. These results can be explained on the basis of the stability of $(>Se\therefore Se<)^+$ radical. The $(>Se\therefore Se<)^+$ radical of SeEOH decays faster (k=1.52 ± 0.08 x 10^9 $M^{-1}s^{-1}$) compared to that of SePOH (k=1.03 ± 0.3 x 10^9 $M^{-1}s^{-1}$) and SeBOH (k=9.4 ± 0.2 x 10^8 $M^{-1}s^{-1}$). Due to higher rate constant for the decay of $(>Se\therefore Se<)^+$ radical of SeEOH, the self decay of $(>Se\therefore Se<)^+$ radical will compete with the electron transfer reaction (k=~10^9 $M^{-1}s^{-1}$) with a given redox couple. This will lead to loss of $(>Se\therefore Se<)^+$ radicals during the measurement and results in lower value of estimated value than the true value.

3.3.3 Analysis of products formed during reaction of •OH radical with SeROH

The $(>Se\therefore Se<)^{+}$ radicals formed in the above reactions may undergo disproportionation reaction to form selenoxide as one of the products according to equation 3.17 and 3.19.[123a]

$$> Se^{2+} \xrightarrow{H_2O} > Se = O + 2H^{+} \qquad (3.19)$$

Formation of selenoxide can be confirmed by their direct identification using HPLC or by utilising its reaction with thiols. In the present study, both these methods were utilised to estimate the G value of $SeROH_{ox}$. For this, 3 ml of N_2O saturated solutions of 5 mM SeROH were irradiated using γ-source with a total absorbed dose of 830 Gy. The samples were eluted from HPLC column using 5:95 acetonitrile:water as mobile phase followed by absorption detection at 240 nm. The observed HPLC chromatogram of the radiolysed SeROH solutions showed two major peaks corresponding to SeROH and $SeROH_{ox}$. Fig. 3.16 shows the HPLC chromatogram of radiolysed samples of (a) SeEOH, (b) SePOH and (c) SeBOH. Under present experimental condition, SeEOH, SePOH and SeBOH were eluted at 4.4, 10.2 and 36.9 minutes, respectively while their corresponding selenoxides were eluted at 2.8, 3.2 and 3.8 minutes, respectively. The G-value of $SeROH_{ox}$ was calculated from the calibration curve obtained from the HPLC chromatogram generated by injecting 0.05 mM - 1.25 mM pure $SeROH_{ox}$ (Fig. 3.16 (d)) and the results are listed in table 3.5.

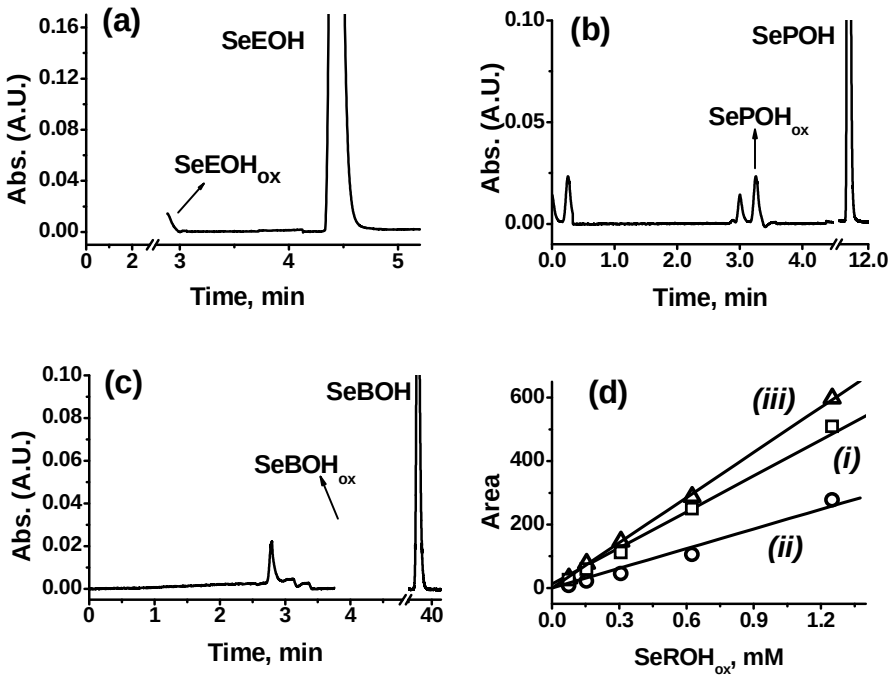

Fig. 3.16: *HPLC chromatogram showing the formation of (a) $SeEOH_{ox}$, (b) $SePOH_{ox}$ and (c) $SeBOH_{ox}$ through γ-radiation induced radiolytic degradation of N_2O saturated aqueous solution of 5 mM SeROH. Fig. (d) shows the calibration curve plotted by analysis of absorption peak area for the known concentrations (0.05 μM-1.25 mM) of (i) $SeEOH_{ox}$, (ii) $SePOH_{ox}$ and (iii) $SeBOH_{ox}$.*

In general selenoxides are unstable and undergo decomposition; therefore quantitative estimations by direct monitoring of $SeROH_{ox}$ may be subjected to errors. Therefore an indirect method was employed by utilizing their reaction with DTT. Selenoxides oxidize DTT to form its disulfide (DTT_{ox}) and parent selenium compound as shown in equation 3.20.

$$> \boldsymbol{Se} = \boldsymbol{O} + \boldsymbol{DTT} \rightarrow \boldsymbol{DTT_{ox}} + > \boldsymbol{Se} + 2\boldsymbol{H_2O} \qquad (3.20)$$

DTT_{ox} formed during this reaction can be detected and quantified using HPLC. For this, 180 µl of radiolysed SeROH samples (N_2O saturated aqueous solution of 5 mM seROH at pH 7) were incubated with 20 µl DTT (final concentration-2 mM) for 5 minutes to allow the reaction to complete. The resulting reaction mixture was injected to HPLC and eluted with 5:95 acetonitrile:water containing 0.1% TFA followed by absorption detection at 240 nm. Fig. 3.17 shows the chromatogram for DTT treated radiolyzed sample of SeEOH, where SeEOH, DTT and DTT_{ox} were observed at 4.3, 6.8 and 10.6 minutes, respectively. The amount of DTT_{ox} formed during the reaction was estimated by using the calibration plot made from the HPLC chromatogram obtained by injecting 0.1 mM- 0.6 mM pure DTT_{ox}.

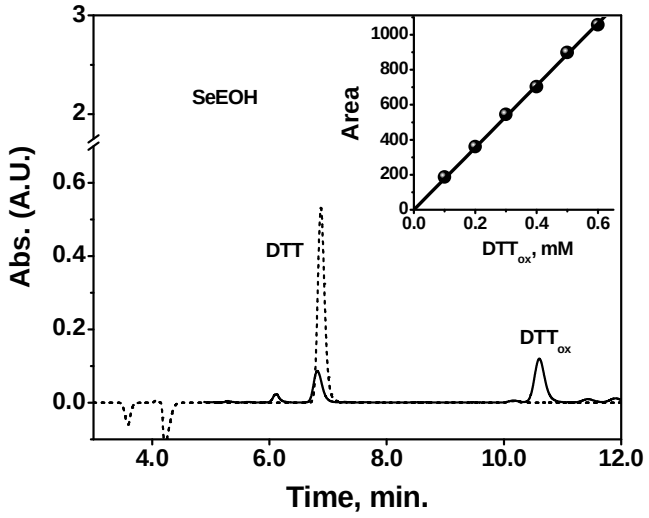

Fig. 3.17: *HPLC chromatogram for the reaction mixture containing irradiated SeEOH (5 mM) and 2 mM DTT. Inset shows the calibration plot for the area of DTT_{ox} peak as a function of DTT_{ox} concentration (0.1 mM-0.6 mM).*

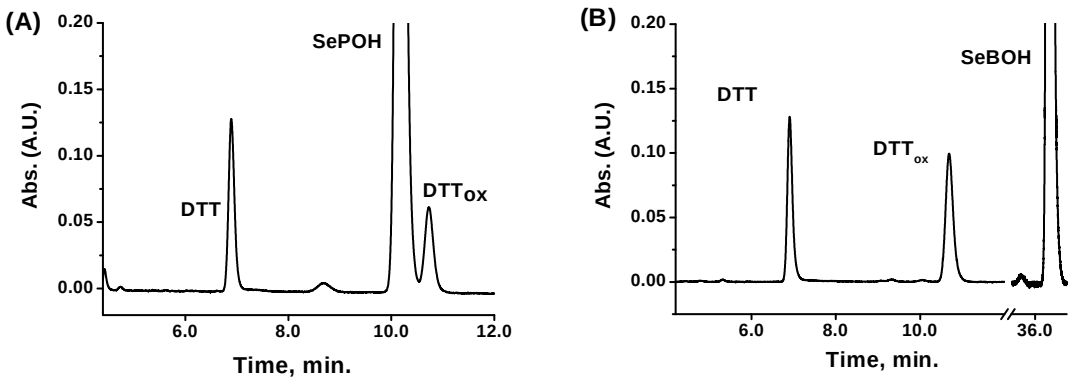

Fig. 3.18: *HPLC chromatogram showing formation of DTT_{ox} on treating irradiated 5 mM of (A) SePOH and (B) SeBOH with 2 mM DTT.*

Fig. 3.18 represents the HPLC chromatograms of reaction mixtures containing 2 mM DTT and radiolyzed samples of 5 mM of (A) SePOH and (B) SeBOH. Using this method, the G-value of selenoxides was estimated to be (0.23 ± 0.02), (0.29 ± 0.02) and (0.31 ± 0.03) µmol/J for SeEOH, SePOH and SeBOH, respectively. These values are close to that observed by direct method (table 3.5), indicating stability of the selenoxides. The estimated values of $SeEOH_{ox}$, $SePOH_{ox}$ and $SeBOH_{ox}$ corresponded to 38.3%, 48.3% and 51.6% of the G-value of $^{\bullet}OH$ (0.6 µmol/J). The results further signify that the G-value of selenoxide increases with increasing alkyl chain length.

Table 3.5: *The G-values of $SeROH_{ox}$ and HCHO formed during reaction of $^{\bullet}OH$ radical with SeROH compounds at pH 7.*

Compounds	SeEOH	SePOH	SeBOH
$SeROH_{ox}$ (µmol/J)	0.20 ± 0.02	0.26 ± 0.02	0.29 ± 0.03
HCHO (µmol/J)	0.11 ± 0.01	< 0.05	< 0.05

Schoneich et al have earlier reported that the reaction of •OH radical with bis(2-ethanol)sulfide (SEOH), a sulfur analogue of SeEOH, generated HCHO as one of the major products.[124b] Anticipating similar reaction for SeROH (Scheme 3.3), experiments were performed to detect HCHO.

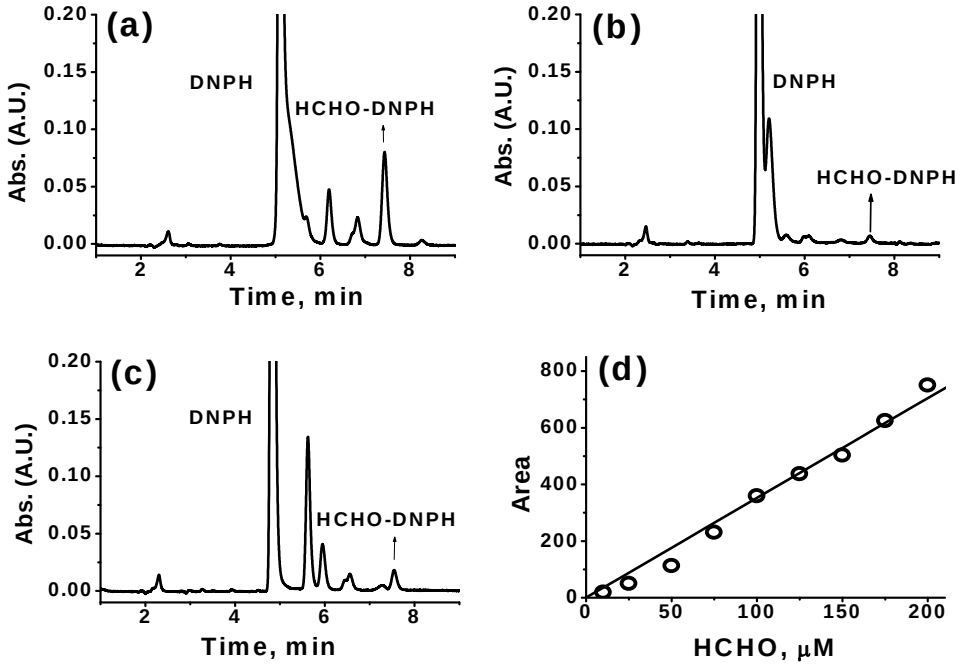

Fig. 3.19: *HPLC chromatograms generated by reaction of acidified DNPH (4 mM) with radiolyzed samples of 5 mM of (a) SeEOH, (b) SePOH and (c) SeBOH. Fig. (d) shows the calibration curve plotted by analysis of absorption peak area for the known concentrations (10 μM-200 μM) of HCHO-DNPH.*

For this, N_2O saturated aqueous solution of 5 mM SeROH were γ-radiolyzed with an absorbed dose of 830 Gy. These radiolyzed samples (180 μl) were further treated with 20 μl of 4 mM of acidified DNPH solution. HCHO reacts with acidified solution of DNPH

to form its hydrazone derivative (DNPH-HCHO) which can be easily detected using its absorption at 345 nm and quantified by HPLC measurements.[102] The different samples were then injected to HPLC and eluted using acetonitrile:water (60:40; v/v) mixture containing 0.1 % TFA as mobile phase. Under these experimental conditions, DNPH and DNPH-HCHO were eluted at 5.1 and 7.4 minutes, respectively, as shown in fig. 3.19 (a-SeEOH, b-SePOH and c-SeBOH). The G-value of HCHO was estimated using calibration plot obtained from the HPLC chromatogram generated by injecting known concentrations (10 μM-200 μM) of HCHO-DNPH (Fig. 3.19(d)) and the results are listed in table 3.5.

The G-value of HCHO was estimated to be 0.11 ± 0.01 μmol/J for SeEOH, which corresponds to ~ 18 % of the G-value of $^{\bullet}$OH radical (0.6 μmol/J). In case of SePOH and SeBOH, the G-value of HCHO was negligible and was less than 2%, of the total $^{\bullet}$OH radical. Using similar procedures, Schoneich et al reported a G-value of ~0.27 μmol/J for HCHO for the reaction of $^{\bullet}$OH radical with SEOH which corresponds to ~ 46% of the G-value of $^{\bullet}$OH radical.[124b] The unusually lower G-value of HCHO in SeEOH as compared to SEOH suggests that (>Se$\therefore$OH) radical of SeEOH decays to from (>Se$\therefore$Se<)$^{+}$ radical predominantly rather than HCHO formation. In contrast, the reaction of $^{\bullet}$OH radical with sulfur compound, SEOH results in formation of HCHO as major product and does not form (>S$\therefore$S<)$^{+}$ radical even at very high (0.1 M) concentration of SEOH.

3.3.4 Quantum chemical calculations

To compliment the experimental results obtained by pulse radiolysis experiments, energetics for the possible reaction pathways for the $^{\bullet}$OH radical reaction with the SeROH

was calculated by employing quantum chemical calculations at B3LYP/6-31+G(d,p) level.[146] Optimized ground state geometry of SeROH compounds in water was found to have C_1 point group and was free from any non-bonding interactions between selenium and oxygen atom of the hydroxyl group.

As seen in fig. 3.20, the HOMO is localized on selenium atom for all SeROH compounds.

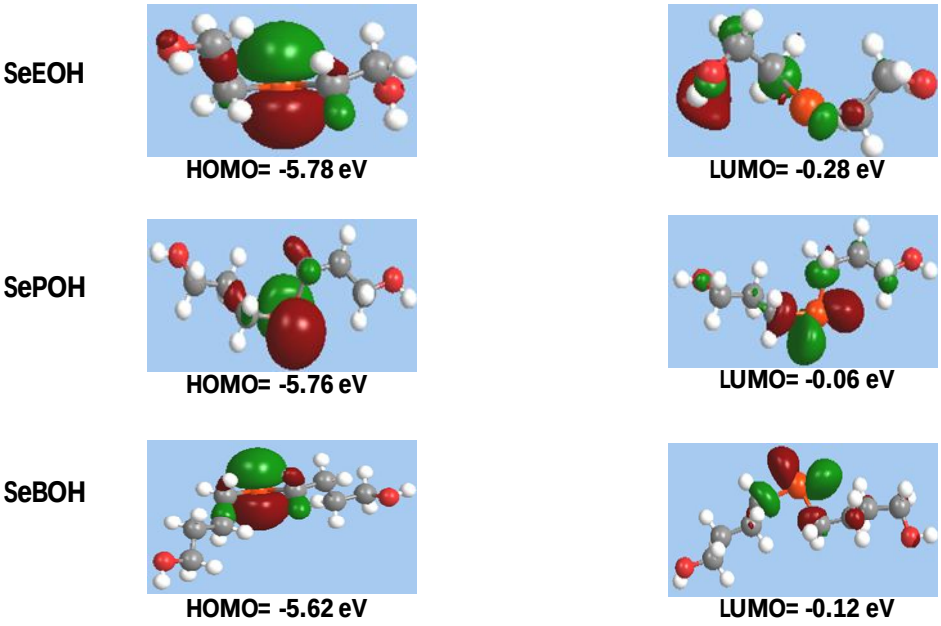

Fig. 3.20: *HOMO and lowest unoccupied molecular orbital (LUMO) images of SeROH compounds.*

Further, geometry of all the possible transients formed during $^{\bullet}$OH radical reaction with SeROH was optimized at UB3LYP/6-31+G (d,p) level. The feasibility of various possible reactions was estimated in terms of energy (B3LYP ground state energy) change (ΔE) during the reaction. Fig. 3.20 gives the pictorial view of energetics of different

pathways of the reaction of $^{\bullet}$OH radical with SeEOH. The values in the parenthesis represent the ΔE values in kcal/mol for a given reaction. As seen in fig. 3.21, the initial addition of $^{\bullet}$OH radical at selenium centre of SeEOH is endothermic (ΔE=+3.8 kcal/mol). Out of the three possible decay pathways of (>Se∴OH) radical, proton catalyzed formation of (>Se$^{\bullet+}$) radical is exoergic (ΔE=-82.5 kcal/mol) while formation of HCHO is endoergic (ΔE=+38 kcal/mol). This further supports the experimental observation that (>Se∴OH) decayed mainly through proton catalyzed dehydration to form (>Se$^{\bullet+}$) radical and only a small fraction leads to the formation of HCHO.

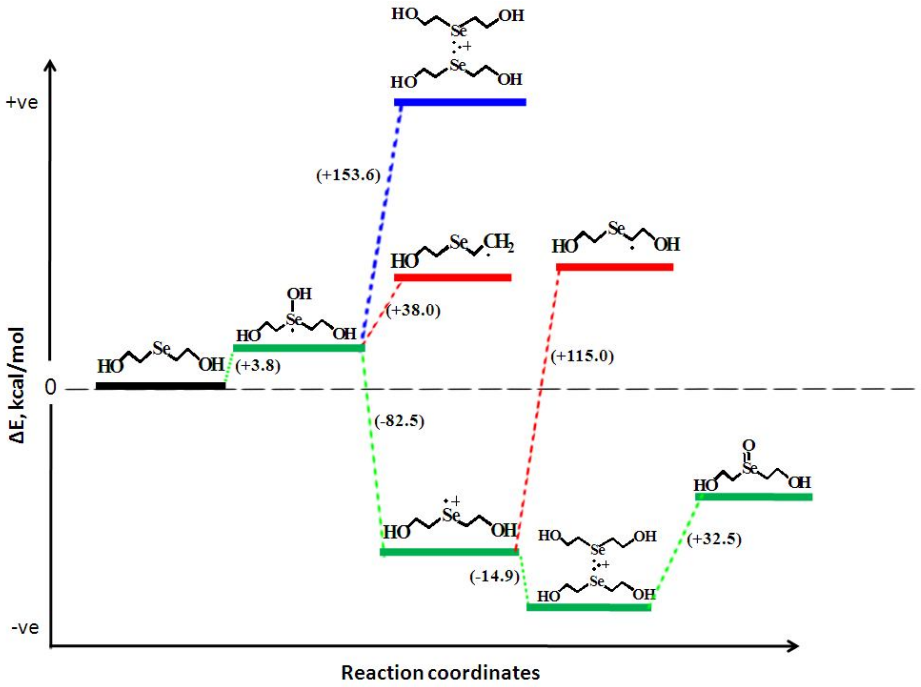

Fig. 3.21: *Energetics of the possible pathways for the reaction of $^{\bullet}$OH radical with SeEOH. The values in the parenthesis represent ΔE in kcal/mol for given reaction.*

Similar calculations were performed for SePOH and SeBOH and their different transients produced during their reaction with $^{\bullet}$OH radical. Figs. 3.22 and 3.23 represent

the pictorial presentation of ΔE for formation of various transients during the reaction of •OH radical with SePOH and SeBOH. The initial addition of •OH radical on SeROH is endoergic and endoergicity increases with increase in alkyl chain length.

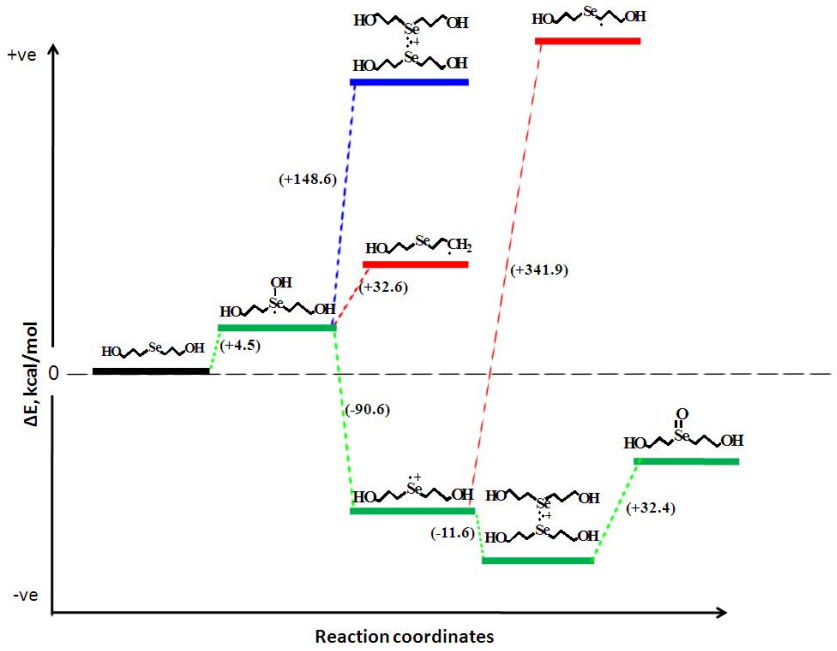

Fig. 3.22: *Energetics of the possible pathways for the reaction of •OH radical with SePOH. The values in the parenthesis represent ΔE in kcal/mol for given reaction.*

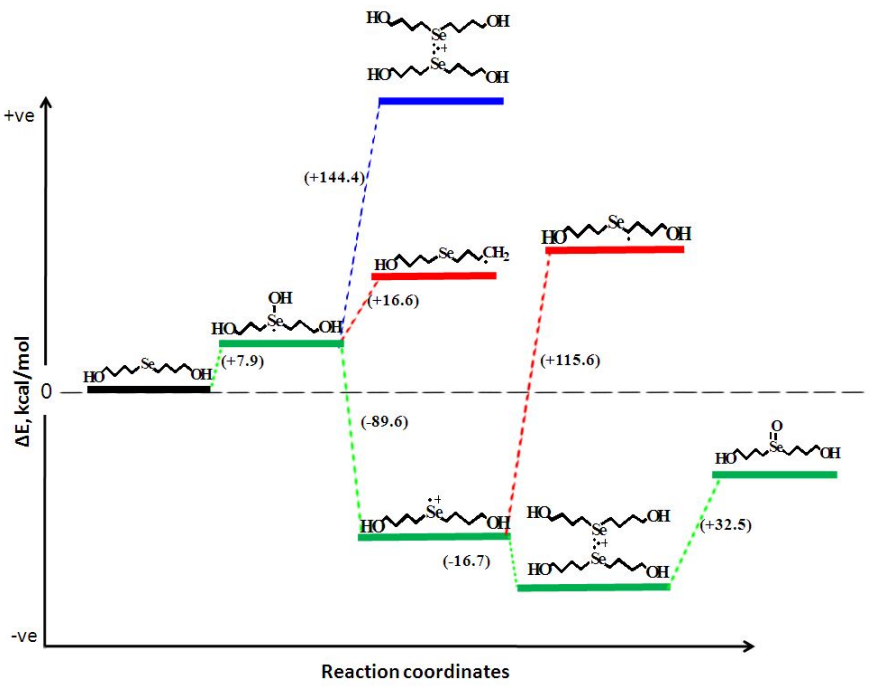

Fig. 3.23: *Energetics of the possible pathways for the reaction of $^{\bullet}$OH radical with SeBOH. The values in the parenthesis represent ΔE in kcal/mol for given reaction.*

The comparative results for the energetics of different pathways for the reaction of $^{\bullet}$OH radical with SeROH are summarized in table 3.6. From ΔE values, it can be stated that proton catalysed dehydration of (>Se∴OH) radical to form (>$Se^{\bullet+}$) radical is exothermic and more favorable in SePOH (ΔE = -90.56 kcal/mol) and SeBOH (ΔE = -89.6 kcal/mol) compared to SeEOH (ΔE = -82.53 kcal/mol). This may be due to possibility of stabilization of (>$Se^{\bullet+}$) radical of SePOH and SeBOH through formation of five and six-membered rings respectively by interaction of the lone pair of oxygen with the selenium centre. Such interaction if occurs in (>$Se^{\bullet+}$) radical of SeEOH, would lead to formation of a strained four-membered ring and therefore would lower the stability of this transient.

Table 3.6: *Energetics of the transients formed during the reaction of $^{\bullet}OH$ radical with SeROH compounds.*

Transients reactions	B3LYP energy change (ΔE, kcal/mol)					
	SeEOH	SePOH	SeBOH	SEOH	SPOH	SBOH
$>Se+^{\bullet}OH \rightarrow (>Se\therefore OH)$	3.49	4.51	7.94	173.81	134.58	258.89
$(>Se\therefore OH) \xrightarrow{H_3O^+} >Se^{\bullet+}+2H_2O$	-82.53	-90.56	-89.60	-82.45	-96.72	-98.71
$(>Se\therefore OH) \rightarrow >Se^{\bullet+}+OH^-$	356.02	340.78	349.56	350.53	347.11	340.79
$>Se^{\bullet+} \xrightarrow{H_2O} \alpha-reducing\ radical+H_3O^+$	115.03	107.84	115.63	109.45	120.31	115.98
$>Se^{\bullet+} \xrightarrow{>Se} (>Se\therefore Se<)^+$	-14.89	-11.57	-16.68	151.68	122.21	236.37
$2(>Se\therefore Se<)^+ \xrightarrow{3H_2O} >Se=O+3>Se+2H_3O^+$	18.45	20.87	23.62	34.57	39.37	36.70

Further, the ($>Se^{\bullet+}$) radical, can decay by two competing reactions: (i) formation of $(>Se\therefore Se<)^+$ radical (Path IIIa in scheme 3.5) and (ii) irreversible loss of proton to form α-reducing radical (Path IIIb in scheme 3.5). As evident from table 3.7, the conversion of ($>Se^{\bullet+}$) radical to $(>Se\therefore Se<)^+$ radical is exothermic (ΔE = -82.53 to -90.56 kcal/mol) while that to form α-reducing radical is endothermic (ΔE = +107.84 to +115.63 kcal/mol), indicating that the former reaction is more favorable compared to the later. On close examination of the optimized structure of ($>Se^{\bullet+}$) radical derived from SeEOH, it was observed that the distance between the selenium centre and the hydrogen atom present at the α-carbon atom is less than the sum of their van der Waal radii, but larger than the normal bond distance indicating presence of non-bonding interactions.[147]

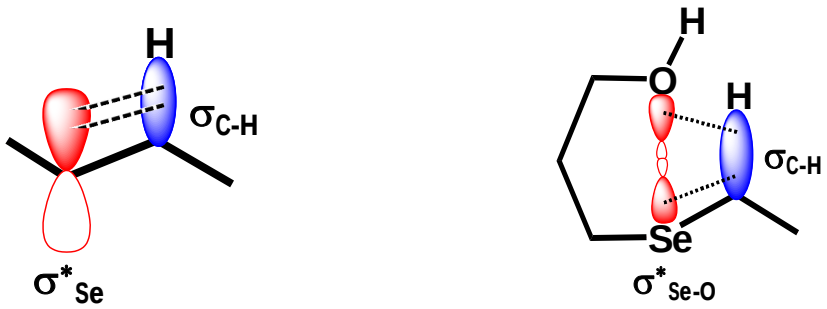

(a) **(b)**

Fig. 3.24: *Non-bonding interactions in (>Se$^{\bullet+}$) radical of (a) SeEOH and (b) SePOH as estimated by quantum chemical calculations in water at UB3LYP/6-31+G(d,p) level.*

The strength of such non-bonding interaction can be extrapolated by performing the natural bond order (NBO) analysis of the orbitals on (>Se$^{\bullet+}$) radical. The non-bonding interaction energy (E_{nb}) is the perturbation induced due to delocalization of an electron density in a bond and the value is directly correlated to the strength of interaction The NBO analysis indicated that in (>Se$^{\bullet+}$) radical of SeEOH, the σ-orbital of α-C-H interacts with the σ* orbital centered at selenium atom (Fig. 3.24a). On the other hand, for SePOH and SeBOH, the σ-orbital of α-C-H interacts with the σ* orbital of Se-O bond (Fig. 3.24b). E_{nb} for these interactions was 1.61, 1.41 and 1.32 kcal/mol for SeEOH, SePOH and SeBOH, respectively. These interactions will lead to irreversible deprotonation to form α-carbon centered radical. Stronger the non-bonding interactions, more will be the formation α-carbon centered radical. This will cause shifting of (>Se∴Se<)$^{+}$ radical equilibrium towards (>Se$^{\bullet+}$) radical (equation 3.4). The calculations clearly support the experimental results that due to stronger interaction between σ-orbital of α-C-H and the σ* orbital centered at selenium atom in SeEOH, the G-value of α-carbon centered radical will be more for SeEOH than for SePOH and SeBOH.

Comparison between organosulfur and organoselenium compounds

It is well established that the sulfur/selenium centered radical cations get stabilized by forming 2c-3e bond. In this, the p-orbital having lone pair electron (either the suitable hetero atom like N or O or another sulfur/selenium atom) overlap with another p-orbital containing unpaired electron on sulfur/selenium to form 2c-3e bond. In selenium, the orbitals are more diffused as compared to sulfur, thereby reducing the orbital overlap and inter electronic repulsion resulting in higher stability of $(>Se\therefore Se<)^{+}$ radical. Also, higher covalent radius in selenium reduces steric congestion at the selenium centre as compared to sulfur. These unique features allow the selenium atom to readily form $(>Se\therefore Se<)^{+}$ radical to the extent that other intermediates like $(>Se\therefore OH)$ radical and $(>Se^{\bullet+})$ radical are not observed. Further, stability of $(>Se\therefore Se<)^{+}$ radical can also be related to the HOMO levels of parent molecule and $(>Se^{\bullet+})$ radical. From the analysis of singly occupied molecular orbital (SOMO) and HOMO of $(>Se^{\bullet+})$ radical and parent SeROH molecule respectively, it was observed that SOMO of $(>Se^{\bullet+})$ radical energy lies close to HOMO of parent molecule (Energy difference < 2 eV). Therefore, overlapping between $(>Se^{\bullet+})$ radical and SeROH molecule becomes energetically favored. However, for sulfur compounds, the energy difference between $(>S^{\bullet+})$ radical and parent sulfur compound is large (Energy difference > 4 eV). This will lead to weak interaction between two sulfur atoms in $(>S\therefore S<)^{+}$ radical and destabilize $(>Se\therefore Se<)^{+}$ radical. As mentioned in table 3.6, the formation of $(>Se\therefore Se<)^{+}$ radical (ΔE=+122.1 kcal/mol) is energetically favored compared to $(>S\therefore S<)^{+}$ radical (ΔE > -11.57 kcal/mol). The high energy barrier makes the formation

of $(>S\therefore S<)^{+}$ less favorable and no $(>S\therefore S<)^{+}$ radical formation has been observed for sulfur analogues experimentally at neutral pH.

Other than stability of $(>Se\therefore Se<)^{+}$ radical, orbital energy levels were also found to affect deprotonation of $(>Se^{\bullet+})$ radical to form α-reducing radicals. As discussed earlier, deprotonation of chalcogen radical cation is favoured by efficient overlap of the p-orbital with the σ-orbital of α-C-H. Being a heavier atom, σ* orbital centered at selenium atom, is higher in energy ($E_{\sigma^{*}(Se)}$=+0.489 eV for SeEOH) than that of sulfur ($E_{\sigma^{*}(S)}$=+0.364 eV, for SEOH). The difference between energy of σ-orbital of α-C-H ($E_{\sigma C-H}$~0.22 eV) and σ* orbital is higher (ΔE= 0.269 eV) in SeEOH than that for SEOH (ΔE= 0.144 eV). Therefore, the non bonding interactions between the σ-orbital of α-C-H with σ* orbital are more favorable in SEOH than in SeEOH, which was further supported by their non bonding interaction energy (E_{nb}) (SeROH; E_{nb}= 1.32-1.61 kcal/mol and SROH; E_{nb}= 3.21-3.67 kcal/mol). These non bonding interactions would lead to easier deprotonation of $(>S^{\bullet+})$ radical and therefore higher G-value of α-reducing radicals in case of SROH compared to SeROH compounds. Since the reaction of $^{\bullet}$OH radical with SeROH compounds generates stable and recyclable transients as compared SROH, selenium compounds can be considered as better radical scavengers than their sulfur analogues.

Based on these results, the mechanism of the reaction of $^{\bullet}$OH radical with SeROH can be summarized in scheme 3.5. The reaction of $^{\bullet}$OH radical with SeROH involves initial attack of $^{\bullet}$OH radical at Se centre to form $(>Se\therefore OH)$ radical (path I). In case of SeEOH, $(>Se\therefore OH)$ radical is stabilized through formation of 6-membered ring which eliminates water molecule and HCHO leading to formation of C-centered radicals (path

IV). Similar reaction in SePOH and SeBOH will involve formation of thermodynamically unstable 7 and 8-membered rings. Therefore in SePOH and SeBOH, formation of C-centered radical is not favored and (>Se∴OH) radical mainly undergoes proton catalysed dehydration to form (>$Se^{\bullet+}$) radical (path II a&b). This radical decays either by path IIIa or IIIb to form (>Se∴Se<)$^{+}$ radical and α-reducing radical, respectively. The (>Se∴Se<)$^{+}$ radical further undergoes dismutation through path (V) and form $SeROH_{ox}$.

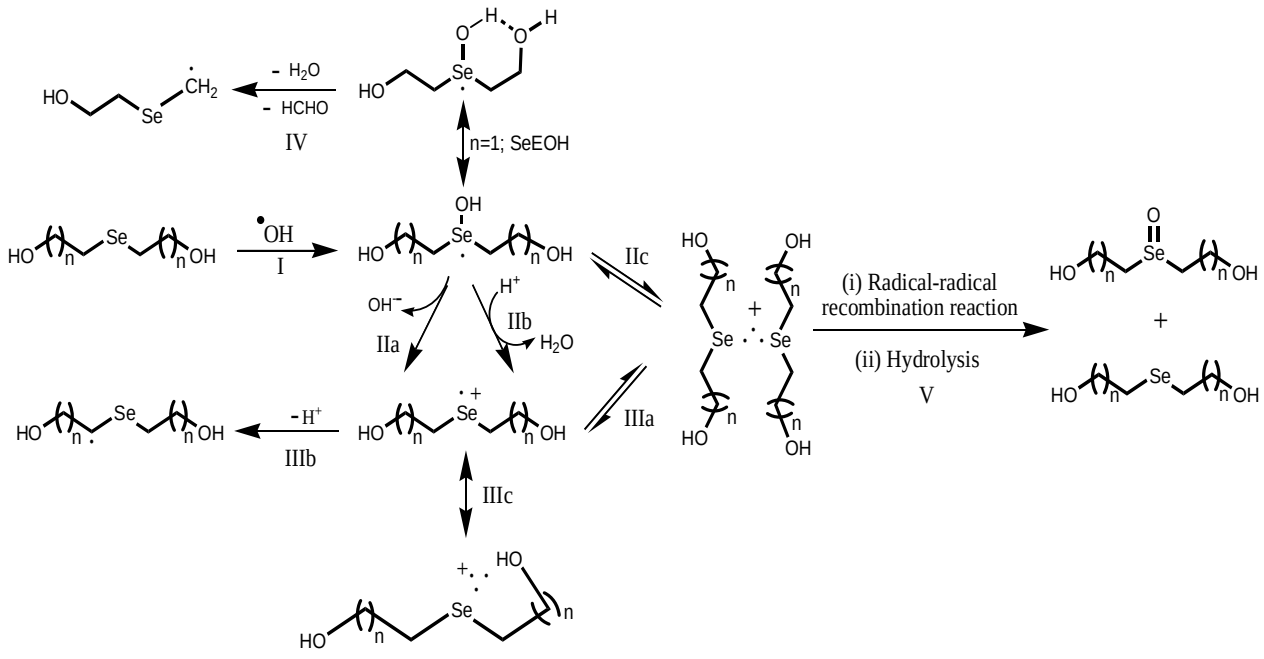

Scheme 3.5: *Proposed mechanism for the possible reactions of •OH radical with SeROH.*

3.3.5 Correlation between free radical scavenging activity and antioxidant activity of SeROH

The stability and nature of one-electron oxidized transient should reflect in their antioxidant activity, therefore ability of SeROH to protect DNA from γ-radiation induced

damage was estimated using DNA damage assay discussed in chapter 2.[108] Fig. 3.25(A-C) shows the gel images of the electrophoretic pattern of the DNA samples exposed to γ-radiation (8 Gy) in the absence and in presence of SeEOH, SePOH and SeBOH respectively. Lane 1 corresponds to control pBR322 DNA, lane 2 corresponds to irradiated DNA and lane 3-12 correspond to irradiated DNA in presence of (0.1 mM-1 mM) of SeROH. From the images it is clear that all the three compounds showed protection towards radiation induced DNA damage in a concentration dependent manner.

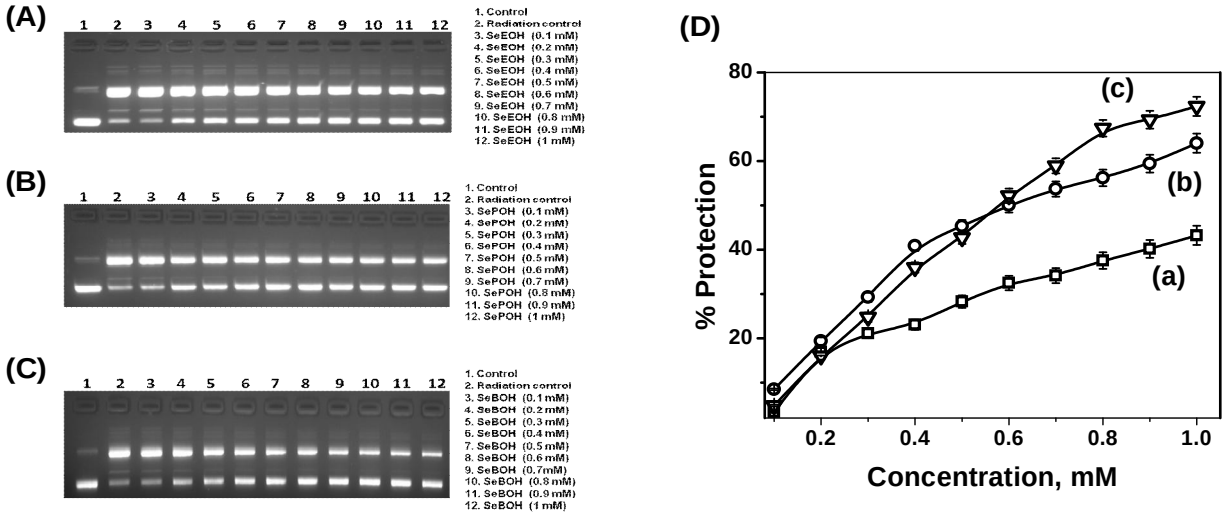

Fig. 3.25: *Panel (A) shows the gel images of unirradiated (lane 1) pBR322, γ-irradiated (8 Gy) pBR322 (lane 2) in absence and (lane 3-12) in presence of 0.1-1 mM SeEOH. Panel (B) and (C) shows the gel images of similar experiment for SePOH and SeBOH. Fig. (D) shows the % protection of pBR 322 by SeROH compounds against radiation induced damage as a function of (a) SeEOH, (b) SePOH and (c) SeBOH concentration.*

The protection for a given concentration of SeROH was calculated by considering the decrease in DNA damage relative to radiation control for which the damage was considered as 100%. The percentage protection of DNA was calculated using the formula

given in equation 2.47 in chapter 2. The IC_{50} value, i.e. the concentration required to protect DNA from radiation induced damage by 50% was estimated to be 0.60 and 0.58 mM for SePOH and SeBOH while for SeEOH, the IC_{50} value was >1 mM. (Fig. 3.25(D)). At a fixed concentration of 1 mM, the respective DNA protection exhibited by SeEOH, SePOH and SeBOH are listed in table 3.7.

Table 3.7: *Comparative results on GPx activity (GSH-NADPH-GSSG coupled assay) and DNA damage assay of SeROH compounds.*

	SeEOH	SePOH	SeBOH
GPx activity Initial velocity (υ), μmol/s	3.8 ± 0.2	5.5 ± 0.2	6.3 ± 0.3
DNA protection (%)* (SeROH = 1 mM)	43 ± 3	64 ± 5	72 ± 5

*(*P<0.01 vs. radiation control- student t-test).*

For better antioxidant activity, in addition to free radical scavenging, these compounds should reduce molecular oxidants (like H_2O_2), so that the radical scavenging activity of SeROH can be correlated with their GPx like activity.[148] For this, 2 mM H_2O_2 was added to 1 mM GSH solution containing 0.3 mM NADPH, 5 Units/ml GR and 0.1 mM of SeROH dissolved in pH 7.4 phosphate buffers. The reaction was monitored by following decrease in absorbance of NADPH at 340 nm as a function of time. Fig. 3.26 shows the decay traces of NADPH at 340 nm as a function of time in absence (blank) and in presence of SeROH. The GPx like activity of SeROH was estimated in terms of the

initial velocity (υ) for the decay of NADPH. For this, these traces were linearly fitted where slope of the trace gives υ and the values of υ for SeROH compounds are listed in table 3.7. The results indicate that the antioxidant activity of SeROH increases with increase in alkyl chain length and followed the pattern SeBOH>SePOH>SeEOH.

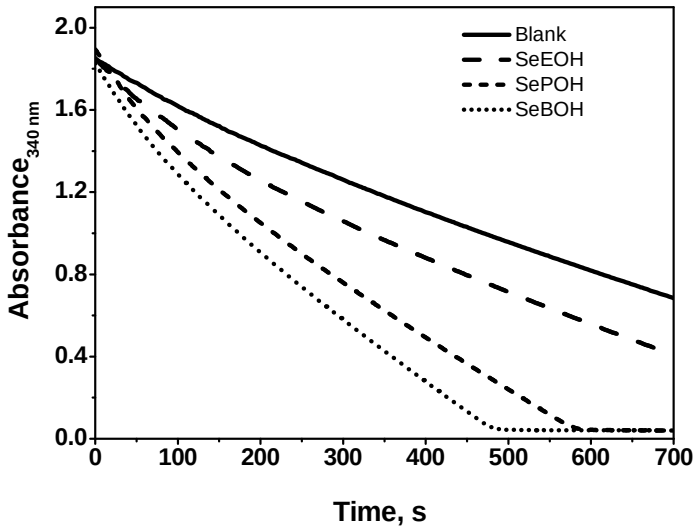

Fig. 3.26: *Absorption-time plot of 0.3 mM NADPH treated with 0.1 mM SeROH containing 2 mM H_2O_2, 1 mM GSH and 4 units/mL GR at pH 7.4.*

The trend in antioxidant activity estimated in terms of GPx activity and DNA protection correlates well with that of G-values of $SeROH_{ox}$ formed by radiolysis. These results indicate that formation of selenoxide during $^{\bullet}OH$ radical reaction is an important parameter for antioxidant activity of organoselenium compounds.

Section-B

Title: Effect of structure on radiation chemistry of organoselenium compounds: Linear vs. Cyclic compound

The studies carried out on the reaction of $^{\bullet}$OH radical with SeROH compounds in section-A showed that the nature and G-value of transients formed during electron transfer reaction of SeROH compounds is affected by their alkyl chain length. These effects were attributed to the variation in HOMO level and extra stability gained by the transients through formation of 5/6-membered rings. Further, to understand the effect of structure on electron transfer reactions on related organoselenium compounds, a comparative study of SeEOH was carried out with its cyclic analogue DHS. The one electron transfer reactions of DHS have been earlier reported in detail in refrence 90.[90] In the present work, an attempt was made to explore the various factors that differentiate radical reactions of the structural isomers. The parameters compared are nature of $(>Se\therefore Se<)^{+}$ radical, G-value of products (different transients and selenoxide) and in vitro antioxidant activity.

3.3.6.1 Pulse radiolysis studies

The $^{\bullet}$OH radical reaction with DHS was studied by pulse radiolyzing the N_2O saturated aqueous solution containing 1 mM DHS at an absorbed dose of 9.2 ± 0.5 Gy and the transient absorption spectrum was recorded. As discussed in reference 90, the transient spectrum showed a single absorption band with wavelength maximum at ~480 nm (Fig. 3.27). The absorbance of this band was found to increase with increase in DHS and $H_2PO_4^{-}$ concentration and was assigned to the formation of $(>Se\therefore Se<)^{+}$ radical of DHS.

Under similar experimental conditions, SeEOH resulted in formation of two absorption bands at ~320 nm and ~490 nm assigned to ($HOCH_2CH_2SeCH_2^{\bullet}$) radical and $(>Se\therefore Se<)^+$ radical, respectively (Fig. 3.27) as discussed earlier in section 3.3.1.

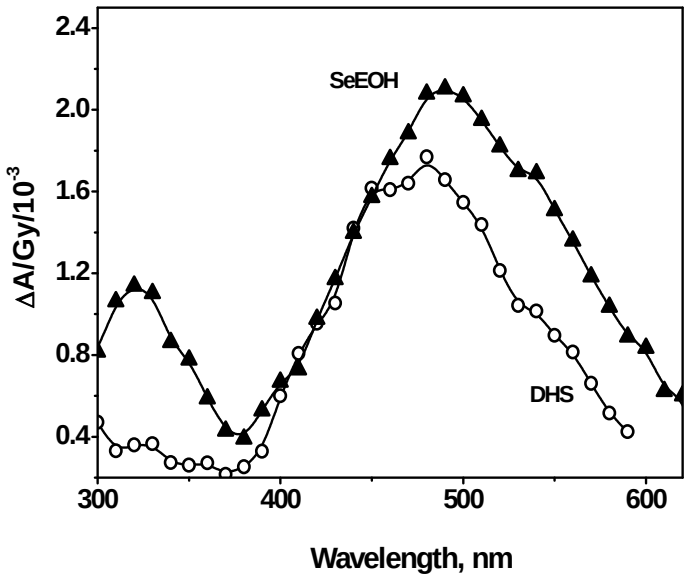

Fig. 3.27: *The transient absorption spectra generated by radiolysis of N_2O saturated aqueous solution of 1 mM SeEOH and 1 mM DHS.*

The decay of $(>Se\therefore Se<)^+$ radical of DHS was found to follow second order kinetics and the rate constant value is listed in table 3.8. The results indicate that $(>Se\therefore Se<)^+$ radical of DHS is moderately stable than that of SeEOH. In line with this, the K values as estimated by following its absorbance at 480 nm as a function of DHS concentration (0.1 mM-1 mM) were found to be higher than SeEOH, indicating higher stability of $(>Se\therefore Se<)^+$ radical of DHS than that of SeEOH.

Table 3.8: *The kinetic properties of (>Se∴Se<)$^{+}$ radical of SeEOH and DHS.*

Compounds	Decay constant (k) for (>Se∴Se<)$^{+}$ radical, $M^{-1}s^{-1}$	Equilibrium constant (K), M^{-1}
SeEOH	(1.52 ± 0.05) x 10^{9}	(1.1 ± 0.2) x10^{4}
DHS	(1.17 ± 0.08) x 10^{9}	(1.8 ± 0.2) x10^{4}

Further, to compare the reactivity of DHS and SeEOH, their reaction with other oxidizing radicals like $N_3^{\bullet}$, $CCl_3O_2^{\bullet}$ and $CO_3^{\bullet-}$ radicals were carried out. The reaction of DHS with these radicals produced similar transient spectra as that obtained for $^{\bullet}$OH radical, indicating that these radicals react with DHS by one electron transfer and form (>Se∴Se<)$^{+}$ radical. The bimolecular rate constants for the reaction of DHS with these radicals are listed in table 3.9. Comparing these results with those obtained for SeEOH, it can be inferred that DHS has higher reactivity towards oxidizing radicals than SeEOH.

Table 3.9: *Bimolecular rate constant values for the reaction of SeEOH and DHS with different free radicals.*

Compounds	Bimolecular rate constant, $M^{-1}s^{-1}$		
	$^{\bullet}$OH radical	$CCl_3O_2^{\bullet}$ radical	$CO_3^{\bullet-}$ radical
SeEOH	(1.0 ± 0.1) x 10^{10}	(4.8 ± 0.1) x10^{8}	(3.0 ± 0.3) x 10^{8}
DHS	(9.1 ± 0.1) x 10^{9}	(8.8 ± 0.3) x10^{8}	(1.3 ± 0.2) x 10^{9}

The higher free radical scavenging activity of DHS as compared to SeEOH, is explained by employing molecular descriptor like HOMO estimated by quantum chemical calculations. Fig. 3.28 represents the optimized structures and corresponding HOMO level of SeEOH and DHS. The HOMO value of DHS is higher than SeEOH due to induction of

ring strain owing to cyclization in DHS. As a result, DHS can be easily oxidized as compared to SeEOH.

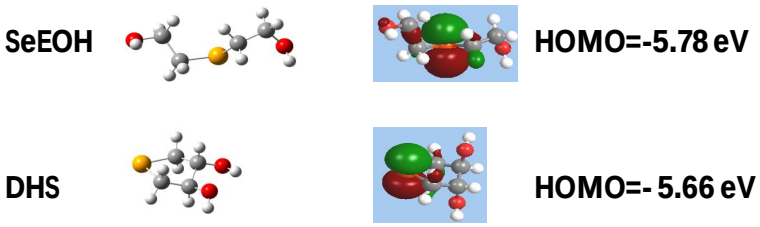

Fig. 3.28: *Optimized structures and HOMO levels of SeEOH and DHS in ground state.*

Further, the ground state geometry of $(>Se\therefore Se<)^{+}$ radical of DHS and SeEOH was optimized using quantum chemical calculations at UB3LYP/6.31+G(d,p) level as shown in fig 3.29. The bond distance between two selenium atoms is less (3.035 Å) in $(>Se\therefore Se<)^{+}$ radical of SeEOH which enhances the inter electronic repulsion and destabilizes the bond. On the other hand in $(>Se\therefore Se<)^{+}$ radical of DHS, Se-Se bond distance (3.071 Å) is comparatively larger. The increase in bond distance between two selenium atoms leads to decrease in inter electronic repulsion and stabilizes the $2\sigma/1\sigma^{*}$ bond. Therefore, $(>Se\therefore Se<)^{+}$ radical of DHS is more stable than that of SeEOH.

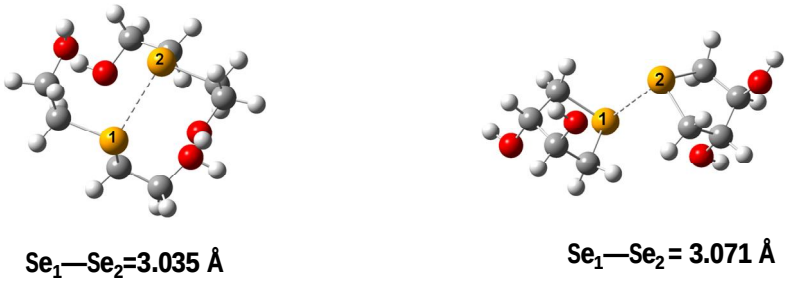

Fig. 3.29: *Optimized structures of $(>Se\therefore Se<)^{+}$ radical of SeEOH and DHS.*

Also, the energetics for the formation of $(>Se\therefore Se<)^{+}$ radical was calculated quantum chemically at B3LYP/6-31+G(d,p) level in water. The formation of $(>Se\therefore Se<)^{+}$ radical was found to be more exothermic for DHS (ΔE=-19.26 kcal/mol) than that of SeEOH (ΔE=-14.89 kcal/mol). These results suggest that formation of $(>Se\therefore Se<)^{+}$ radical is more favourable in case of DHS than SeEOH and support the experimental observations.

3.3.6.2 Estimation of G-value *of transients*

As stated in section 3.3.2, the $(>Se\therefore Se<)^{+}$ radicals are oxidising in nature and can react with reductants like $ABTS^{2-}$ to form $ABTS^{\bullet-}$ radical. This reaction can be utilised to estimate the G-value of oxidising radicals produced during reaction of $^{\bullet}OH$ radical with DHS. For this the formation of $ABTS^{\bullet-}$ radical was followed as a function of DHS concentration by monitoring its absorbance at 645 nm as discussed in section 3.3.2.1. The estimated G-value of $(>Se\therefore Se<)^{+}$ radical was found to be higher for DHS (0.45 ± 0.04 μmol/J) than that for SeEOH (0.22 ± 0.03 μmol/J). These values were found to be in correlation with the K values of $(>Se\therefore Se<)^{+}$ radical of DHS and SeEOH as listed in table 3.9. Similarly, the reaction of $^{\bullet}OH$ radical with DHS was studied in presence of different oxidants like MV^{2+}/Th^{2+}/DQ to estimate the yield of reducing radicals, if any produced. However, under present experimental conditions, no reaction was observed corresponding to reducing radicals of DHS. These results suggest that DHS on reaction with $^{\bullet}OH$ radical forms $(>Se\therefore Se<)^{+}$ radicals as the only transient.

3.3.6.3 Product analysis: HPLC studies

As discussed earlier, HCHO and selenoxides are the important species that can be formed by reaction of $^{\bullet}$OH radical with organoselenium compounds and play important role in defining the antioxidant activity of these compounds. Therefore, the G-value of selenoxide and HCHO was estimated for DHS using steady state radiolysis following similar procedure as used for SeROH compounds, discussed in section 3.3.3. Table 3.10 lists the G-value of HCHO and selenoxides formed during radiolysis of SeEOH and DHS. These results suggest that DHS on reaction with $^{\bullet}$OH radical produced significantly higher amount of (~2 times) of DHS_{ox} than that of SeEOH. Unlike in SeEOH, no HCHO formation was observed during radiolysis of DHS.

Table 3.10: *G-values of HCHO and selenoxides formed during the reaction of $^{\bullet}$OH radical with SeEOH and DHS.*

Compounds	Selenoxide (μmol/J)	HCHO (μmol/J)
SeEOH	0.23 ± 0.04	0.11 ± 0.01
DHS	0.45 ± 0.04	NIL

The comparatively higher G-value of DHS_{ox} can be attributed to higher stability of $(>Se\therefore Se<)^{+}$ radical of DHS than that of SeEOH. As observed earlier in SeROH homologues, G-value of selenoxides has a direct correlation with the antioxidant activity of these compounds; DHS is expected to exhibit higher antioxidant activity than SeEOH. Therefore, antioxidant activity of these compounds was estimated in terms of their reaction

with molecular oxidants (like H_2O_2) and inhibition of radiation induced DNA damage as discussed below.

3.3.6.4 Antioxidant activity

The antioxidant activity of DHS was estimated by studying the protection of pBR322 DNA (250 ng) against radiation (8 Gy) induced damage. Fig. 3.30(A) shows the variation in percentage protection offered by DHS with the gel image shown in the inset. Lane 1 in the gel image corresponds to control DNA while lane 2 and lane 3-19 correspond to irradiated DNA in absence and presence of 0.05-1 mM DHS, respectively. The IC_{50} value of DHS was estimated to be 0.43 mM, whereas SeEOH showed only marginal protection and the IC_{50} vale was not achieved in experimental concentration (up to 1 mM).

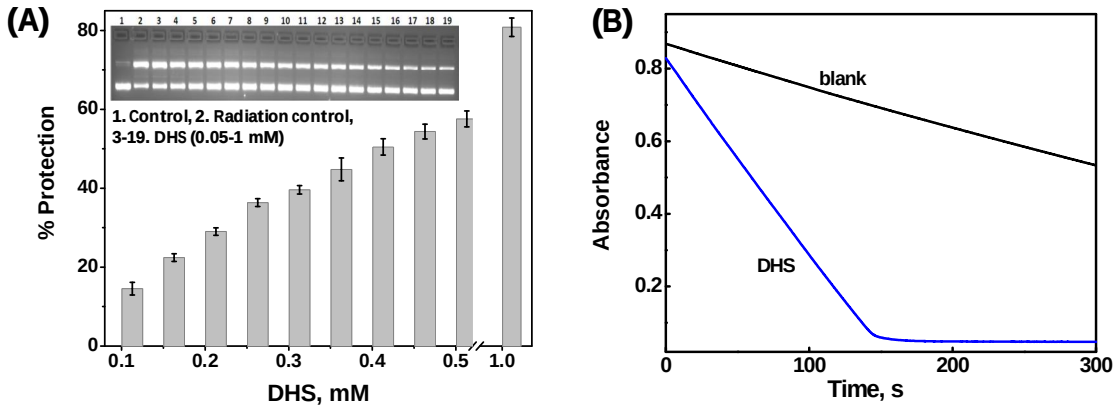

Fig.3.30: *(A) Variation in percentage protection against radiation induced damage as a function of DHS concentration. Inset shows the corresponding gel image, where lane 1 shows control DNA, lane 2 shows irradiated DNA and lanes (3-19) show irradiated DNA pretreated with 0.05-1 mM DHS. Fig. B shows the absorbance-time plot of 0.3 mM of*

NADPH treated with 0.1 mM DHS containing 2 mM H_2O_2, 1 mM GSH and 4 units/mL GR at pH 7.4.

GPx like activity of DHS was estimated using NADPH-GSH-GSSG coupled assay. Fig. 3.30(B) shows the absorbance-time plot of 0.3 mM NADPH in absence (shown as blank) and in presence of 0.1 mM DHS. The comparative results are listed in table 3.11.

Table 3.11: *Summary of results of antioxidant assays performed for SeEOH and DHS.*

Compound	Inhibition of $^{\bullet}$OH induced DNA damage, IC_{50} (mM)	GPx activity, Initial velocity (μmol/s)
SeEOH	> 1 mM	3.8 ± 0.2
DHS	0.43 ± 0.05	8.1 ± 0.4

These results showed that the activity of DHS for scavenging free radicals like $^{\bullet}$OH radical and molecular oxidants like H_2O_2 is higher than that of SeEOH. The higher inhibition of radiation induced damage can be correlated to higher G-value of selenoxide for DHS than that of SeEOH. Overall, it can be stated that DHS exhibits higher activity towards both free radicals and molecular oxidants than its linear analogue SeEOH, mainly due to higher HOMO value and selenoxide yield.

3.4 Conclusions

The electron transfer processes play important role in defining antioxidant activity of redox active organoselenium compounds. One of the primary factors in this process has been their ability to neutralize ROS. With this aim, the reactions of $^{\bullet}$OH radical and other

oxidizing radicals with linear and cyclic selenoethers (SeEOH, SePOH, SeBOH and DHS) were investigated using nanosecond pulse radiolysis. The results are summarized below.

1. Initial reaction of $^{\bullet}$OH radical with these compounds takes place at the selenium centre to form (>Se∴OH), which is then converted to three different types of radicals like, (>Se$^{\bullet+}$) radical, (>Se∴Se<)$^{+}$ radical and α-{bis(hydroxyl alkyl)}selenomethine radical. In all the compounds, (>Se∴Se<)$^{+}$ radical was the major transient formed with absorption maximum in the range of 460-500 nm.
2. The initially formed (>Se∴OH) radical decayed by two major pathways- i) degradation via Barton reaction to form HCHO and C-centered radicals and ii) proton catalyzed dehydration to form (>Se$^{\bullet+}$) radical. The first pathway was observed only in SeEOH and the G-value of HCHO was nearly one third when compared with its sulfur analogue, SEOH.
3. A fraction of (>Se$^{\bullet+}$) radical undergoes deprotonation to form α-{bis(hydroxyl alkyl)}selenomethine radical. The extent of reaction decreased with increase in alkyl chain length.
4. The (>Se$^{\bullet+}$) radical further combined with un-oxidized SeROH molecule to form (>Se∴Se<)$^{+}$ radical. The (>Se∴Se<)$^{+}$ radical decayed by radical-radical reaction followed by hydrolysis to form $SeROH_{ox}$. The G-value of $SeROH_{ox}$ increased with increase in alkyl chain length.
5. The antioxidant activity of SeROH was estimated in terms of GPx activity and inhibition of radiation induced DNA damage, where SeBOH was found to be the most effective, while SeEOH was found to be the least effective. The antioxidant

activity was found to be in direct correlation with radiolytic G-value of selenoxide and HOMO levels of parent molecules.

6. On comparison of cyclic (DHS) and linear analogues (SeEOH), cyclic compound showed higher free radical and molecular oxidants scavenging activity. The higher activity of DHS is due to its higher HOMO level and stable $(>Se\therefore Se<)^{+}$ radical. Among all the four compounds studied, DHS was found to be better antioxidant.
7. Comparative studies between SeROH compounds and their sulfur analogues showed that although the initial step for the reaction of $^{\bullet}OH$ radical (addition to sulfur/selenium atom) is same in both cases, the nature and G-value of the transients formed differ significantly. The molecular descriptors involved in defining these transients included covalent radii of selenium atom, non-bonding interactions and molecular orbital energy levels.
8. The results provide supportive evidence to explain why selenium compounds can be better antioxidants than their sulfur analogues.

Chapter 4

Reaction of peroxynitrite with organoselenium compounds: Role of chemical structure on antioxidant activity.

In this chapter, reactions of three structurally related organoselenium compounds with a molecular oxidant i.e. peroxynitrite and its derived radicals were studied using stopped flow and pulse radiolysis techniques. The reaction products formed were characterized and quantified using nuclear magnetic resonance (NMR) and high performance liquid chromatography (HPLC), respectively. The antioxidant activity of these compounds against peroxynitrite induced damage was estimated and correlated with the yield of selenoxides.

4.1 Introduction

Peroxynitrite is a powerful molecular oxidant, generated by diffusion controlled reaction of $NO^{\bullet}$ radical with $O_2^{\bullet-}$ radical in activated macrophages, endothelial cells, neurons and neutrophils.[149] Peroxynitrite is a strong oxidant and a nitrating species, which is beneficial in inflammatory reactions in terms of oxidative destruction of intruding microorganisms.[150] However, higher concentrations and uncontrolled generation of peroxynitrite can result in unwanted oxidation (oxidative stress) and consecutive destruction of cellular components like lipids, proteins and DNA.[151,152] Excess production of peroxynitrite has been implicated in many pathological conditions like neurodegenerative diseases, infection etc.[153] Peroxynitrite induced nitration and oxidation of proteins may destroy their tertiary structure resulting in protein aggregates that may contribute to the pathogenesis of various neurodegenerative diseases like Alzheimer's and Parkinson's diseases.[154,155] Peroxynitrite induces lipid peroxidation and damages DNA through strand breaks and base modification.[156] Peroxynitrite impairs elements of mitochondrial electron transport system and inhibits the activity of antioxidant enzymes.[157] All these processes lead to cytotoxicity, inflammatory response, loss of immunity in cells and apoptosis of cells.[158]

In view of the toxic effects of peroxynitrite, extensive research is being continued to reduce its toxicity. Detoxification of peroxynitrite can be brought by three approaches: prevention, interception and repair.[159] Prevention approach includes minimizing the probability of simultaneous generation of $NO^{\bullet}$ radical and $O_2^{\bullet-}$ radical. Interception includes scavenging of peroxynitrite by low molecular weight molecules like, CO_2,

ascorbate, etc before reacting with target biomolecules.[160] Repair corresponds to regeneration of normal cell conditions after peroxynitrite induced damage.

The cellular defensive system against peroxynitrite includes enzymes (GPx, myeloperoxidase), metalloproteins and low molecular weight molecules (CO_2, GSH) etc.).[161,162] Metalloproteins like Fe (III) porphyrins, have shown high reactivity towards peroxynitrite and the bimolecular rate constant values were estimated to be (2.0-8.0) x 10^6 $M^{-1}s^{-1}$.[163] Table 4.1 lists rate constants for the reaction of peroxynitrite with some of important compounds.

Table 4.1: *The bimolecular rate constants for the reaction of some important peroxynitrite scavengers.*

Compounds	Rate constant, $M^{-1}s^{-1}$	Reference
Myeloperoxidase	$2.0 \pm 0.1 \times 10^7$	164
CO_2	$5.8 \pm 0.2 \times 10^4$	38
Fe(III) porphyrins	(2.0-8.0) x 10^6	163
Cys	$2.6 \pm 0.2 \times 10^3$	165
Ascorbate	$2.4 \pm 0.2 \times 10^2$	160
Ebselen	$2.0 \pm 0.1 \times 10^6$	166
GPx	$8.0 \pm 0.2 \times 10^6$	167
SeMet	$3.0 \pm 0.2 \times 10^3$	168
GSH	$1.4 \pm 0.2 \times 10^3$	161a
Met	$1.6 \pm 0.2 \times 10^2$	169
SeCys	$6.6 \pm 0.3 \times 10^5$	170
MeSeCys	$1.9 \pm 0.1 \times 10^3$	84b

Due to the high concentration (~2 mM) of CO_2 in cellular system, it reacts with peroxynitrite with a bimolecular rate constant of $5.8 \pm 0.2 \times 10^4$ $M^{-1}s^{-1}$ to generate new oxidants ($CO_3^{\bullet-}$ radical and $NO_2^{\bullet}$ radical).[38] These radicals play important role in peroxynitrite mediated oxidative processes and are considered to be responsible for damage to biomolecules like proteins, DNA etc.[39] In proteins, thiols are the main targets of peroxynitrite where they are oxidized to either disulfides or sulfoxides.[171] The reactions of peroxynitrite with biomolecules can take place via one-electron transfer, two-electron transfer and sometimes via oxygen atom transfer. The two electron transfer reaction leads to formation of sulfenic acid (RS-OH) which being very unstable reacts with another thiol molecule to form disulfides. Whereas, one-electron transfer reaction results in formation of thiyl radicals ($RS^{\bullet}$) which further dimerize to form disulfides. Formation of $RS^{\bullet}$ radical has been confirmed by electron paramagnetic resonance (EPR) studies for reaction of peroxynitrite with Cys and GSH.[25] There are reports where peroxynitrite has been found to react with thiols via competing one- and two-electron transfer pathways. For example, the reaction of peroxynitrite with Met and 2-keto-4-thiomethylbutanoic acid (TMBA) takes place via both one and two-electron transfer resulting in a mixture of ethylene and corresponding sulfoxides as products.[37]

Due to the similarity between chemical properties of sulfur and selenium, selenium based compounds have also been explored for scavenging of peroxynitrite. The search for selenium based compounds for detoxification of peroxynitrite started with ebselen by Masumoto and co-workers in mid 90's where they found that ebselen reacts with peroxynitrite with a bimolecular rate constant of 2.0×10^6 M^{-1} s^{-1} and protect DNA from peroxynitrite induced single strand breaks.[172] Similarly, other compounds like 2-

(methylseleno)benzanilide, SeMet, CysSeSeCys were reported to scavenge peroxynitrite and attenuate peroxynitrite induced nitration and oxidation reactions.[172] Immediately after that GPx was observed to degrade peroxynitrite inside cells effectively.[167] GPx not only reduced peroxynitrite induced oxidation but also nitration of proteins. Sies et.al proposed that GPx exhibited peroxynitrite reductase like catalytic activity and reduced peroxynitrite catalytically in presence of GSH as shown in Scheme 4.1.[173]

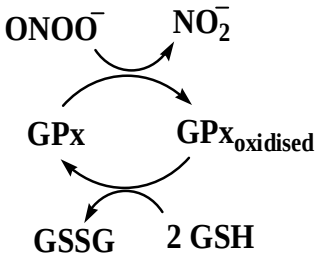

Scheme 4.1: *Representative reaction mechanism for the reaction of peroxynitrite with GPx.*

Briviba et.al. by kinetics studies showed that GPx reacted with peroxynitrite with a rate constant of (8.0 ± 0.3) $x10^6$ $M^{-1}s^{-1}$ which has been attributed to SeCys residue (in –SeH form) present in the active site of the enzyme.[167] In the presence of peroxynitrite, -SeH moiety of SeCys is oxidized to the selenenic acid (-SeOH). This intermediate is then reduced back to the (-SeH) form at the expense of two reducing equivalents of GSH and thus the redox cycle for peroxynitrite is completed. This is also called as peroxynitrite reductase activity.

Interesting feature of organoselenium compounds is that the scavenging ability of these compounds is higher by 10-100 folds in magnitude than their sulfur counterparts.[23]

For example, SeMet reacts with peroxynitrite with a bimolecular rate constant of (3.0 ± 0.2) x 10^3 compared to (1.6 ± 0.2) x 10^2 for Met.[167,169] Similarly, SeCys (~300 times) has shown much higher reactivity compared to Cys.[165,170] The activity of these compounds has been studied by their ability to prevent peroxynitrite induced DHR123 oxidation, protein nitration, DNA damage and cellular toxicity.[174,175] Similarly, organoselenium compounds like, selenourea, CysSeSeCys, SeMet were found to inhibit the oxidation of DHR123 by peroxynitrite. Andreza et al have shown that GPx, ebselen and diphenyldiselenide inhibit peroxynitrite-mediated protein tyrosine nitration and apoptosis in endothelial cells.[161a]

Among the low molecular weight organoselenium compounds studied so far, ebselen exhibited the highest reactivity for peroxynitrite (2.0 x 10^6 M^{-1} s^{-1}).[167] It reacts with peroxynitrite to form selenoxide which in the presence of thiols can regenerate the original active form. Recent studies on ebselen and its derivatives showed that selenoxides formed during the reaction with peroxynitrite are highly unstable and undergo hydrolysis to from corresponding seleninic acid.[176] This pathway inhibits the thiol mediated regeneration of ebselen which in turn decreases the peroxynitrite reductase activity. Most of the organoselenium compounds synthesized so far have shown lower reactivity than ebselen. Also, their applications are limited due to poor water solubility. Overall, the development of potent catalytic organoselenium compounds to degrade peroxynitrite is limited by their poor water solubility, instability of the intermediates and intrinsic cytotoxicity.

Present study explores DHS, a cyclic selenolane and a GPx mimic alongwith its structurally related derivatives as probable peroxynitrite scavengers.[90,177] Considering the reactivity of DHS towards molecular oxidants (like H_2O_2) and free radicals ($^{\bullet}OH$), DHS is

also expected to react with peroxynitrite. With this aim, an attempt has been made to understand the reaction kinetics, mechanism and nature of end products for the reaction of DHS with peroxynitrite. To understand the influence of functional groups and structural changes on peroxynitrite scavenging activity, comparative studies have been performed on SeEOH, a linear analogue of DHS and MAS, an amino substituted derivative of DHS.[94,96b] The chemical structures of these compounds are given in scheme 4.2

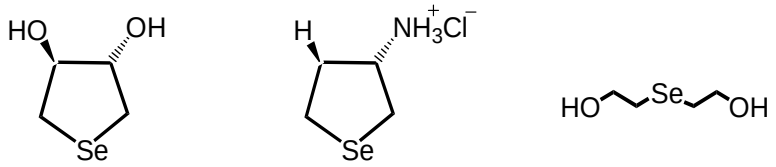

(DHS) **(MAS)** **(SeEOH)**

Scheme 4.2: *Chemical structure of DHS, MAS and SeEOH.*

4.2 Materials and methods

The kinetics of reaction between peroxynitrite and organoselenium compounds was studied by following the decay of peroxynitrite at 302 nm by stopped flow technique and the instrumental details are given in chapter 2. The $CO_3^{\bullet-}$ and $NO_2^{\bullet}$ radicals were generated by pulse radiolyzing N_2O saturated aqueous solution of 0.1 M Na_2CO_3 and 0.1 M $NaNO_2$, respectively with an average absorbed dose of 15 Gy using linac facility. The yield of nitrate (NO_3^-) formed by isomerisation of peroxynitrite was calculated by monitoring the formation of nitro-resorcinol according to the reported procedure by Zhang et al.[178] The selenoxides were identified using NMR and MS techniques. The quantification of selenoxides was done using HPLC technique using thiol-disulfide method,as discussed earlier in chapter 3. Here, GSH ($k_{GSH+ONOO^-}$=7.3 x 10^2 $M^{-1}s^{-1}$) was

used in place of DTT, as DTT itself reacts with peroxynitrite with a rate constant of ~10^3 $M^{-1}s^{-1}$ and can interfere with reaction of peroxynitrite with organoselenium compounds. The DNA damage and cellular toxicity was determined by gel electrophoresis and MTT assays, respectively and the details are given in chapter 2.

4.3 Results and discussion

4.3.1 Kinetics studies

Peroxynitrite has a pKa value of 6.8 and exists in equilibrium with its protonated form peroxynitrous acid (ONOOH) as shown in equation 4.1.[37]

$$ONOO^- + H^+ \underset{}{\overset{pKa=6.8}{\rightleftharpoons}} ONOOH \qquad (4.1)$$

ONOOH is a very strong oxidizing species with reduction potential of (1.20 ± 0.05) V measured at pH 7.[37] It is relatively unstable and decays either by homolytic cleavage to form $^{\bullet}OH$ and $NO_2^{\bullet}$ radicals or through isomerization to form nitrate ion (NO_3^-) as shown in equation 4.2 and 4.3, respectively. At pH 7.4, in absence of any substrate, isomerization reaction dominates and accounts for 70% of the peroxynitrous acid decomposition reaction.

$$ONOOH \xrightarrow{k_1} NO_2^{\bullet} + {}^{\bullet}OH \qquad (4.2)$$

$$ONOOH \xrightarrow{k_2} NO_3^- + H^+ \qquad (4.3)$$

In the presence of substrate, ONOOH can also form a high energy species [ONOOH]* more reactive than $^{\bullet}OH$ radical. [ONOOH]* can react with substrate through one electron transfer reaction as shown in equation 4.4.

$$\mathbf{ONOOH + Substrate \xrightarrow{k_3} one\text{-}e\ oxidised\ Products + NO_2^-} \quad (4.4)$$

At physiological pH (i.e. 7.4) ~80% of it exists as peroxynitrite (anionic form) and only ~20 % will exist as protonated form. Peroxynitrite undergoes self dissociation (k_4=1.3 s^{-1}) with first order kinetics and rearranges to form NO_3^- according to equation 4.5.[179]

$$\mathbf{ONOO^- \xrightarrow{k_4} NO_3^-} \quad (4.5)$$

In presence of any substrate, peroxynitrite can react through one electron or two electron oxidation (equation 4.6) or by oxygen atom transfer (equation 4.7).

$$\mathbf{ONOO^- + Substrate \xrightarrow{k_5'} 1e^- /2e^- oxidised\ products} \quad (4.6)$$

$$\mathbf{ONOO^- + Substrate \xrightarrow{k_5''} NO_2^- + Oxy\text{-}Products} \quad (4.7)$$

Here, k_5' and k_5'' are the rate constants for the reaction of peroxynitrite with substrate through electron transfer (equation 4.6) and oxygen atom transfer (equation 4.7), respectively. Under suitable redox conditions, NO_2^- can react with oxy-products formed and regenerate the parent compound (equation 4.8).

$$\mathbf{NO_2^- + Oxy\text{-}Products \xrightarrow{k_6} NO_3^- + Substrate} \quad (4.8)$$

In the present study, the reaction of peroxynitrite with organoselenium compounds was studied under pseudo first order conditions, where the rate of disappearance (k_{obs}) of peroxynitrite at a fixed pH can be given by equation 4.9.

$$k_{obs} = k_4 + k_5[Substrate] \quad (4.9)$$

Here $k_5=k_5'+k_5''$ is the total rate constant for the reaction of substrate with peroxynitrite having contribution from both reactions shown in equation 4.6 and 4.7. The bimolecular rate constant was estimated from the linear plot of k_{obs} as a function of organoselenium compound concentration according to equation 4.9. The intercept of the linear plot gives the rate constant (k_4) for the self decay of peroxynitrite while slope gives the bimolecular rate constant (k_5) for the reaction. The k_{obs} values were calculated by following the absorbance of peroxynitrite at 302 nm as a function of time using stopped flow technique at pH 7.5. Fig. 4.1(A) represents the absorption-time plot of 0.1 mM peroxynitrite in absence (trace a) and in presence of different concentrations (0.5 mM-4 mM) of DHS (trace b-e). In the absence of DHS, peroxynitrite decayed by following first order kinetics. On addition of DHS, the decay became faster in a concentration dependant manner. The individual decay traces were fitted to first order reaction kinetics according to equation 4.10.

$$Y(t) = at + b + \exp(-k_{obs}t) \quad (4.10)$$

where Y(t) is the time dependent absorbance of peroxynitrite at 302 nm and a, b represent slope and baseline (absorbance at infinite time) of the decay trace, respectively. The estimated k_{obs} values showed a linear variation with DHS concentration. Fig. 4.1(B) shows the linear fitting of the k_{obs} values as a function of DHS concentration.

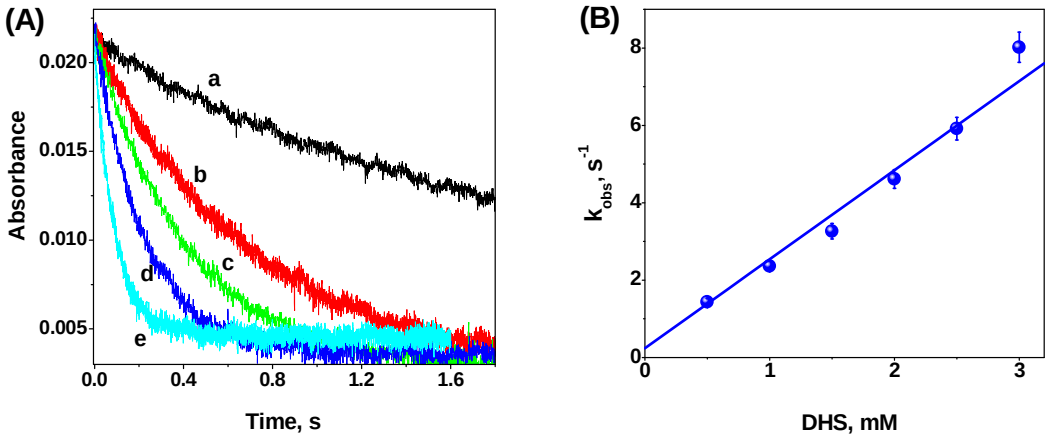

Fig. 4.1: *(A) Absorption-time plot of 0.1 mM peroxynitrite (a) in absence and in presence of (b) 0.5 mM, (c) 1 mM, (d) 2 mM and (e) 3 mM DHS. Fig. B shows the linear plot of* k_{obs} *as a function of DHS concentration.*

From the intercept of the linear plot (according to equation 4.9), the calculated value of k_4 was found to be (0.21 ± 0.02) s^{-1} which agrees with the earlier reported values for the self decay constant of peroxynitrite at pH 7.5.[180] The bimolecular rate constant for the reaction of DHS with peroxynitrite was estimated to be (2.2 ± 0.3) x 10^3 $M^{-1}s^{-1}$. Similarly, the reaction of SeEOH and MAS with peroxynitrite was studied. Fig. 4.2(A) and 4.3(A) represent the decay traces of peroxynitrite in absence (trace a) and in presence of 0.5 mM-3 mM MAS (trace b-e) and 0.5 mM-3 mM SeEOH (trace b-e), respectively. Both MAS and SeEOH showed similar reaction kinetics pattern as that of DHS. The k_{obs} values showed a linear variation as a function of MAS and SeEOH concentration as shown in fig. 4.2(B) and 4.3(B), respectively. The bimolecular rate constant values for the reaction of peroxynitrite with SeEOH, MAS are listed in table 4.2.

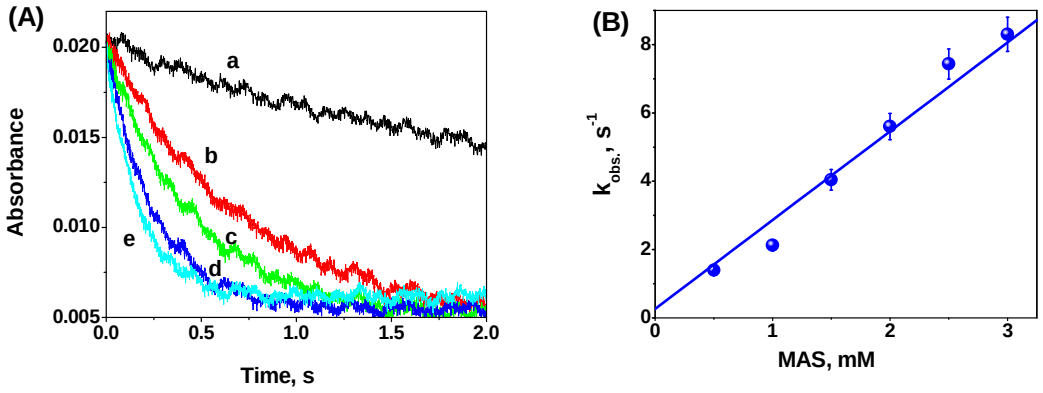

Fig. 4.2: *(A) Absorption-time plot of 0.1 mM peroxynitrite (a) in absence and in presence of (b) 0.5 mM, (c) 1 mM, (d) 2 mM and (e) 3 mM MAS. Fig. B shows the linear plot of* k_{obs} *as a function of MAS concentration.*

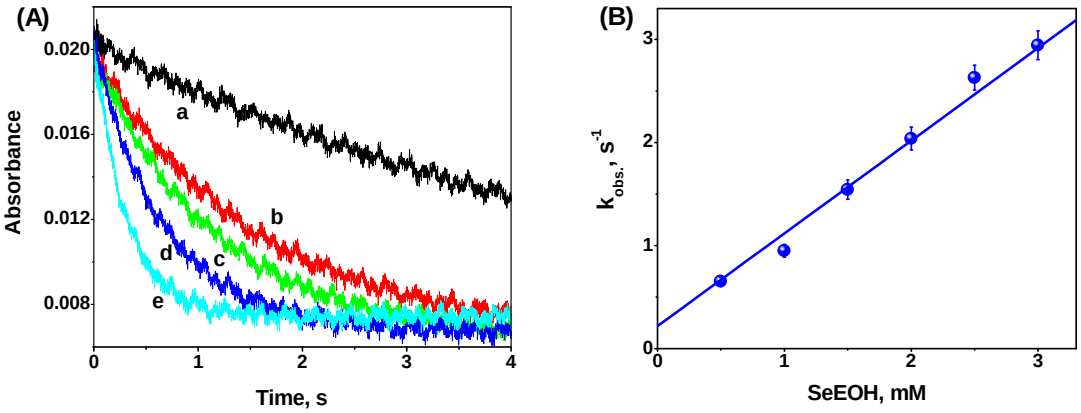

Fig. 4.3: *(A) Absorption-time plot of 0.1 mM peroxynitrite (a) in absence and in presence of (b) 0.5 mM, (c) 1 mM, (d) 2 mM and (e) 3 mM SeEOH. Graph B shows the linear plot of* k_{obs} *as a function of SeEOH concentration.*

From the results, it can be stated that both DHS and MAS have nearly similar reactivity towards peroxynitrite while SeEOH reacts marginally slowly with peroxynitrite.

The rate constants for these compounds were also determined by competition kinetics using DHR123 as a reference solute.[175]

Table 4.2: *Bimolecular rate constant values for the reaction of organoselenium compounds with peroxynitrite at pH 7.5.*

Compounds	Bimolecular rate constant (k_5, $M^{-1}s^{-1}$) x 10^3	
	using stopped flow technique	using competition kinetics
DHS	2.2 ± 0.3	1.9 ± 0.2
MAS	2.0 ± 0.2	1.6 ± 0.1
SeEOH	1.6 ± 0.1	0.9 ± 0.1

Peroxynitrite oxidizes DHR123 to give rhodamine123 with a bimolecular rate constant (k_7) of 8.2 x 10^3 $M^{-1}s^{-1}$ as given in equation 4.11. Formation of rhodamine 123 can be easily monitored as it gives intense fluorescence with peak maximum at 536 nm when excited at 510 nm. In presence of organoselenium compounds, DHR123 undergoes competitive reaction with peroxynitrite (equation 4.12).

$$\mathbf{ONOO^- + DHR\,123 \xrightarrow{k_7} Rhodamine\,123} \qquad (4.11)$$

$$\mathbf{ONOO^- + DHS/MAS/SeEOH \xrightarrow{k_5} Products} \qquad (4.12)$$

Fig. 4.4(A (a-f)) shows the fluorescence spectra of rhodamine123 as a function of DHS concentration (0-100 μM). It can be seen that the fluorescence intensity of rhodamine123 decreased on addition of DHS in a concentration dependent manner. Similarly, fluorescence intensity of rhodamine123 also decreased in presence of both

SeEOH and MAS as shown in fig. 4.4(B). At any given concentration, the decrease in fluorescence intensity was more for DHS than that for MAS and SeEOH.

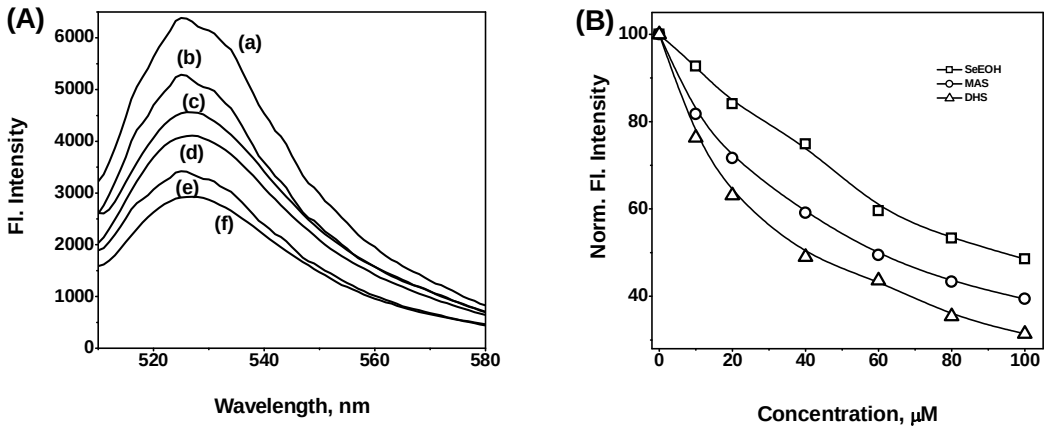

Fig. 4.4: *(A) The fluorescence spectra of rhodamine123 in absence (a) and in presence of (b) 20 μM, (c) 40 μM, (d) 60 μM, (e) 80 μM and (f) 100 μM DHS containing peroxynitrite (5 μM) and 0.1 mM DTPA in 10 mM phosphate buffer at pH 7.4. Graph B shows the gradual decrease in fluorescence intensity of rhodamine123 as a function of SeEOH, MAS and DHS concentration.*

If F_0 and F are the fluorescence intensities of rhodamine123 at 536 nm in the absence and in presence of DHS/MAS/SeEOH, respectively, then k_5 will be given by equation 4.13.

$$\frac{F_0}{F} - 1 = \frac{k_5}{k_7} \frac{[DHS / MAS / SeEOH]}{[DHR123]} \qquad (4.13)$$

The slope of the linear plot of (F_0/F-1) as a function of [DHS/MAS/SeEOH]/[DHR123] gives the ratio (k_5/k_7) of rate constants of the two

reactions (Fig. 4.5). The values of k_5 for DHS, MAS and SeEOH have been calculated by substituting k_7 and the results are listed in table 4.2.

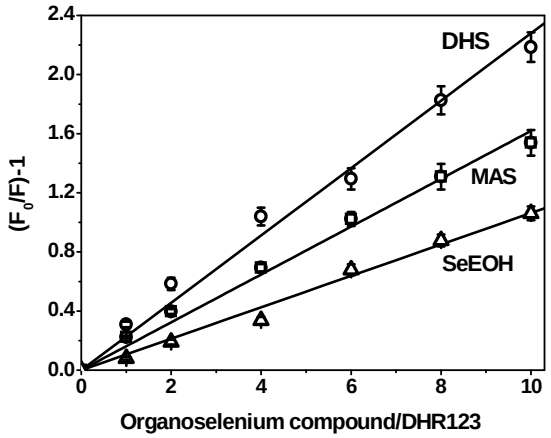

Fig. 4.5: *Linear plot for variation of (F_0/F-1) as a function of concentration ratio of organoselenium compound and DHR123 ([Organoselenium compound]/[DHR123]).*

The rate constants determined by competition kinetics are comparable to those obtained by kinetic method using stopped flow spectrometer. From these results, it is clear that the rate constants for the reaction of peroxynitrite with DHS and MAS are comparable while that with SeEOH is lower. The rate constants of these compounds are comparable with those for SeMet, MeSeCys, SeCysA, etc. but are quite low compared to ebselen.

4.3.2 Reaction with secondary radicals of peroxynitrite

Under physiological conditions, where the concentration of CO_2 is > 1.3 mM, peroxynitrite rapidly reacts with CO_2 with a rate constant of (k_7=5.8 ± 0.2) x 10^4 $M^{-1}s^{-1}$ to form nitroso-peroxocarbonate $[ONOO\text{-}CO_2]^-$ which subsequently decays to form $CO_3^{\bullet-}$ and $NO^{\bullet}_2$ radicals as shown in equation 4.14.[38]

$$ONOO^- + CO_2 \rightarrow [ONOO - CO_2]^- \rightarrow NO_2^{\bullet} + CO_3^{\bullet -} \quad (4.14)$$

Considering the higher rate constant and cellular concentration of CO_2 compared to organoselenium compounds being studied, the reaction of peroxynitrite with CO_2 will dominate over the direct reaction of peroxynitrite with substrate. These resultant radicals ($CO_3^{\bullet -}$, $E°(CO_3^{\bullet -}/CO_3^{2-})$ = +1.78 V and $NO_2^{\bullet}$, $E°(NO_2^{\bullet}/NO_2^-)$ = +0.99 V vs NHE) are oxidizing in nature.[39,181] For an efficient scavenger of peroxynitrite, it is important to see how they scavenge these radicals along with direct scavenging of peroxynitrite. Therefore organoselenium compounds were also tested for their ability to scavenge $CO_3^{\bullet -}$ and $NO^{\bullet}_2$ radicals using pulse radiolysis technique.

$CO_3^{\bullet -}$ radical exhibits absorbance at ~600 nm ($\varepsilon_{600\ nm}$=1680 $M^{-1}cm^{-1}$) which can be utilised to monitor its reaction with organoselenium compounds. Fig. 4.6(A) shows the absorption-time plot of $CO_3^{\bullet -}$ radical in absence and in presence of 10 µM DHS. In the absence of DHS, $CO_3^{\bullet -}$radical decayed by second order kinetics with 2k/εl value of (5.7 ± 0.1) x 10^7 s^{-1} at pH 7.4. On addition of 10 µM DHS, $CO_3^{\bullet -}$radical decayed very fast and the reaction was found to follow first order kinetics.

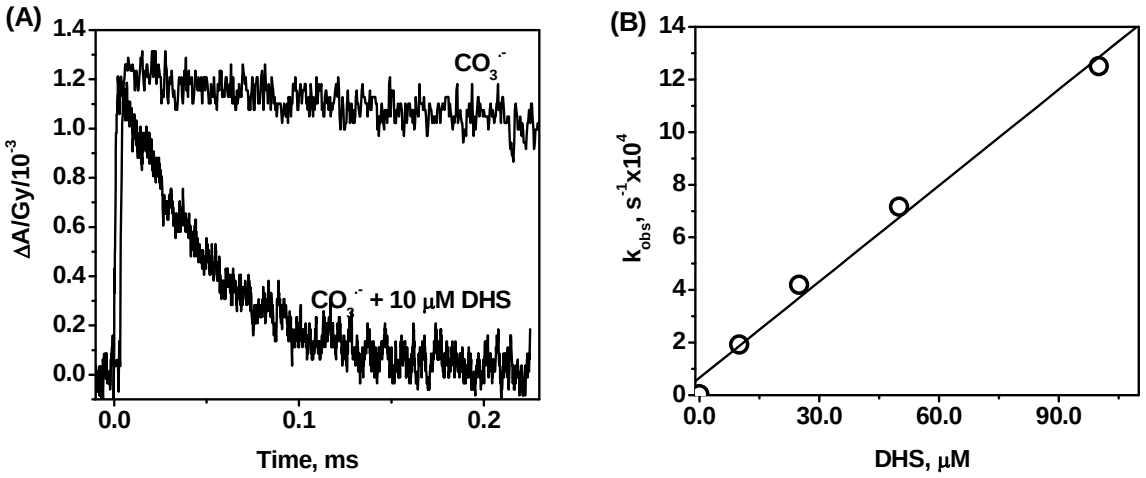

Fig. 4.6: *(A) The absorption-time plot of $CO_3^{\bullet-}$ radical at 600 nm in absence and presence of 10 μM DHS at pH 7.5. Fig. B shows the linear fit of k_{obs} as a function of DHS concentration (10-100 μM).*

The bimolecular rate constant (k_8) for the reaction of DHS with $CO_3^{\bullet-}$ radical was estimated from the linear plot of k_{obs} at 600 nm as a function of DHS (10 -100 μM) as shown in fig. 4.6B and was found to be (1.2 ± 0.2) x 10^9 $M^{-1}s^{-1}$. Similarly, studies were carried out for reaction of $CO_3^{\bullet-}$ radical with MAS and SeEOH. Fig. 4.7 (A) represents the decay traces of $CO_3^{\bullet-}$ radical in absence and in presence of 10 μM MAS and SeEOH, indicating that the decay of $CO_3^{\bullet-}$ radical becomes faster in the presence of SeEOH and MAS. To estimate the bimolecular rate constant for these reactions, k_{obs} for the decay of $CO_3^{\bullet-}$ radical was plotted as a function of SeEOH and MAS as shown in fig 4.7(B). The estimated bimolecular rates constant values were (9.8 ± 0.5) x 10^8 $M^{-1}s^{-1}$ and (6.5 ± 0.3) x 10^8 $M^{-1}s^{-1}$ for MAS and SeEOH, respectively.

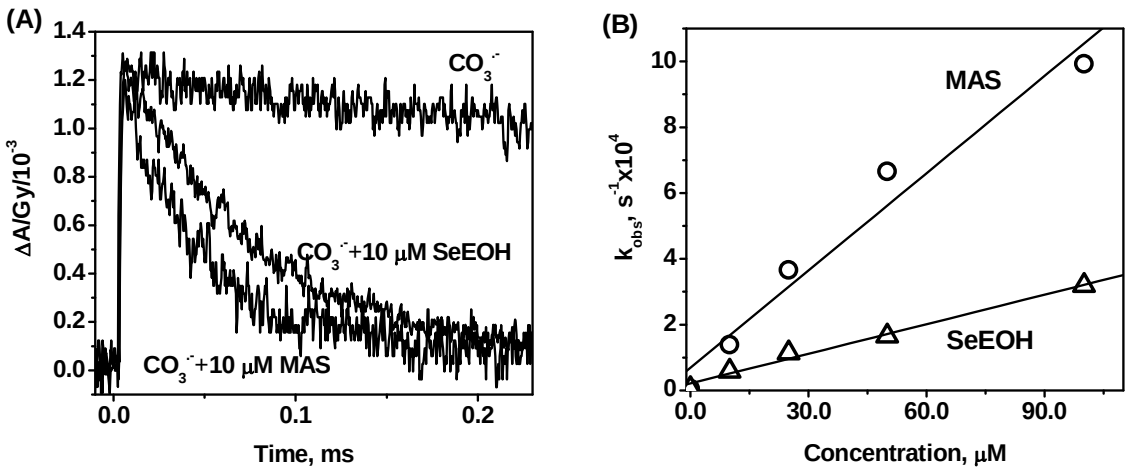

Fig. 4.7: *(A) The absorption-time plot of $CO_3^{\bullet-}$ radical at 600 nm in absence and presence of 10 μM MAS/SeEOH at pH 7.5. Fig. B shows the linear fit of k_{obs} as a function of MAS/SeEOH concentration (10-100 μM).*

To understand the reaction of organoselenium compounds with $CO_3^{\bullet-}$ radical, transient absorption spectra were recorded. Fig. 4.8(A&B) represents the transient spectra generated by reaction of $CO_3^{\bullet-}$ radical with DHS and MAS, respectively. The transient absorption spectra showed characteristic absorption band at ~480 nm. This absorption band was attributed to formation of dimer radical cation $(>Se\therefore Se<)^+$ of DHS and MAS as discussed in chapter 3. Formation of $(>Se\therefore Se<)^+$ radical is expected to occur through one–electron oxidation to form selenium centered radical cation $(>Se)^{\bullet+}$, followed by its subsequent reaction with parent organoselenium compounds as shown in equation 4.15. The transient absorption spectrum for the similar study on SeEOH could not be performed.

$$CO_3^{\bullet-} + >Se \xrightarrow{-CO_3^{2-}} >Se^{\bullet+} \underset{}{\overset{>Se}{\rightleftharpoons}} (>Se\therefore Se<)^+ \qquad (4.15)$$

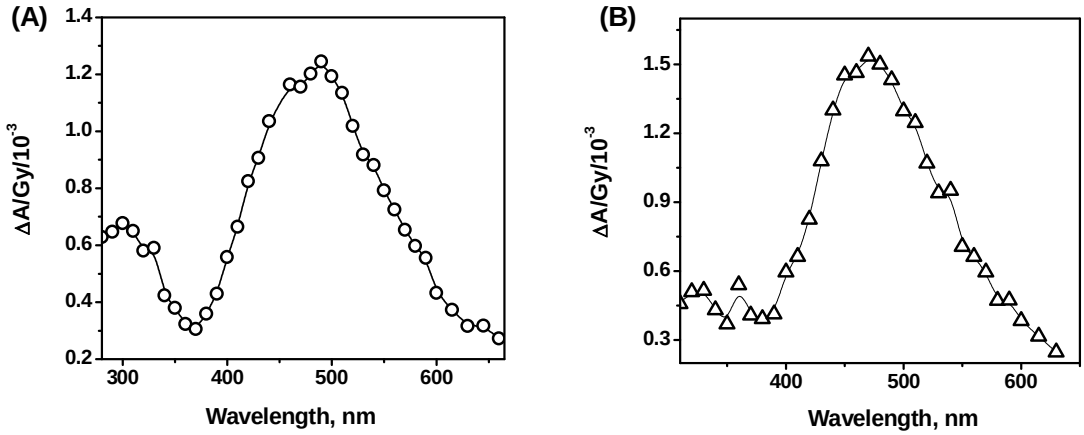

Fig. 4.8: *The transient absorption spectra generated by pulse radiolyzing N_2O saturated solution of (A) 1 mM DHS and (B) 1 mM MAS containing 0.1 M Na_2CO_3 at pH 7.4.*

Similarly, the reaction of DHS with $NO_2^{\bullet}$ radical was carried out using pulse radiolysis. However, no absorption band was observed in transient absorption spectra generated by pulse radiolysis of aqueous solution of DHS containing 0.1 M $NaNO_2$ indicating no reaction between $NO_2^{\bullet}$ radical and DHS under these present experimental conditions. The results were also confirmed by employing competition kinetics using $ABTS^{2-}$ as a reference solute.[182] $NO_2^{\bullet}$ radical reacts with $ABTS^{2-}$ to form $ABTS^{\bullet-}$ radical, formation of which can be monitored from its absorbance at 645 nm. In absence of DHS, a formation trace was observed for $ABTS^{\bullet-}$ radical at 645 nm on radiolysing N_2O saturated solution of 0.1 M $NaNO_2$ containing 100 μM of $ABTS^{2-}$. If DHS reacts with $NO_2^{\bullet}$ radical, they would compete with $ABTS^{2-}$ and a decrease in yield of $ABTS^{\bullet-}$ radical would be observed. However, no difference in absorbance of $ABTS^{\bullet-}$ radical was observed in the presence of 10 μM-500 μM of DHS indicating that DHS does not react with $NO_2^{\bullet}$ radical.

Similarly, no reaction was observed between $NO_2^{\bullet}$ radical and MAS or SeEOH. This could be due to the unfavorable redox potential of these compounds compared to $NO_2^{\bullet}$ radical.

4.3.3 Characterization of reaction products of organoselenium compounds with peroxynitrite

To understand the mechanism of the reaction of peroxynitrite with organoselenium compounds, detailed product analysis was carried out using NMR, HPLC and MS techniques. The results obtained are discussed below.

Fig. 4.9(A) shows the ^{77}Se NMR spectra of reaction mixture containing 60 mM DHS in heavy water (D_2O) and 20 mM peroxynitrite. The ^{77}Se NMR spectra showed two peaks at 69 ppm and 940 ppm. Using the earlier reported ^{77}Se NMR spectra of DHS by Iwaoka et al, the NMR peak at 69 ppm was attributed to DHS while that at 940 ppm was attributed to DHS_{ox}.[96a] No other peak was observed in ^{77}Se NMR spectra for this reaction. Similarly, ^{77}Se NMR spectra for reaction of MAS with peroxynitrite gave two signals at 120 ppm and 944 pm corresponding to MAS and MAS_{ox}, respectively as shown in fig. 4.9(B). Similar studies on SeEOH could not be carried out due to some experimental difficulties. However, it was expected that SeEOH would follow similar mechanism as DHS.

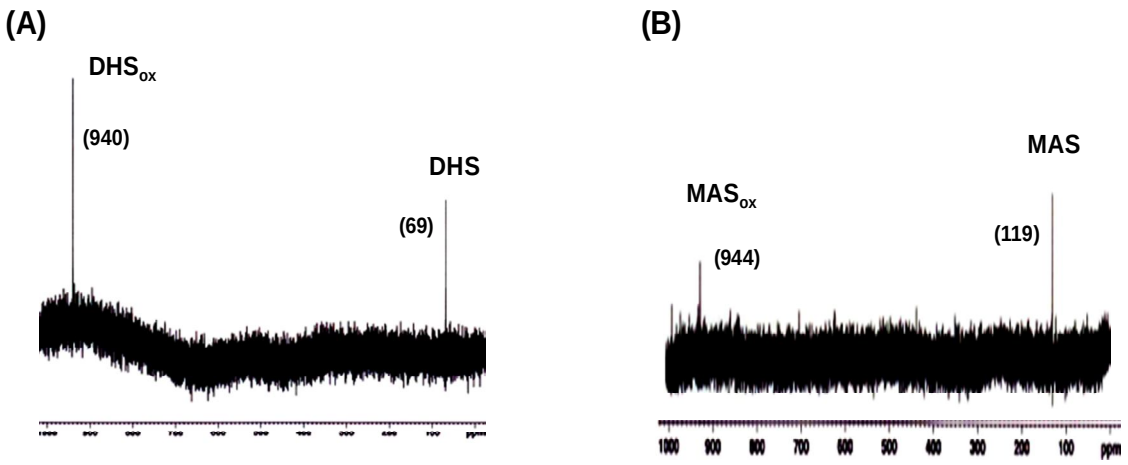

Fig. 4.9: *^{77}Se NMR spectra of 60 mM (A) DHS and (B) MAS incubated with 20 mM peroxynitrite in D_2O as solvent.*

Formation of DHS_{ox} and MAS_{ox} was further confirmed by ^{13}C NMR spectra recorded for the reaction mixture containing 20 mM peroxynitrite and 60 mM DHS/MAS. The ^{13}C NMR of peroxynitrite treated DHS gave six signals corresponding to DHS δ (27.52 ppm, 78.89 ppm) and DHS_{ox} δ (54.11 ppm, 58.57 ppm, 79.6 ppm, 80.03 ppm). These results indicate that the primary reaction of these compounds with peroxynitrite is either electron transfer followed by hydrolysis or oxygen atom transfer to form the selenoxides (>Se=O) and NO_2^- as shown in equation 4.16.

$$>Se + ONOO^- \longrightarrow >Se{=}O + NO_2^- \qquad (4.16)$$

To further confirm the formation of selenoxides during the reaction of DHS and MAS with peroxynitrite, MS measurements were carried out. Fig. 4.10 (A & B) shows the mass spectra of the reaction mixture containing 0.5 mM peroxynitrite incubated with 1 mM DHS and MAS respectively. DHS showed an intense peak at m/z value of 185

corresponding to presence of DHS_{ox}. Similarly, for the reaction of MAS with peroxynitrite two major peaks were obtained at m/z values of 152 and 168. These mass peaks were attributed to molecular ion peaks of MAS and MAS_{ox}. These results confirmed the formation of corresponding selenoxides during the reaction of peroxynitrite with organoselenium compounds under study. Similar studies with SeEOH were not performed.

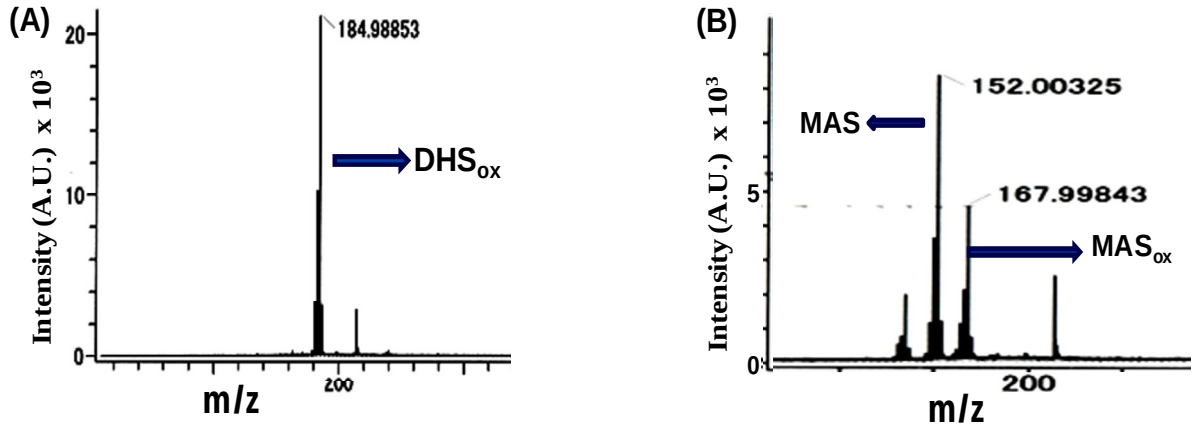

Fig. 4.10: *Mass spectra generated by reaction of 0.5 mM peroxynitrite with 1 mM (A) DHS and (B) MAS.*

4.3.4 Estimation of selenoxide by HPLC analysis

The amount of selenoxides formed during the reaction of peroxynitrite with organoselenium compounds under study, HPLC measurement were carried out. Selenoxides are known to react with thiols like DTT and GSH quantitatively and this reaction can be used to estimate their yields. GSH reduces selenoxides to give parent selenium compound and GSSG as given in equation 4.17. The amount of GSSG formed during the reaction can be easily detected and quantified using HPLC technique and represents the amount of selenoxide present in reaction mixture.

$$> Se = O + 2GSH \rightarrow\!\!> Se + GSSG + H_2O \qquad (4.17)$$

As GSH reacts directly with peroxynitrite (k=5.8 x10^2 $M^{-1}s^{-1}$), there can be error in the estimation of yield of GSSG by following reaction 4.17.[161a] Therefore, in order to avoid reaction of peroxynitrite with GSH, first the organoselenium compounds (0.1 mM) was treated with stoichiometric amount of peroxynitrite (0.1 mM) and the reaction was allowed to complete (mixture was incubated for 5 min) followed by addition of GSH (1 mM). It is expected that by this time all the peroxynitrite would have been consumed by the selenium compound and nothing would remain to react with GSH. The reaction components were eluted using 5:95 acetonitrile:water containing 0.1% TFA.

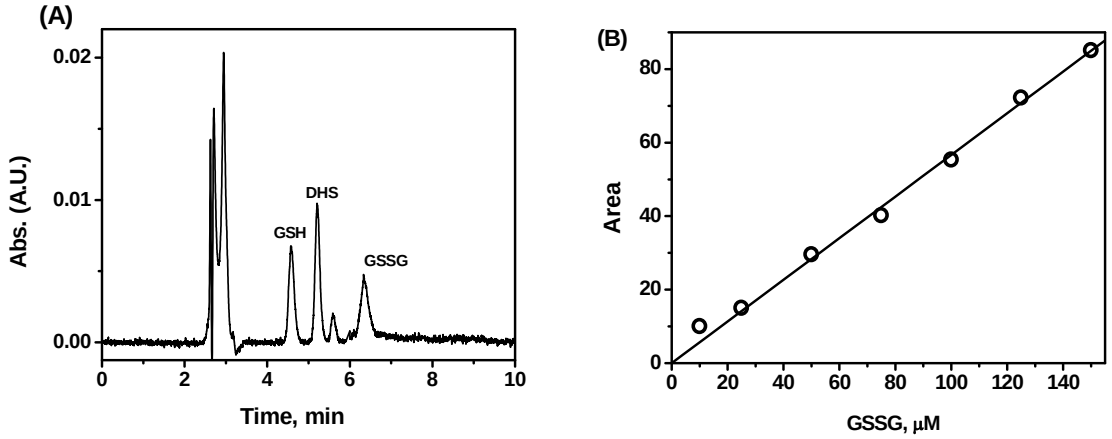

Fig. 4.11: *(A) HPLC chromatogram generated by reaction of 0.1 mM peroxynitrite with 0.1mM DHS in the presence of 1 mM GSH. Fig (B) shows the calibration plot of area under GSSG peak at 6.3 min as a function of GSSG concentration (10-150 μM).*

Fig. 4.11 (A) represents the HPLC chromatogram obtained for the reaction of peroxynitrite treated DHS with GSH. Among the different reaction components, GSH eluted first, followed by DHS and GSSG with retention time of 4.6 min, 5.1 min and 6.3

min, respectively. For quantification of GSSG, standard calibration curve (GSSG peak area v/s GSSG concentration) was made by using known concentration (10-150 μM) of GSSG standards. The area under GSSG peak for each reaction sample was calculated and plotted against GSSG concentration to make a calibration plot as shown in fig. 4.11(B). From the calibration curve, the estimated yield of DHS_{ox} was 63 ± 5 μM.

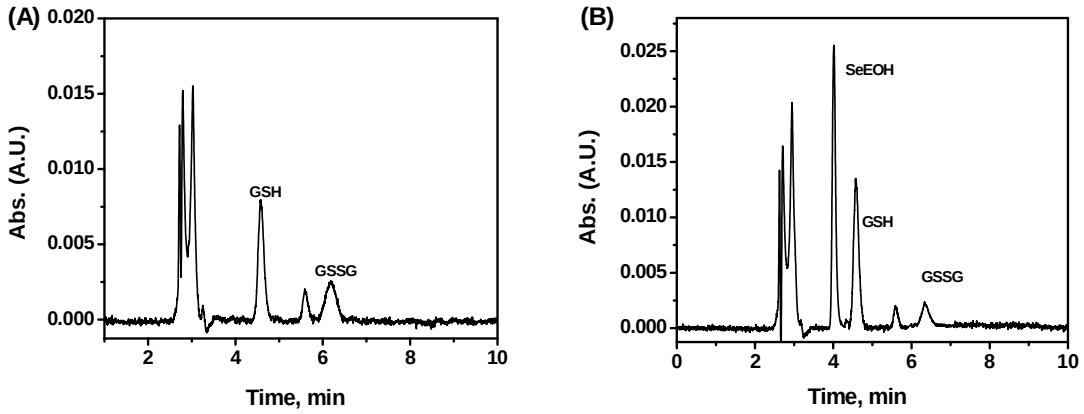

Fig. 4.12: *HPLC chromatogram generated by reaction of 0.1 mM peroxynitrite with (A) 0.1mM MAS and (B) 0.1 mM SeEOH.*

Similarly, the reaction of 0.1 mM MAS/SeEOH with 0.1 mM peroxynitrite was carried out. After 5 minutes, the reaction samples were treated with 1 mM GSH and injected to HPLC. Fig. 4.12(A&B) represents the HPLC chromatogram obtained for the reaction of peroxynitrite with MAS and SeEOH, respectively. From the calibration plot of GSSG, the estimated yield of MAS_{ox} and $SeEOH_{ox}$ were 40 ± 3 μM and 28 ± 2 μM. The estimated yield of DHS_{ox}, MAS_{ox} and $SeEOH_{ox}$ corresponded to 63 ± 5%, 40 ± 3% and 28 ± 2% of the peroxynitrite concentration (0.1 mM) used for the measurement. The yield of selenoxide formed during the reaction of peroxynitrite with MAS and SeEOH was much lower than that for DHS. Lower yield of MAS_{ox} could be due to involvement of the amine

group of MAS in direct reaction with peroxynitrite (nitration or nitrosation).[183] The contribution of these reactions would decrease the fraction of peroxynitrite undergoing direct oxygen-atom transfer to MAS. The relatively low yield of $SeEOH_{ox}$ may be due to poor stability of $SeEOH_{ox}$. Moreover, its reaction with both peroxynitrite and its derived radicals is very slow. As a result of this, the self decay of peroxynitrite through isomerisation can compete with its reaction with SeEOH. This results in decrease in overall yield of $SeEOH_{ox}$.

The selenoxides obtained by above method will have contribution from both direct reaction with peroxynitrite (equation 4.12) and reaction with its derived species i.e. $CO_3^{\bullet-}$ radical (equation 3.19, 3.22 and 4.15). In a separate experiment, the yield of selenoxides formed on the reaction of DHS, MAS and SeEOH with $CO_3^{\bullet-}$ radical was estimated by HPLC using GSH-GSSG method. For this, the reaction mixture containing 5 mM DHS/MAS/SeEOH and 0.1 M Na_2CO_3 was irradiated with γ-radiation (720 Gy). The irradiated samples were then incubated with 2 mM GSH for 5 minutes and amount of GSSG formed was calculated by HPLC measurements. The radiation chemical yield (G) of DHS_{ox}, MAS_{ox} and $SeEOH_{ox}$ under these conditions was estimated to be 0.60 ± 0.03, 0.32 ± 0.02 and 0.24 ± 0.01 μmol/J, respectively which correspond to 87%, 46% and 35% of $CO_3^{\bullet-}$ radical formed ($G_{CO3}^{\bullet-}$ =0.69 μmol/J) due to radiolysis.

As stated earlier, under some conditions, selenoxides formed during the reaction of organoselenium compounds with peroxynitrite, can react with NO_2^- as shown in equation 4.8. If such a reaction occurs, it will lead to conversion of NO_2^- to NO_3^- and regeneration

of parent compound (equation 4.8 and 4.16). Therefore, to estimate the contribution of this reaction, the conversion of NO_2^- to $NO_3^-$was studied and discussed below.

4.3.5 NO_2^- to NO_3^- conversion by selenoxides

As seen in equation 4.8, the reaction of NO_2^- with selenoxides results in formation of NO_3^-. The reaction can be monitored by estimating the amount of NO_3^- formed during the reaction. For this, the reaction of NO_3^- with resorcinol to form nitro-resorcinol was utilised as earlier reported by Zhang et al.[178] At acidic pH, resorcinol in presence of NO_3^- form nitro-resorcinol which can be monitored from its absorption at 505 nm (ε=1.7 x 10^4 $M^{-1}cm^{-1}$). This reaction is quantitative and amount of nitro-resorcinol formed can be directly correlated with amount of NO_3^- present in the reaction system. For the present experiment, 0.3 mM peroxynitrite solution was incubated with 0.1 mM of organoselenium compounds at pH 7.4 for 5 minutes. To this, acidic solution of 11 mM resorcinol containing 0.1 M H_2SO_4 was added and further incubated for 2 minutes. To estimate the extent of self isomerisation, buffered (pH 7.4) peroxynitrite solution was treated with acidic solution of resorcinol and was used as control. The amount of nitro-resorcinol formed was estimated from its absorbance at 505 nm. In the absence of organoselenium compounds, the amount of NO_3^- formed was estimated to be 6.8 ± 0.02 μM. In presence of 0.1 mM organoselenium compounds, the yield of NO_3^- increased significantly and the estimated values were 13.4 ± 0.6 μM, 9.9 ± 0.3 μM and 3.8 ± 0.2 μM for DHS, MAS and SeEOH, respectively. Also, the bimolecular rate constant for the reaction of NO_2^- with selenoxides was estimated by monitoring the kinetics of the formation of nitro-resorcinol at 505 nm. For this, 2 mM of DHS_{ox} was treated with 25 μM-200 μM $NaNO_2$ in presence

of 5 mM acidified resorcinol and the rate constant (k_{obs}) for the formation of nitro-resorcinol was estimated. From the linear plot of k_{obs} as a function of $NaNO_2$ concentration, the bimolecular rate constant was estimated. The bimolecular rate constant for the reaction of NO_2^- with DHS_{ox}, MAS_{ox} and $SeEOH_{ox}$ were estimated to be (19.8 ± 0.6), (14.5 ± 0.4) and (11.6 ± 0.7) $M^{-1}s^{-1}$, respectively. As most (~85-90%) of peroxynitrite reacts mainly with CO_2 and only a fraction z~10-15%) reacts directly with organoselenium compounds, the yield of NO_2^- formed would be only ~10-15% of initial amount of peroxynitrite and contribution of NO_2^- to NO_3^- would be negligible in comparison to GSH mediated regeneration of organoselenium compounds.

To further confirm the role of $DHS_{ox}/MAS_{ox}/SeEOH_{ox}$ in conversion of NO_2^- to NO_3^-, direct reaction between DHS_{ox} and NO_2^- was carried out. According to equation 4.8, this reaction leads to conversion of selenoxide to organoselenium compound which can be easily monitored by HPLC measurements. For this, 0.2 mM of $NaNO_2$ solution was incubated with 1 mM of DHS_{ox} and injected to HPLC. Fig. 4.13 shows the chromatogram of 1 mM DHS_{ox} (a) in absence and (b) in presence of NO_2^-. As seen in fig. 4.13(b), in absence of NO_2^- only one peak was observed at 3.2 minutes corresponding to DHS_{ox}. On addition of 0.2 mM $NaNO_2$, DHS_{ox} peak decreased with appearance of a new peak at 4.8 minutes corresponding to DHS.

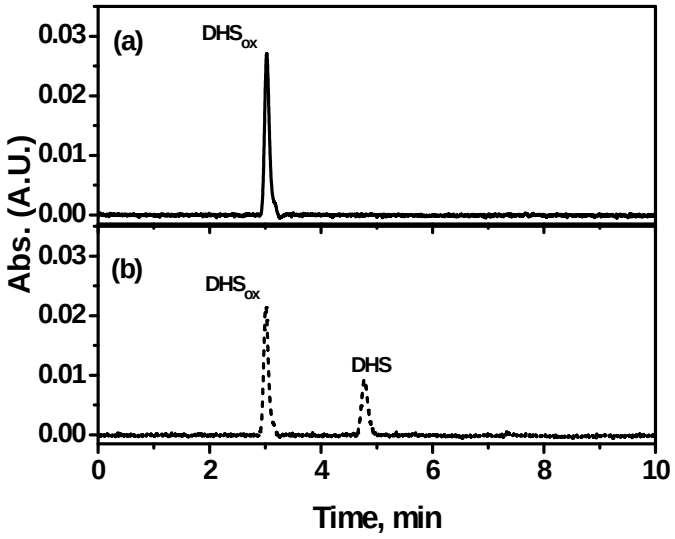

Fig. 4.13: *HPLC chromatogram of 1 mM DHS_{ox} (a) in absence and (b) in the presence of 0.2 mM $NaNO_2$ in 70 mM phosphate buffer at pH 7.4.*

The amount of DHS formed was calculated by plotting a calibration curve of the known concentration of standard DHS sample. From the calibration curve, the amount of DHS formed was estimated to be 0.15 ± 0.03 mM and accounts for ~ 75 % of total NO_2^- concentration (0.2 mM). Similar studies on MAS and SeEOH could not be done due to the instability of MAS_{ox} and $SeEOH_{ox}$. These results indicate that selenoxides of DHS/MAS/SeEOH have the ability to convert NO_2^- to NO_3^- and regenerate parent molecule i.e. DHS/MAS/SeEOH. These results showed that although the initial reaction of these compounds with peroxynitrite leads to formation of selenoxides and NO_2^-, these products further react to generate less reactive NO_3^-. This reaction can be of advantage as it provides a catalytic pathway for reduction of oxidative stress induced by peroxynitrite and nitrosative stress induced by NO_2^-.[184] The overall reaction of these organoselenium compounds with peroxynitrite is summarised below.

As stated earlier and shown in scheme 4.3, only 10% of initial peroxynitrite reacts directly with organoselenium compounds while ~90% of peroxynitrite reacts with CO_2 to to form $CO_3^{\bullet-}$ and $NO_2^{\bullet}$ radicals via $[ONOO\text{-}CO_2]^-$ adduct with a yield of ~65% as represented in scheme 4.3. In case of DHS, about 90% of $CO_3^{\bullet-}$ radicals are scavenged by DHS to form corresponding DHS_{ox} and if this is the primary reaction for formation of selenoxide, the reaction of peroxynitrite with DHS should generate selenoxide with a yield of ~60% relative to amount of peroxynitrite used. The experimental yield (63%) of DHS_{ox} matches quite well with these results.

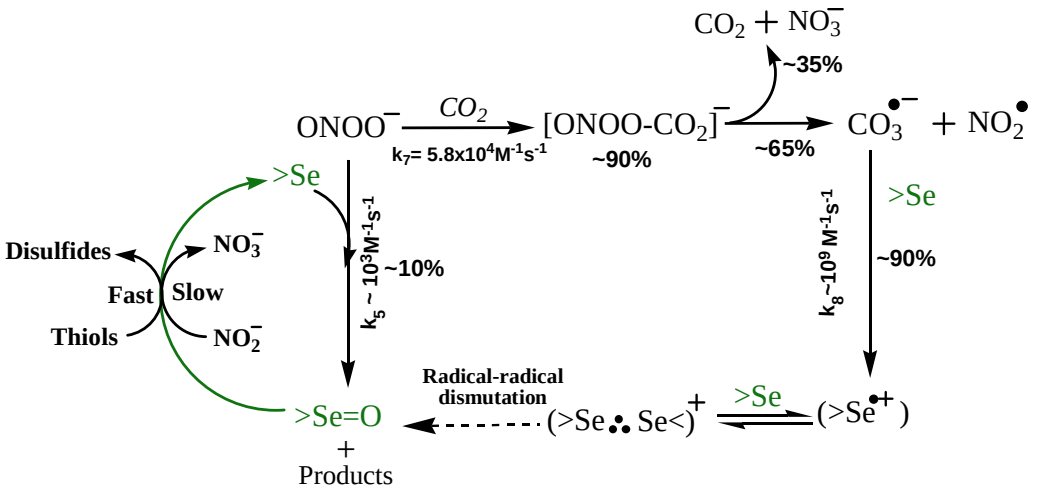

Scheme 4.3: *Schematic presentation for the catalytic degradation of peroxynitrite by organoselenium compounds and contribution of different pathways.*

Unlike DHS, for MAS and SeEOH, direct correlation between kinetically calculated and experimentally estimated amount of selenoxide was not observed. The calculated yield of MAS_{ox} (~55%) and $SeEOH_{ox}$ (~42%) were found to be higher than the observed values (MAS_{ox}=40%, $SeEOH_{ox}$=28%). This was attributed to involvement of side reactions and instability of MAS_{ox} and $SeEOH_{ox}$. In the above scheme 4.3, formation of

selenoxide is crucial as it can be regenerated back to parent organoselenium compound in the presence of thiols. The selenoxide derived from most of the other selenium antioxidants are unstable and undergo degradation either due to fast hydrolysis to form seleninic acid (as found in ebselen) or by *syn*-elimination as in SeCys.[170,176] In contrast, DHS_{ox} is quite stable and does not undergo degradation. Therefore, the yield and stability of selenoxides could play a major role while deciding the antioxidant activity of selenium compounds.

The above studies indicate that these compounds should be able to protect biomolecules against peroxynitrite induced damage. To assess the ability of DHS/MAS/SeEOH to prevent peroxynitrite induced damage in vitro experiments were carried out and discussed below.

4.3.6 Effect of organoselenium compounds on peroxynitrite induced DNA damage

Peroxynitrite and its degraded products are found to be genotoxic and induce strand breaks in DNA, leading to transformation of super coiled (SC) double stranded DNA to linear (LN) and circular forms.[108] The protection ability of organoselenium compounds against peroxynitrite induced damage to pBR322 DNA was estimated using gel electrophoresis as discussed earlier in section 2.10.2 in chapter 2. Fig. 4.14 (A) shows the gel images of the electrophoretic pattern of the control DNA(lane 1), DNA treated with peroxynitrite in the absence (lane 2) and in the presence of 0.1 mM to 1 mM DHS (lane 3-0.1 mM, lane 4-0.2 mM, lane 5-0.4 mM, lane 6-0.6 mM, lane 7-0.8 mM, lane 8-1 mM).

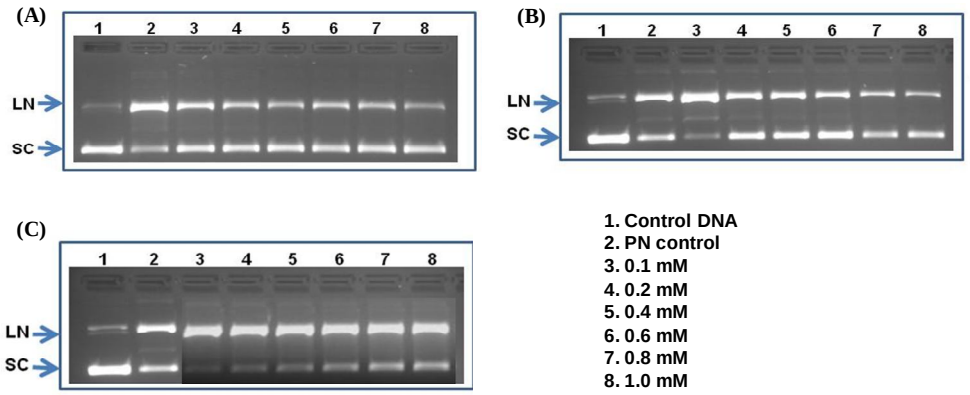

Fig. 4.14: *Gel images of control pBR322 (lane 1) and pBR322 treated with 0.5 mM peroxynitrite in absence (lane 2) and the presence 0.1-1.0 mM (lane 3-8) of (A) DHS, (B) MAS and (C) SeEOH. LN and SC refer to linear and super coiled form of pBR322.*

To estimate the percentage damage, fraction of SC-DNA in each lane was calculated and that in control sample was taken as 1. The percentage protection was estimated by using equation 2.46 in chapter 2. It was found that treatment of peroxynitrite leads to considerable decrease (~70%) in intensity of SC-DNA compared to that of control DNA. On addition of DHS, the band intensity of SC-DNA increased and that of LN-DNA decreased in concentration dependent manner. Similarly, fig. 4.14 (B & C) shows the gel images of pBR322 alone (lane 1) and treated with peroxynitrite in presence of 0-1 mM MAS and SeEOH (lane 2-8), respectively.

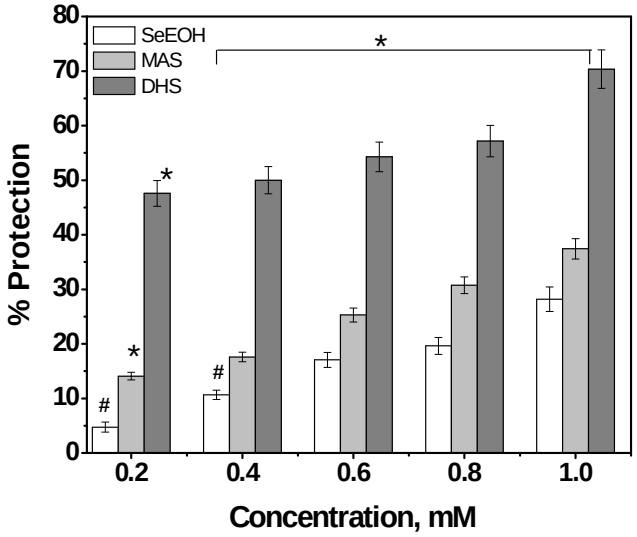

Fig. 4.15: *Concentration dependent protection shown by organoselenium compounds towards peroxynitrite induced DNA damage. Data presented are mean ± SEM of three independent sets of experiments. (*P<0.001, t-TEST)*

Fig. 4.15 represents the percentage protection exhibited by the organoselenium compounds against peroxynitrite induced DNA damage as a function of concentration. From the graph it can be inferred that all the three compounds under study showed protection to DNA against peroxynitrite induced damage in a concentration dependent manner. At any given concentration, DHS showed better protection than MAS and SeEOH. The IC_{50} value, i.e. the concentration required to protect DNA from peroxynitrite induced damage by 50% was estimated to be 0.42 mM for DHS. The same could not be estimated for MAS and SeEOH and is expected to be >1 mM for MAS and SeEOH. At a fixed concentration of 1 mM, the respective values of DNA protection exerted by DHS, MAS and SeEOH are 70 ± 4%, 37 ± 3% and 28 ± 3%, respectively.

4.3.7 Effect of organoselenium compounds on peroxynitrite induced cytotoxicity

As stated earlier, peroxynitrite and its derived radicals are cytotoxic, therefore to see the effect of organoselenium compounds on peroxynitrite induced cellular toxicity MTT assay was performed on CHO cells and the experimental details are given in section 2.10.1 in chapter 2.[107] First, these compounds were evaluated for their toxicity in CHO cells in absence of peroxynitrite. The results indicated that DHS did not show any toxicity upto 5 mM concentration; however SeEOH and MAS showed slight toxicity (< 5%) when used in mM range. To avoid intrinsic toxicity of SeEOH and MAS, compound concentration was limited up to 0.5 mM only. Pretreated cells with 0-0.5 mM DHS, MAS and SeEOH for 4 hours, were exposed to 0.5 mM peroxynitrite for 10 minutes and cellular toxicity was measured by MTT assay. Fig. 4.16 shows the percentage viability of cells exposed to peroxynitrite without and with organoselenium compound treatment. Addition of 0.5 mM peroxynitrite to CHO cells resulted in reduction of cell viability by ~18%. Pretreatment of cells with DHS, MAS and SeEOH up to a concentration of 0.3 mM did not show any significant effect on cell viability. However at higher concentrations (0.3 mM - 0.5 mM), DHS exhibited concentration dependent protection whereas, SeEOH and MAS showed marginal protection, suggesting that DHS is better than SeEOH or MAS in protecting the CHO cells from peroxynitrite induced cytotoxicity. The protection exhibited by DHS, MAS and SeEOH at a fixed concentration of 0.5 mM, was 63 ± 4, 29 ± 3 and 23 ± 3%, respectively.

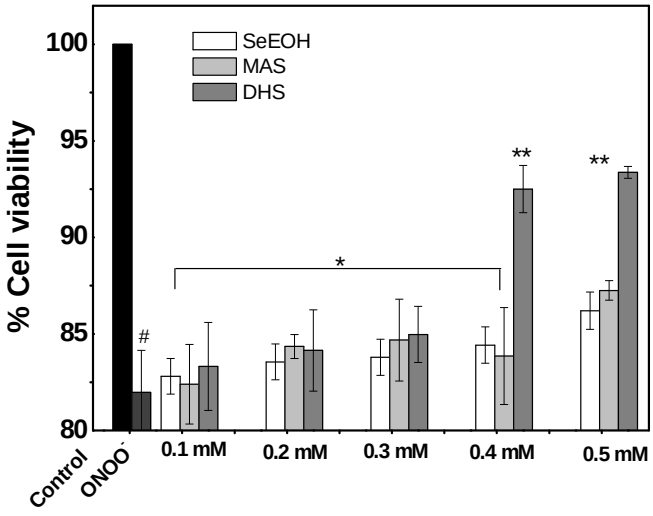

Fig. 4.16: *Concentration dependent protection shown by organoselenium compounds towards peroxynitrite (0.5 mM) induced cellular toxicity in CHO cells. Control refers to absence of peroxynitrite and organoselenium compounds. Data are mean ± S.E.M. from two independent experiments, each one assayed in triplicate. #P < 0.001 vs. control; *P < 0.05 and **P < 0.01 vs. peroxynitrite-treated cells.*

In both the assays (DNA damage and cellular toxicity), DHS showed significantly higher protection (~2 times) against peroxynitrite induced damage than MAS or SeEOH. Also, HPLC measurements showed that the yield of selenoxide obtained for reaction of peroxynitrite with DHS (~63%) was higher than that for MAS (~40%) and SeEOH (~28%). Overall, these results confirmed that the antioxidant activity of these compounds, estimated in terms of protection against peroxynitrite induced damage, can be directly correlated to the yield of selenoxide formed during their reaction with peroxynitrite. Formation of selenoxide is very important as it can regenerate the parent compound in the presence of thiols. Also, regeneration of parent organoselenium compounds through

reaction of NO_2^- with selenoxide may contribute to overall catalytic degradation of peroxynitrite.

4.4 Conclusions

Peroxynitrite is a powerful molecular oxidant, contributing significantly to pathophysiology of many diseases associated with oxidative stress. Present study signifies the reactivity and mechanism of the reaction of low molecular weight and water soluble organoselenium compounds having GPx like activity with peroxynitrite. Three different types of organoselenium compounds, DHS (cyclic), SeEOH (linear) and 3-monoamineselenolane (MAS-functional analogue of DHS) were tested for their scavenging ability towards peroxynitrite. The results for this study are summarized below.

1. DHS, MAS and SeEOH scavenge peroxynitrite with bimolecular rate constants in the order of ~10^3. DHS showed the highest reactivity followed by MAS. SeEOH was found to be the least reactive towards peroxynitrite.

2. All the three compounds also scavenge $CO_3^{\bullet -}$ radical and NO_2^- and the activity followed the order DHS > MAS > SeEOH. None of these compounds in given experimental conditions, react with $NO_2^{\bullet}$ radical.

3. The reaction of peroxynitrite with organoselenium compounds resulted in formation of their corresponding selenoxides i.e. DHS_{ox}, MAS_{ox} and $SeEOH_{ox}$. The percentage yield of selenoxides formed on reaction of DHS, MAS and SeEOH with peroxynitrite was 63 ± 5%, 40 ± 3% and 28 ± 2%.

4. These compounds also showed protection against peroxynitrite induced cellular toxicity and pBR322 DNA damage. DHS showed preferentially higher (two times) antioxidant activity and was attributed to the higher yield of selenoxide formed during its reaction with peroxynitrite and its derived radicals.

5. The studies propose that formation of stable selenoxides during oxidation of organoselenium compounds and their easy reversibility to parent selenium compound using thiols is an important criterion for enabling such compounds to act as efficient antioxidants.

Chapter 5

Studies on binding of organoselenium compounds with gold nanoparticles (GNP) and effect on their redox properties

This chapter explores the binding of two structural isomers DHS and SeEOH with GNP. This includes interaction of GNP with selenium compounds to form Se-GNP nanocomposites and their characterization using different analytical techniques like absorption spectroscopy, DLS, TEM, SERS, etc. Further, electron transfer reactions of these nanocomposites have been studied to understand the influence of GNP binding on redox properties of selenium compounds.

5.1 Introduction

Inorganic colloidal nanoparticles depending on the material they consist of, possess a number of different properties such as high electron density, strong optical absorption photoluminescence, etc.[185] Among the metal nanoparticles, GNP occupy the central place due to its ease of preparation, outstanding colloidal stability and unique physico-chemical properties.[186] Historically, the use of GNP originated from Egypt and China around 5th century B.C., where it was widely used as pigment in enamel, silk fabric and glass.[187] In the middle ages, GNP has been used for treatment of various diseases such as dysentery, epilepsy and tumors. The actual scientific research on GNP started when Faraday in the year 1857, reported the formation of a deep red solution of colloidal gold by reduction of an aqueous solution of chloroaurate ($AuCl_4^-$) using phosphorus in carbon disulfide (CS_2).[188] Since then, there have been a lot of reports signifying the importance of GNP and its unique properties with special application in material science and medicines.[189]

GNP allows a wide range of ligands to be encapsulated through non-covalent interactions or chemical conjugation. It has provided a novel platform for nano biotechnology and biomedicine because of surface conjugation with biomolecules and remarkable optical properties related to the localized surface plasmon resonance (SPR).[190] Also, functionalized GNP has shown promising results in target specific drug delivery and detection of biomolecules like thiols, proteins and nucleic acids.[191] Recently, GNP have been proposed as novel radio sensitizing agents for killing of cancer cells due to their strong photoelectric absorption coefficient.[192]

For medical and therapeutic application, maintaining the stability of GNP is very important. This can be achieved by surface functionalization with a suitable ligand. Such surface functionalization can help in passivation of GNP surface and suppress its aggregation. For this, it is necessary to identify suitable ligands and understand ligand interactions with GNP. Binding of ligand with GNP surface can lead to change in photo physical/chemical behavior of GNP as well as in the electronic properties of ligand.[193] The optical and chemical properties of these nanocomposites can be tuned by the strength of ligand interaction with GNP which in turn depends on the size of GNP and structure of ligand.[194] A wide range of ligands containing thiols, amines and carboxylate functional groups have been studied as substrates for the surface modification of GNP.[195,196] Being a soft electrophile, binding of GNP with soft nucleophiles like sulfur and phosphorus ligands has been found to be advantageous. The binding of organosulfur compounds especially organothiols to GNP has been well studied. The high binding affinity of thiols to GNP has been explored for surface modification to improve stability, functionality and toxicity for many biomedical applications.[197] GSH, Cys and CysA coated GNP have been used for imaging of cancer cells.[198] Self assembled layers (SAM) of thiols like GSH, dihydrolipoic acid, 2-mercapto ethanol, etc., on GNP surface have applications in nanotechnology and diagnostics.[199] Thiol functionalization of GNP takes place through covalent interaction between sulfur and surface gold atoms. In alkyl thiolates, alkyl chain attached to sulfur atom although does not interact with GNP directly but affects the adsorption energy involved in the formation of SAM.[199a,200] Although the interaction between ligands having heteroatom like phosphorus, nitrogen and sulfur with GNP for surface passivation have been well explored, such studies with selenium compounds are not much reported.[201]

Selenium, the heavier member of chalcogen group is comparatively more polarizable and a better nucleophile. This property will lead to strong covalent interaction between selenium and gold atoms present on the surface of GNP. Therefore, surface functionalization of GNP with selenium compounds can be advantageous. The first report on interaction of organoselenium compounds with GNP was published in 1992 by Samant and co-workers where they showed the formation of an ordered SAM of docosaneselenol on gold surface.[202] Bandopadhyay et al reported formation of SAM of different aromatic and aliphatic organoselenium compounds on GNP surface. They showed that the aliphatic chains of alkaneselenoates produced considerably denser packing than alkanethiol on gold surface.[203]. The SERS studies on aromatic selenium compounds like benzeneselenol, diphenyl diselenide, dibenzyl diselenide, dioctyl diselenide, and benzyl phenyl selenide showed that along with the Au-Se interaction, additional interactions exist between the benzene ring and GNP surface which results in higher stabilization of GNP nanocomposites as compared to analogous aliphatic selenium compounds.[204] Han et.al. further showed that the binding of aliphatic diselenides to GNP surface results in cleavage of Se-Se bond leading to formation of GNP-selenolate nanocomposites similar to that of organic disulfides.[26] The binding of alkyl diselenides to GNP was also found to alter their redox behavior where the GNP nanocomposites showed faster electron transfer compared to parent selenium compounds.[205] Xang et. al. using cyclic voltametery, have shown that binding on GNP leads to increase in one-electron reduction potential of aliphatic diselenides like dioctyldiselenide.[206] From the different studies carried out on selenium-GNP binding, it is anticipated that the change in structure of organoselenium compounds can significantly affect its mode of interaction with GNP and in turn its electron transfer

properties. Till now, the studies carried out on binding of organoselenium compounds with GNP are mainly limited to characterization of ligand-GNP surface interactions. However, the effect of such ligand-GNP interaction on electron transfer properties of organoselenium compounds has not been well understood. Therefore it becomes important to understand the structure dependent interaction of organoselenium compounds with GNP and its effect on their redox properties.

Here in this chapter, binding of two organoselenium compounds, DHS and SeEOH with GNP of different sizes was carried out (Scheme 5.1). DHS and SeEOH are structural isomers and have shown differential GPx like activity.[94] The binding of DHS with GNP surface is expected to change the electron density on selenium centre which in turn will be reflected in its redox properties and also its antioxidant activity.

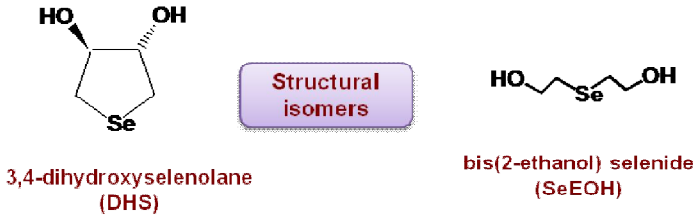

Scheme 5.1: *Chemical structure of SeEOH and DHS.*

5.2 Materials and methods

GNP samples were prepared by treating aqueous solution of $KAuCl_4$ and Na_3-citrate according to Turkewich method with slight modification and the detailed synthesis is given in chapter 2.[98] The characterization of GNP and Selenium-GNP conjugates was carried out by using techniques such as absorption spectrophotometer, DLS, TEM and

SERS. The electron transfer reactions of SeEOH/DHS-GNP were studied by employing their reaction with $ABTS^{\bullet-}$ radical and $^{\bullet}OH$ radicals.

5.3 Results and Discussion

5.3.1 Absorption spectroscopic studies of GNP: GNP of four different sizes (GNP1 (brown color), GNP2 (pink color), GNP3 (wine red color) and GNP4 (purple color)) were prepared and are shown in fig. 5.1(A). GNP shows absorption spectrum in the range of 510-800 nm due to the presence of SPR, which is highly specific to its size and shape. The absorption band is also affected by dielectric constant of the medium, surface functionalization and interparticle distance.[207] Fig. 5.1(B) shows the absorption spectra of the GNP samples with absorption maxima at 510 nm, 522 nm, 527 nm and 531 nm for 7 nM of GNP1, GNP2, GNP3 and GNP4, respectively. The red shift in absorption maximum from GNP1 to GNP4 indicates that the size of GNP follows the order GNP4 > GNP3 > GNP2 > GNP1. The broadness of the absorption peak can be related to the dispersity in the GNP size. As, the full width at half maximum (FWHM) value is higher for GNP4 followed by GNP3, GNP2 and GNP1, suggesting increase in particle size distribution with increase in GNP size.

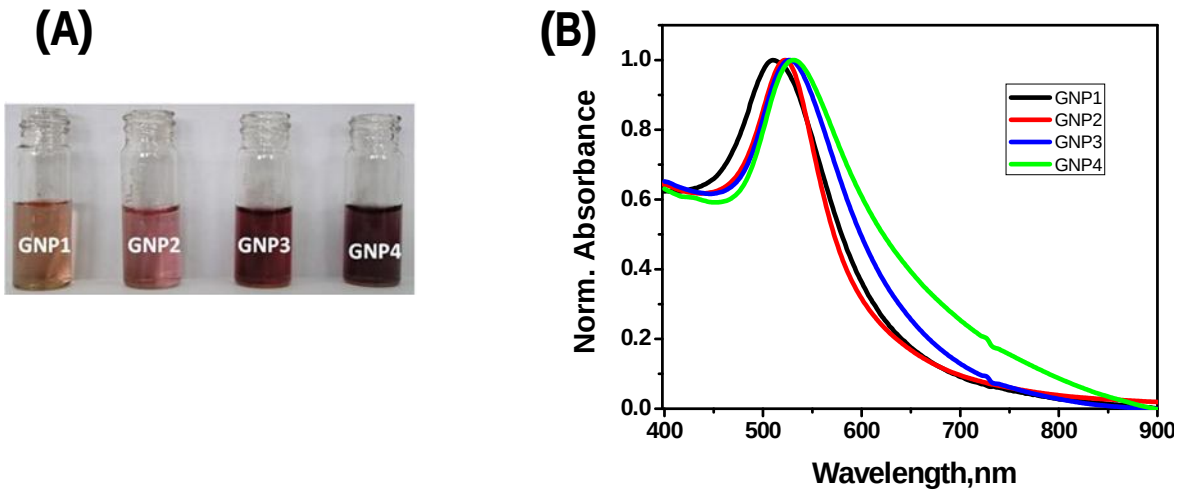

Fig. 5.1: *(A) Images of GNP samples and (B) normalized absorption spectra of 7 nM GNP1, GNP2, GNP3 and GNP4.*

5.3.2 Binding of DHS with GNP

5.3.2.1 Absorption spectroscopic studies: As, the SPR band of GNP is very sensitive to its environment, it can be used to study the interaction of a ligand with GNP. Therefore, the binding of DHS with GNP was studied by following the absorption spectra of GNP as a function of DHS concentration. For this, GNP samples were incubated with different concentration of DHS (0.05 mM-5 mM) for 5 minutes and absorption spectra were recorded. Fig. 5.2 shows the variation in absorption spectra of GNP1 as a function of DHS concentration (0.1 mM-2 mM). In the presence of DHS, the absorbance of GNP1 at 510 nm decreased and the spectra were red shifted to 520-580 nm. The spectral changes in the SPR band of GNP on addition of DHS indicated that DHS induces aggregation of GNP.[208]

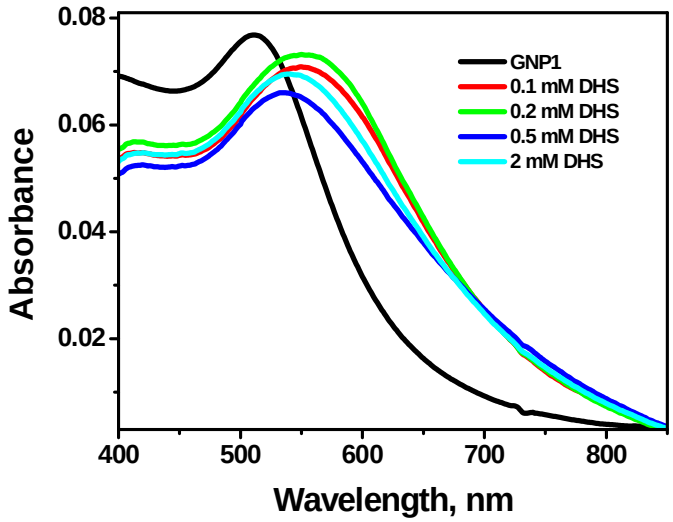

Fig. 5.2: *Variation in absorption spectra of GNP1 as a function of DHS concentration (0.1 mM-2 mM).*

Similarly, the absorption spectra of GNP2, GNP3 and GNP4 were recorded in presence of DHS. Fig. 5.3 shows the change in absorption spectra of GNP2 as a function of DHS concentration (0.05 mM-1 mM). In absence of DHS, GNP2 exhibited its peak maximum at 522 nm which on addition of 0.1 mM of DHS decreased considerably with concomitant evolution of a new absorption band at ~ 720 nm (Fig. 5.3).

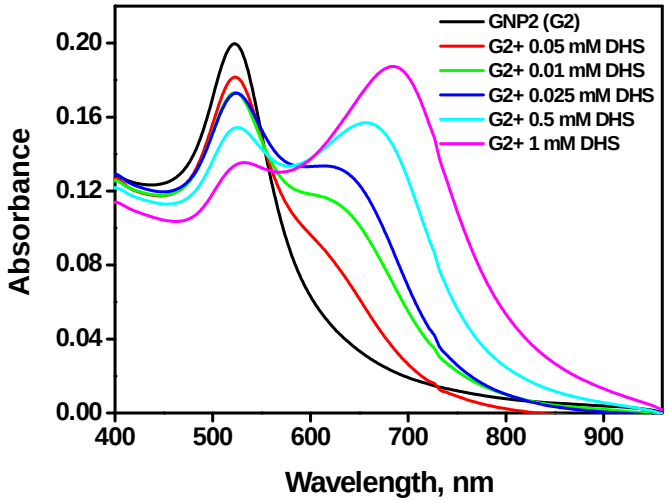

Fig. 5.3: *Variation in absorption spectra of GNP2 as a function of DHS concentration (0.05 mM-1 mM).*

The red shift in SPR band (520 nm) of GNP2 to ~720 nm, in presence of DHS indicates that the interaction of DHS with GNP2 leads to aggregation. Similar studies were carried out for GNP3 and GNP4. As shown in fig. 5.4 (A), addition of DHS (0.1 mM-1 mM) to GNP3, resulted in decrease in the absorbance at 527 nm with evolution of a new absorption band at ~720 nm. Similarly, addition of (0.05 mM-1 mM) DHS to GNP4 solution shifted its SPR band from 531 nm to ~750 nm as represented in fig. 5.4(B). These results indicate that DHS interacts with GNP and causes aggregation in GNP solution.

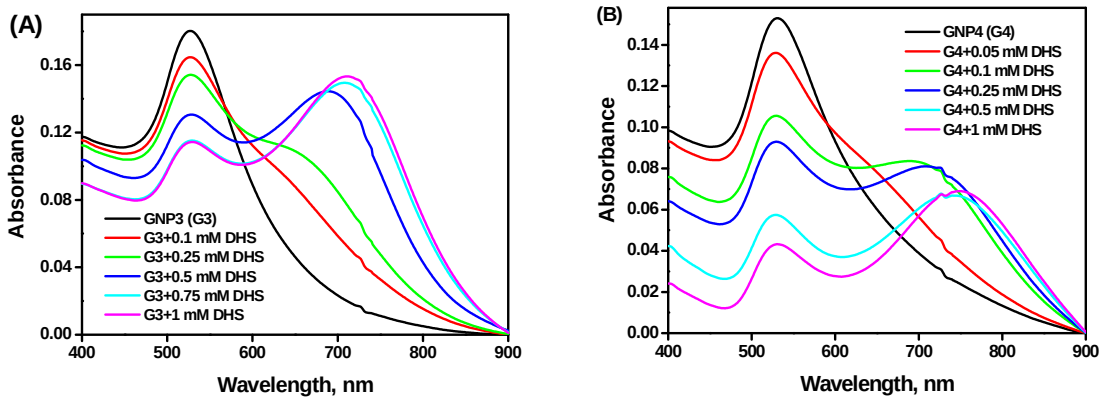

Fig. 5.4: *Absorption spectra of (A) GNP3 and (B) GNP4 as a function of DHS concentration (0 mM-1 mM).*

Further, to estimate the strength of binding interaction between DHS and GNP, binding constant (K) was calculated as described below.

Estimation of K: The change in absorbance of GNP at 520 nm as function of DHS concentration was used to calculate the binding constant between GNP and DHS. The process of binding of DHS with GNP can be expressed by equation 5.1.

$$\mathbf{DHS} + \boldsymbol{GNP} \rightleftharpoons \mathbf{[DHS} - \boldsymbol{GNP]} \tag{5.1}$$

For the above reaction, K can be expressed by:

$$\boldsymbol{K} = \frac{\boldsymbol{[DHS - GNP]}}{\boldsymbol{[GNP][DHS]}} \tag{5.2}$$

As, each GNP has large number of binding sites (n) on its surface, the total number of sites available for binding of DHS will be given by product of n and GNP concentration ([GNP]). Considering this, equation 5.2 can be rewritten as:

$$\boldsymbol{K} = \frac{\boldsymbol{[DHS-GNP]}}{\boldsymbol{n[GNP][DHS]}} \tag{5.3}$$

At equilibrium, total DHS (initial concentration of DHS, $[DHS]_0$) can be expressed as sum of free DHS and GNP bound DHS ([GNP-DHS]). Therefore, free form of DHS will be given by [DHS]=($[DHS]_0$-[DHS-GNP]). Also, due to existence of multiple binding sites on GNP surface, most of GNP binding sites remain unoccupied and it can be assumed that n[GNP]~ $n[GNP]_0$ where GNP_0 is the initial concentration of GNP. Substituting these values in equation 5.3, we get

$$\boldsymbol{K} = \frac{\boldsymbol{[DHS-GNP]}}{\boldsymbol{n[GNP]_0([DHS]_0-[DHS-GNP])}} \tag{5.4}$$

Rearranging above equation 5.4,

$$\boldsymbol{[DHS-GNP]} = \frac{\boldsymbol{nK[GNP]_0[DHS]_0}}{1+\boldsymbol{nK[GNP]_0}} \tag{5.5}$$

The initial absorbance A_0 is due to GNP, as DHS does not absorb in wavelength region of 350-900 nm. Therefore, at any concentration of DHS, the absorbance A_{eq} will be the sum of absorbance due to free GNP and DHS-GNP. Therefore, the change in absorbance is given by:

$$\Delta A = A_0(GNP) - A_{eq}(DHS - GNP) \tag{5.6}$$

$$\Delta A = \varepsilon(GNP)l[GNP]_0 - \varepsilon\left(DHS - GNP\right)l[DHS - GNP] \tag{5.7}$$

$$\Delta A = \Delta\varepsilon l[DHS - GNP] \tag{5.8}$$

where l is the optical path length, which is 1 cm and Δε corresponds to the differential extinction coefficient at 520 nm. From equations (5.5) and (5.8), we get

$$\Delta A = \Delta\varepsilon l \frac{nK[GNP]_0[DHS]_0}{1 + nK[GNP]_0} \tag{5.9}$$

which is rearranged to give modified Benesi-Hildebrand equation as given in equation (5.10).[209]

$$\frac{1}{\Delta A} = \frac{1}{nK\ell\Delta\varepsilon[DHS]_0[GNP]_0} + \frac{1}{\Delta\varepsilon\ell[GNP]_0} \tag{5.10}$$

Using equation 5.10, nK value can be calculated experimentally by linear fit of the double reciprocal plot ($1/\Delta A$ vs $1/[DHS]_0$) as shown in fig. 5.5, where the ratio of intercept and slope will give the product of n and K.

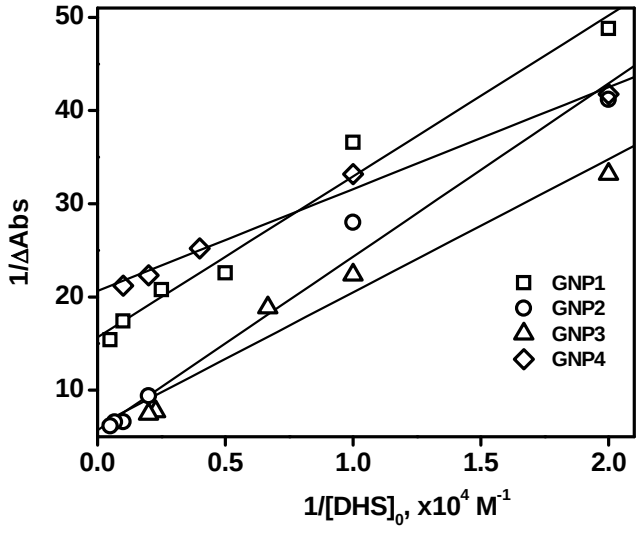

Fig. 5.5: *Double reciprocal plot for change in absorbance of GNP1, GNP2, GNP3 and GNP4 at 520 nm as a function of DHS concentration (0.05 mM-0.5 mM) as per equation 5.10.*

For this, the change in absorbance of SPR band of GNP (520 nm) was monitored as function of $[DHS]_0$ and absorption data were fitted linearly according to equation 5.10. The calculated values of nK for GNP1-4 are listed in table 5.1. The n value was calculated as following:

Calculation of n: Assuming GNP to be a spherical shaped nanoparticle with face centered cubic (FCC) structure[210] (density, ρ=19.3 g/cm^3), the average number of gold atoms (N) present in GNP of diameter D will be given by[211]

$$N = \frac{\pi \rho D^3}{6M} = 30.89602 D^3 \qquad (5.11)$$

where M (196.97 g/mole) is the atomic weight of gold atom. If N_{Total} is the total numbers of gold atoms involved in the formation of GNP of a given size, then the number of GNP particles in a given volume V (mL) can be calculated as:

$$\text{Number of particles of GNP} = \frac{N_{Total}}{N} \tag{5.12}$$

This number can be expressed in terms of GNP concentration i.e. [GNP] as per equation 5.13, where N_A is Avogadro number.

$$[GNP] = \frac{N_{Total}}{NVN_A} = \frac{N_{Total}}{30.89602D^3VN_A} \tag{5.13}$$

If V_{DHS} is the volume of DHS added to a fixed volume (V_{GNP}) of GNP solution of, then 'n' which also represents the number of moles of DHS present on surface of GNP (1 mole) can be estimated using equation 5.14.[212]

$$n = \left(\frac{\text{no. of moles of DHS}}{\text{no. of moles of GNP}}\right) = \frac{[DHS]xV_{DHS}}{[GNP]xV_{GNP}} \tag{5.14}$$

Under given experimental conditions, the 'n' value were calculated using equation 5.14 and are listed in table 5.1. The results indicate that the K values for DHS-GNP increase with decrease in the size of GNP. This can be explained on the basis of size dependent electronic behavior of GNP. With decrease in GNP size, the number of surface atoms increases. This leads to increase in electron density on GNP surface and makes the small sized GNP more susceptible for interaction with incoming ligand. Therefore, small sized

GNP would interact with DHS more strongly and show higher K values as compared to larger sized GNP.

Table 5.1: *Binding constant for the binding of GNP with DHS.*

S.No	nK, M^{-1}	Number of binding sites, n	K $x10^{-3}$, M^{-1}
GNP1	4.5 $x10^{2}$	1.9 x 10^{4}	23.6 ± 0.8
GNP2	5.0x 10^{3}	5.2 x 10^{5}	9.7 ± 0.4
GNP3	9.1 x 10^{3}	2.4$x10^{6}$	3.8 ± 0.2
GNP4	2.7 x 10^{4}	3.0 x 10^{7}	0.9 ± 0.1

5.3.2.2 DLS and TEM studies

The red shift observed in absorption spectra of GNP on addition of DHS may be due to aggregation of particles. To resolve this, size measurement studies were carried out for GNP in presence of DHS using DLS technique.[213] Due to overlapping absorption by GNP1 and DHS-GNP1 with wavelength of the excitation laser, it was difficult to monitor the changes in GNP1 size. Fig. 5.6 shows the time dependent exponential decay of correlation function ($G_1(\tau)$) for 7 nM GNP2 in absence and presence of 0.1 mM DHS. The data were fitted to monomodal distribution and as per equation 2.41 and 2.43, the hydrodynamic diameter of GNP2 was estimated to be (15 ± 3) nm, which in presence of 0.1 mM DHS increased to (34 ± 4) nm. By following similar procedure, the hydrodynamic diameter of GNP3, GNP4 and its aggregates in presence of DHS were estimated and the values are given in table 5.2.

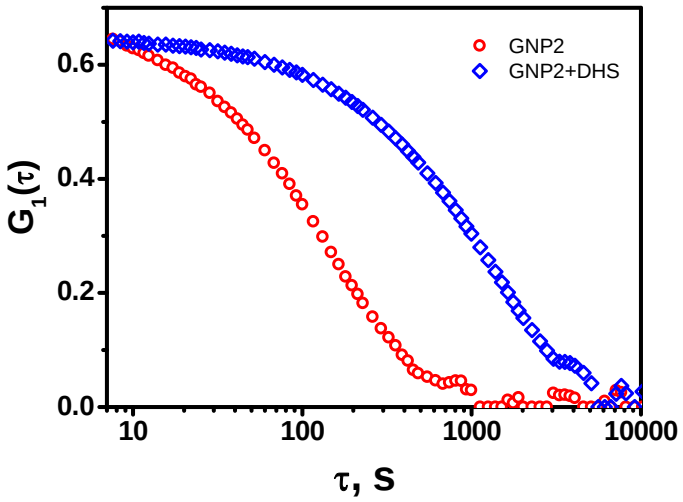

Fig. 5.6: *Plot of $G_1(\tau)$ as a function of time (τ) for 7 nM GNP2 in absence and in presence of 0.1 mM DHS. (Polydispersity index (PI) < 0.1)*

The hydrodynamic diameter of DHS bound GNP increased with increase in DHS concentration (0.1-1.0 mM), indicating increase in aggregation due to DHS. DLS technique gives the hydrodynamic diameter of the nanoparticles which includes the actual size of nanoparticles and thickness of associated solvent layer. Therefore to get the actual size of GNP and DHS-GNP, TEM measurements were carried out.

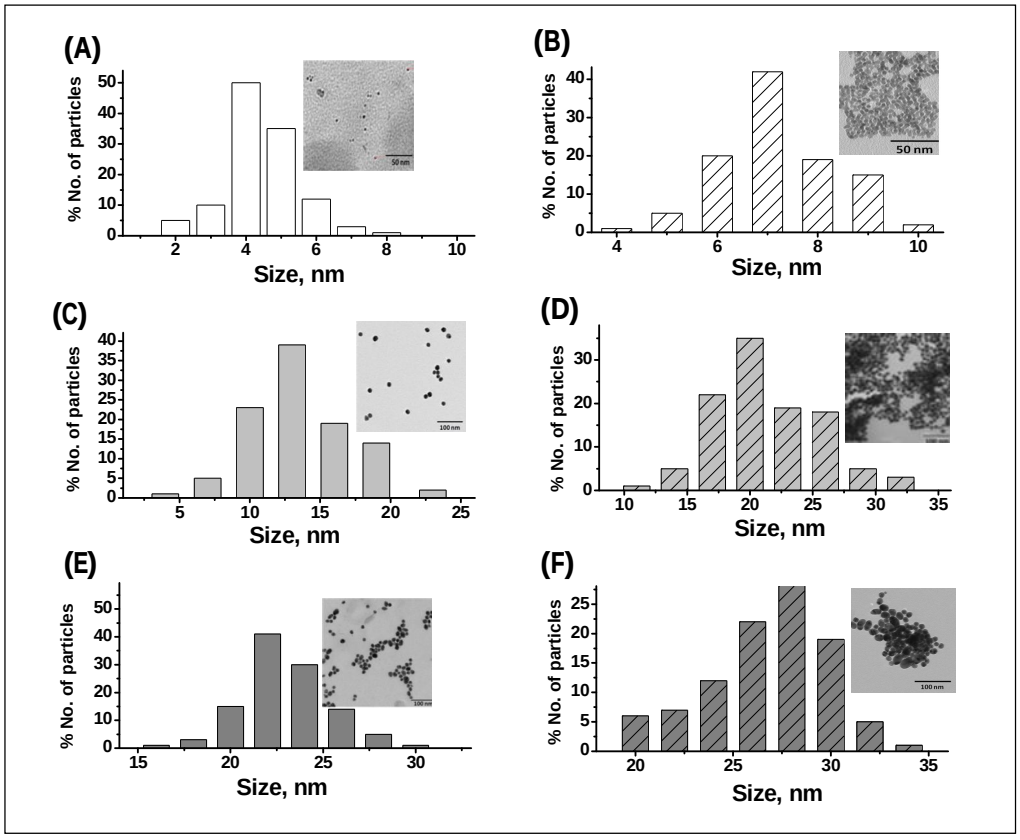

Fig. 5.7: *Size distribution of (A) GNP1, (B) GNP1-DHS, (C) GNP2, (D) GNP2-DHS, (E) GNP3 and (F) GNP3-DHS as observed by TEM measurements. Inset shows the corresponding TEM images.*

Fig. 5.7(A,C,E) represent the size distribution of GNP1, GNP2 and GNP3 with their TEM images given as inset. The measured values for the average diameter of GNP1, GNP2 and GNP3 were 4 ± 2 nm, 12 ± 3 nm and 21 ± 4 nm, respectively. Fig. 5.7(B,D,F) represent the size distribution of GNP1, GNP2 and GNP3 in the presence of 1 mM DHS. The average diameter values were 7 ± 3 nm, 20 ± 6 nm and 27 ± 8 nm for GNP1-DHS, GNP2-DHS and GNP3-DHS, respectively. The results indicate that addition of 1 mM DHS leads to a small increase in GNP size. Insets of fig. 5.7(B,D,F) show TEM images of

GNP1, GNP2 and GNP3 in presence of DHS, which confirmed that addition of DHS leads to aggregation of GNP as given in scheme 5.2.

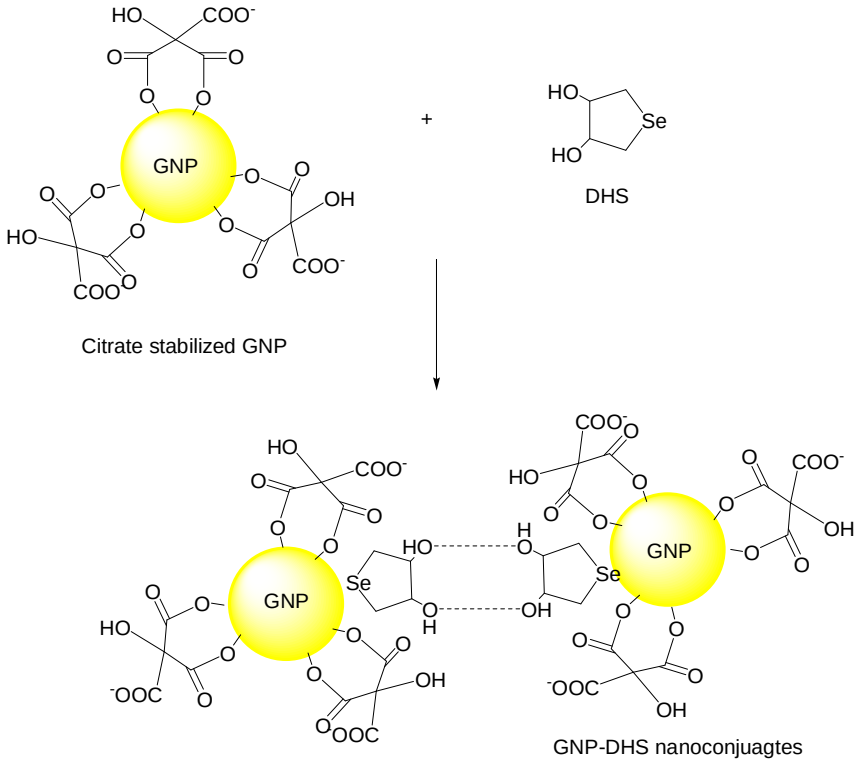

Scheme 5.2: *Possible inter particle interactions between DHS and GNP.*

In analogy with selenium compounds studied earlier for their functionalization of GNP surface, it is presumed that DHS binds with GNP via selenium atom and hydroxyl groups of DHS remain free. The hydroxyl groups can participate in intermolecular hydrogen bonding and can act as a linker between two particles. This will cause decrease in inter particle distance and results in aggregation of DHS-GNP. The estimated size values of GNP by both DLS and TEM, in absence and in presence of 1 mM DHS are summarized in table 5.2.

Table 5.2: *Size of GNP and DHS-GNP as measured by TEM and DLS techniques.*

S.No	GNP diameter (nm)		DHS-GNP diameter (nm)	
	TEM	DLS	TEM	DLS
GNP1	4 ± 2	------	7 ± 3	------
GNP2	12 ± 3	15 ± 3	20 ± 6	34 ± 4
GNP3	21 ± 4	25 ± 3	27 ± 8	79 ± 6
GNP4	----	58 ± 5	----	195 ± 8

5.3.2.3 ζ-potential measurements: Metal nanoparticles acquire stability either due to steric repulsion or due to electrostatic stabilization.[214] GNP with negatively charged citrate ions as capping agent, are electrostatically stabilized and their stability can be measured in terms of ζ-potential values. In general, a stable colloidal system of citrate capped GNP shows ζ-potential values in the range of -30 to -40 mV. The effect of binding of DHS with GNP on stability of GNP was assessed by monitoring the change in its ζ-potential as a function of DHS concentration (0.05 mM-1 mM).

As seen in fig. 5.8, ζ-potential of GNP2 decreases gradually with increase in DHS concentration. Similarly the ζ-potential values of GNP1, GNP3 and GNP4 decreased with increasing DHS concentration. The ζ-potential values for GNP1-4 in absence and presence of 0.1 mM DHS are listed in table 5.3.

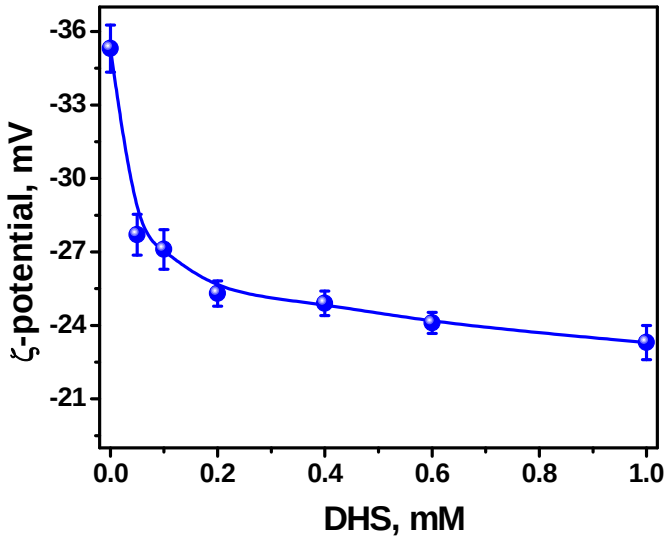

Fig. 5.8: *Variation in ζ-potential of GNP2 as a function of DHS concentration (50 μM-1 mM).*

Binding of a neutral ligand like DHS will cause removal of citrate ions from the surface of GNP surface resulting in decrease in surface charge of the GNP. As, DHS concentration increases, more number of citrate ions would be replaced from GNP surface resulting in DHS concentration dependent decrease in ζ-potential values.

Table 5.3: *ζ –potential measurement results for the binding of DHS with GNP.*

S. No	ζ -potential (mV)		Change in ζ –potential, mV
	Blank GNP	DHS	
GNP1	-46.1 ± 0.5	-39.1 ± 0.8	7.0 ± 0.6
GNP2	-39.5 ± 2.9	-31.6 ± 1.5	7.9 ± 0.5
GNP3	-38.2 ± 1.7	-28.6 ± 1.2	9.6 ± 0.7
GNP4	-34.5 ± 0.9	-25.3 ± 0.4	9.2 ± 0.6

5.3.2.4 Raman and SERS studies

SERS is a commonly used technique to understand the binding and mode of interaction between a substrate and metal nanoparticles. GNP surface is rich in electrons and can share its surface electron density with the bound ligands. Depending upon the orientation of the ligand on GNP surface, Raman intensity of selected vibration modes of the ligand are enhanced and therefore the site and nature of interaction between a ligand and noble metal surface can be explicitly understood by this technique.[215] Therefore, SERS studies were carried out for determining the orientation of DHS on GNP surface. Fig. 5.9 represents the Raman spectra of (a) DHS and SERS spectra of (b) DHS-GNP2, (c) DHS-GNP3 and (d) DHS-GNP4.

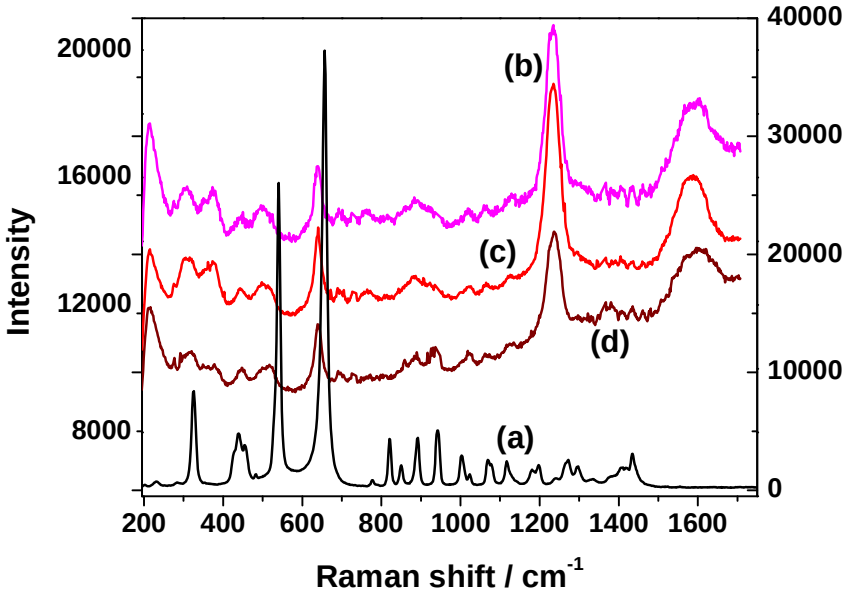

Fig. 5.9: *(a) Raman spectrum of pure DHS. Spectra (b), (c) and (d) represent the SERS spectra of 0.1 mM of DHS in presence of 7 nM of GNP2, GNP3 and GNP4, respectively.*

The assignment of Raman bands was done using the Raman spectra of selenolane as reported earlier by Kimelfeld et.al.[216] This compound is a five membered cyclic selenide and has similar structural features as that of DHS (two hydroxyl (OH) groups of DHS are replaced by hydrogen (H) in selenolane). Therefore, it was used as a reference to assign the Raman peaks of DHS. The assignment was further supported by quantum chemical calculated Raman specra of DHS using DFT at B3LYP/6-61+G(d,p) level in water (section 2.11 in chapter 2). The experimentally observed Raman and SERS peaks along with peak assignment are given in table 5.4.

Table 5.4: *Assignment of Raman peaks of DHS and SERS peaks of DHS-GNP.*

S. No	Raman peak (selenolane), cm^{-1}	Raman peak (DHS), cm^{-1}		SERS peak, cm^{-1}	Assignment
		Theory	Experimental		
1.	357	332	324		Se-deformation
2.	475	441	439		Se-deformation
3.	584	575	540		C-Se-C stretching
4.	612	661	656	636	C-Se-C stretching
5.	782	762	776		C-Se-C stretching
6.	866	833	820		β-CH_2 bending (rocking)
7.	950	872	848		C-C stretching
8.	985	963	941		α-CH_2 bending (rocking)
9.	1170	1115	1180		α-CH_2 bending (twisting)
10.	1249	1205	1234	1234	α-CH_2 bending (wagging)
11.	1307	1265	1294		β-CH_2 bending (twisting)
12.	1340	1353	1379		β-CH_2 bending (rocking)

As, the local field polarization due to electromagnetic radiation is primarily perpendicular to the metallic surface, only the vibrational modes of DHS which have their

dipole moment oriented perpendicular to the nanoparticles surface are strongly enhanced while others are not observed in SERS.[217] From the SERS results, it is clear that binding of GNP with DHS leads to enhancement in mainly C-Se-C stretching modes (636 cm^{-1}) and α-CH_2 bending modes (1234 cm^{-1}). No SERS peaks were observed corresponding to β-CH_2 group and OH groups. The structural rigidity in DHS offers resistance to any change in geometry while binding on GNP surface. This would allow only few atoms to directly interact with GNP surface. Thus DHS binds with GNP mainly through selenium atom with marginal interaction via α-CH_2 group. These interactions will force DHS to orient in a way that C-Se-C plane of DHS lies on GNP surface and β-CH_2 groups away from the GNP surface.

The binding of GNP with a ligand is expected to be influenced by the structure of the ligand. Therefore, to understand the effect of change in structure of organoselenium compounds on binding with GNP, similar studies were carried out with SeEOH, a linear analogue of DHS.

5.3.3 Binding of SeEOH with GNP

5.3.3.1 Absorption-spectroscopic studies*:* The characterization of the SeEOH-GNP was done by using absorption spectrometry technique. For this, 7 nM of GNP1 solution was incubated with different concentrations of SeEOH for 5 minutes and the absorption spectra were recorded. As seen in the fig. 5.10, on addition of 0.1 mM SeEOH, the SPR absorbance of GNP1 decreases and the absorption spectra becomes broad with a red shift (~ 4 nm) in peak maximum. With increase in SeEOH concentration (upto 4 mM), further

red shift was observed and the spectra became broader. The results indicate that addition of SeEOH to GNP1 solution leads to aggregation of GNP1.

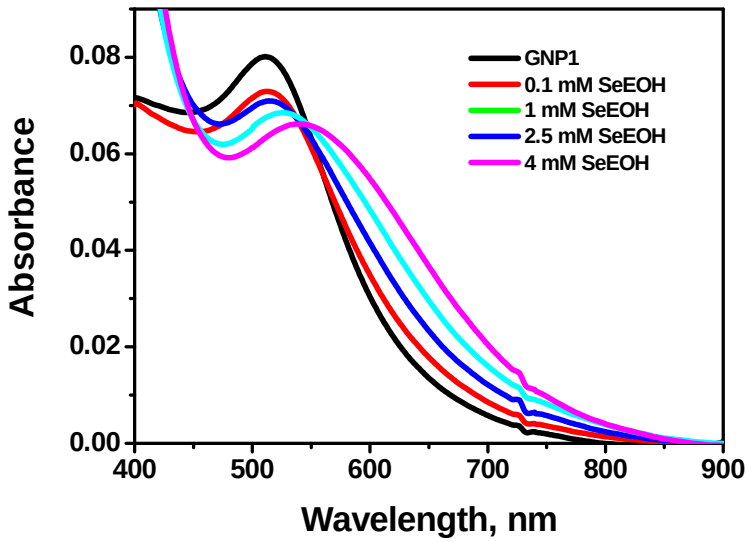

Fig. 5.10: *The absorption spectra of GNP1 in absence and in presence of 0.1 mM-4 mM SeEOH.*

Similar studies were carried out for the binding of SeEOH with GNP2, GNP3 and GNP4. Fig. 5.11 represents the absorption spectra of GNP2 in absence and in presence of different concentration of SeEOH (10-100 μM). On addition of 10 μM SeEOH, the absorbance at 522 nm decreased with increase in absorbance in the 600-700 nm region. On further increase in SeEOH concentration, a new absorption band was evolved at ~680 nm with concomitant decrease in absorbance at 522 nm.

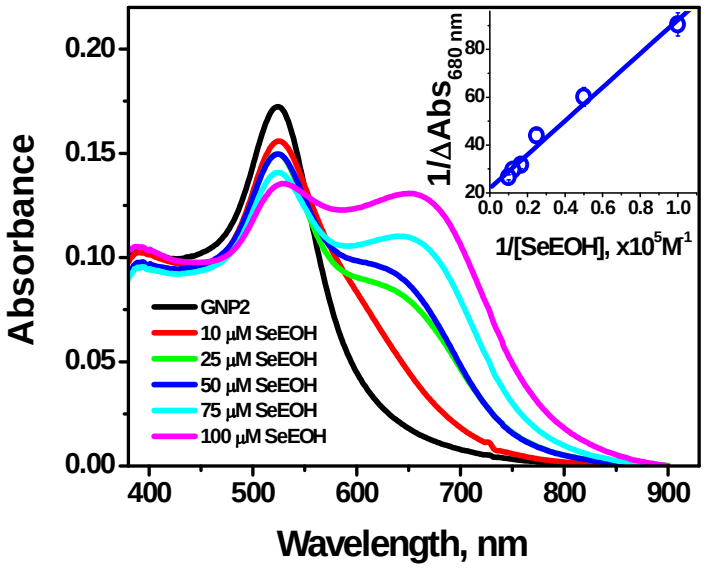

Fig. 5.11: *Variation in absorption spectra of GNP2 as a function of SeEOH concentration (10 µM-100 µM). Inset shows double reciprocal plot for GNP absorbance at 520 nm as a function of SeEOH concentration.*

Similar features were seen for binding of SeEOH with GNP3 and GNP4. The change in absorption spectra of GNP on addition of SeEOH indicates the interaction between SeEOH and GNP. The extent of interaction was estimated by monitoring the changes in the absorbance at 520 nm with SeEOH concentration. Inset of fig. 5.11 shows the double reciprocal plot for variation in absorbance of GNP as a function of SeEOH concentration. From this, nK values for the binding of SeEOH with GNP were calculated using equation 5.10 replacing DHS with SeEOH. The calculated K values for the binding of SeEOH with GNP1, GNP3 and GNP4 are listed in table 5.5.

Table 5.5: *Estimation of binding constant for SeEOH-GNP*.

S. No	nK, M^{-1}	K x 10^{-2}, M^{-1}
GNP1	$9.9x10^{2}$	5.2 ± 0.1
GNP2	$3.1x10^{4}$	5.9 ± 0.2
GNP3	$9.1x\ 10^{4}$	3.8 ± 0.1
GNP4	$1.2x\ 10^{5}$	0.40 ± 0.02

From the results, it can be stated that the binding strength between SeEOH and GNP increases with decrease in GNP size up to 15 nm and does not change on further decrease in GNP size. Under identical experimental conditions, K values obtained for SeEOH-GNP are higher than those of DHS-GNP by an order of magnitude, which indicates stronger interaction in SeEOH-GNP than in DHS-GNP (table 5.1 & 5.5). These results further suggest that SeEOH can passivate the surface energy of the GNP to a greater extent than DHS.

Another interesting observation is the differential spectral shift in SPR band of GNP, for DHS-GNP and SeEOH-GNP. The red shift in SPR band is indicative of aggregation of GNP. The larger red shift for DHS-GNP as compared to SeEOH-GNP indicates higher aggregation. Also, the two systems showed different FWHM values in their absorption spectra under similar experimental conditions. The FWHM values of the SPR band reflect the polydispersity in particle size.[218] For a given concentration, DHS-GNP showed higher FWHM values compared to SeEOH-GNP indicating higher polydispersity in DHS-GNP than SeEOH-GNP.

5.3.3.2 DLS and TEM studies: The effect of binding of SeEOH on size of GNP was estimated by DLS. For this, size of GNP was measured as a function of SeEOH concentration. Fig. 5.12 represents the variation of $G_1(\tau)$ as a function of time for GNP2 in absence and presence of 0.1 mM SeEOH.

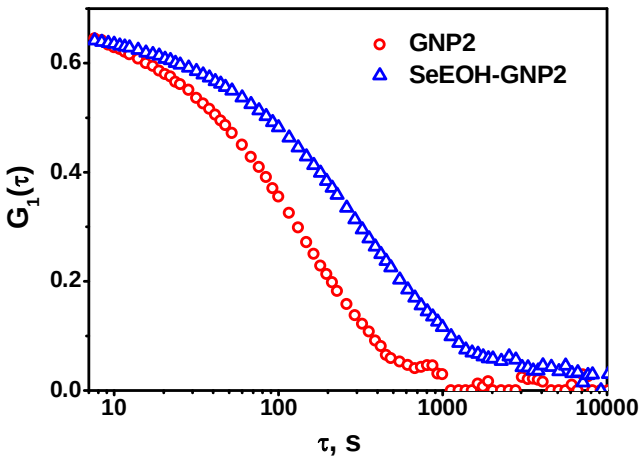

Fig. 5.12: *Plot of* $G_1(\tau)$ *as a function of time for 7 nM GNP2 in absence and in presence of 0.1 mM SeEOH. (PI < 0.1)*

From the decay of $G_1(\tau)$, the diffusion coefficient and diameter of the particles were calculated as discussed earlier in section 2.8 in chapter 2. The hydrodynamic diameter for GNP2 was found to increase from 12 ± 3 nm to 15 ± 3 nm on addition of 0.1 mM SeEOH. Similar trend was observed for GNP3 and GNP4 and the results are listed in table 5.6. These results were further confirmed by TEM measurements. Fig. 5.13(A,C,E) show the particle size distribution of GNP1, GNP2, GNP3 along with their TEM images in insets. Similarly, fig. 5.13(B,D,F) show the particle size distribution of GNP1-SeEOH, GNP2-SeEOH and GNP3-SeEOH along with their TEM images in insets. The results

confirmed that addition of SeEOH did not cause much increase in GNP hydrodynamic size but cause aggregation of GNP.

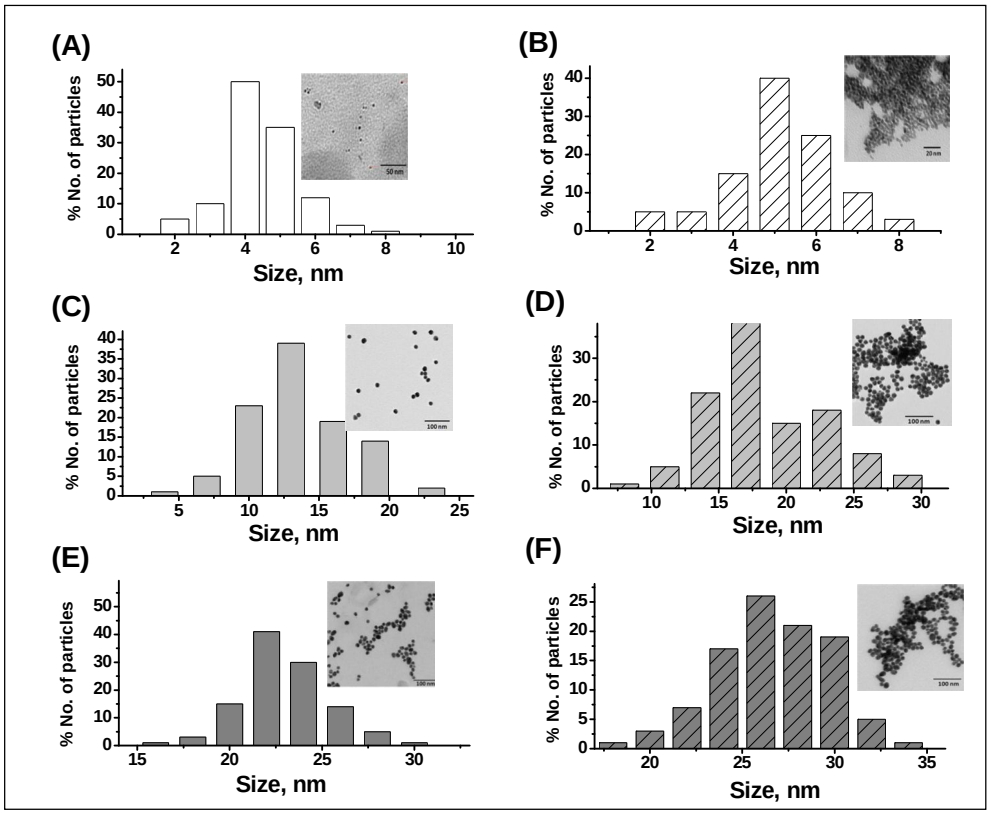

Fig. 5.13: *Size distribution analysis of TEM images of (A) GNP1, (B) GNP1-SeEOH, (C) GNP2, (D) GNP2-SeEOH, (E) GNP3 and (F) GNP3-SeEOH. Insets show the corresponding TEM images.*

The average size of GNP1, GNP2, GNP3 and their SeEOH composites are given in table 5.6. In comparison with DHS-GNP, SeEOH-GNP have smaller size and lower aggregation. These results are in accordance with the absorption data where DHS-GNP exhibit larger red shift in SPR band of GNP than SeEOH-GNP.

Table 5.6: *Size of GNP and GNP-DHS as measured by TEM and DLS techniques.*

S.No	GNP		SeEOH-GNP	
	TEM	DLS	TEM	DLS
GNP1	4 ± 2		5 ± 2	
GNP2	12 ± 3	15 ± 3	17 ± 5	26 ± 5
GNP3	21 ± 4	25 ± 3	26 ±5	69 ± 5
GNP4		58 ± 5		140 ± 10

5.3.3.3 ζ-potential measurements

To understand the effect of binding of SeEOH on stability of GNP, ζ-potential measurements were carried out. Fig. 5.14 shows the change in ζ-potential of GNP2 as a function of SeEOH concentration (50 μM-1 mM). On addition of SeEOH up to a concentration of 0.2 mM, a sharp decrease in ζ-potential value was observed. However, at higher SeEOH concentration (>0.2 mM), only marginal changes were observed in ζ-potential values of GNP which may be due to saturation of the binding sites on GNP surface. Similarly, ζ-potential measurements were carried out for GNP1, GNP3 and GNP4 in absence and in presence of 0.1 mM SeEOH and the results are listed in table 5.7. It is clear that the ζ-potential values of GNP decreased on addition of SeEOH. The decrease in ζ-potential of GNP is attributed to replacement of citrate ions from GNP surface by electrically neutral SeEOH molecules.

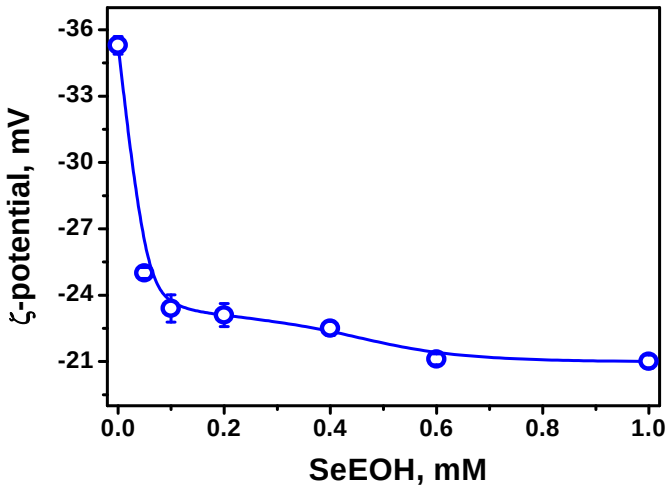

Fig. 5.14: *Variation in ζ-potential of GNP as a function of SeEOH concentration (0.05 mM-1 mM).*

Comparing the ζ-potential values for DHS-GNP and SeEOH-GNP, as given in table 5.3 and 5.7, respectively, it can be stated that both DHS and SeEOH lead to decrease in ζ-potential of GNP, but the decrease is more prominent for SeEOH than DHS. This indicates that the binding of SeEOH with GNP results in more efficient displacement of the negatively charged citrate from GNP surface than DHS. However, as indicated by absorption spectra, DLS and TEM studies, the extent of aggregation is less in SeEOH-GNP than DHS-GNP. These contrasting results can be understood by considering the higher binding constant of SeEOH for binding with GNP as compared to that of DHS. The stronger interactions in SeEOH-GNP would passivate GNP surface energy more effectively and thus provide higher stability than DHS-GNP.

Table 5.7: *ζ -potential values for GNP and SeEOH-GNP.*

S.No	ζ -potential (mV)		Change in ζ –potential, mV
	Blank GNP	SeEOH	
GNP1	-46.1 ± 0.5	-30.1 ± 0.5	16.0 ± 0.8
GNP2	-39.5 ± 2.9	-27.6 ± 0.8	11.9 ± 0.6
GNP3	-38.2 ± 1.7	-24.2 ± 1.6	14.0 ± 0.7
GNP4	-34.5 ± 0.9	-21.6 ± 2.4	12.9 ± 0.6

5.3.3.4 Raman and SERS studies

To further understand the nature of interactions in SeEOH-GNP, SERS measurements were carried out. For this, first Raman spectra of neat SeEOH was recorded and the various peaks were assigned using Raman spectra of its sulfur analogue, bis(ethanol)sulfide (SEOH) as reported by Farquharson et al.[219] The Raman peak assignment was further supported by quantum chemical calculations done at B3LYP/6-31G+(d,p) level in water. The peak positions and their assignments are listed in table 5.8 and shown pictorially in fig. 5.15.

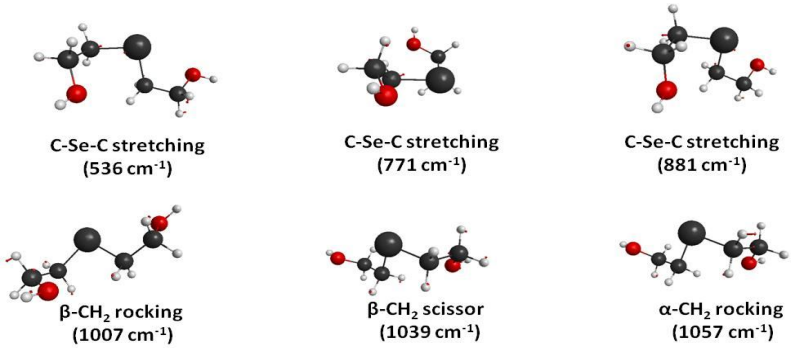

Fig. 5.15: *Pictorial presentation for the different Raman vibrational modes of SeEOH. Arrow shows the direction of movement of corresponding atom.*

Table 5.8: *Assignment of Raman peaks of SeEOH and SERS peaks of SeEOH-GNP.*

S. No	Raman peak (SEOH), cm^{-1}	Raman peak (SeEOH), cm^{-1}		SERS peak, cm^{-1}	Assignment
		Theory	Experimental		
1.	510.9	466	449		S/Se-deformation
2.	529.9	536	562	551	C-Se-C stretching
3.	698.1	771	668	672	C-Se-C stretching
4.	1015.2	984	1003	999	α CH_2 bending (rocking)
5.	1059.9	1007,1039 1057	1055	1023 1047	β CH_2 bending (rocking & scissor)
6.	1127.8	1132	1124	1112	α CH_2 bending (rocking)
7.	1198.4	1192	1186	1170	α CH_2 bending (rocking)
8.	1298.8	1263	1276	1251	CH_2 bending (twisting)
9.	1332.6	1366	1321	1322	β-CH_2 bending (wagging)
10.	1502.0	1440	1467	1455	CH_2 bending (twisting)
11.	1558.0	1568	1563	1557	β-CH_2 bending (wagging)

The standard Raman spectrum of SeEOH (Fig. 5.16 (a)) showed characteristic peaks at 344 cm^{-1}, 449 cm^{-1}, 562 cm^{-1} and 668 cm^{-1}, along with broad and overlapping peaks ranging from 800 cm^{-1} to 1600 cm^{-1}. The Raman peaks observed in the spectrum at 344 cm^{-1} and 449 cm^{-1} are due to Se-deformation band while peaks at 562 cm^{-1} and 668 cm^{-1} correspond to C-Se-C stretching mode. Fig. 5.16(b, c & d) show the SERS spectra obtained on treating 0.1 mM SeEOH with 7 nM of GNP2, GNP3 and GNP4, respectively, in the frequency range 300-2000 cm^{-1}. For SeEOH-GNP2 two small but broad peaks were observed at 551 cm^{-1} and 672 cm^{-1} corresponding to C-Se-C symmetric and asymmetric stretching modes, respectively. At larger GNP size, along with the above peaks, a new sharp peak in the wave number region 1000-1050 cm^{-1} and small overlapping peaks from 1100-1500 cm^{-1} were observed corresponding to α-CH_2 and β-CH_2 bending modes.

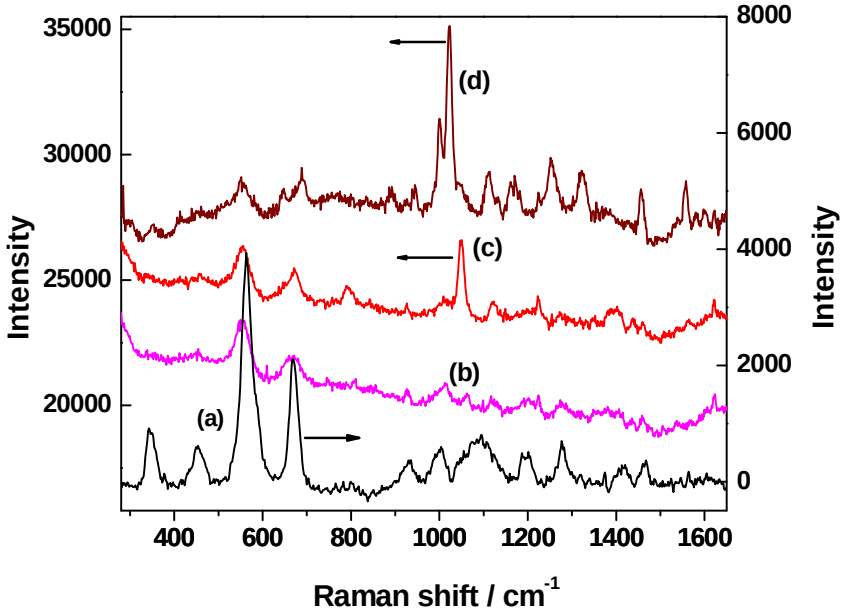

Fig. 5.16: *(a) Raman spectra of pure SeEOH. SERS spectra of 0.1 mM of SeEOH in presence of 7 nM (b) GNP2, (c) GNP3 and (d) GNP4, respectively.*

The enhancement in C-Se-C stretching peak indicates that the binding of SeEOH with GNP takes place through selenium atom. Enhancement in the intensity of CH_2 bending modes indicates interaction of alkyl chain of SeEOH with GNP surface.

Comparing SERS data of DHS-GNP and SeEOH-GNP, the mode of binding in these two compounds appears to be very different. For DHS-GNP the major enhancement was observed in C-Se-C stretching mode (636 cm^{-1}), confirming that the binding of DHS on GNP surface occurs mainly through selenium centre (Scheme 5.3). However, in case of SeEOH-GNP, along with C-Se-C stretching mode (551 cm^{-1}), α-CH_2 bending modes (1023 cm^{-1}) and β-CH_2 bending modes (1112 cm^{-1}) were also found to be enhanced. This enhancement is attributed to interaction of alkyl chain of SeEOH with GNP surface as shown in scheme 5.3. If such interaction takes place, it is expected that in SeEOH-GNP,

the alkyl chain attached to selenium atom, may remain parallel to GNP surface. This kind of interaction appears to be dominating for larger GNP probably due to the fact that the surface curvature decreases with increase in GNP size. In SeEOH, both α-CH_2 and β-CH_2 vibration modes were enhanced, while in case of DHS only the α-CH_2 mode was enhanced.

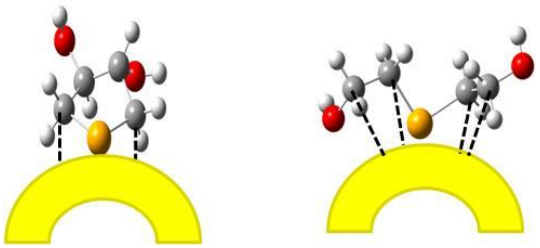

Scheme 5.3: *Orientation of DHS and SeEOH molecules on the GNP surface as suggested by SERS studies.*

Table 5.9: *SERS analysis for SeEOH-GNP and DHS-GNP.*

Compounds		GNP2	GNP3	GNP4
SeEOH	C-Se-C stretching Peak shift (cm^{-1})	9.7	9.7	11.8
	α-CH_2 bending (wagging) Peak shift (cm^{-1})	---	9	32.1
DHS	C-Se-C stretching Peak shift (cm^{-1})	20	16	18
	α-CH_2 bending (wagging) Peak shift (cm^{-1})	1.8	1.8	0.6

The different modes of interaction with GNP can also be explored in terms of shift in the SERS peak relative to parent Raman peak. As mentioned in table 5.9, the C-Se-C stretching peak of SeEOH/DHS shifted to lower wave number on binding with GNP. This is due to the fact that the binding of DHS/SeEOH would lead to transfer of electron density from selenium atom to GNP surface which would result in weakening of C-Se bond.

Comparing the peak shift in C-Se-C stretching of SeEOH and DHS due to binding with GNP, it can be said that transfer of electron density from selenium atom to GNP surface is higher in DHS than that in SeEOH. These results indicate that even though the binding of both SeEOH and DHS with GNP takes place through selenium atom; their orientations differ significantly.

The above studies indicate that the binding of DHS/SeEOH with GNP may lead to differential change in electron density on selenium atom of DHS/SeEOH. This would affect electron transfer ability of these compounds. Therefore, electron transfer reactions of DHS/SeEOH and their GNP were studied as discussed in next section.

5.3.4 Electron transfer properties

5.3.4.1 Reaction with $ABTS^{\bullet-}$ radical: To assess the influence of GNP binding on redox properties of DHS/SeEOH, electron transfer reaction between DHS/SeEOH and $ABTS^{\bullet-}$ radical was carried out in absence and presence of GNP. The reaction of DHS and SeEOH with $ABTS^{\bullet-}$ radical can be shown as equation 5.15.

$$\boldsymbol{DHS / SeEOH + ABTS^{\bullet-} \rightarrow DHS^{\bullet+} / SeEOH^{\bullet+} + ABTS^{2-}} \qquad (5.15)$$

The progress of the reaction was monitored by following the absorbance of $ABTS^{\bullet-}$ radical which shows strong absorbance at 420 nm and a broad absorption band in 600-900 nm region.[220] As GNP and its SeEOH/DHS composites absorb in the wavelength range of 400-600 nm, the reaction was monitored at 820 nm to avoid the interference due to GNP and SeEOH/DHS.

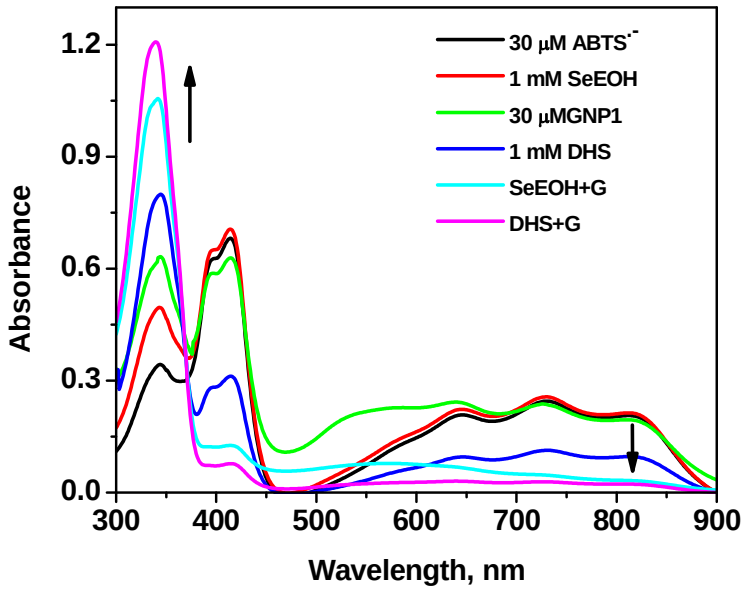

Fig. 5.17: *Absorption spectra of 30 µM* $ABTS^{\bullet-}$ *radical in absence and in presence of SeEOH-GNP and DHS-GNP. Downward and upward arrows show decrease in* $ABTS^{\bullet-}$ *radical absorbance at 420 nm and 600 nm-800 nm with concomitant increase in 345 nm peak corresponding to* $ABTS^{2-}$ *on addition of SeEOH/DHS in free and GNP-bound state.*

Fig. 5.17 shows the absorption spectra of $ABTS^{\bullet-}$ radical in absence and presence of SeEOH/DHS and their GNP nanocomposites. As indicated in the fig. 5.17, the absorbance of $ABTS^{\bullet-}$ radical did not change significantly in the presence of SeEOH and GNP1, while in presence of 1 mM DHS, the absorbance at 600-850 nm decreased significantly with concomitant increase in absorbance at 345 nm due to formation of $ABTS^{2-}$. On the other hand, when the $ABTS^{\bullet-}$ radical solution was mixed with 1 mM SeEOH/DHS containing 7 nM GNP(1-4), the absorbance of $ABTS^{\bullet-}$ radical decreased almost completely with the formation of $ABTS^{2-}$ ion. These results indicate that GNP1 and SeEOH individually do not react with $ABTS^{\bullet-}$ radical. Fig. 5.18 (A) represents the absorption-time plots of $ABTS^{\bullet-}$ radical alone and in presence of 1 mM DHS, 7 nM GNP1

and DHS-GNP (1-4). Similarly, Fig. 5.18 (B) represents the absorption-time plot of $ABTS^{\bullet-}$ radical alone and in presence of 1 mM SeEOH, 7 nM GNP1 and SeEOH-GNP (1-4). The results showed that organoselenium compounds after binding with GNP show enhanced reactivity towards $ABTS^{\bullet-}$ radical. It should be noted that SeEOH which is not reactive to $ABTS^{\bullet-}$ radical, becomes reactive in presence of GNP.

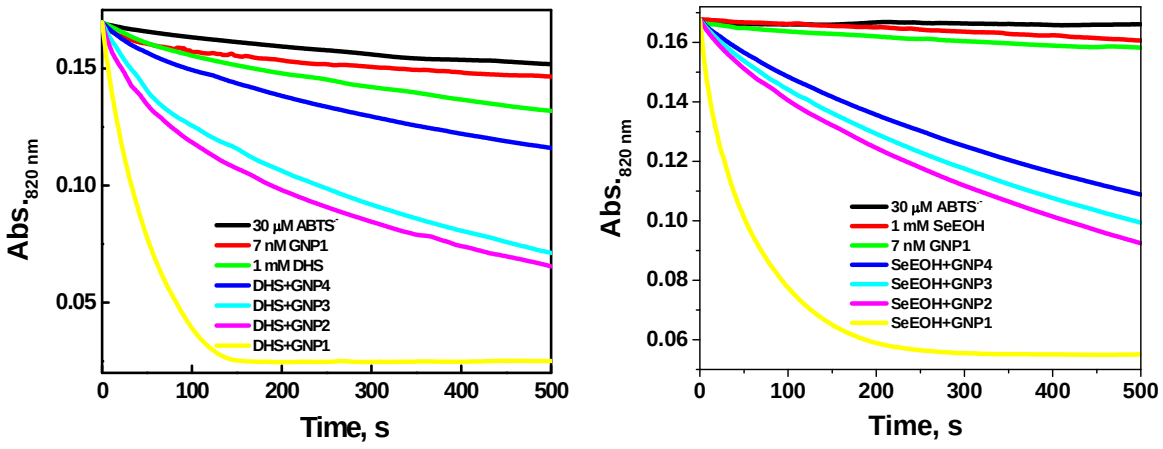

(A) (B)

Fig. 5.18: *(A) Absorbance –time plot of 30 µM $ABTS^{\bullet-}$ radical alone and in presence of 7 nM GNP1, 1 mM DHS, DHS-GNP1, DHS-GNP2, DHS-GNP3 and DHS-GNP4. Fig. (B) shows the absorbance –time plot of 30 µM $ABTS^{\bullet-}$ radical alone and in presence of 7 nM GNP1, 1 mM SeEOH and SeEOH-GNP1, SeEOH-GNP2, SeEOH-GNP3 and SeEOH-GNP4.*

The observed rate constant (k_{obs}) for the decay of $ABTS^{\bullet-}$ radical was estimated by fitting the decay traces to first order kinetics as given in equation 2.25. In absence of any reductant (SeEOH/DHS/GNP), $ABTS^{\bullet-}$ radical decayed through radical-radical reactions with a k_{obs} value of $(3.7 \pm 0.3) \times 10^{-6}$ s^{-1}. The k_{obs} values for the reaction of $ABTS^{\bullet-}$ radical with SeEOH, DHS, SeEOH-GNP and DHS-GNP are summarized in table 5.10.

Table 5.10: *The observed rate constants (k_{obs}) for the reduction of $ABTS^{\bullet-}$ radical.*

S. No	($k_{ABTS^{\bullet-}+GNP}$), s^{-1}	($k_{ABTS^{\bullet-}+DHS}$), s^{-1}	($k_{ABTS^{\bullet-}+SeEOH}$), s^{-1}
In absence of GNP	$(3.7 \pm 0.3) \times 10^{-6}$	$(0.97 \pm 0.05) \times 10^{-3}$	$(7.96 \pm 0.08) \times 10^{-5}$
GNP1	$(2.1 \pm 0.1) \times 10^{-4}$	$(1.08 \pm 0.07) \times 10^{-2}$	$(5.39 \pm 0.08) \times 10^{-3}$
GNP2	$(1.1 \pm 0.1) \times 10^{-4}$	$(3.52 \pm 0.05) \times 10^{-3}$	$(2.12 \pm 0.05) \times 10^{-3}$
GNP3	$(9.5 \pm 0.5) \times 10^{-5}$	$(2.94 \pm 0.09) \times 10^{-3}$	$(1.85 \pm 0.09) \times 10^{-3}$
GNP4	$(6.7 \pm 0.3) \times 10^{-5}$	$(2.39 \pm 0.08) \times 10^{-3}$	$(1.37 \pm 0.07) \times 10^{-3}$

The results listed in table 5.10 indicate that the reducing ability of both DHS and SeEOH increases in presence of GNP. Also the increase in reducing activity in presence of GNP (1-4) was observed to be higher (5-10 times) for SeEOH than DHS. In particular, binding of GNP1 to SeEOH lead to ~150 folds increase in its k_{obs} value while only ~ 10 folds increase was observed for DHS-GNP1.

The increase in the rate constant for the reaction of $ABTS^{\bullet-}$ radical with DHS/SeEOH absorbed on GNP surface may arise due to two factors: a) Co-adsorption of reactants ($ABTS^{\bullet-}$ radical and DHS/SeEOH) and b) stability of intermediates ($DHS^{\bullet+}$/$SeEOH^{\bullet+}$) formed during the reaction. The possibility of co-adsorption of $ABTS^{\bullet-}$ radical along with DHS/SeEOH on GNP surface would lead to increase in proximity between these reactants. However, this possibility was ruled out by UV-visible and SERS studies which showed that on addition of GNP1 to $ABTS^{\bullet-}$ radical solution, the absorption spectrum was found to be only sum of individual spectra due to GNP1 and $ABTS^{\bullet-}$ radical indicating the independent existence of GNP1 and $ABTS^{\bullet-}$ radical in the solution. Also, SERS studies on $ABTS^{\bullet-}$ radical solution containing GNP1 did not show any peaks

indicating no interaction between GNP1 and $ABTS^{\bullet-}$ radicals. This suggested that the increase in the rate of reaction between DHS-GNP/SeEOH-GNP and $ABTS^{\bullet-}$ radical may be due to stabilization of the intermediates formed during the reaction. This can be explained by considering scheme 5.4 which shows that $ABTS^{\bullet-}$ radical oxidizes DHS/SeEOH bound to GNP, to its radical cation ($DHS^{\bullet+}$/$SeEOH^{\bullet+}$). GNP surface being electron rich, would act like a pool of electrons for $DHS^{\bullet+}$/$SeEOH^{\bullet+}$; these radicals would accept electron from GNP surface and undergo subsequent reduction to regenerate parent DHS/SeEOH by electron transfer from the GNP plasmon.

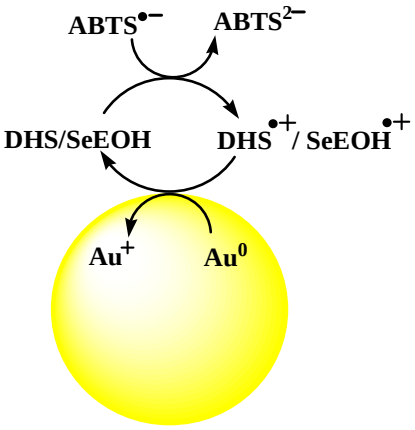

Scheme 5.4: *Possible mechanism for the reaction of* $ABTS^{\bullet-}$ *radical with SeEOH/DHS absorbed on GNP surface.*

Interestingly, the rate of reduction of $ABTS^{\bullet-}$ radical was found to increase with decrease in GNP particle size (table 5.10). For a fixed concentration of GNP (7 nM), the rate of reduction of $ABTS^{\bullet-}$ radical was the highest for GNP1 and the lowest for GNP4. Fig. 5.19 represents the linear dependence of the k_{obs} with the reciprocal of the diameter of GNP. With decrease in GNP diameter, the surface to volume ratio increases which causes

increase in electron density on the surface of GNP. This will make lower sized GNP more reactive towards electron transfer from GNP surface to $DHS^{\bullet+}$/$SeEOH^{\bullet+}$ and lead to increase in rate of overall reaction.

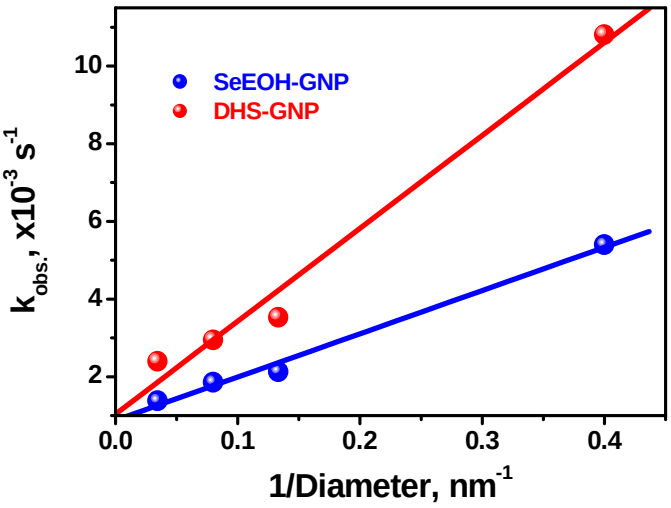

Fig. 5.19: *Linear fit for the variation of k_{obs} for reaction of $ABTS^{\bullet-}$ radicals with DHS/SeEOH-GNP composites as function of (diameter)$^{-1}$ of GNP.*

5.3.4.2 Pulse radiolysis studies

Like $ABTS^{\bullet-}$ radicals, $^{\bullet}OH$ radicals are powerful oxidizing radicals and are known to participate in electron transfer reactions with organoselenium compounds. Due to the short life time of these radicals, the reactions must be followed in micro to milli second time scales to understand the electron transfer processes. Earlier, using pulse radiolysis, we have shown that both DHS and SeEOH on reaction with $^{\bullet}OH$ radicals undergo one-electron oxidation to produce $>Se^{\bullet+}$ radical. The ($>Se^{\bullet+}$) radical on association with parent molecule can form $(>Se\therefore Se<)^{+}$ radical as discussed in chapter 3 (equation 3.4). The $(>Se\therefore Se<)^{+}$ radical showed a characteristic absorption band in the range of 480-500 nm.

Since binding to GNP can influence the reactivity of SeEOH/DHS, the reactions of $^{\bullet}$OH radicals with DHS and SeEOH in presence of GNP were studied. In ABTS$^{\bullet-}$ radical studies, composites of GNP2-4 showed lower enhancement in electron transfer ability of DHS/SeEOH and most significant results were obtained for GNP1, therefore pulse radiolysis studies were restricted to GNP1 only. For this, N_2O saturated aqueous solutions of 1 mM SeEOH/DHS mixed with 7 nM GNP1 at pH 7 were subjected to pulse radiolysis and the transients were detected by absorption spectrometry. As seen in fig. 5.20(A), the transient absorption spectrum obtained on $^{\bullet}$OH radical reaction of DHS and DHS-GNP have similar spectral features with absorption maximum at 480 nm. In analogy with earlier studies on DHS, this absorption band was assigned to $(>Se\therefore Se<)^{+}$ radical. These results indicate that the mechanism of reaction of $^{\bullet}$OH radical with DHS remains unaltered in the presence of GNP1 and generated $(>Se\therefore Se<)^{+}$ radical as the major observable transients.

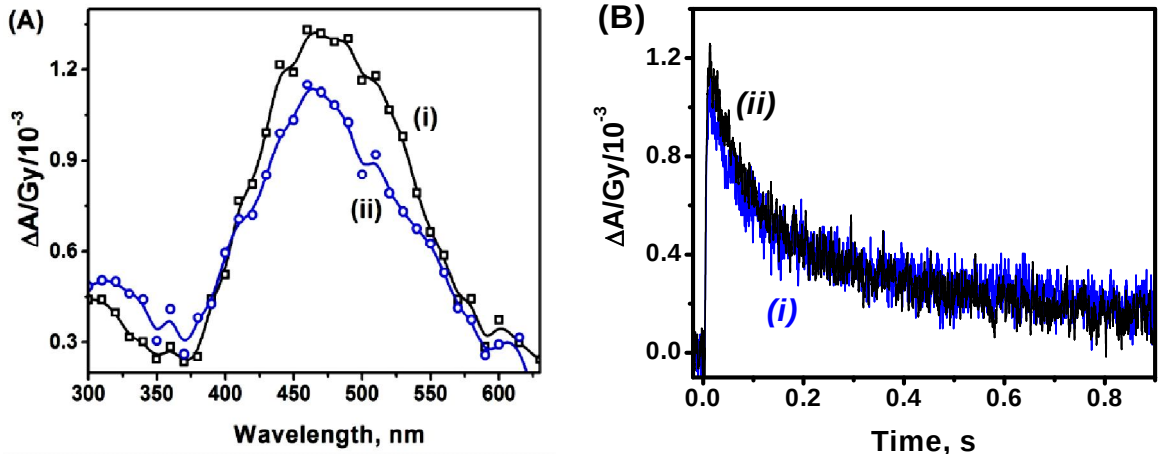

Fig. 5.20: *(A) Transient absorption spectra obtained on pulse radiolysing N_2O saturated aqueous solution of 250 µM DHS (i) in absence and (ii) in presence of 7 nM GNP1 at pH 7 at an absorbed dose of (10.2±0.5) Gy. Fig. (B) shows the absorption-time plot at 480 nm due to $(>Se\therefore Se<)^{+}$ radical in absence and presence of 7 nM GNP1.*

Fig. 5.20(B) shows the absorbance –time plot of the $(>Se\therefore Se<)^{+}$ radical of DHS at 480 nm in absence and presence of GNP1. In both cases, $(>Se\therefore Se<)^{+}$ radical decayed by second order kinetics and no significant difference was observed in the kinetic behavior of $(>Se\therefore Se<)^{+}$ radical in absence and presence of GNP1 as shown in inset of fig. 5.20(B). In a similar way, the transient spectrum for the reaction of $^{\bullet}OH$ radical with SeEOH was recorded both in absence and in presence of GNP1. As shown in fig. 5.21(A) the reaction of $^{\bullet}OH$ radical with SeEOH and SeEOH-GNP1 generates similar transient absorption spectra with absorption maxima at ~480 nm which was assigned to $(>Se\therefore Se<)^{+}$ radical of SeEOH. The decay of $(>Se\therefore Se<)^{+}$ radical followed second order kinetics with $2k/\varepsilon l$ value of $(1.05 \pm 0.08) \times 10^{6}\ s^{-1}$, and $(6.03 \pm 0.05) \times 10^{5}\ s^{-1}$ in the absence and presence of GNP1 respectively (Fig. 5.21(B)), indicating that the $(>Se\therefore Se<)^{+}$ radical is stabilized on GNP surface.

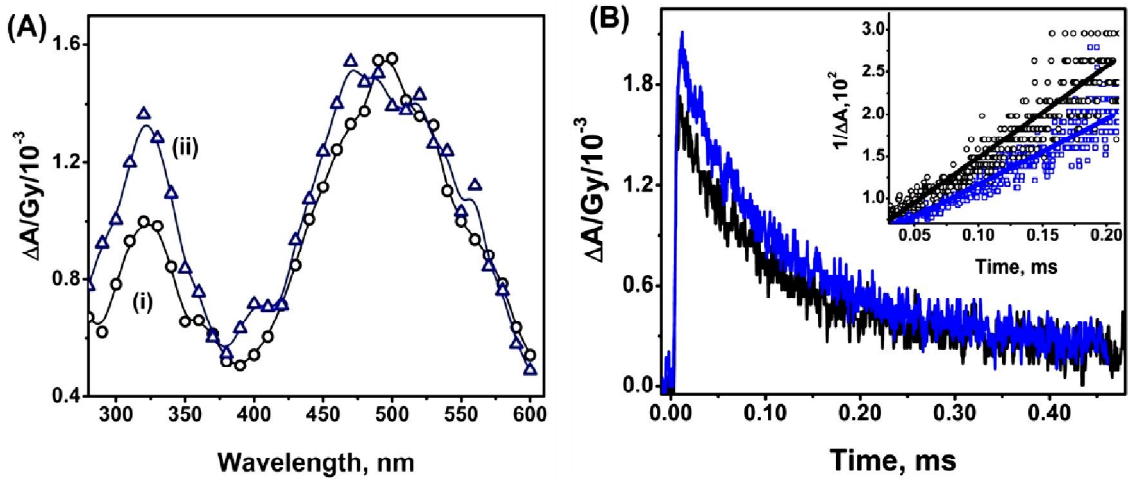

Fig. 5.21: *(A) Transient absorption spectrum obtained on reaction of $^{\bullet}OH$ radical with 250 µM SeEOH (i) in absence and (ii) presence of 7 nM GNP1 at pH 7. Fig B shows the absorption-time plot at 480 nm. Inset of fig (B) shows the plot of reciprocal of absorbance*

*at 480 nm due to (>Se∴Se<)$^+$ radical in absence (□) and presence of 7 nM GNP1 (**O**). The slope of the linear fit gives the 2k/εl for (>Se∴Se<)$^+$ radical decay.*

On the other hand, the kinetics of (>Se∴Se<)$^+$ radical of DHS did not change in presence or absence of GNP1. These results indicate that the (>Se∴Se<)$^+$ radical of SeEOH is stabilized to a higher extent as compared to DHS. This can be understood by considering the steps involved in formation of (>Se∴Se<)$^+$ radical. The one-electron transfer reaction of $^\bullet$OH radical with SeEOH/DHS leads to formation of >Se$^{\bullet+}$ radical as discussed in detail in chapter 3. This >Se$^{\bullet+}$ radical exists in equilibrium with (>Se∴Se<)$^+$ radical. The experimentally observed decay of (>Se∴Se<)$^+$ radical comprises of both its self decay (equation 3.19) and its conversion to >Se$^{\bullet+}$ radical (equation 3.15). Therefore, any factor which will affect the stability of >Se$^{\bullet+}$ radical, would also influence decay profile of (>Se∴Se<)$^+$ radical. >Se$^{\bullet+}$ radical can undergo deprotonation to form α-C centered radical (equation 3.17) which is assisted by overlapping of a σ orbital of α C-H bond with the p-orbital of selenium atom. As indicated by SERS studies, interaction of alkyl chain of SeEOH will lead to bending of CH_2 moiety towards GNP surface. This will result in lower overlapping between σ orbital of α-CH_2 and p-orbital of selenium atom and deactivate the deprotonation pathway. Thus the binding of SeEOH with GNP causes to preferential formation of (>Se∴Se<)$^+$ radical. Accordingly, in presence of GNP the radiation chemical yield (G-value) of selenoxide formed by disproportionation reaction of (>Se∴Se<)$^+$ radical is also expected to increase. To confirm this, the G-value of selenoxide (DHS_{ox}/$SeEOH_{ox}$) formed on reaction of $^\bullet$OH radical with DHS/SeEOH in absence and presence of GNP1 was estimated. For this, the

radiolyzed solution of DHS/SeEOH and DHS-GNP/SeEOH-GNP were incubated with DTT, where DTT reacts with DHS_{ox}/$SeEOH_{ox}$ quantitatively to form oxidised DTT (DTT_{ox}) as given in equation 3.23. The G-value of DHS_{ox}/$SeEOH_{ox}$ was estimated by monitoring the amount of DTT_{ox} using HPLC in the absence and presence of GNP1 at different absorbed doses (80 Gy to 250 Gy).

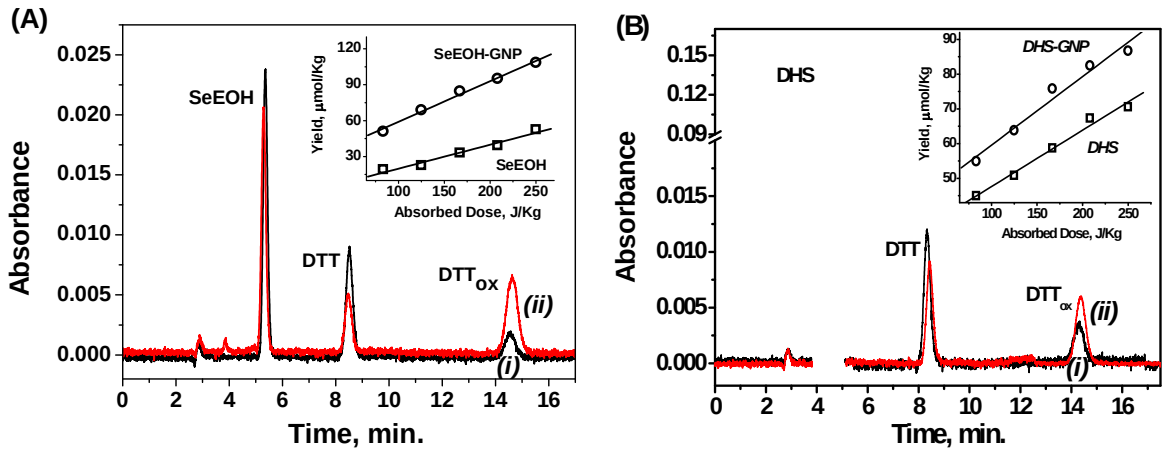

Fig. 5.22: *Estimation of* DHS_{ox}/$SeEOH_{ox}$ *formed on γ-radiolysis of* N_2O *purged aqueous solution of 1 mM (A) SeEOH and (B) DHS in absence (i) and (ii) in presence of 7 nM GNP1 (Absorbed dose=167±5 Gy). Insets of fig. (A) and (B) show the linear variation in the amount of selenoxide formed as a function of absorbed dose (80-250 Gy).*

Fig. 5.22 shows the HPLC chromatogram of DTT treated with radiolysed samples of (A) SeEOH, and (B) DHS in absence and presence of GNP1. The retention time of SeEOH, DHS, DTT and DTT_{ox} were 4.3, 5.4, 8.3 min. and 14.4 min, respectively. The amount of DHS_{ox}/$SeEOH_{ox}$ was calculated in terms of DTT_{ox} from the standard calibration curves of DTT_{ox} as shown in inset of fig. 5.22 (A&B). The slope of the linear plot corresponds to the G-value of the DHS_{ox}/$SeEOH_{ox}$.

Recently, Sicard-Roselli, et. al. have demonstrated that the G-value of •OH radical increases in the presence of GNP which in turn depends on the dose rate, size and concentration of the nanoparticles.[221] Therefore, the G-value of •OH radical was estimated in presence of GNP1. For this N_2O saturated solution of coumarin in absence and presence of 7 nM GNP1 was used as dosimeter. •OH radicals on reaction with coumarin form 7-hydroxy coumarin (7-HOC) as one of the products, formation of which can be monitored by its fluorescence at 456 nm.[221] The quantification of •OH radical in terms of 7-HOC formed in the presence of GNP1 was done using the calibration plot of fluorescence intensity of 7-HOC vs. •OH concentration) as shown in fig. 5.23.

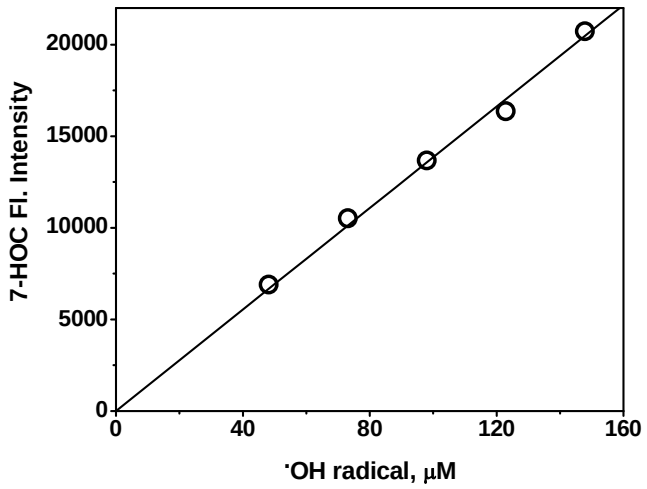

Fig. 5.23: *Calibration plot for the fluorescence of 7-HOC as a function of •OH radical concentration (50-150 μM).*

The estimated G-value of •OH radical in the absence and presence of GNP1 was estimated to be (0.6 ± 0.05) and (0.86 ± 0.08) μmol/J, respectively. Since the G-value of •OH radical increased in the presence of GNP, G-value of DHS_{ox}/$SeEOH_{ox}$ obtained in

absence and in presence of GNP1 was normalized with respective $G_{\bullet OH}$ values. After normalization, G-value of $SeEOH_{ox}$ was found to be (39.6 ± 6.0) % and (51.7 ± 4.0) % of $G_{\bullet OH}$, for SeEOH and SeEOH-GNP. Under similar experimental condition, G-value of DHS_{ox} was estimated to be (51.0 ± 7.0) % and (56.0 ± 5.0) % of the total $^{\bullet}OH$ radical in the absence and presence of GNP1 respectively. These results showed that the percentage increase in G-value of selenoxide is higher for SeEOH-GNP than that for DHS-GNP. Formation of selenoxide is very important as it can regenerate parent DHS molecule in the presence of thiols.

During radiolysis of SeEOH, it has also been found that HCHO is formed as one of the reaction products (equation 3.21). Since $G_{\bullet OH}$ increased in the presence of GNP1, it is also expected to increase the G-value of HCHO (G_{HCHO}). Therefore, the formation of HCHO during γ-radiolysis of SeEOH and DHS was monitored both in absence and presence of GNP1. The value of G_{HCHO} was estimated using DNPH derivatization method as discussed earlier in chapter 3.[102] For this, N_2O purged solution of 1 mM SeEOH/DHS and their GNP composites were exposed to γ-radiation (80-250 Gy) followed by HPLC measurements. Fig. 5.24 shows the HPLC chromatogram of DNPH treated radiolyzed sample of SeEOH (i) in absence and (ii) in presence of 7 nM GNP1 with an absorbed dose of 167 Gy.

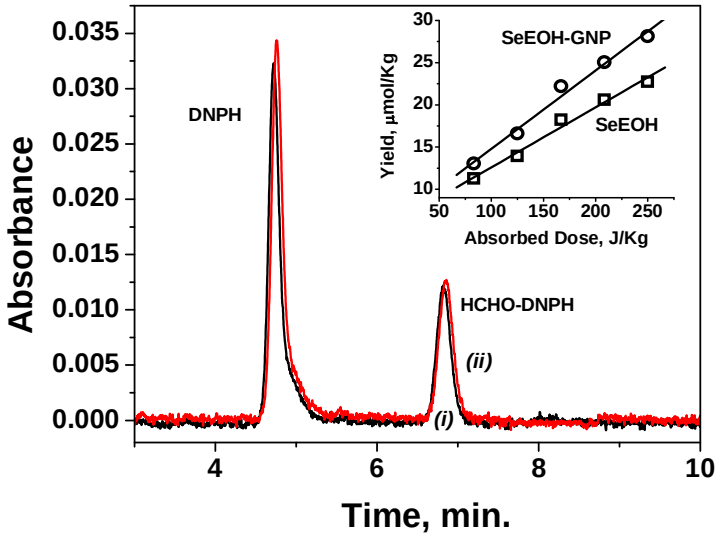

Fig. 5.24: *HPLC chromatogram obtained for the reaction of DNPH with γ-radiolyzed samples of (i) 1 mM SeEOH and (ii) 1 mM SeEOH incubated with 7 nM GNP1 in N_2O saturated conditions (Absorbed dose=167 Gy). Insets (A) and (B) show the linear variation in the amount of formaldehyde formed as a function of absorbed dose.*

G_{HCHO} was found to be 0.091 ± 0.008 and 0.12 ± 0.01 µmol/J for SeEOH and SeEOH-GNP1, respectively. The respective normalized G_{HCHO} for SeEOH in absence and in presence of GNP1 was estimated to be (15 ± 2)% and (13 ± 2)% of $G_{\bullet OH}$. No HCHO formation was observed for radiolysis of DHS both in free form and GNP1 composited form. These results indicate that although the presence of GNP1 increased the G-value of selenoxides considerably, the formation of HCHO was not much affected. Here, the increase in G-value of selenoxides can play important role in modulation of antioxidant properties of these compounds as selenoxides can regenerate parent organoselenium compounds in the presence of thiols like, DTT providing catalytic degradation of free radicals.

5.4 Conclusions

With an aim to understand how the binding of simple organoselenium compounds with GNP can affect their electron transfer ability, detailed investigations on the binding of two structural isomers, i.e. SeEOH (linear) and DHS (cyclic) with GNP of four different sizes were carried out. The results obtained are summarized below:

1. Binding of SeEOH and DHS with GNP lead to red shift in SPR band of GNP from ~520 nm to ~700 nm and induced aggregation. The binding constant was higher for SeEOH than DHS.
2. The aggregation of GNP on addition of DHS and SeEOH was confirmed by DLS and TEM. Under similar experimental conditions, the size of DHS-GNP was larger compared to that of SeEOH-GNP. Also, the ζ-potential of GNP decreased on binding with both SeEOH and DHS.
3. The binding of DHS on GNP surface occured through selenium atom majorly with its C-Se-C plane lying parallel to GNP surface. Whereas, SeEOH was bound to GNP surface through both selenium atom and alkyl chain.
4. The binding of GNP with SeEOH and DHS modulated the redox properties of SeEOH and DHS. The free radical ($ABTS^{\bullet-}$) radicals scavenging activity of SeEOH and DHS was enhanced in presence of GNP.
5. Pulse radiolysis studies on the reaction of $^{\bullet}OH$ radical with SeEOH and DHS in absence and in presence of GNP showed formation of similar transients i.e. dimer radical cation $(>Se\therefore Se<)^{+}$. Presence of GNP did not lead to any change in the G-value

and kinetic behavior of $(>Se\therefore Se<)^{+}$ radical of DHS. However, $(>Se\therefore Se<)^{+}$ radical from SeEOH decayed more slowly in presence of GNP.

6. In presence of GNP1, the G-value of $SeEOH_{ox}$ increased significantly whereas no increase in G-value of DHS_{ox} was observed. This suggests that it is possible to modulate selenoxide formation of simple selenoethers using GNP conjugation which in turn can influence their antioxidant activity.

Chapter 6

Summary and Outlook

This chapter summarizes the results obtained from different studies carried out in the thesis with their future implications.

Free radicals and molecular oxidants, collectively known as reactive oxygen species (ROS) are important entities generated during various biochemical reactions in the cells. Excess generation of ROS causes imbalance in the cellular redox homeostasis, resulting in oxidizing environment termed as 'oxidative stress', which has been implicated in several diseased states. To protect from oxidative stress, nature has equipped cells with a defense system which involves different enzymes like SOD, GPx, etc. along with low molecular weight molecules like vitamins, thiols, etc., collectively called as antioxidants. Out of these, GPx is an important redox regulating enzyme, containing selenium in the active centre, having ability to reduce hydroperoxides at the expense of cellular thiols. Selenium shares same group as sulfur in the periodic tables and sulfur compounds play crucial biochemical role in regularizing cellular redox homeostasis. Selenium is a micronutrient and its deficiency has been linked with many diseases. Due to all these advantages, selenium in both organic and inorganic form is attracting researchers to develop them as redox regulating supplements as well as new drugs. Several new organoselenium compounds are being developed in such a way that these compounds possess both free radical scavenging and GPx like activity, wherein these compounds exhibit catalytic reduction of molecular oxidants like H_2O_2 and peroxynitrite. During such reactions, these compounds undergo several types of electron transfer reactions. Even though the enzymatic activity of organoselenium compounds have been studied extensively, there are not many reports on free radical reactions and electron transfer reactions of these compounds which are necessary for understanding their role in GPx and antioxidant activity.

Therefore the motivation behind the present thesis work is to study redox reactions between free radical or molecular oxidants and simple organoselenium compounds, which are structurally related. The organoselenium compounds studied under present work were water soluble selenoethers that differed either in alkyl chain length substitution or in cyclic vs. linear structures. Further, the electron transfer reactions were monitored in conditions where the organoselenium compounds have been conjugated to GNP. Both one-electron and two-electron transfer reactions in these organoselenium compounds were kinetically monitored followed by identification and estimation of the transient intermediate and reaction products. Further, important molecular descriptors associated with these electron transfer reactions were quantified using quantum chemical calculations. A correlation between these molecular descriptors with the structure of organoselenium compounds and their antioxidant activity has been made in detail. The overall results have been presented in three parts. The first part explains the effect of chemical structure on one-electron transfer reactions of organoselenium compounds and nature of transients formed during these reactions. In the second part, role of structural changes and electron density at the selenium atom in organoselenium compounds was explored for their activity against molecular oxidants (peroxynitrite). In the third part of the thesis, studies were carried out on tuning of the electron transfer reactions of organoselenium compounds to get a desired reaction product through conjugation with GNP. The important findings have been summarized here.

In chapter 3, detailed studies were carried out to understand the effect of structural changes on free radical (e.g. $^{\bullet}OH$ and $CCl_3O_2^{\bullet}$) reactions of organoselenium compounds. The studies were performed using pulse radiolysis and the transients were characterized by

absorption spectrometry. For this, three homologous aliphatic selenoethers (SeROH), (SeEOH, SePOH and SeBOH) were employed. The initial reaction of $^{\bullet}$OH radical with SeROH was similar, irrespective of the alkyl chain length, i.e oxidative addition of $^{\bullet}$OH radical on selenium atom to give (>Se$\therefore$OH) radical. However, the stability and decay pattern of (>Se$\therefore$OH) radical varied with length of alkyl chain. One of the major pathways for the decay of (>Se$\therefore$OH) radical was conversion to ((>Se$\therefore$Se<)$^{+}$) radical via proton catalyzed formation of (>Se$^{\bullet+}$) radical and its subsequent reaction with SeROH. The stability of the (>Se$\therefore$Se<)$^{+}$ radical increased with increase in alkyl chain length. This direct correlation was also reflected in the final yield of the selenoxides ($SeROH_{ox}$) formed by disproportionation reaction of (>Se$\therefore$Se<)$^{+}$ radical. Another pathway for the decay of (>Se$\therefore$OH) radical is degradation to form carbon centered radicals and HCHO via Barton reaction, similar to that observed in analogous organosulfur compounds. However, the yield of HCHO formed during radiolysis of SeEOH was quite low (~11%) when compared with its sulfur analogue, where HCHO yield was estimated to be about 46% of the $^{\bullet}$OH radical yield. No HCHO or higher aldehydes formation was observed for SePOH and SeBOH. Formation of both carbon centered radical and HCHO is implicated to induce oxidative stress. These results were further supported by quantum chemical calculations, where it was observed that the stability of (>Se$\therefore$Se<)$^{+}$ radical could be correlated to the energy difference between HOMO of parent molecule and SOMO of (>Se$^{\bullet+}$) radical. Similar calculations when performed with sulfur analogues, confirmed the lower yield of (>S$\therefore$S<)$^{+}$ radical in organosulfur compounds. Further, the energy of non-bonding interaction, E_{NB} has been calculated between the radical cation centre and –CH bond (at α

position to Se atom). Higher E_{NB} in sulfur compounds as compared to analogous selenium compounds has been attributed to higher radiolytic degradation in the sulfur compounds. In view of all these special properties, organoselenium compounds are recommended as better antioxidants than organosulfur compounds.

As an extension of this study the results for SeEOH were compared with its cyclic isomer DHS. Earlier, a comparative study on the GPx activity of SeEOH and DHS showed that DHS exhibits higher GPx activity than SeEOH.[94] The differential activity was attributed to increase in its HOMO energy on cyclization. $^{\bullet}$OH radical reaction with SeEOH and DHS, indicated that although both the compounds produced $(>Se\therefore Se<)^{+}$ as the major reaction species the two differed in the final reaction products. In SeEOH, a fraction of $(>Se\therefore OH)$ radicals was converted to C-centered radicals and HCHO, while the same was not observed in DHS. The $(>Se\therefore Se<)^{+}$ radical of DHS was found to be more (~1.6 times) stable than that of SeEOH. Also the yield of selenoxide was found to be ~2 times higher for DHS than SeEOH. The higher yield of DHS_{ox} was attributed to the formation of stable $(>Se\therefore Se<)^{+}$ radical. Quantum chemical studies further suggested that radiolytic degradation pathways like formation of HCHO and deprotonation of $(>Se^{\bullet+})$ radical are suppressed for DHS due to unavailability of non-bonding interaction in $(>Se\therefore OH)$ radical and $(>Se^{\bullet+})$ radical.

In chapter 4, detailed studies were carried out to investigate the reaction of DHS and SeEOH with peroxynitrite, a potent molecular oxidant. To understand the effect of change in functional group on antioxidant behavior of these compounds, similar studies were extended with MAS, a monoamino substituted analogue of DHS. The bimolecular

rate constant values (in ~10^3 $M^{-1}s^{-1}$) for the reaction of these compounds with peroxynitrite, as obtained from stopped flow and competition kinetics, were found to be in the order of DHS > MAS > SeEOH. The characterization of products formed during the reaction of peroxynitrite with organoselenium compounds was done using ^{77}Se NMR and MS measurements where corresponding selenoxides were found to be the only detectable products. The yield of selenoxides was estimated by HPLC measurements and found to be the highest for DHS followed by MAS and SeEOH. Further, the reactions of these compounds with peroxynitrite derived species ($CO_3^{\bullet-}$, $NO_2^{\bullet}$ and NO_2^-) were carried out. Being oxidizing in nature, these radicals also can enhance the damage caused by peroxynitritre. All the three compounds reacted with $CO_3^{\bullet-}$ radical and generated $(>Se\therefore Se<)^+$ radical through one-electron oxidation while no reaction was observed with $NO_2^{\bullet}$ radical. The selenoxides showed ability to convert NO_2^- to less reactive NO_3^- followed by regeneration of parent organoselenium compound. In addition, DHS showed significantly higher protection (~ 2 times) against peroxynitrite induced DNA damage and cellular toxicity compared to MAS and SeEOH and was directly correlated to higher yield of DHS_{ox} formed during its reaction with peroxynitrite. These results emphasized that formation of a stable selenoxide makes DHS exhibit higher antioxidant and peroxynitrite reductase activity than the other compounds.

As, seen in the above studies, the electron density on selenium atom is an important factor in deciding the antioxidant activity of these selenoethers. Other than structural and functional group changes, electron density can also be modulated through formation of metal nanoconjugates. Therefore, studies were carried out on binding of organoselenium compounds (SeEOH and DHS) with GNP and influence of such binding on redox

properties of these compounds, in chapter 5. For this, GNP of four different size (GNP1-4 nm, GNP2-12 nm, GNP3-21 nm and GNP4-45 nm) were prepared and characterized by DLS, TEM and ζ- potential. Addition of both SeEOH and DHS led to shift in SPR band of GNP from ~520 nm to 680-720 nm region indicating aggregation of GNP due to its interaction with SeEOH/DHS. SeEOH showed 2-4 times higher value of binding constant with GNP than DHS at all sizes. Under similar experimental conditions, addition of SeEOH resulted in larger decrease in ζ-potential of GNP than that by DHS. The differential binding interaction of DHS and SeEOH with GNP were resolved by SERS, which indicated that plane of SeEOH molecule lies parallel to GNP surface and SeEOH-GNP interaction occurs through both selenium atom and alkyl chain. Whereas, DHS interacts with GNP only through selenium atom and no significant interaction was observed from alkyl chain. The nanoconjugation with GNP surface was found to modulate the electron transfer reaction of both SeEOH and DHS with $ABTS^{\bullet-}$ radical. The presence of GNP enhanced the rate of reaction of both DHS and SeEOH with $ABTS^{\bullet-}$ radical by several folds and among the four different sizes of GNP, GNP1 showed highest enhancement. The binding of SeEOH with GNP1 stabilized the $(>Se\therefore Se<)^{+}$ radical formed during reaction of SeEOH with $^{\bullet}OH$ radical along with increase in the yield of $SeEOH_{ox}$ in presence of GNP1. However, no such effects were seen for DHS-GNP nanoconjugates. These results suggested that stronger interaction of SeEOH with GNP surface increased the nucleophilicity of SeEOH and stabilized the transients formed during its one-electron transfer reactions. This study provides an alternative route of modulating electron transfer reactions of simple organoselenium compounds with the help of GNP nanoconjugates.

In summary, this thesis provides an insight into how structural factors, chemical kinetic parameters along with molecular descriptors like HOMO, non-bonding interaction, enthalpy change, etc can be used for designing organoselenium based antioxidants with enhanced activity against both free radicals and molecular oxidants. These molecular studies further confirm that compared to analogous sulfur compounds, organoselenium compounds act as better antioxidants due to favorable molecular parameters.

Future Perspectives

Low molecular weight organoselenium compounds represent a special class of antioxidants which can exhibit both GPx like catalytic activity or free radical scavenging activity, through the intermediacy of selenoxides. Therefore, it is necessary to understand the correlation between structural features of the organoselenium compounds and stability of their selenoxide. In the present work, it was showed that selenoxides can be formed via radical-radical reaction of $(>Se\therefore Se<)^{+}$ radical, therefore new molecules should be designed in such a way that selenium centre acquires stabilization either through non-bonding interactions or by hemi bonding with other electron rich centers. Use of metal nanoparticles opens another way to modify the antioxidant activity of organoselenium compounds. In the present study, it was shown that conjugation of organoselenium compounds with GNP resulted in enhancement in their electron transfer efficiency and the formation of Se-GNP nanocomposites can be beneficial in the modification of antioxidant activity of these compounds. Also, these nanocomposites can be used to enhance the cellular uptake of the organoselenium compounds and increase their bio availability. Therefore future studies should be addressed to use GNP-composites of organoselenium

compounds for targeted therapy as both selenium compounds and gold nanoparticles have specific bioactivity especially in the design of anticancer drugs.

References

1. J. J. Berzelius, *Afhandl. Fys. Kemi Mineralogi*, 1818, **6**, 42.
2. J. Beld, K. J. Woycechowsky and D. Hilvert, *Biochemistry*, 2007, **46**, 5382-5390.
3. J. Rost and S. Rapoport, *Nature*, 1964, **201**, 185-185.
4. B. Mishra, A. Sharma, S. Naumov and K. I. Priyadarsini, *J. Phys. Chem. B*, 2009, **113**, 7709–7715.
5. M. Jonsson, J. Lind, G. Merenyi and T. E. Eriksen, *J. Chem. Soc. Perkin Trans. 2*, 1995, 67-70.
6. a) R. J. Shamberger, *Biochemistry of Selenium*; Plenum press, New York, 1983; b) A. Bock, *In Encyclopedia of Inorganic Chemistry*, R. Bruce-King, Ed., Wiley New York, 1994.
7. a) A. L. Moxon, *In Alkali Disease or Selenium Poisoning*, Bulletins, 1937, **311**, 1-88.; b) S. H. Knight, O. A. Beath, *Wyoming Agric. Exp. Station Bull.*, 1937, **221**, 2–64.
8. S. G. Knott and C. W. R. McCray, *Aust. Vet. J.*, 1959, **35**, 161–165.
9. P. J. Peterson and G. W. Butler, *Nature*, 1967, **213**, 599–600.
10. D. D. Magg and M. W. Glen, Toxicity of selenium: farm animals in *Selenium in Biomedicine, Conn. AVI, Westport*, 1967, 127–140.
11. A. A. Nelson, O. G. Fitzhugh and H. O. Calvery, *Cancer Research*, 1943, **3**, 230-236.
12. K. Schwarz and C. M. Foltz, *J. Am. Chem. Soc.*, 1957, **79**, 3292–3293.

13. a) J. B. Jones and T. C. Stadtman, *J. Bio. Chem.*, 1981, **256**, 656-663; b) J. E. Cone, R. M. DelRio, J. N. Davis and T. C. Stadtman. *Proc. Natl. Acad. Sci.*, 1976, **73**, 2659-2663.

14. J. T. Rotruck, A. L Pope, H. E. Ganther, A. B. Swanson, D. G. Hafeman and W. G. Hoekstra, *Science*, 1973, **179**, 588-590.

15. a) G. N. Schrauzer, D. A. White and C. J. Schneider, *Bioinorg. Chem.*, 1977, **7**, 23-34.; b) G.F. Combs and W. P. Graya, *Pharma. Therap.*, 1998, **79**, 179–192.

16. World Health Organization, *In Trace elements in human nutrition and health, Geneva*, 1996

17. European Food Safety Authority, *In Tolerable Upper Intake Levels for Vitamins and Minerals*, 2006, 65-76.

18. K. Bierla, J. Szpunar, A. Yiannikouris and R. Lobinski,, *Trends Anal. Chem.*, 2012, **41**, 122–132.

19. C. J. Gobler, A. V. Lobanov, Y. Z. Tang, A. A. Turanov, Y, Zhang, M. Doblin, G. T. Taylor, S. A. Sanudo-Wilhelmy, I. V. Grigoriev and V. N. Gladyshev, *ISME J.*, 2013, **7**, 1333-1343.

20. V. N. Gladyshev and D. L. Hatfield, *J. Biochem. Sci.*, 1999, **6**, 151–160.

21. J. R. Arthur, R. Nicol and G. J. Beckett, *Am. J. Clin. Nutr.*, 1993, **57**, 236S–239S.

22. E. S. J. Arner, *Biochim. Biophys. Acta*, 2009, **1790**, 495–526.

23. a) B. Eberle, H. J. Haas, *J. Trace Elem. Electro. Health Dis.*, 1993, **7**, 217–221.; b) V. Mostert, *Arch. Biochem. Biophys.*, 2000, **376**, 433–438.

24. S. J. Fairweather-Tait, R.Collings and R. Hurst, *Am. J. Clin. Nutr.*, 2010, **91**, 1484S–1491S.

25. V. Ducros and A. Favier, *EMC Endocrinol. Nutr.*, 2004, **1**, 19–28.

26. a) M. Baqui, D. Botero, B. Gereben, C. Curcio, J. W. Harney, D. Salvatore, K. Sorimachi, P. R. Larsen and A. C. Bianco, *J. Biol. Chem.*, 2003, **278**, 1206–1211.; b) M. M. A. Baqui, B. Gereben, J. W. Harney, P. R. Larsen and A. C. Bianco, *Endocrinology*, 2000, **141**, 4309–4312.; c) A. C. Bianco, D. Salvatore, B. Gereben, M. J. Berry and P. R. Larsen, *Endocr. Rev.*, 2002, **23**, 38–89.

27. R. Arrojo'eDrigo and A. C. Bianco, *Int. J. Biochem. Cell Biol.*, 2011, **43**, 1432–1441.

28. S. Gromer, J. Eubel, B. Lee and J. Jacob, *Cell. Mol. Life Sci.*, 2005, **62**, 2414–2437.

29. M. L. Bareither and H. G. Verhage, *Am. J. Anat.*, 1981, **162**, 107–118.

30. R. F. Burk, G. E. Olson, V. P. Winfrey, K. E. Hill and D. P. Yin, *Am. J. Physiol.: Gastrointest. Liver Physiol.*, 2011, **301**, G32–G38.

31. C. Galbusera, P. Orth, D. Fedida and T. Spector, *Biochem. Pharmacol.*, 2006, **71**, 1747-1752.

32. a) J. D. Rush and W. H. Koppenol, *J. Biol. Chem.*, 1986, **261**, 6730-6733.; b) J. D. Rush and W. H. Koppenol, *J. Inorg. Biochem.*, 1987, **29**, 199-215.; c) J. D. Rush and W. H. Koppenol, *J. Am. Chem. Soc.*, 1988, **110**, 4957-4963.; d) D. E. Cabelli, J. D. Rush, M. J. Thomas and B. H. J. Bielski, *J. Phys. Chem.*, 1989, **93**, 3579-3586.; e) J. D. Rush, Z. Maskos and W. H. Koppenol, *FEBS Lett.*, 1990, **261**, 121-123.

33. G. R. Buettner, T. P. Doherty and L. K. Patterson, *FEBS Letters*, 1983, **158**, 143-146.

34. L. J. Ignarro, FASEB J., 1989, 3, 31-36.; b) T. M. Dawson, V. L. Dawson and S. H. Snyder. *Annals. of Neurology*, 1992, **32**, 297-311.

35. N. V. Blough and O. C. Zafiriou, *Inorg. Chem.*, 1985, **24**, 3502–3504.

36. a) C. Gagnon, F. A. Leblond and J. G Filep, *FEBS Letters*, 1998, **431**, 107-110.; b) B. Alvarez, L. Piacenza, F. Irigoin, G. Peluffo and R. Radi, *Arch. Biochem. Biophys.*, 2004, **432**, 222-232.

37. W. H. Koppenol, J. J, Moreno, W. A. Pryor, H. Ischiropoulos and J. S. Beckman, *Chem. Res. Toxicol.*, 1992, **5**, 834-842.

38. a) M. G. Bonini and O. Augusto, *J. Bio. Chem.*, 2001, **276**, 9749–9754.; b) M. G. Bonini, R. Radi, G. F. Sueta, A. M. Ferreirai and O. Augusto, *J. Bio. Chem.*, 1999, **274**, 10802–10806.

39. O. Augusto, M. G. Bonini, A. M. Amanso, E. Linares, C. X. Santos and S. L. Menezes, *Free Rad. Bio. Med.*, 2002, **32**, 841–859.

40. R. Radi, *J. Biol. Chem.*, 2013, **288**, *26464-26472.*

41. R. F. Cathcart, *Med. Hypotheses,* 1985, **18**, 61-77.

42. H. wiseman, *FEBS Letters*, 1993, **326**, 285-288.

43. a) J. Thorne and M. J. Campbell, *Proc. Nutri. Soc.*, 2008, **67**, 115-127.; b) P. R. Holt, N. Arber and B. Halmos, *Cancer Epidem. Biomark. Prev.*, 2002, **11**, 113–119.; c) M. Lipkin and H. L. Newmark, *J. Am. Coll. Nutr.*, 1999, **18**, 392S-397S.; d) H. L. Newmark, *Adv. Exp. Med. Biol.*, 1994, **364**,109-114.

44. E. Niki, *Free Radic. Biol. Med.*, 2014, **66**, 3-12.

45. a) K. I. Priyadarsini, *Curr. Pharm. Res.*, 2013, **19**, 2093-2100.; b) P. Malik and T. K. Mukherjee, *Chinese. J. Bio.*, 2014, 1-8.

46. a) A, M. Mileo and S. Miccadei, *Oxi. Med. Cell.Long.*, 2016, 1-17.; b) S. Gorlach, J. Fishna and U. lewandowska, *Cancer Lett.*, 2016, 1-17.

47. a) G. Annia and A. J. Raul, *RSC Adv.*, 2011, **1**, 1763-1771.; b) C. M. Jones, A. Lawrence, P. Wardman and M. J. Burkitt, *Biochem. Soc. Trans.*, 2003, **31**, 1337-1339.

48. a) A. Gulizar, *Yonsei Med. J.*, 2004, **45**, 776-788.; b) F. P. Chen, Y. C. Huang, C. C. Lin, H. M. Wang and F. F. Chiang, *FASEB J.*, 2013, **27**, 113S-114S.

49. a) P. Rose, M. Whiteman, P. K. Moore and Y. Z. Zhu, *Nat. Prod. Rep.*, 2005, **22**, 351–368.; b) V. M. Dirsch, A. K. Kiemer, H. Wagner and A. M. Vollmar, *Atherosclerosis*, 1998, **139**, 333–339.

50. a) Y. P. Lei, H. W. Chen, L. Y. Sheen and C. K Lii, *J. Nutr.*, 2008, **138**, 996–1003.; b) E. W. Son, S. J. Mo, D. K. Rhee and S. Pyo, *Int. Immunopharmacol.*, 2006, **6**, 1788–1795.

51.) a) N. Ide and B. H. S. Lau, *J. Pharm. Pharmacol.*, 1997, **49**, 908–911.; b) N. Ide and B. H. Lau, *J. Nutr.*, 2001, **131**, 1020–1026.; c) K. M. Kim, S. B. Chun, M. S. Koo, W. J. Choi, T. W. Kim, Y. G. Kwon, H. T. Chung, T. R. Billiar and Y. M. Kim, *Free Radic. Biol. Med.*, 2001, **30**, 747–756.

52. X. L. Chen, G. Dodd and C. Kunsch, *Inflamm. Res.*, 2009, **58**, 513–521.

53. a) M. Zakkar, K. Van der Heiden, A. LuongLe, H. Chaudhury, S. Cuhlmann, S. S. Hamdulay, R. Krams, I. Edirisinghe, I. Rahman, H. C arlsen, D. O. Haskard, J. C. Mason and P.C. Evans, *Arterioscler. Thromb. Vasc. Biol.*, 2009, **29**, 1851–1857.; b) C. S. Piao, S. Gao, G. H. Lee, S. Kim, B. H. Park, S. W. Chae, H. J. Chae and S. H. Kim, *Pharmacol. Res.*, 2010, **61**, 342–348.

54. W. M. Randle and J. E. Lancaster, *In Allium Crop Science- Recent Advances. CABI Publishing, New York*, 2002, 329–356.

55. A. Muller, E. Cadenas, P. Graf and H. Sies, *Biochem. Pharmacol*., **1984**, *33*, 3235-3239.

56. a) H. Sies, Free Radic. Biol. Med., 1993, 14, 313-323.; b) B. K. Sarma and G. Mugesh, *J. Am. Chem. Soc.*, 2005, **127**, 11477-11485.

57. G. Mugesh, A. Panda, H. B. Singh, N. S. Punekar and R. J. Butcher, *J. Am. Chem. Soc.*, 2001, **123**, 839-850.; b) G.Mugesh and W.W. du Mont, *Chem. Eur. J.*, 2001, **7**, 1365–1370.

58. S. S. Zade, S. Panda, S. K. Tripathi, H. B. Singh and G. Wolmershauser, *Eur. J. Org. Chem.*, 2004, 3857–3864.

59. a) R. M. Rosa, D. J. Moura, A. C. Romano e Silva, J. Saffi, J. A. Pegas-Henriques, *Mutat. Res.*, 2007, **631**, 44–54.; b) R. Brandao, C. I. Acker, M. R. Leite, N. B. Barbosa and C.W Nogueira, *J. Appl. Toxicol*., 2009, **29**, 612–618.

60. M. Iwaoka and S. Tomoda, *J. Am. Chem. Soc.*,1994, 116, 2557-2561.

61. T. G. Back, B. P. Dyck and M. Parvez, *J. Org. Chem.*, 1995, **60**, 703–710.

62. K. P. Bhabak and G. Mugesh, *Chem. Eur. J,*. 2008, **14**, 8640-8651.

63. T. Wirth, *Molecules*, 1998, **3**, 164-166.

64. T. G. Back and Z. Moussa, *J. Am. Chem. Soc.*, 2002, **124**, 12104-12105.

65. D. J. Press, E. A. Mercier, D. Kuzma, and T. G. Back, *J. Org. Chem.*, 2008, **73**, 4252–4255.

66. P. Prabhu, B. G. Singh, M. Noguchi, P. P. Phadnis, V. K. Jain, M. Iwaoka and K. I. Priyadarsini, *Org. Biomol. Chem.*, 2014, **12**, 2404-2412.

67. a) T. G. Back and Z. Moussa, *J. Am. Chem. Soc.*, 2003, **125**, 13455-13460.; b) T. G. Back and Z. Moussa, *J. Am. Chem. Soc.*, 2002, **124**, 12104–12105.

68. a) A. Kunwar, B. Mishra, A. Barik, L. B. Kumbhare, R. Pandey, V. K. Jain and K. I. Priyadarsini, *Chem. Res. Toxicol.*, 2007, **20**, 1482–1487.; b) A. Kunwar, P. Bansal, S. J. Kumar, P. P. Bag, P. Paul, N. D. Reddy, L. B. Kumbhare, V. K. Jain, R. C. Chaubey, M. K. Unnikrishnan and K. I. Priyadarsini. *Free Radic. Biol. Med.*, 2010, **48**, 399–410.

69. T. G. Back, Z. Moussa and M. Parvez, *Angew. Chem. Int. Ed.*, 2004, **43**, 1268 –1268.

70. F. Kumakura, B. Mishra, K. I. Priyadarsini and M. Iwaoka, *Eur. J. Org. Chem.*, **2010**, 440–445.

71. P. Prabhu, P. P. Bag, B. G. Singh, A. Hodage, V. K. Jain, M. Iwaoka, and K. I. Priyadarsini, *Free Rad. Res.*, 2011, **45**, 461–468.

72. S. Yoshida, F. Kumakura, I. Komatsu, K. Arai, Y. Onuma, H. Hojo, B. G. Singh, K. I. Priyadarsini and M. Iwaoka, *Angew. Chem. Int. Ed.*, 2011, **50**, 2125–2128.

73. a) K. Briviba, I. Roussyn, V. S. Sharov and H. Sies, *Biochem. J.*, 1996, **319**, 13-15.; b) O. Skaff, D. I. Pattinson, P. E. Morgan, R. Bachana, V. K. Jain, K. I. Priyadarsini and M. J. Davies, *Biochem. J.*, 2012, **441**, 305–316.

74. H. Tsukagoshi, M. Koketsu, M. Kato, M. Kurabayashi, A. Nishina and H. Kimura. *FEBS J.*, 2007, **274**, 6046-6054.

75. R. Scurlock, M. Rougee, R. V. Bensasson, M. Evers and N. Dereu, *Photochem. Photobiol.*, 1991, **54**, 733-736.

76. B. Mishra, K. I. Priyadarsini, H. Mohan and G. Mugesh, *Bioorg. Med. Chem. Lett.*, 2006, **16**, 5334–5338.

77. M. T. Zimmerman, C. A. Bayse, R. R. Ramoutar and J. L. Brumaghim, J. Inorg. Biochem., 2015, 145, 30–40.

78. S. Kumar, J. Yan, J. F. Poon, V. P. Singh, X. Luc, M. Karlssonott, L. Engman and S. Kumar, *Angew. Chem. Int. Ed.*, 2016, **55**, 3729-3733.

79. a) O. Skaff, D. I. Pattison and P. E. Morgan, *Biochem. J.*, 2012, **441**, 305-316.; b) C. Schoneich, V. Narayanaswami, K. D. Asmus and H. Sies, *Arch. Biochem. Biophys.*, 1990, **282**, 18-25.; c) R. Scurlock, M. Rougee, R. V. Bensasson, M. Evers and N. Dereu, *Photochem. Photobiol.*, 1991, **54**,733-736.

80. B. Mishra, K. I. Priyadarsini and H. Mohan, *J. Phy. Chem. A*, 2006, **110**, 1894-1900.

81. T. Tobien , H. Hungerbuhler and K. D. Asmus, *Phosphorus, Sulfur and Silicon*, 2009, **95**, 249-263.

82. H. Masumoto and H. Sies. *Chem. Res. Toxicol.*, 1996, **9**, 262-267.

83. H. Masumoto and H. Sies, *Chem. Res. Toxicol.*, 1996, **9**, 1057-1062.

84. a) B. S. Kumar, A. Kunwar, B. G. Singh, A. Ahmad and K. I. Priyadarsini, *Biol. Trace Elem. Res.*, 2011, **140**, 127–138.; b) C. Storkey, D. I. Pattison, M. T. Ignasiak, C. H. Schiesser and M. J. Davies, *Free Rad. Bio. Med.*, 2015, **89**, 1049–1056.

85. B. Mishra and K. I. Priyadarsini. *Rad. Phys. Chem.*, 2008, **77**, 1294–1299.

86. a) B. Mishra, A. Sharma, S. Naumov and K. I. Priyadarsini, *J. Phys. Chem. B*, 2009, **113**, 7709-7715.; b) S. Padmaja, G. L. Squadrito, J. N. Lemercier, R. Cueto and W. A. Pryor. *Free Rad. Bio. Med.*, 1996, **21**, 317-322.

87. B. Mishra, L. B. Kumbhare, V. K. Jain and K. I. Priyadarsini. *J. Phys. Chem. B*, 2008, **112**, 4441-4446.

88. a) B. Mishra, A. Barik, A. Kunwar, L. B. Kumbhare, K. I. Priyadarsini and V. K. Jain, *Phosphorus, Sulfur, and Silicon*, 2008, **183**, 1018–1025.; b) B. S. Kumar, A.

Kunwar, A, Ahmad L. B. Kumbhare, V. K. Jain and K. I. Priyadarsini. *Rad. Environ. Biophys.*, 2009, **48**, 379-384.

89. S. Padmaja, G. L. Squadrito and W. A. Pryor. *Arch. Biochem. Biophys.*, 1998, **349**, 1-6.

90. B. G. Singh, E. Thomas, F. Kumakura, K.Dedachi, M. Iwaoka and K. I.Priyadarsini, *J. Phys. Chem. A*, 2010, **114**, 8271–8277.

91. G. V. Buxton, C. L. Greenstock, H. W. Phillips and R. B. Alberta, *J. Phy. Chem. Ref. Data*, 1988, **17**, 513-886.

92. R. Overend and G. Paraskevopoulos, *J. Phys. Chem.*, 1978, **82**, 1329–1333.

93. P. Neta, R. E. Huie and A. B. Ross, *J. Phys. Chem. Ref. Data*, 1988, **17**, 1027-1258..

94. K. Arai, F. Kumakura, M. Takahira, N. Sekiyama, N. Kuroda, T. Suzuki and M. Iwaoka, *J Org Chem.*, 2015, **80**, 5633-5642.

95. S. Dey, N. Ghavale, A. S. Hodage, V. K. Jain, G. Kedarnath, L. B. Kumbhare, P. P. Phadnis, P. C. Parashiva, K. I. Priyadarsini and A. Wadawale, *BARC/2009/I/003*.

96. a) M. Iwaoka, T. Takahashi and S. Tomoda, *Heteroatom Chem.*, 2001, **12**, 293-299.; b) K. Arai, K. Moriai, A. Ogawa, M. Iwaoka, *Chem. Asian J.*, 2014, **9**, 3464-3471.

97. R. M. Uppu, G. L. Squadrito, R. Cueto and W. A. Pryor, *Nitric Oxide-B: Physio. Patho. Proc.*, 1996, **29**, 311-333.

98. J. Turkevich, P. C. Stevenson and J. Hillier, *Discuss. Faraday Soc.*, 1951, 55-75.

99. M. Brust, M. Walker, D. bethel, D. J. Schiffrin and R. T. Whyman, *Chem. Soc. Chem. Commun.*, 1994, **7**, 801-802.

100. S. N. Guha, P. N. Moorthy, K. Kishore, D. B. Naik, K. N. Rao, *Proc. Indian Acad. Sci., Chem. Sci.* **1987**, *99*, 261-271.

101. G. V. Buxton, C. C. Stuart, *J. Chem. Soc. Faraday Trans*. **1995**, *91*, 279-281.

102. A. Soman, Y. Qiu and Q. Chan Li, *J. Chrom. Sci.*, 2008, **46**, 461-465.

103. R. Finsy, *Adv. Coll. Interf. Sci.*,1994, **52**, 79-143.

104. C. Miller, *Proc. Roy. Soc. Lond.*, 1924, **106**, 724-749.

105. R. J. Hunter, *In Zeta Potential in Colloid Science: Principles and Applications*, Harcourt Brace Jovanovich Publications Sydney, 1988.

106. E. L. Ru and P. Etchegoin, *In Principles of surface enhanced Raman spectroscopy*, Elsevier, 2009.

107. M. J. Aardema, R. D. Snyder, C. Spicer, K. Divi, T. Morita, R. J. Mauthe, D. P. Gibson, S. Soelter, P. T. Curry, V. Thybaud, G. Lorenzon, D. Marzin, E. Lorge, *Mutat. Res.*, 2006, **607**, 61-87.

108. M. Maiorinoa, A. Roveria, F. Ursini and C. Gregolin, *J. Free Rad. Biol. Med*., 1985, **1**, 203-207.

109. a) F. Jensen, *In Introduction to computational chemistry*, John Wiley and Sons, Chichester, England, 2007.; b) C. J. Cramer, *In Essentials of computational chemistry*, John Wiley & Sons Ltd., Chichester, 2002.

110. A. V. Marenich, C. J. Cramer, D. G. Truhlar, *J. Phys. Chem. B* **2009**, *113*, 6378–6396.

111. M. W. Schmidt, K. K, Baldridge, J. A. Boatz, S. T. Elbert, M. S. Gordon, J. H. Jensen, S. Koseki, N. Matsunaga, K. A. Nguyen, S. J. Su, T. L. Windus, M. Dupuis and J. A. Montgomery, *J. Comput. Chem.*, 1993, **14**, 1347-1358.

112. E. Reed, L. A. Curtiss, F. Weinhold, *Chem. Rev*. **1988**, *88*, 899-926.

113. S. J. K. Jensen, *J. Mol. Struc.*, 2003, **666**, 387–392.

114. M. A. Valko, B. D. Leibfritz, J. Moncola, T. D. Mark, C. Cronin, M. Mazura and D. J. Telser, *Int. J. Biochem. Cell Bio.*, 2007, **39**, 44–84.

115. a) K. D. Asmus, D. Bahnemanann, D. M. Bonifacic and H. A. Gillis, *Faraday Discuss. Chem. Soc.*, 1977, **63**, 213-225.; b) M. Bonifacic, G. L. Hug and C. Schoneich, *J. Phys. Chem. A*, 2000, **104**, 1240-1245.

116. a) W. F. Wang, M. N. Schuchmann, H. P. Schuchmann, W. Knolle, J. V. Sonntag and C. V. Sonntag, *J. Am. Chem. Soc.*, 1999, **121**, 238-245.; b) K. I. Priyadarsini and B. G. Singh, *Proc. Natl. Acad. Sci., India, Sect. A-Phys. Sci.*, 2016, **86**, 459-464.

117. *G.* Meissner, A. Henglein and *G.* Beck, *Z. Naturforsch., E Anorg. Chem., Org. Chem., Biochem., Biophys., Biol.*, 1967, **22B**, 13.

118. a) B. C. Gilbert, J. P. Larkin and R. O. C. Norman, *J. Chem. Soc., Perkin Trans.*, 1973, **2**, 272-277.; b) B. C. Gilbert, D. K. C. Hodgeman and R. O. C. Norman, *J. Chem. Soc., Perkin Trans.*, 1973, **2**, 1748-1752.

119. a) M. Bonifacic, H. Mijckel, D. Bahnemann and K. D. Asmus, *J.Chem. Soc., Perkin Trans.*, 1975, **2**, 675-685.; b) E. Janata, D. Veltwisch and K. D. Asmus, *Radiat. Phys. Chem.*, 1980, **16**, *43*-49.

120. a) W. T. Dixon, R. O. C. Norman and A. J. Buley, *J. Chem. Soc.*, 1964, 3625-3634.; b) D. Veltwisch, E. Janata and K. D. Asmus, *J. Chem. Soc. Perkin Trans.*, 1980, **2**, 146-153.

121. a) K. D. Asmus, D. Bahnemann, M. Bonifaeie and H. A. Gillis, Fara*day Discuss. Chem. Soc.*, 1977, **63**, 213-225.; K. D. Asmus, D. Bahnemann, C. H. Fischer and D. Veltwisch, *J. Am. Chem. Soc*., 1979, **101**, 5322-5329.; K. D. Asmus, *Acc. Chem. Res.*, 1979, **12**, 436-442.

122. B. M. Hoffman, J. E. Roberts, T. *G.* Brown, C. H. Kang and E. Margoliash, *Proc. Natl. Acad. Sci. U.S.A.*, 1979, **76**, 6132-3136.

123. K. O. Hiller, B. Masloch, M. Gobl and K. D. Asmus, *J. Am. Chem. Soc.*, 1981, **103**, 2734-2743.

124. K. D. Asmus, M. Gobl, K. O. Hiller, S. Mahling and J. Monig, *J. Chem. Soc. Perkin Trans.II*, 1985, 641-646.

125. a) C. Schoneich, A. Aced and K. D. Asmus, *J. Am. Chem. Soc.*, 1993, **115**, 11376-11383.; b) B. L. Miller, T. D. Williams and C. Schoneich, *J. Am. Chem. Soc.*, 1996, **118**, 11014-11025.

126. a) C. Schoneich and K. Bobrowski, *J. Am. Chem.* Soc., 1993, **115**, 6538-6543.; b) K. Bobrowski, G. L. Hug, B. Marciniak, B. Miller and C. Schoneich, *J. Am. Chem. Soc.*, 1997, **119**, 8000-8011.

127. R. Badiello and E. M. Fielden, *Int. J. Rad. Bio.*, 1970, **17**, 1-14.

128. M. Tamba, S. Bonora and R. Badiello, *Zeitschrift Fur Naturforschung-Section B J. Chem. Sci.*, 1974, **29**, 571-572.

129. M. Tamba and R. Badiello, *Int. J. Rad. Bio.*, 1973, **23**, 435-445.

130. B. Mishra, D. K. Maity, K. I. Priyadarsini, H. Mohan and J. P. Mittal., *J. Phys. Chem. A*, 2004, **108**, 1552-1559.

131. B. Mishra, P. A. Hassan, K. I. Priyadarsini and H. Mohan. *J. Phys. Chem. B*, 2005, **109**, 12718-12723.

132. B. Mishra, S. Kumar and K. I. Priyadarsini, *Rad. Phys. Chem.*, 2008, **77**, 125–130.

133. A. Assmann, M. Bonifacic, K. Briviba, H. Sies and K. D. Asmus, *Free Radic. Res.*, 2000, **32**, 371-6.

134. T. Nauser, S. Dockheer, R. Kissner, and W. H. Koppenol, *Biochemistry*, 2006, **45**, 6038-6043.

135. B. G. Singh, E. Thomas, S. N. Sawant, K. Takahashi, K. Dedachi, M. Iwaoka and K. I. Priyadarsini, *J. Phys. Chem. A*, 2013, **117**, 9259−9265.

136. T. Tobien, M. Bonifacic, S. Naumov and K. D. Asmus, *Phys. Chem. Chem. Phys.*, 2010, **12**, 6750–6758.

137. B. G. Singh, S. A. Nadkarni, V. K. Jain and K. I. Priyadarsini, *RSC Adv.*, 2015, **5**, 66621–66627.

138. M. Bonifacic, I. Stefanic, G. L. Hug, D. A. Armstrong and K. D. Asmus, *J Am. Chem. Soc.*, 1998, **120**, 9930–9940.

139. Z. B. Alfassi and R. H. Schuler, *J.Phys. Chem.*, 1985, **89**, 3359-3363.

140. W. Wang, M. N. Schuchmann, H. P. Schuchmann, W. Knolle, J. V. Sonntag and C. V. Sonntag, *J. Am. Chem. Soc.*, 1999, **121**, 238-245.

141. T. N. Das and K. I. Priyadarsini, *J. Phys. Chem.*, 1994, **98**, 5212-5278.

142. B. S. Wolfenden and R. L. Willson, *J. Chem. Soc. Perkin Trans.*, 1982, **11**, 805-812.

143. S. Solar, W. Solar, N. Getoff, J. Holcman and K. Sehested, *J. Chem.Soc. Faraday Trans.*, 1982, **78**, 2467-2477.

144. D. Meisel and G. Czapski, *J. Phys. Chem.*, 1975, **79**, 1503–1509.

145. S. N. Guha, P. N. Moorthy, K. Kishore, D. B. Naik and K. N. Rao, *Proc. Indian Acad. Sci., Chem. Sci.*, 1987, **99**, 261-271.

146. B. K. Sarma and G. Mugesh, *Chem. Phys. Chem.*, 2009, **10**, 3013-3020.; M. Iwaoka, H. Komatsu, T. Katsuda and S. Tomoda, *J. Am. Chem. Soc.*, 2004, **126**, 5309-5317.

147. A. J. Mukherjee, S. S. Zade, H. B. Singh and R. B. Sunoj, *Chemical Reviews*, 2010, **110**, 4357-4416.

148. O. Makogon, R. Flyunt, T. Tobien, S. Naumov and M. Bonifacic, *J. Phys. Chem. A*, 2006, **112**, 5908-5916.

149. a) P. Pacher, J. S. Beckman and L. Liaudet, *Physiol. Rev.*, 2007, **87**, 315-424.; b) W. H. Koppenol, J. J. Moreno, W. A. Pryor, H. Ischiropoulos and J. S. Beckman, *Chem. Res. Toxicol.*, 1992, **5**, 834-842.

150. a) K. N. Houk, K. R. Kondroski and W. A. Pryor, *J. Am. Chem. Soc.*, 1996, **118**, 13002-13006.; b) R. S. Ronson, M. Nakamura, J V Johansen, *Cardiovasc. Res.*, 1999, **44**, 47-59.

151. a) R. Kissner and W. H. Koppenol, *J. Am. Chem. Soc.*, 2002, **124**, 234-239.; b) V. M. Darley-Umsar, N. Hogg, V. J. O'Leary, M. T. Wilson and S. Moncada, *Free Rad. Res. Comm.*, 1992, **17**, 9-20.; c) W. M. Deen, S. R. Tannenbaum and J. S. Beckman, *FASEB J.*, 2002, **16**, 1144.; d) B. Alvarez and R. Radi, *Amino Acid*, 2003, **25**, 295-311.

152. B. Epe, D. Ballmaier, I. Roussyn, K. Briviba and H. Sies, *Nucleic Acid Res.*, 1996, **24**, 4105-4110.

153. A. G. Estevez, R. Radi, L. Barbeito, J. T. Shin, J. A. Thompson and J. S. Beckman, *Neurochem.* 1995, **65**, 1543-1550.

154. M. A. Smith, P. L. Harris, L. M. Sayre, J. S. Beckman and George Perry, *J. Neuro.*, 1997, **17**, 2653–2657.

155. M. Ebadi, S. K. Sharma, P. Ghafourifar, H. Brown-Borg and H. E. Refaey, *Meth. Enzymol.*, 2005, **396**, 276-298.

156. M. G. Salgo, K. Stone, G. L. Squadrito, J. R. Battista and W. A. Pryor, *Biochem. Biophy. Res. Comms.,* 1995, **210**, 1025-1030.

157. a) M. Ebadi and S. K. Sharma, *Antioxid Redox Signal*., 2003, **5**, 319-335.; b) J. Boczkowski,·C. L. Lisdero, S. Lanone, M. C. Carreras, M. Aubier and J. J. Poderoso, *Biol. Signals Recept.,* 2001, **10**, 66–80.

158. a) S. Csaba, *Toxicol. Lett.*, 2003, **140**, 105-112.; b) D. Rachmilewitz, J. S. Stamler, F. Karmeli, M. E. Mullins, D. J. Singel, J. Loscalzo, R. J. Xavier and D. K. Podolsky, *Gastroenterology*, 1993, **105**, 1681-1688.

159. G. E. Arteel, K. Briviba and H. Sies, *FEBS Letters*, 1999, **445**, 226-230.

160. Bartlett, D. F. Church, P. L. Bounds and W. H. Koppenol, *Free Rad. Biol. Med.*, 1995, **18**, 85-92.

161. a) F. A. de Bem, B. Fiuza, P. Calcerrad, P. M. Brito, G. Peluffo, C. P. Dinis, M. Trujillo, J. T. Rocha, R. Radi and L. M Almeida, *Nitric Oxide*, 2013, **31**, 20-30.; b) R. Radi, *Chem. Res. Toxicol.*, 1996, **9**, 828–835.

162. a) S. V. Lymar and J. K. Hurst, *J. Am. Chem. Soc.*,1995, **117**, 8867-8868.; b) J. E. Barker, J.P. Bolanos, J. M. Land, J. B. Clark and S. J. Heales, *Dev. Neurosci.*, 1996, **18**, 391-396.

163. M. K. Stern, M. P. Jensen and K. Kramer, *J. Am. Chem. Soc.*, 1996, **118**, 8735 – 8736.

164. R. Floris, S. R. Piersma, G Yang, P Jones, and R Wever, *Eur. J. Biochem.*, 1993, **215**, 767–775.

165. R. Radi, J. S. Beckman, K. M. Bush and B. A. Freeman, *J. Biol. Chem.*, 1991, **266**, 4244-4250.

166. H. Masumoto, R. Kissner, W. H. Koppenol and H. Sies, *FEBS Lett.*, 1996, **398**, 179-182.

167. K. Briviba, R. Kissner, W. H. Koppenol, and H. Sies, *Chem. Res. Toxicol.*, 1998, **11**, 1398-1401.

168. S. Padmaja, G. L. Squadrito, J. N.Lemercier, R. Cueto and W. A. Pryor, *Free Rad. Bio.Med.*, 1997, **23**, 917–926.

169. W. A. Pryor, X. Jin, and G. L. Squadrito, *Proc. Nati. Acad. Sci. USA*, **91**, 11173-11177.

170. C. Storkey, D. I. Pattison, M. T. Ignasiak, C. H. Schiesser and M. J. Davies, *Free Rad. Bio. Med.*, 2015, **89**, 1049–1056.

171. H. Ischiropoulos, L. Zhu, J. Chen, H. M. Tsai, J. C. Martin, C. D. Smith and J. S. Beckman, *Arch. Biochem. Biophys.*, 1992, **298**, 431-437.

172. I. Roussyn, K. Briviba, H. Masumoto and H.Sies, *Arch. Biochem. Biophy.*, 1996, **330**, 216–218.

173. H. Sies, V. S. Sharov, L.O. Klotz, and K. Briviba, *J. Biol. Chem.*, 1997, **272**, 27812–27817.

174. J. Glebska and W. H. Koppenol, *Free Rad. Bio. Med.*, 2003, **35**, 676–682.

175. M. Tien, B. S. Berlett, R. L. Levine, P. B. Chock and E. R. Stadtman, *Proc. Natl. Acad. Sci. USA*, 1999, **96**, 7809-7814.

176. K. P. Bhabak, A. A. Vernekar, S. R. Jakka, G. Roy and G. Mugesh, *Org. Biomol. Chem.*, 2011, **9**, 5193-5200.

177. S. Chakraborty, S. K. Yadav, M. Subramanian, K. I. Priyadarsini, M. Iwaoka and S. Chattopadhyay, *Free Rad. Res.*, 2012, **46**, 1378-1386.

178. J. Z. Zhang and C. J. Fischer, *Marine Chemistry*, 2006, 99, 220-226.

179. C. E. Richeson, P. Mulder, V. W. Bowry and K. U. Ingold, *J. Am. Chem. Soc.*, 1998, **120**, 7211–7219.

180. C. Molina, R. Kissner and W. H. Koppenol, *Dalton Trans.*, 2013, **42**, 9898-9905.

181. D. B. Medinas, G. Cerchiaro, D. F. Trindade and O. Augusto, *IUBMB Life*, 2007, **59**, 255-262.

182. B. S. Wolfenden and R. L. Willson, *J. Chem. Soc. Perkin Trans.II*, 1982, 805-812.

183. R. M. Uppu and W. A. Pryor, *J. Am. Chem. Soc.*, 1999, **121**, 9738-9739.

184. a) J. P. Spencer, M. Whiteman, A. Jenner and B. Halliwell, *Free Radic. Biol. Med.*, 2000, **28**, 1039-1050.; b) J. P. Eiserich, M. Hristova, C. E. Cross, A. D. Jones, B. A. Freeman, B. Halliwell and A. V. Der-Vliet, *Nature*, 1998, **391**, 393-397.

185. a) Y. J. Zhang, H. Rao, Z. Xianfang, W. Lianzhou and W. Chenxu, *Chinese Sci. Bull.*, 2012, **57**, 2-3.: b) V. V. Mody, R. Siwale, A. Singh and H. R. Mody, *J. Pharm. Bioallied Sci.*, 2010, **2**, 282–289.

186. a) E. Boisselier and D. Astruc, *Chem. Soc. Rev.*, 2009, **38**, 1759-1782.; b) M. C. Daniel and D. Astruc, *Chem. Rev.*, 2004, **104**, 293-346.; c) H. J. Haick and D. Phys, *Appl. Phys.*, 2007, **40**, 7173-7186.; d) M. Zayats, R. Baron, I. Popov and I. Willner, *Nano Lett.*, 2005, **5**, 21-25.

187. D. Compton, L. Comish and E. Lingen, *Gold Bull.*, 2003, **36**, 10-16.

188. M. Faraday, Philos. *Trans. R. Soc. London*, 1857, **147**, 145-181.

189. a) W. Zhao, M. A. Brook and Y. F. Li, *Chem. Bio. Chem.*, 2008, **9**, 2363-2371.; b) U. F.Bunz and V. M. Rotello, *Angew. Chem. Int. Ed.*, 2010, **49**, 3268-3271.; c) R. A.

Sperling, P. R. Gil, F. Zhang, M. Zanella and W. J. Parak, *Chem. Soc. Rev.*, 2008, **37**, 1896-1908.

190. C. R. Patra, R. Bhattacharya, D. Mukhopadhyay, P. Mukherjee, *Adv. Drug Deliv. Rev.*, 2010, **62**, 346–361.

191. a) S. Rana, A. Bajaj, R. Mout and V. M. Rotelloa, *Adv. Drug Deliv. Rev.*, 2012, **64**, 200–216.; b) M. M. Joseph, S. R. Aravind, S. K. George, K. R. Pillai, S. Mini and T. T. Sreelekha, *Coll. Surf. B: Biointerf.*, 2014, **116**, 219-227.

192. a) R. S. Norman, J. W. Stone, A. Gole, C. J. Murphy and T. L. Sabo-Attwood, *Nano Lett.*, 2007, **8**, 302–306.; b) W. S. Kuo, C. N. Chang, Y. T. Chang and C. S. Yeh, *Chem. Commun.*, 2009, 4853–4855.

193. S. K. Ghosh and T. Pal, *Chem. Rev.*, 2007, **107**, 4797-4862.; b) X. Liu, M. Atwater, J. Wang and Q. Huo, *Coll. Surf. B: Biointerf.*, 2007, **58**, *3–7.*

194. P. K. Jain, K. S. Lee, I. H. El-Sayed and M. A. El-Sayed, *J. Phys. Chem. B*, 2006, **110**, 7238-7248.

195. S. Y. Lin, Y. T. Tsai, C. C. Chen, C. M. Lin and C. Chen, *J. Phys. Chem. B*, 2004, **108**, 2134–2139.

196. a) S. M. Ansar, R. Haputhanthri, B. Edmonds, D. Liu, L. Yu, A. Sygula and D. Zhang, *J. Phys. Chem. C*, 2011, **115**, 653–660.; b) M. A. Aziz, J. P. Kim and M. Oyama, *Gold Bull.*, 2014, **47**, 127–132.; c) R. A. Sperling and W. J. Parak, *Phil. Trans. R. Soc. A*, 2010, **368**, 1333–1383.

197. a) H. Gu, P. L. Ho, E. Tong, L. Wang and B. Xu, *Nano Lett.*,2003, **3**, 1261–1263.; b) J. Gil-Tomas, S. Tubby, I. P. Parkin, N. Narband, L. Dekker, S. P. Nair, M. Wilson and C. Street, *J. Mater. Chem.*, 2007, **17**, 3739–3746.

198. J. Gao, X. Huang, H. Liu, F. Zan and J. Ren, *Langmuir*, 2012, **28**, 4464−4471.

199. a) T. Sen and A. Patra, *J. Phys. Chem. C*, 2009, **113**, 13125–13132.; b) S. X. Zhang, N. Wang, H. J. Yu, Y. M. Niu and C. Q. Sun, *Bioeletrochemistry*, 2005, **67**, 15−22.; c) S. Roux, B. Garcia, J. L. Bridot, M. Salome, C. Marquette, L. Lemelle, P. Gillet, L. Blum, P. Perriat and O. Tillement, *Langmuir*, 2005, **21**, 2526−2536.; d) B. C. Mei, K. Susumu, I. L. Medintz, J. B. Delehanty, T. J. Mountziaris and H. J. Mattoussi, *Mater. Chem.*, 2008, **18**, 4949−4958.; e) F. Chai, C. G. Wang, T. T.Wang, L. Li and Z. M. Su, *ACS Appl. Mater. Interf.*, 2010, **2**, 1466−1470.; f) P. Ghosh, G. Han, M. De, C. K. Kim and V. M. Rotello, *Adv. Drug Deliv. Rev.*, 2008, **60**, 1307−1315.

200. Y. Joseph, I. Besnard, M. Rosenberger, B. Guse, H.Nothofer, J. M. Wessels, U. Wild, A. Knop-Gericke, D. Su, R. Schlo1gl, A. Yasud and T. Vossmeyer, *J. Phys. Chem. B*, 2003, **107**, 7406-7413.

201. a) H. M. Zakaria, A. Shah, M. Konieczny, J. A. Hoffmann, A. J. Nijdam and M. E. Reeves, *Langmuir*, 2013, **29**, 7661−7673.; b) K. Vangala, K. Siriwardana, E. S. Vasquez, Y. Xin, C. U. Pittman, K. B. Walters and D. Zhang, *J. Phys. Chem. C*, 2013, **117**, 1366−1374.

202. M. G. Samant, C. A. Brown and J. G. Gordon, *Langmuir*, 1992, **8**, 1615-1618.

203. a) K. Bandyopadhyay and K. Vijayamohanan, *Langmuir*, 1999, **15**, 5314-5322.; b) K. Bandyopadhyay and K. Vijayamohanan, *Langmuir*, 1998, **14**, 625-629.

204. S. W. Han and K. J. Kim, *Coll. Interf. Sci.*, 2001, **240**, 492–497.

205. S. Antonello, G. Arrigoni, T. Dainese, M. D. Nardi, G. Parisio, L. Perotti, A. Rene, A Venzo and F. Maran, *ACS Nano*, 2014, 2788–2795.

206. J. Choi, Y. J. Lee, H. Kang, J. W. Han and J. Noh, *Bull. Korean Chem. Soc.*, 2008, **29**, 1229-1232.

207. X. Liu, M. Atwater, J. Wang and Q. Huo, *Coll. Surf. B: Biointerf.*, 2007, **58**, 3–7.

208. a) J. W. S. Rayleigh, *Philos. Mag.*, 1907, **14**, 60-65.; b) L. M. Landau and E. M. Lifshitz, *In Electrodynamics of Continuous Media; Pergamon: Oxford*, 1971.; c) J. D. Jackson, *In Classical Electrodynamics*, Wiley: New York, 1975.; G. Mie, *Ann. Phys.*, 1908, **25**, 377.

209. C. P. Shah, B. Mishra, M. Kumar, K. I. Priyadarsini and P. N. Bajaj, *Curr. Sci.*, 2008, **95**, 1426-1432.

210. R. C. Mucic, J. J. Storhoff, C. A. Mirkin, R. L. Letsinger, *J. Am. Chem. Soc.*,1998, **120**, 12674-12675.

211. a) H. Zhang, I. Hussain, M. Brust, A. I. Cooper, *Adv. Mater.*, 2004, **16**, 27-30.; b) X. D. Cui, A. Primak, X. Zarate, J. Tomfohr, O. F. Sankey, A. L. Moore, T. A. Moore, D. Gust, L. A. Nagahara and S. M. Lindsay, *J. Phys. Chem. B*, 2002, **106**, 8609-8614.

212. X. Liu, M. Atwater, J. Wang and Q. Huo, *Coll. Surf. B - Biointerf.*, 2007, **58**, 3–7.

213. H. Jans, X. Liu and Q. Huo, *Anal Chem.*, 2009, **81**, 9425–9432.

214. T. Doane, C. Hungchuang, R. Hill and C. Burda, *Acc. Chem. Res.*, 2012, **45**, 317-326.

215. D. Zhang and S. M. Ansar, *Anal. Chem.*, 2010, **82**, 5910–5914.

216. Y. M. Kimelfeld, A. Usmanov, G. N. Zhizmn, V. A. Vdovin, N. N. Magdesieva, *J. Struc. Chem.*, 1971, **11**, 1056-1058.

217. M. Moskovits and J. S. Suh, *J. Phys. Chem.*, 1984, **88**, 5526–5530.

218. M. R. Johan, L. C. Chong and N. A. Hamizi, *Int. J. Electrochem. Sci.*, 2012, **7**, 4567-4573.

219. F. Inscore and S. Farquharson, *SPIE*, 2006, 1-8.

220. B. S. Wolfenden and R. L Willson, *J. Chem. Soc. Perkin Trans.-II*, 1982, 805-812.

221. C. S. Roselli, E. Brun, M. Gilles, G. Baldacchino, C. Kelsey, H. McQuaid, C. Polin, N. Wardlow and F. Currell, *Small*, 2014, **10**, 3338–3346.